



Ghent University
Faculty of Pharmaceutical Sciences
Laboratory of Radiopharmacy

**Design and evaluation of novel PET and
SPECT tracers for imaging the
monoamine system and the P-gp
transporter**

Sylvie De Bruyne

Pharmacist

Thesis submitted to obtain the degree of
Doctor in Pharmaceutical Sciences

2009

Promotor : Prof. Dr. Apr. F. De Vos

The author and the promoter give the authorization to consult and to copy parts of this thesis for personal use only. Any other use is limited by the Laws of Copyright, especially the obligation to refer to the source whenever results from this thesis are cited.

De auteur en promoter geven de toelating dit proefschrift voor consultering beschikbaar te stellen en delen ervan te kopiëren voor persoonlijk gebruik. Elk ander gebruik valt onder de beperkingen van het auteursrecht, in het bijzonder met betrekking tot de verplichting uitdrukkelijk de bron te vermelden bij het aanhalen van resultaten uit dit proefschrift.

Gent, augustus 2009

De promoter :

Prof. Dr. Filip De Vos

De auteur :

Sylvie De Bruyne



JORGE CHAM ©THE STANFORD DAILY

The first practical application of a radioisotope was made by George de Hevesy in 1911. At the time de Hevesy was a young Hungarian student working in Manchester with naturally radioactive materials. Not having much money he lived in modest accommodation and took his meals with his landlady. He began to suspect that some of the meals that appeared regularly might be made from leftovers from the preceding days or even weeks, but he could never be sure. To try and confirm his suspicions de Hevesy put a small amount of radioactive material into the remains of a meal. Several days later when the same dish was served again he used a simple radiation detection instrument - a gold leaf electroscope - to check if the food was radioactive. It was, and de Hevesy's suspicions were confirmed.

DANKWOORD

Je zou verwachten dat het enige stuk dat in het Nederlands geschreven wordt het snelst en eenvoudigst zou schrijven. Dit blijkt niet zo te zijn...

Eerst en vooral wil ik *Prof Guido Slegers* bedanken om mij 5 jaar geleden de kans te geven dit doctoraatswerk aan te vatten.

Mijn promotor *Prof Dr Apr Filip De Vos* bedank ik om mij de mogelijkheid te geven dit doctoraatsonderzoek volledig zelfstandig en in alle vrijheid te voltooien.

Volgende laboratoria en mensen wil ik bedanken voor de vlotte samenwerking: de mensen van het *Laboratorium voor Medicinale Chemie* voor de NMR-analyses en hulp bij scheikundige problemen, *Medisip (Steven D. en Prof S. Staelens)* voor het opnemen en verwerken van de scans, *Prof K. Rice, Prof N. Colabufo and Prof R. Silvestri* voor het leveren van producten. Het *IBA team (Jan, John, Cedric)* bedank ik voor de vele bestralingen en jullie flexibiliteit in het voorzien van bestraaltijd. De telefoontjes met jullie waren altijd leuk en zorgden voor wat ontspanning tijdens het stressen aan de 11C-module. *Joban*, bedankt om de 11C-module ineen te knutselen, te onderhouden en je hulp bij technische problemen!

(Ex)-collega's (Bart, Veerle, Ludo, Ruth, Elke, Ingrid, Rien, Peter, Lieve, Joeri, Dirk, Fijo, Davy, Nico, Ghilaine, Valerie, Magali, Liesbet, Leoni, Caroline, Lieselotte en Dominique) ik vond het heel prettig om met jullie samen te werken. Jullie waren altijd bereid naar mijn frustraties te luisteren en te helpen waar nodig. *Wim, Davy, Nico, Ghilaine, Valerie*, de koffiepauzes met jullie waren ideale momenten om te ontspannen en natuurlijk ook te roddelen ☺. *Wim*, merci voor de assistentie bij computerproblemen. *Ingrid*, ik ken niemand anders met zoveel onderzoeksenthoustiasme. De fietsritjes naar en van het labo waren altijd héél ontspannend. *Dominique*, de happy hours met jou waren telkens een feest ☺. *Liezeloze*, merci voor alle cyclotron-assistentie. *Caroline en Magali*, jullie zijn zeer sociale collega's die altijd tijd maakten voor een ontspannende babbel. *Liesbet*, het was prettig samenwerken met zo een begripvolle en geduldige collega. Ik ben je enorm dankbaar voor het nalezen

Acknowledgements

van de volgende 200 pag. *Leonie*, ik had dit op voorhand niet verwacht maar ik vond het héél gezellige jaren in “ons” syntheseslabo. Ik heb me altijd goed geamuseerd tijdens de vele uren in het labo. Ik kon altijd bij jou terecht voor raad over experimenten en de resultaten. *Liesbet en Leonie*, merci voor de vele injecties. Alle (ex)-collega’s: bedankt voor de leuke jaren op het labo en de drie fantastische en memorabele weekends! De labo-avondjes waren ook steeds iets om naar uit te kijken.

Sofie, Ine, Marjan, Margriet, Ellen en Ilse, ik ben blij dat ik jullie tijdens mijn farmaciejaren heb leren kennen en kijk altijd uit naar de gezellige vrouwenavonden met jullie (die veel te weinig voorkomen). *Sofie, Ine en Marjan*, jullie hebben me overtuigd van het feit dat ik wel geschikt was om te doctoreren en daar ben ik jullie nog steeds heel dankbaar voor. *Ilse*, dankzij jou ben ik op het labo radiofarmacie terecht gekomen. Jammergenoeg zijn we er niet beide kunnen beginnen.

Vrienden, bedankt voor alle interesse en steun tijdens de voorbije jaren. Dankzij jullie kon ik de stress van het doctoraatswerk eventjes vergeten!

Mijn ouders ben ik dankbaar mij de kans te geven om te studeren en me daarin ook volledige vrijheid te geven. Zonder jullie had ik nooit dit stukje tekst hier kunnen schrijven. Zowel mijn als Wouter zijn *familie* en dan in het bijzonder mijn en zijn pa wil ik bedanken voor de vele uren werk in Aalter. Dankzij jullie kunnen we binnenkort verhuizen naar een mooi huis met tuin!

Tenslotte wil ik ook “*mijn drie jongens*” bedanken. De twee kleinste zorgden ervoor dat ik nooit alleen was tijdens de saaie uren achter de computer. Wouter, je bent wellicht net zo blij als ik dat dit doctoraat afgewerkt is, al is het maar omdat je computers nu weer veilig zijn ☺. Aangezien ik je voor teveel dingen dankbaar om dit in enkele woorden te kunnen zeggen en neerschrijven ga ik het eenvoudig houden: *Beesie*, merci voor alles!

TABLE OF CONTENTS

List of Abbreviations

Thesis Outline	1
Chapter 1: General Introduction	5
1.1. Medical imaging	7
1.1.1. HISTORICAL BACKGROUND	7
1.1.2. PET	8
1.1.3. SPECT	9
1.1.4. SMALL ANIMAL IMAGING	11
1.2. Neuroimaging	12
1.2.1. RADIOPHARMACEUTICALS	12
1.2.2. NEUROIMAGING WITH PET AND SPECT	14
1.3. References	14
Chapter 2: Blood-brain barrier transport	17
2.1. The blood-brain barrier	19
2.1.1. GENERAL	19
2.1.2. INFLUX IN THE BRAIN	20
2.1.3. EFFLUX OUT THE BRAIN	22
2.2. P-glycoprotein	22
2.2.1. HISTORICAL BACKGROUND	22
2.2.2. EXPRESSION, STRUCTURE AND FUNCTION	23
2.2.3. PHYSIOLOGICAL ROLE OF P-GP	26
2.3. Modulation of P-gp	27
2.3.1. SUBSTRATES	27

2.3.2.	INHIBITORS	29
2.3.3.	IMAGING OF P-GP	30
2.4.	References	32
 Chapter 3: Catecholamine system in the brain		39
3.1.	Catecholamine pathways in the brain	41
3.1.1.	GENERAL INTRODUCTION	41
3.1.2.	NORADRENERGIC SYSTEM IN THE BRAIN	42
3.1.3.	DOPAMINERGIC SYSTEM IN THE BRAIN	43
3.2.	Catecholamine transporters	45
3.2.1.	GENERAL INTRODUCTION	45
3.2.2.	HISTORICAL BACKGROUND	46
3.2.3.	STRUCTURE, FUNCTION AND MECHANISM	46
3.2.4.	NOREPINEPHRINE TRANSPORTER	48
3.2.4.1.	<i>Structure and localization</i>	48
3.2.4.2.	<i>NET and human diseases</i>	49
3.2.4.3.	<i>Imaging of NET</i>	51
3.2.5.	DOPAMINE TRANSPORTER	54
3.2.5.1.	<i>Structure and localization</i>	54
3.2.5.2.	<i>Psychostimulants and DAT</i>	55
3.2.5.3.	<i>Role of DAT in human disorders</i>	57
3.2.5.4.	<i>Imaging of DAT</i>	58
3.3.	Monoamine oxidase	60
3.3.1.	GENERAL INTRODUCTION	60
3.3.2.	EXPRESSION AND STRUCTURE	61
3.3.3.	SUBSTRATES AND INHIBITORS	62
3.3.4.	PHYSIOLOGICAL ROLE IN HEALTH AND DISEASE	64
3.3.5.	IMAGING OF MAO	65
3.4.	References	67

Scope and Aims	79
Chapter 4: Materials and Methods	85
4.1. General	87
4.2. Animals	88
4.3. Carbon-11 as radionuclide	88
4.3.1. GENERAL	88
4.3.2. PRODUCTION OF $^{11}\text{CH}_4$	89
4.3.3. SYNTHESIS OF $^{11}\text{CH}_3\text{I}$	90
4.4. Iodine-123 as radionuclide	90
4.4.1. GENERAL	90
4.4.2. NUCLEOPHILIC IODINATION	90
4.4.3. ELECTROPHILIC IODINATION	91
4.5. Experimental procedures	91
4.5.1. SPECIFIC ACTIVITY	91
4.5.2. LOG $D_{7.4}$	92
4.5.3. METABOLITE STUDY	92
4.6. References	93
Chapter 5: Synthesis and preliminary <i>in vivo</i> evaluation of $[^{123}\text{I}]$-(<i>S,S</i>)-IPBM for mapping the norepinephrine transporter	95
5.1. Abstract	97
5.2. Introduction	98
5.3. Materials & Methods	99
5.3.1. ORGANIC SYNTHESIS	99
5.3.1.1. <i>Cold reference compound synthesis</i>	100
5.3.1.2. <i>Precursor synthesis</i>	104
5.3.2. ENANTIOMERIC PURITY	109

5.3.3.	RADIOCHEMISTRY	109
5.3.4.	QUALITY CONTROL	110
5.3.5.	BIODISTRIBUTION STUDY	111
5.4.	Results & Discussion	112
5.4.1.	ORGANIC SYNTHESIS	112
5.4.2.	ENANTIOMERIC PURITY	113
5.4.3.	RADIOCHEMISTRY	114
5.4.4.	QUALITY CONTROL AND LOG D _{7,4}	114
5.4.5.	BIODISTRIBUTION STUDY	115
5.5.	Conclusion	117
5.6.	References	118

Chapter 6: Radiosynthesis and *in vivo* evaluation of [¹¹C]-labelled pyrrole-2-carboxamide derivatives for MAO-A imaging

		121
6.1.	Abstract	123
6.2.	Introduction	124
6.3.	Materials & Methods	125
6.3.1.	GENERAL	125
6.3.2.	RADIOCHEMISTRY	126
6.3.2.1.	[¹¹ C]-RS 2315	126
6.3.2.2.	[¹¹ C]-RS 2360	127
6.3.3.	IN VITRO CHARACTERIZATION	127
6.3.4.	BIODISTRIBUTION STUDIES	128
6.3.5.	BLOCKING STUDIES	128
6.3.6.	METABOLITE ANALYSIS	129
6.3.7.	IMAGING STUDY	129
6.4.	Results & Discussion	131

6.4.1. RADIOSYNTHESIS	131
6.4.1.1. [¹¹ C]-RS 2315	132
6.4.1.2. [¹¹ C]-RS 2360	132
6.4.2. IN VITRO CHARACTERIZATION	133
6.4.2.1. <i>Quality control, specific activity and stability</i>	133
6.4.2.2. <i>Log D_{7.4}</i>	133
6.4.3. BIODISTRIBUTION STUDIES	134
6.4.4. BLOCKING STUDIES	136
6.4.5. METABOLITE ANALYSIS	138
6.4.6. PET SCANS	140
6.5. Conclusion	141
6.6. References	143

Chapter 7: Synthesis, radiosynthesis and *in vivo* evaluation of [¹²³I]-FMIP for imaging the dopamine transporter

7.1. Abstract	147
7.2. Introduction	148
7.3. Materials & Methods	150
7.3.1. ORGANIC SYNTHESIS	150
7.3.1.1. <i>(4-(2-(Bis(4-fluorophenyl)methoxy)ethyl)piperidin-1-yl)-(4-hydroxyphenyl)methanone (2)</i>	150
7.3.1.2. <i>4-((4-(2-(Bis(4-fluorophenyl)methoxy)ethyl)piperidin-1-yl)-methyl)phenol (3)</i>	151
7.3.1.3. <i>4-((4-(2-(Bis(4-fluorophenyl)methoxy)ethyl)piperidin-1-yl)-methyl)phenyltrifluoromethanesulfonate (4)</i>	152
7.3.1.4. <i>4-(2-(Bis(4-fluorophenyl)methoxy)ethyl)-1-(4-(tributylstannyl)-benzyl)piperidine (5)</i>	152
7.3.1.5. <i>4-(2-(Bis(4-fluorophenyl)methoxy)ethyl)-1-(4-iodobenzyl)-</i>	

Table of Contents

<i>piperidine (FMIP)</i>	153
7.3.2. RADIOCHEMISTRY	154
7.3.3. IN VITRO CHARACTERIZATION	154
7.3.4. BIODISTRIBUTION STUDY	155
7.3.5. REGIONAL BRAIN DISTRIBUTION STUDY	155
7.3.6. BLOCKING STUDY	156
7.3.7. PLASMA BINDING	156
7.3.8. METABOLITE ANALYSIS	157
7.3.9. BLOOD-BRAIN BARRIER TRANSPORT INHIBITION STUDY	157
7.3.10. REGIONAL BRAIN DISTRIBUTION AFTER CSA PRETREATMENT	158
7.4. Results & Discussion	158
7.4.1. ORGANIC SYNTHESIS	158
7.4.1.1. <i>Precursor synthesis</i>	159
7.4.1.2. <i>Synthesis of FMIP</i>	160
7.4.2. RADIOSYNTHESIS	160
7.4.3. IN VITRO CHARACTERIZATION	161
7.4.4. BIODISTRIBUTION STUDY	162
7.4.5. REGIONAL BRAIN DISTRIBUTION STUDY	165
7.4.6. BLOCKING STUDY	166
7.4.7. PLASMA PROTEIN BINDING AND METABOLITE ANALYSIS	167
7.4.8. BLOOD-BRAIN BARRIER TRANSPORT INHIBITION STUDY	169
7.4.9. REGIONAL BRAIN DISTRIBUTION AFTER CSA PRETREATMENT	169
7.5. Conclusion	170
7.6. References	172

Chapter 8: <i>In vivo</i> evaluation of [¹²³I]-FMIP for imaging the P-glycoprotein transporter	175
8.1. Abstract	177
8.2. Introduction	178
8.3. Materials & Methods	179
8.3.1. BIODISTRIBUTION STUDIES IN MICE	179
8.3.2. DOSE ESCALATION STUDY	179
8.3.3. METABOLITE ANALYSIS	180
8.3.4. U-SPECT SCAN	181
8.4. Results & Discussion	182
8.4.1. RADIOCHEMISTRY	182
8.4.2. BIODISTRIBUTION STUDIES	182
8.4.2.1. <i>Biodistribution study in normal FVB mice</i>	183
8.4.2.2. <i>Influence of CsA pretreatment</i>	184
8.4.2.3. <i>Influence of gene depletion</i>	184
8.4.2.4. <i>Influence of CsA pretreatment in mdr1a (-/-) mice</i>	185
8.4.3. DOSE ESCALATION STUDY	186
8.4.4. METABOLITE ANALYSIS	187
8.4.5. U-SPECT SCAN	189
8.5. Conclusion	191
8.6. References	194
Chapter 9: Radiosynthesis and <i>in vivo</i> evaluation of [¹¹C]-MC80 for P-gp imaging	197
9.1. Abstract	199
9.2. Introduction	200
9.3. Materials & Methods	201
9.3.1. GENERAL	201

9.3.2.	RADIOCHEMISTRY	202
9.3.3.	IN VITRO CHARACTERIZATION	203
9.3.4.	BIODISTRIBUTION STUDY	203
9.3.5.	METABOLITE ANALYSIS	204
9.4.	Results & Discussion	205
9.4.1.	RADIOSYNTHESIS	205
9.4.2.	IN VITRO CHARACTERIZATION	205
9.4.2.1.	<i>Quality control, specific activity and stability</i>	205
9.4.2.2.	<i>Log D_{7.4}</i>	205
9.4.3.	BIODISTRIBUTION STUDIES	205
9.4.3.1.	<i>Biodistribution study in FVB mice</i>	205
9.4.3.2.	<i>Biodistribution study after CsA pretreatment</i>	207
9.4.3.3.	<i>Biodistribution study in mdr1a (-/-) mice</i>	209
9.4.3.4.	<i>Biodistribution study after pretreatment with cold compound</i>	210
9.4.4.	METABOLITE ANALYSIS	212
9.4.4.1.	<i>Metabolism study in FVB mice</i>	213
9.4.4.2.	<i>Metabolism study after CsA pretreatment</i>	213
9.4.4.3.	<i>Metabolism study in mdr1a (-/-) mice</i>	213
9.5.	Conclusion	214
9.6.	References	215
	Summary	217
	Samenvatting	223
	Curriculum Vitae	229

LIST OF ABBREVIATIONS

ABC	ATP binding cassette
ADAM	2-((2-((Dimethylamino)methyl)phenyl)thio)-5-iodophenylamine
ADHD	Attention Deficit Hyperactivity Disorder
ATP	Adenosine Triphosphate
BBB	Blood-Brain Barrier
β -CIT	RTI-55, 2 β -Carbomethoxy-3 β -(4-iodophenyl)nortropane
β -CFT	WIN 35,428, 2 β -Carbomethoxy-3 β -(4-fluorophenyl)nortropane
BH ₃	Borane
Bq	Becquerel
calcd	Calculated
CDCl ₃	Deuterated Chloroform
CH ₄	Methane
CH ₂ Cl ₂	Dichloromethane
CH ₃ Cl	Chloroform
CH ₃ CN	Acetonitrile
CH ₃ I	Methyl Iodide
CNS	Central Nervous System
COMT	Catecholamine-O-methyltransferase
cpm	Counts per minute
CsA	Cyclosporin A
CT	Computed Tomography
Ci	Curie

List of Abbreviations

Da	Dalton
DASB	3-Amino-4-(2-dimethylaminomethylphenylsulfanyl)benzotrile
DAT	Dopamine Transporter
DMF	Dimethylformamide
DMSO	Dimethylsulfoxide
DNA	Desoxyribonucleic Acid
DOPA	Dihydroxyphenyl-alanine
ECD	Ethyl Cysteinate Diethylester
EI	Electron Impact
ESI-MS	Electrospray Ionization Mass spectrum
Et ₃ N	Triethylamine
Eu(hfc) ₃	Europium tris[3-heptafluoropropylhydroxymethylene)-(-)-camphorate]
eV	Electron Volt
FECNT	2β-Carbomethoxy-3β-(4-chlorophenyl)-8-(2-fluoroethyl)nortropane
FMeNER	Fluoromethyleboxetine
FMIP	4-(2-(Bis(4-fluorophenyl)methoxy)ethyl)-1-(4-iodobenzyl)piperidine
FP-CIT	Fluoropropyl- 2β-carbomethoxy-3β-(4-iodophenyl)nortropane
FT-NMR	Fourier Transform NMR
GBR 13119	1-((4-Fluorophenyl)(phenyl)methoxy)ethyl)-4-(3-phenylpropyl)piperazine,
GBR 12909	1-(2-(Bis(4-fluorophenyl)methoxy)ethyl)-4-(3-phenylpropyl)piperazine

HCl	Hydrochloric Acid
HCOOH	Formic Acid
H ₂ O ₂	Hydrogen Peroxide
HPLC	High Performance Liquid Chromatography
IBZM	Iodobenzamide
ID	Injected Dose
IPBM	2-[α -(2-Iodophenoxy)benzyl]morpholine
i.v.	Intravenously
<i>J</i>	Coupling Constant
kb	Kilobase
K ₃ EDTA	Tripotassium Ethylenediaminetetraacetate
MAO	Monoamine Oxidase
MC80	6,7-Dimethoxy-2-(6-methoxy-naphthalen-2-ylmethyl)-1,2,3,4-tetrahydro-isoquinoline
MC90	6,7-Dimethoxy-2-(6-hydroxy-naphthalen-2-ylmethyl)-1,2,3,4-tetrahydro-isoquinoline
MeNER	Methylreboxetine
MeOH	Methanol
MHz	Megahertz
m.p.	Melting Point
MPP ⁺	1-Methyl-4-phenylpyridinium
MPTP	1-Methyl-4-phenyl-1, 2, 3, 6-tetrahydropyridine
MRI	Magnetic Resonance Imaging
MW	Molecular Weight

List of Abbreviations

NaH	Sodium Hydride
NaHCO ₃	Sodium Bicarbonate
NaI	Sodium Iodide
NaI(Tl)	Sodium Iodide doped with Thallium
NaOH	Sodium Hydroxide
Na ₂ SO ₄	Sodium Sulfate
NBD	Nucleotide Binding Domain
n.c.a.	No Carrier Added
NET	Norepinephrine Transporter
NH ₄ OH	Ammonium Hydroxide
NMR	Nuclear Magnetic Resonance
NMRI	Naval Medical Research Institute
PBS	Phosphate Buffered Saline
PD	Parkinson's Disease
PE2I	<i>N</i> -(3-iodopro-2 <i>E</i> -enyl)-2β-carbomethoxy-3β-(4-methylphenyl)nortropane
PET	Positron Emission Tomography
P-gp	Permeability-glycoprotein
p.i.	Post Injection
ppm	Parts per Million
ROI	Region of Interest
RP-HPLC	Reversed Phase-HPLC
RS 2315	<i>N</i> -phenethyl-1 <i>H</i> -pyrrole-2-carboxamide
RS 2360	(<i>R</i>)- <i>N</i> -(1-cyclohexylethyl-1 <i>H</i> -pyrrole-2-carboxamide
RS 2115	<i>N</i> -phenethyl-1 <i>H</i> -pyrrole-2-carboxamide
RS 2226	(<i>R</i>)- <i>N</i> -(1-cyclohexylethyl-1 <i>H</i> -pyrrole-2-carboxamide

SD	Standard Deviation
SERT	Serotonin Transporter
SPECT	Single Photon Emission Computed Tomography
$T_{1/2}$	Half-life
T_r	Retention Time
TBAH	Tetrabutylammonium hydroxide
THF	Tetrahydrofuran
TLC	Thin Layer Chromatography
TMD	Transmembrane Domain
TMS	Trimethylsilane
UV	Ultraviolet
VOI	Volumes of Interest
WAY100635	<i>N</i> -(2-[4-(2-methoxyphenyl)-1-piperazinyl]ethyl)- <i>N</i> -(2-pyridyl)cyclohexanecarboxamide
δ	Chemical Shift

Thesis Outline



THESIS OUTLINE

Neuroimaging has provided the means to elucidate healthy physiological processes in human beings along with the causes and consequences of neurological and psychiatric disorders. The use of suitable radiopharmaceuticals assists clinicians in the diagnosis and care of patients with brain disorders. The human brain consists of millions of inter-communicating neurons. Mental processes are driven by the complex interplay of neurotransmitter systems and their disruption underlies many diseases of the central nervous system. A prerequisite of efficient drug treatment of diseases of the central nervous system is that sufficient amounts of the drug enter the brain. An important factor determining this bioavailability is the capability to accumulate in the brain. Active transport by P-glycoprotein (P-gp) from the brain back into the bloodstream has a major impact on drug resistance to psychotropic drugs.

In this thesis we aimed to develop radiotracers for targets of the dopamine and norepinephrine system that causes neurotransmitter inactivation being the norepinephrine transporter, the dopamine transporter and monoamine oxidase. By the discovery that one of the designed radiotracers is modulated by P-gp, the focus of this thesis was redirected towards imaging of P-gp function and expression.

Chapter 1 gives a short overview of the medical imaging techniques and describes the requirements of a valuable radiopharmaceutical for SPECT or PET imaging.

Chapter 2 discusses the blood-brain barrier and the transport of compounds across this barrier. One of the most important transport mechanisms limiting brain uptake of drugs, P-gp, is detailed in this chapter.

The dopamine and norepinephrine system and more specifically the dopamine transporter, the norepinephrine transporter and monoamine oxidase, are discussed in **Chapter 3**.

In **Chapter 4** the general material and methods are described.

The lack of a valuable radiotracer for the norepinephrine transporter, leads us to the development of an iodinated reboxetine analogue, [^{123}I]-(*S,S*)-IPBM, to visualize this transporter. **Chapter 5** reports the synthesis, radiosynthesis and preliminary evaluation of [^{123}I]-(*S,S*)-IPBM.

In **Chapter 6** the radiolabelling as well as the *in vivo* characterization of two [^{11}C]-labelled pyrrole-2-carboxamide derivatives, [^{11}C]-RS 2315 and [^{11}C]-RS 2360, are described. *In vitro*, RS 2315 and RS 2360 were both potent inhibitors of monoamine oxidase-A. The search for new ligands for MAO-A with optimal kinetic properties is justified by the lack of an ideal ligand and the observation that fluctuations in MAO-A functionality are associated with human diseases and tobacco addiction.

The synthesis along with the radiolabelling and *in vivo* evaluation of [^{123}I]-FMIP as a selective radiotracer for the dopamine transporter is reported in **Chapter 7**. FMIP has nanomolar affinity for the dopamine transporter and better selectivity over the other monoamine transporters compared to the already existing ligands for dopamine transporter imaging with SPECT.

The contribution of P-gp to the low brain uptake of [^{123}I]-FMIP along with its potential as P-gp imaging agent are investigated in **Chapter 8**. To date, no iodinated SPECT ligands for P-gp imaging have been published.

Finally, **Chapter 9** describes the radiolabelling of an *in vitro* characterized substrate (MC80) of the P-gp pump with ^{11}C and the evaluation of this tracer *in vivo* for its potential to image P-gp function or expression.

Chapter 1

General Introduction



Chapter 1

General Introduction

1.1. Medical imaging

1.1.1. HISTORICAL BACKGROUND

The first known method for medical imaging made use of X-rays and has been discovered in 1895 by Wilhelm Röntgen. Nowadays there exist different imaging techniques that can be divided into two categories: structural and functional imaging.

Structural imaging is primarily aimed at anatomical localisation of pathological processes. Besides X-rays, computed tomography (CT) and magnetic resonance imaging (MRI) are the most important ones. Due to their short wavelength, X-rays penetrate through most tissues depending on the density of the tissue. The detection of X-rays on a photographic plate, providing an image that is in accordance with the density of the tissues. This makes them especially useful in the detection of pathology of the skeletal system. To a lesser extent, they are also used for identifying some disease processes in soft tissue. Imaging alternatives for soft tissues are CT and MRI. CT has been developed in 1967 and is still the gold standard in the diagnosis of a large number of different disease entities. CT also uses X-rays but here, the X-ray source rotates around the patient, resulting in a high quality three dimensional image (resolution of 1 mm). MRI has been discovered a few years later than CT and is not only used for structural but also for functional imaging. MRI technology is based on nuclear magnetic resonance (NMR). The advantage of MRI is that it provides high contrast images between

the different types of soft tissues within the body without exposing subjects to ionizing radiation.

Functional imaging is, rather than anatomical imaging, focussed on physiological processes like metabolism, blood flow, receptor binding, etc. The pivotal functional imaging techniques, Positron Emission Tomography (PET) and Single Photon Emission Computed Tomography (SPECT), belong to the domain of nuclear medicine. Widespread clinical use of nuclear medicine began in the early 1950's. Unlike the use of X-rays and CT where radiation is passed through the body, nuclear imaging modalities detect the radiation emitted by the human body after administration of radiopharmaceuticals. This provides very accurate images of the area of the body being investigated. Depending on the radiopharmaceutical used, information about certain biological changes or processes is gathered, leading to knowledge or diagnosis of diseases (For review see Guy, 1996; Wolbarst and Hendee, 2006).

1.1.2. PET

PET is a non-invasive imaging method used to study physiological, biochemical and pharmacological processes in the human body. PET utilizes positron (β^+) emitting isotopes. Positrons are particles with an equal mass as electrons, but with a positive charge. The positron travels a short distance in tissue until it interacts with an electron, in a process called annihilation. The total mass of positron and electron is converted into electromagnetic energy, producing two photons of 511 keV emitted under an angle of 180° (Wong and Brasic, 2001; Lewellen, 2008). A PET scanner contains a set of detectors arranged in a ring surrounding the object to be imaged (Figure 1.1). The pair of photons produced from a single annihilation will be detected almost simultaneously on opposing pairs of scintillation detectors as a coincidence event. The rings of scintillation detectors register thousand of coincidence events emitted from the subject and convert them into an electrical signal that can be registered. The acquired emission data

are then converted into a tomographic image via computerised reconstruction algorithms. Theoretically, PET has a resolution of 2 - 4 mm (Wong and Brasic, 2001; Lewellen, 2008; Ganguly et al., 2009).

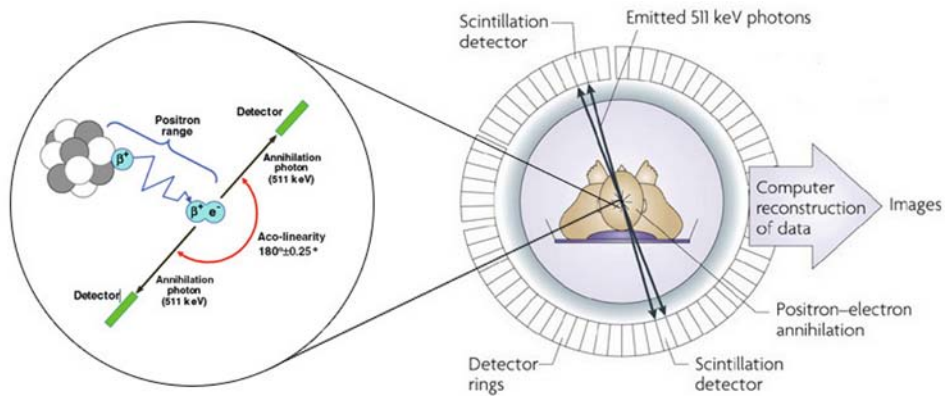


Figure 1.1 Principle of PET camera

Radionuclides commonly used in PET are ^{18}F ($T_{1/2} \approx 110$ min), ^{11}C ($T_{1/2} \approx 20.4$ min), and ^{15}O ($T_{1/2} \approx 2$ min). The stable counterparts of ^{11}C and ^{15}O are the building blocks of all living matter which makes it possible to incorporate them into the molecules of interest without changing their pharmacological or physiological properties. On the other hand, the presence of an on-site cyclotron is required to produce the radionuclides with relative short half-lives, immediately prior to use (Wong and Brasic, 2001).

1.1.3. SPECT

The origin of SPECT can be found in the groundbreaking experiments on emission tomography performed approximately 50 years ago (Kuhl and Edwards, 1963). SPECT is used to gain information on physiological parameters or certain biological processes based on the *in vivo* distribution of the radioactivity,

measured by external mapping of the location and density of the emitted photons.

SPECT cameras detect single photons and consist of a collimator, one or more scintillation crystals and photomultiplier tubes (Figure 1.2). The properties of these three parts determine the sensitivity and spatial resolution of the SPECT camera. The use of a collimator restricts the flow of photons to only those that reach the detector in a ninety degree angle, allowing localisation of the radionuclide. Thereafter, the scintillation crystal absorbs the energy from the photons and converts it to visible light which can be detected by the photomultiplier tubes. A sodium iodide crystal, doped with thallium (NaI(Tl)) is commonly used as the scintillator in SPECT imaging. Subsequently, the photomultiplier tubes convert these light photons into an electrical charge which is then amplified to a detectable level. Three dimensional tomographic images in the coronal, horizontal and sagittal planes are reconstructed by computer software programs from the data collected (Ruth, 2009).

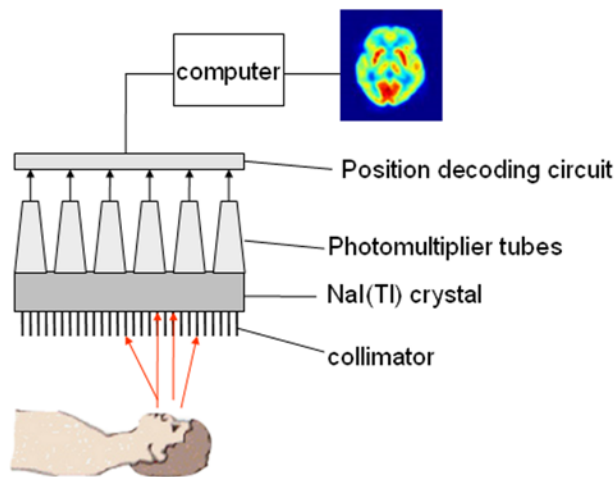


Figure 1.2 Schematic view of a SPECT camera

Two- and triple-head rotating cameras have been developed resulting in improved sensitivity and higher spatial resolution. Workable resolution is about 6

mm, which is low compared to PET cameras. Because a PET camera only detects the coincidence events, there is no need for a collimator, improving the sensitivity and resolution of the PET camera.

The ideal radionuclide for SPECT imaging possesses a relative short half-life and emits photons in high abundance and with sufficient energy to penetrate the body without undesirable scatter or attenuation. ^{99m}Tc ($T_{1/2} \approx 6$ h, 140.5 keV) is the best and least expensive radionuclide but its metallic characteristics make it difficult to work with. Another commonly used isotope is ^{123}I ($T_{1/2} \approx 13.2$ h, 159 keV). SPECT radionuclides are not commonly found in nature which makes it difficult to incorporate them into biological active molecules without changing the physiological properties of the molecule (Kung, 1991).

1.1.4. SMALL ANIMAL IMAGING

Small animal imaging requires, due to the size of the subjects involved, higher spatial resolution than most clinical systems can provide. This has led to the development of μSPECT and μPET (Peremans et al., 2005). To achieve a higher spatial resolution, scanners must use higher-resolution detectors and obtain finer spatial sampling while maintaining the sensitivity as high as possible (Sossi and Ruth, 2004; Rowland et al., 2008).

Preclinical μSPECT mainly use pinhole collimation achieving spatial resolution of 0.5 to 2 mm. The major limitation of pinhole μSPECT is the reduced field of view and subsequently the reduced sensitivity. By setting up additional pinholes and focusing them on different regions, it is possible to increase the field of view, improve the sensitivity, and obtain high spatial resolution when using sufficiently small pinhole diameters (Beekman et al., 2005; Rowland et al., 2008; Vanhove et al., 2008).

Enhancement of preclinical PET is mainly focussed on improved photon detection material. Compared to the commonly used detection material NaI(Tl), Lutetium Orthosilicate has a high density and high light yield. This allows

reduction in the size of individual crystals and thus leads to higher spatial resolutions while maintaining the same sensitivity (Ruth, 2009). As well as the hardware improvement, development of software that provides more accurate data quantification and image reconstruction contributes to the successful application of preclinical PET and SPECT (Sossi and Ruth, 2004; Rowland et al., 2008).

1.2. Neuroimaging

The human brain is a complex organ, consisting of millions of intercommunicating neurons. Due to the complexity of the central nervous system (CNS) our knowledge about CNS disorders is still limited. The understanding of biochemical abnormalities relating to disease and disease processes is pivotal to the future development of effective diagnosis, treatment and management of neurological and psychiatric illness. Since the development of suitable radioligands in the late 1970's, the use of non-invasive imaging modalities (PET and SPECT) is a valuable tool for *in vivo* brain mapping and drug development in the future (Wong and Brasic, 2001; Gee, 2003).

1.2.1. RADIOPHARMACEUTICALS

Radiopharmaceuticals can be divided into two categories being: diagnostic and therapeutic radiopharmaceuticals. For the preparation of radiopharmaceuticals, a radionuclide is coupled to a drug with a certain target in the human body. In this thesis, only radiopharmaceuticals for brain imaging will be discussed. The development of new and improved radiopharmaceuticals is a research field that is actively explored. To obtain a new, valuable radiopharmaceutical, some critical points have to be considered during the radiotracer development (Kung, 1991). First, a possible interesting radiotracer must be selected out of the thousand molecules designed by chemists; preferentially, a molecule with high *in vitro*

affinity (K_d in nanomolar range) and selectivity (at least more than 10) for its target. Subsequently, radiolabelling opportunities that do not alter the affinity and selectivity are required. Lipophilicity is another important parameter since it determines the ability of the molecule to cross the blood-brain barrier (BBB). The lipophilicity is often expressed by the $\log D_{7.4}$, which is the logarithm of the partition coefficient between n-octanol and water at physiological pH. An ideal $\log D_{7.4}$ should be between 1.5 and 3 (Waterhouse, 2003). A molecule that is too hydrophilic ($\log D_{7.4} < 1.5$) will not pass the BBB by passive diffusion. Elevated values of $\log D_{7.4}$ on the other hand, result in high nonspecific binding. The ability of the molecule to penetrate the BBB is not only determined by the partition coefficient. The molecular weight has to be lower than 650 g/mol, the molecule may not be charged and binding to plasma proteins must be reversible. The presence of multispecific xenobiotics transporters at the BBB can cause efflux of the molecule out of the brain. Consequently, a lower brain uptake than expected from its lipophilicity is observed. P-glycoprotein is an example of such a transporter (For review see Stöcklin, 1992; Elsinga, 2002).

When preparing radiopharmaceuticals, the chemical, radiochemical and radionuclidic purity are of great importance. This implies that the tracer solution has to be free of unlabelled and labelled impurities and undesirable radionuclides. Further is the specific activity, expressed as the amount of radioactive molecules over the total mass of those molecules present in the tracer solution, also of critical importance. Specific activity is usually formulated as GBq/ μmol or Ci/ μmol . As most radiotracers for brain imaging are injected intravenously, special requirements including pH, isotonicity, sterility and apyrogenicity are necessary.

When all the mentioned requirements are fulfilled, the radiopharmaceutical can be evaluated *in vivo*. It is important that the administered radiotracer is highly distributed to the organ of interest resulting in a high target to non-target ratio. The radiotracer must interact with the system in a known and reproducible fashion. Rapid metabolism of the radiopharmaceutical is undesirable when the

specific binding of the radiopharmaceutical to its target must be detected. Radiolabelled metabolites can bind to other molecules or take part in unknown biochemical processes and result in nonspecific accumulation of radioactivity. The presence of radiometabolites in plasma that cannot cross the BBB does not disturb the signal to noise ratio (Elsinga, 2002; Stöcklin, 1992).

1.2.2. NEUROIMAGING WITH PET AND SPECT

The ability of SPECT and PET to image specific biomolecules in the living brain provides a unique tool for clinical researchers. Given this, it is not surprising that over the last decade a large number of radiotracers have been developed to image and quantify the various neurotransmitter systems. As mentioned before, development of a suitable radioligand is fraught with problems and there are many compounds reported in the development phase that never reached the end point of *in vivo* use in man.

Some radiopharmaceuticals successful in clinical SPECT studies are [^{99m}Tc]ECD (tracer for cerebral blood flow), [¹²³I]IBZM (dopamine D2 receptor tracer), [¹²³I]ADAM (serotonin transporter tracer) and the dopamine transporter tracer [¹²³I]FP-CIT (for review see Camargo, 2001; Zipursky et al., 2007; Sharma and Ebadi, 2008).

The most important clinically used PET brain tracers are [¹⁸F]DOPA, [¹¹C]raclopride (dopamine D2 receptor tracer), [¹¹C]DASB (serotonin transporter tracer), and the serotonin 5-HT_{1A} receptor tracer [¹¹C]WAY100635 (For Review see Fowler et al., 2003; Shiue and Welch, 2004; Zipursky et al., 2007).

1.3. References

- Beekman FJ, van der Have F, Vastenbouw B, van der Linden A, van Rijk P et al. U-SPECT-I: A novel system for submillimeter-resolution tomography with radiolabeled molecules in mice. *J Nucl Med* 2005; 46:1194-1200.
- Camargo EE. Brain SPECT in neurology and psychiatry. *J Nucl Med* 2001; 42:611-23.

- Elsinga PH. Radiopharmaceutical chemistry for positron emission tomography. *Methods* 2002; 27:208-17.
- Fowler JS, Ding YS and Volkom ND. Radiotracers for positron emission tomography imaging. *Sem in Nucl Med* 2003; 33:14-27.
- Ganguly BN, Mondal NN, Nandy M and Roesch F. Some physical aspects of positron annihilation tomography: A critical review. *Q J Nucl Med Mol Imaging* 2009; 279:685-98.
- Gee AD. Neuropharmacology and drug development. *Br Med Bull* 2003; 65:169-77.
- Guy CN. The second revolution in medical imaging. *Contemporary Physics* 1996; 37:15-45.
- Kuhl DE and Edwards RQ. Image separation radioisotope scanning. *Radiology* 1963; 80:653-62.
- Kung HF. Overview of radiopharmaceuticals for diagnosis of central nervous disorders. *Crit Rev Clin Lab Sci* 1991; 28:269-81.
- Lewellen TK. Recent developments in PET detector technology. *Phys Med Biol* 2008; 53:R287-R317.
- Peremans K, Cornelissen B, Van Den Bossche B, Audenaert K and Van de Wiele C. A review of small animal imaging planar and pinhole SPECT γ camera imaging. *Vet Radiol Ultrasound* 2005; 46:162-70.
- Rowland DJ and Cherry SR. Small-animal preclinical nuclear medicine instrumentation and methodology. *Semin Nucl Med* 2008; 38:209-22.
- Ruth TJ. The use of radiotracers in life sciences. *Rep Prog Phys* 2009; 72:1-23.
- Sharma S and Ebadi M. SPECT neuroimaging in translational research of CNS disorders. *Neurochem Int* 2008; 52:352-62.
- Shiue CY and Welch MJ. Update on PET radiopharmaceuticals: life beyond fluorodeoxyglucose. *Radiol Clin N Am* 2004; 42:1033-53.
- Sossi V and Ruth TJ. Micropet imaging: in vivo biochemistry in small animals. *J Neural Transm* 2005; 112:319-30.
- Stöcklin G. Tracers for metabolic imaging of heart and brain. *Eur J Nucl Med* 1992; 19:527-51.
- Vanhove C, Defrise M, Lahoutte T and Bossuyt A. Three-pin-hole collimator to improve axial spatial resolution and sensitivity in pinhole SPECT. *Eur J Nuc Med Mol Imaging* 2008; 35:407-15.
- Waterhouse RN. Determination of lipophilicity and its use as a predictor of blood-brain barrier penetration of molecular agents. *Mol Imaging Biol* 2003; 5:376-389.
- Wolbarst AB and Hendee WR. Evolving and experimental technologies in medical imaging. *Radiology* 2006; 238:16-39.
- Wong DF and Brasic JR. In vivo imaging of neurotransmitter systems in neuropsychiatry. *Clin Neurosci Res* 2001; 1:35-45.
- Zipursky RB, Meyer JH and Verhoeff P. PET and SPECT imaging in psychiatric disorders. *Can J Psychiatr Nurs* 2007; 52:146-157.

Chapter 2

Blood-brain barrier transport



Chapter 2

Blood-brain barrier transport

2.1. The blood-brain barrier

2.1.1. GENERAL

The brain is a very delicate organ and homeostasis in the neural microenvironment is essential for the perfect functioning of the brain. Therefore, the brain must be protected against metabolic fluctuations in blood composition. However, at the same time contact with blood must be maintained for nutrient supply and waste disposal. This complex task is accomplished by the blood-brain barrier (BBB) (Aigner et al., 1997). The existence of such a barrier between blood and brain was first demonstrated by Ehrlich (1885). At the end of the 1960's, the tight junctions and the fine structural localization of the BBB were discovered (Reese and Karnovsky 1967; Brightman and Reese 1969).

The BBB is not the only barrier that limits drug transport to the brain parenchyma. There are two more barriers described: 1) blood-cerebrospinal-fluid barrier (presented by the choroid plexus epithelium in the ventricles) and 2) the ependyma (epithelial layer of cells covering the brain tissue in the ventricles and limiting the transport of compounds from the cerebrospinal-fluid to the brain tissue). Based on total blood flow and its wide vascular bed, the BBB is functionally the most important global influx barrier. The human BBB has a total blood vessel length of approximately 600 km with an estimated surface of 20 m² (Pardridge 2002; de Boer and Gaillard 2007).

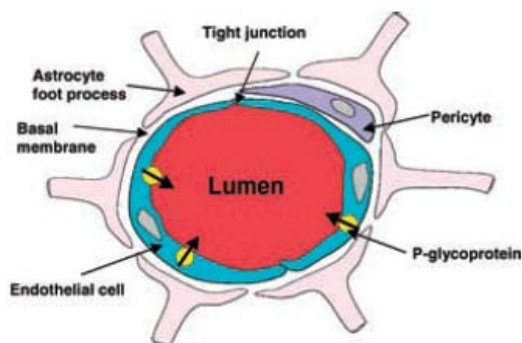


Figure 2.1 Schematic brain capillary (Löscher, 2007)

Brain capillary endothelial cells, pericytes, astrocytes and neuronal cells (Figure 2.1) compose the BBB (Rubin and Staddon 1999; Ballabh et al., 2004; de Boer and Gaillard 2007). Brain capillary endothelial cells are distinguished from peripheral endothelial cells. Their specific characteristics such as tight junctions prevent paracellular transport of compounds from blood to the brain. Furthermore, low vesicular transport, high metabolic activity and lack of fenestrations prevent transcellular transport of xenobiotics to the brain. These specific features are induced and maintained by the astrocytes as well as by the neuronal endings. This barrier is very efficient and makes the brain practically inaccessible for lipid-insoluble compounds and large molecules. As a consequence, the therapeutic value of many promising drugs is diminished and cerebral diseases proved to be most refractory to therapeutic interventions. Given the prevalence of brain diseases, this is a considerable problem (Oldendorf 1977; Brightman 1977; Aigner 1997; Bodor and Buchwald 1999).

2.1.2. INFLUX IN THE BRAIN

Invasive drug delivery and drug delivery based on BBB transport are the two strategies used to bring molecules into the brain. The invasive strategy is rarely applied and will therefore not be discussed in this thesis (For review see Pardridge 1997; 2002; 2007). The non-invasive strategy can be divided into two

main drug transport possibilities across the BBB: passive diffusion and active transport systems.

Passive diffusion of substances through the BBB depends on molecular weight, lipophilicity and intermolecular forces (Levin 1980; Pardridge 1998; Bodor and Buchwald 1999; Habgood et al., 2000). There is a molecular weight threshold of approximately 650 g/mol with respect to drug penetration through the BBB. The more lipid-soluble a drug, the more easily it will move from the polar environment of the blood across the nonpolar BBB. Lipophilicity can be measured by the partition coefficient between octanol and water. The intermolecular forces are determined by the functional groups of the molecule. Measurement of the surface activity, which takes into account the hydrogen binding capabilities and the hydrophobic properties, can predict the ability of substances to passively diffuse through the BBB (Pardridge 1998).

Active transport systems can be divided into absorptive-, carrier- or receptor-mediated transport. Absorptive-mediated transcytosis is initiated by the binding of cationic substances to negative charges on the plasma membrane. This process does not involve specific plasma membrane receptors. Upon binding of the cationic compound to the plasma membrane, endocytosis occurs (de Boer et al., 2003). The carrier-mediated transport is used for blood-to-brain transport of nutrients and vitamins. At least eight different nutrient transport systems have been identified, with each transporting a group of nutrients of the same chemical structure. A tool for enhancing BBB transport of drugs is to modify the drugs structurally to mimic the endogenous nutrients (For review see Pardridge 2002; 2007). Receptor-mediated transport enables larger endogenous molecules, such as peptides, proteins and genes to specifically enter the brain. Conjugation of exogenous molecules such as recombinant proteins and antisense agents to brain transport vectors makes it possible to deliver them to the brain. The brain transport vector is comprised of endogenous peptides or peptidomimetic

monoclonal antibodies that undergo receptor-mediated transport (For Review see Pardridge 1999; 2002; 2007; de Boer and Gaillard 2007).

2.1.3. EFFLUX OUT OF THE BRAIN

To maintain homeostasis of the brain, the BBB combines restricted entering of endogenous and exogenous compounds to the brain with specialized transport mechanisms for efflux of these compounds out of the brain. These multispecific xenobiotic transporters are conventionally grouped into families based on molecular and functional similarities. Several different drug transporter families have been identified, including the organic anion transporter, multidrug resistance-associated protein, multidrug resistance protein, organic anion transporting polypeptide, organic cation transporter, concentrative nucleoside transporter and equilibrative nucleoside transporter subfamilies (Zhang et al., 2004; Huai-Yun et al., 1998; Bauer et al., 2005; Kim, 2005). The first described drug efflux transporter was P-glycoprotein (P-gp), followed by several members of the multidrug resistance-associated protein family and more recently breast cancer related protein (For review see Taylor 2002; de Boer 2003; Bauer et al., 2005; Löscher and Potschka 2005; Dallas et al., 2006). To date, P-gp is the best known and most important drug efflux pump.

2.2. P-glycoprotein

2.2.1. HISTORICAL BACKGROUND

The ATP-binding cassette (ABC) family of transport proteins represents one of the largest families of proteins in living organisms. Its members have been found in each kind of organism examined so far. These transporters mediate drug absorption, distribution and excretion and therefore play a central role in cellular physiology (Ayrton and Morgan 2001). It is difficult to characterize a

physiological system in depth without identifying a role for an ABC transporter. Over the last 15 years, there has been a significant increase in the molecular characterization of transport proteins in animals and man. There are seven known distinct subfamilies of ABC transporters, designated A - G. P-gp, the most important transporter, belongs to the ABCB subfamily (For review see Klein et al., 1999; Dean et al., 2001; Schinkel and Jonker 2003; Sun et al., 2003).

P-gp is the most extensively studied mammalian ABC transporter and is often regarded as the prototype for understanding the biochemical mechanisms. In 1976, Juliano and Ling identified this efflux pump. Because the glycoprotein they found appeared to be unique to mutant cells that displayed altered drug permeability, they named it permeability-glycoprotein (P-glycoprotein or P-gp). The discovery of P-gp was groundbreaking because it explained multidrug resistance, a frequently observed phenomenon in tumours (Juliano and Ling, 1976). In 1989, two independent research groups found expression of P-gp at the human BBB (Cordon-Cardo et al., 1989; Thiebaut et al., 1989). P-gp is highly expressed at the luminal membrane of endothelial cells which is a perfect localization to protect the brain from xenobiotics (Biegel et al., 1995; Beaulieu et al., 1997). Therefore, P-gp is generally recognized to be the most important element of the selective, active BBB for efflux of xenobiotics and has been the main focus of BBB research over the last decade.

2.2.2. EXPRESSION, STRUCTURE AND FUNCTION

In humans, P-gp is encoded by two genes, MDR1 and MDR2. Only the MDR1 gene, located on chromosome 7q21, is responsible for the multidrug resistance. The closely related MDR2 gene, also called MDR3, is involved in intrahepatic cholestasis (Klein et al., 1999). In contrast to humans, mice have three genes encoding P-gp: *mdr1a* (also called *mdr3*), *mdr1b* (also called *mdr1*) and *mdr2*. As in humans, the *mdr2* gene does not contribute to multidrug resistance. The tissue distribution of *mdr1a* and *mdr1b* differ from each other, but together these

proteins cover the same areas as the single MDR1 P-gp in humans. This suggests that mouse *mdr1a* and *mdr1b* together fulfil the same physiological role(s) as MDR1 in human (Croop et al., 1989; Chen et al., 1986; van der Bliek et al., 1988; Hsu et al., 1989; Gros et al., 1986; Devault and Gros 1990).

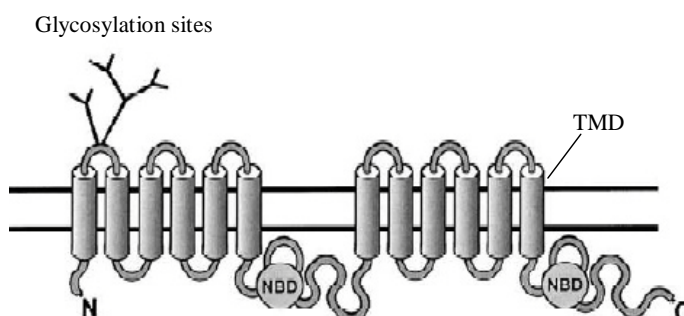


Figure 2.2 Predicted Secondary structure of P-gp (Schinkel et al., 1999)

TMD = transmembrane domain; NBD = nucleotide binding domain

The MDR1 gene product (Figure 2.2) is a 170 kDa transmembrane protein that consists of 1280 amino acids. It is organized as a single polypeptide consisting of two similar halves; a carboxy and an amino halve (Dey et al., 1997). Each part consists of a transmembrane domain containing six helices and an intracellular ATP-binding site also known as nucleotide binding domain (NBD). Intracellular and extracellular loops connect the transmembrane segments with the first extracellular loop being highly N-glycosylated. The NBD contains three conserved domains among the ABC transporters: walker A and B domains and a signature motif (C). The NBD binds and hydrolyzes ATP which provides the energy for active drug export that can occur against a large concentration gradient. Binding of substrates occur at the transmembrane domains (Gottesman et al., 1996; Sauna and Ambudkar, 2001; Higgins and Linton 2004; For review see Endicott and Ling 1989; Gottesman and Pastan, 1993; Bosch and Croop 1998; Gottesman and Ambudkar 2001; Ambudkar et al., 2005).

Table 2.1 mRNA expression of P-gp (adapted from Croop et al., 1989; Schinkel et al., 1999)

Tissue	MDR1 (human)	mdr1a (mouse) 3	mdr1b (mouse) 1
Stomach	+	-	+
Intestines	+++	+++	+
Liver	+++	+	+
Adrenal gland	++++	++++	++++
Ovary	+	+	++
Testis	+	+	-
Kidney	+++	+	++
Uterus	+	(+)	+
Pregnant uterus	++	(+)	++++
Brain	++	+	-
Skeletal muscle	+	+	+
Heart	Data not available	+	+
Lung	+	++	+
Spleen	+	+	+

The relative expression is indicated by +, and very low or undetectable levels with -

Apart from expression in the BBB, drug-transporting P-gp pumps are expressed in a range of other tissues (Table 2.1). The most prominent sites are the endometrium of the pregnant uterus, the apical surface of mucosal cells in the small and large intestines, the biliary canalicular membrane of hepatocytes and the luminal membrane of proximal tubular epithelial cells in the kidney. High levels are also located in the adrenal glands of mice and humans. This tissue distribution suggests that P-gp plays a role in excreting toxic xenobiotics and metabolites into intestinal lumen, bile and urine, respectively (Figure 2.3). In addition, moderate levels were found in a range of other tissues (Thiebaut et al., 1987; Croop et al., 1988; Cordon-Cardo et al., 1989).

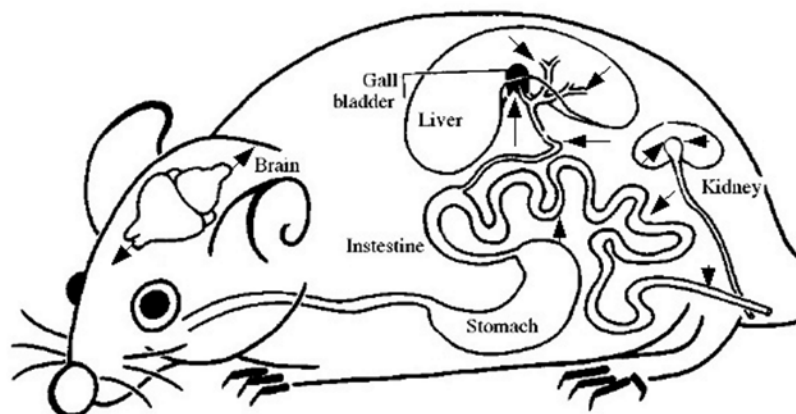


Figure 2.3 Schematic drawing of the organ distribution of P-gp in the mouse
(modified from Schinkel, 1997)

2.2.3. PHYSIOLOGICAL ROLE OF P-GP

Firm evidence for the purpose of P-gp came from studies in which *mdr1* genes were inactivated by insertional mutagenesis (For review see Borst and Ambudkar, 1996; Ambudkar et al., 1999; Schinkel, 1999). The physiological function of P-gp at the BBB is to protect the brain from potentially harmful substances by exporting these substances out of the brain. Intestinal P-gp is an important factor in limiting the entry of substrate drugs from the intestinal lumen to the bloodstream. Therefore it can have a major negative effect on the oral bioavailability of drugs. Intestinal P-gp can further contribute to the direct excretion of drugs from the bloodstream into the intestinal lumen. The bile canalicular P-gp contributes to the hepatobiliary excretion of drugs. Together these effects can result in a markedly slower elimination of drugs from the bloodstream and in a clear shift from primarily fecal to primarily urinary excretion of some drugs. Expression of P-gp in the placenta suggests a role for P-gp in protecting the foetus from toxic xenobiotics. Because of its localization in steroid-secreting glands, P-gp might be involved in secretion of steroids, or in protecting the plasma membranes of steroid-secreting cells from the toxic effects

of high steroid concentration (Schinkel 1997; Ambudkar et al., 1999; Schinkel 1999; Tanigawara 2000). Taking together, the physiological function of P-gp is the protection of the cells and organism against toxic compounds.

Since the finding that resistance to anticancer drugs in human cancers is due to the expression of the P-gp transporter (Chen et al., 1986) it has become clear that P-gp also has a major impact on drug resistance to psychotropic drugs like anti-epileptics (Löscher and Potschka, 2001; Luna-Tortós et al., 2008), anti-HIV drugs (Kim et al., 1998; Huisman et al., 2000), antidepressants and others (Schinkel et al., 1996; Wang et al 2003; Linnet and Ejsing, 2008; Schinkel and Jonker 2003).

The degree of expression and the functionality of the MDR1 gene product can directly affect the distribution, absorption and elimination of P-gp substrates. Consequently, variations in the expression levels and activity of P-gp have a major impact on the therapeutic efficacy of many drugs. This implicates that absorption of drugs is variable among individuals (Kim et al., 2001; Ambudkar et al., 2003; Ebinger et al., 2006; Brinkmann et al., 2001). Currently, more than 100 mutations in the human P-gp gene have been identified (Maeda et al., 2008). Some of these polymorphisms are directly related to human diseases such as epilepsy (Löscher 2007; Kwan and Brodie 2005; Siddiqui et al., 2003), Parkinson disease (Kortekaas et al., 2005), Alzheimer disease (Lam et al., 2001; Vogelgesang et al., 2002) and others (Turgut et al., 2008; Langford et al., 2004; Löscher and Potschka 2005).

2.3. Modulation of P-gp

2.3.1. SUBSTRATES

P-gp recognizes and transports a structurally, chemically and pharmacologically diverse range of compounds with molecular weights between 200 Da and 1900

Da. Drugs that are found to be substrate for P-gp include anthracyclines (daunorubicin), vinca alkaloids (vincristine), calcium channel blockers (verapamil), anti-emetics (domperidone), the immunosuppressivum Cyclosporin A (CsA) and so on (Table 2.2) (Bauer et al., 2005; Linnet and Ejsing, 2007).

Table 2.2 Examples of drugs transported by P-gp

Cardiovascular medication	Cytotoxic agents
Verapamil	Doxorubicin
Diltiazem	Daunorubicin
Digoxin	Paclitaxel
Carvedilol	Opioids
Lovastatin	Morphine-6-glucuronide
Anti-emetics	Phentanyl
Domperidone	Loperamide
Ondansetron	Antibiotics
HIV protease inhibitors	Erythromycin
AZT	Rifampicin
Ritonavir	Others
Saquinavir	Dexamethason (glucocorticoid)
Immunosuppressive drugs	Doxorubicin (antineoplastic)
Cyclosporin A	Midazolam (benzodiazepine)
Tacrolimus	Ivermectin (antihelminthic)

The mechanism by which P-gp recognizes this wide range of substrates is less clear at the moment (Schinkel et al., 1996; Tanigawara, 2000; Bart et al., 2000; Linnet and Ejsing, 2008). Given the potential of P-gp to affect bioavailability and tissue distribution, particularly CNS drug distribution, it would be very useful to understand the structural features that make a compound a substrate or inhibitor of P-gp. However, specific structure-activity models of a P-gp pharmacophore have proven to be difficult to develop. A general pharmacophore with two or three electron donor groups in a fixed spatial separation has been suggested by Seelig et al. (1998). It has also been proposed that a planar aromatic domain and the presence of a basic nitrogen atom are features of substrates but drugs lacking these features could also be transported (Sun et al., 2003). The only common

denominator for all P-gp substrates is their amphipatic nature (Schinkel et al., 2003). Partitioning into the lipid membrane is the rate-limiting step for the interaction of a substrate with P-gp. Dissociation of the P-gp-substrate complex is determined by the number and strength of the hydrogen bonds formed between the substrate and the transporter. If two substrates are applied simultaneously to P-gp, the compound with the highest potential to form hydrogen bonds, generally act as an inhibitor (Seelig et al., 2000).

2.3.2. INHIBITORS

In view of the potential contribution of P-gp to the drug resistance observed during chemotherapy in a number of clinical tumors, there is a widespread interest in the use of so-called P-gp reversal or modulating agents. Co-administration of such blockers with conventional chemotherapy in cancer patients might reverse the P-gp-mediated multidrug resistance of the tumor, and thus enhance the response to therapy. Another therapeutic implication of these reversal agents is the enhancement of brain uptake of some drugs. This is favourable for therapy when the intended pharmacological target is positioned behind the BBB. Keeping in mind the protective role of P-gp at the BBB, P-gp modulators should be used carefully.

Because of the potentially important therapeutic implications of reversal agents, several P-gp blockers with high efficacy and low toxicity have been developed. Reversal agents are as diverse in structure as the previously identified transported drugs. In fact, many compounds initially identified as reversal agents turned out to be themselves transported by P-gp, which suggests that they inhibit transport of other compounds in a competitive manner (Schinkel 1997; Huisman et al., 2000; Varma et al., 2003).

Based on the specificity and affinity, P-gp inhibitors are classified into three generations. First-generation inhibitors are pharmacological actives, which are in clinical use for other indications but have shown to inhibit P-gp. These include

verapamil, CsA, reserpine and tamoxifen. The use of these compounds is limited by their side effects when administered with a dose that is required to inhibit P-gp. Valsopodar, biricodar and GF120918 are examples of second-generation modulators. They are analogues of the first-generation compounds but lack the pharmacological activity of the original molecule and possess usually a higher P-gp affinity. Despite their better pharmacological profile, these agents display lack of absolute selectivity thereby limiting their clinical use. Most of them are often inhibitors of other ABC transporters or cytochrome P₄₅₀3A. Third-generation inhibitors are the most potent, highly selective P-gp modulators, having only little influence on cytochrome P₄₅₀3A drug metabolism and showing only little interaction with chemotherapeutic agents. Members of this class are zosuquidar, tariquidar, laniquidar and ONT-093 (Tan et al., 2000; Varma et al., 2003; Fricker and Miller 2004; Nobili et al., 2006).

2.3.3. IMAGING OF P-GP

Non-invasive imaging of P-gp functionality or expression with PET or SPECT could have several applications. PET or SPECT could be applied to evaluate the efficacy of candidate modulators that have passed initial *in vitro* screening assays. It might also allow selection of the proper modulator and dosing schedule for the individual patient. Information on the dynamic transport of P-gp will avoid unnecessary treatment with modulators in those patients who will not benefit. Another interesting application could be the monitoring of P-gp functionality in psychiatric and neurological disorders which could implicate the efflux pump as a possible cause in these diseases. So far, several radioligands for PET and SPECT have been proposed among which [¹¹C]verapamil, [¹¹C]N-desmethyl-loperamide (Lazarova et al., 2008), [¹¹C]loperamide (Zoghbi et al., 2007), [¹¹C]colchicine (Levchenko et al., 2000), [¹¹C]carvedilol (Elsinga et al., 2005) and [¹⁸F]MPPF (Lacan et al., 2008; Passchier et al., 2000) for PET and [^{99m}Tc]sestamibi and [^{99m}Tc]tetrofosmin (Ballinger et al., 1996) for SPECT (For review see Elsinga et

al., 2004; Elsinga et al., 2005; Vaidyanathan and Zalutsky, 2004) (Figure 2.4). Two of them, [^{11}C]verapamil and [$^{99\text{m}}\text{Tc}$]sestamibi, have been used in clinical trials and will be discussed briefly.

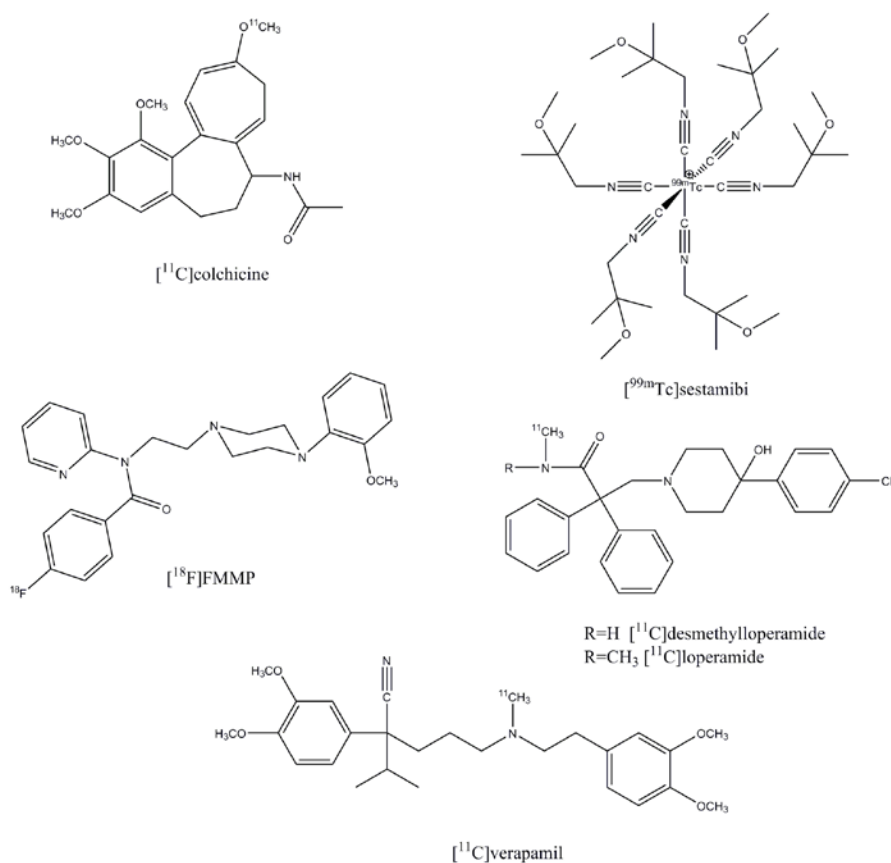


Figure 2.4 Tracers evaluated for imaging P-gp

[$^{99\text{m}}\text{Tc}$]sestamibi is a radiopharmaceutical used clinically to study myocardial perfusion (Mandalapu et al., 1999). It was demonstrated that [$^{99\text{m}}\text{Tc}$]sestamibi, a substrate for P-gp as well as for multidrug resistance protein 1, is especially useful for imaging P-gp expression in tumors rather than brain (Kostakoglu et al., 1996; Barbarics et al., 1998 for review see Hendrikse et al., 1999).

Differences in tissue concentrations of [^{11}C]verapamil was demonstrated between *mdr1a* knock-out mice and wild type mice. The brain uptake of [^{11}C]verapamil is

remarkably higher in *mdr1a* knock-out mice (9.5 fold) as well as after pretreatment with CsA (10.6 fold) indicating that [¹¹C]verapamil is effectively transported by P-gp at the BBB (Hendrikse et al., 1998). Evaluation of [¹¹C]verapamil for *in vivo* imaging of P-gp functionality in non-human primates proved its usefulness as a tool for evaluating P-gp function (Lee et al., 2006). Nevertheless, metabolism of [¹¹C]verapamil makes the determination of a pharmacokinetic model, and so absolute quantification, more complex (Syvanen et al., 2008; Luurtsema et al., 2004).

2.4. References

- Aigner A, Wolf S and Gassen HG. Transport and detoxication: principles, approaches, and perspectives for research on the blood – brain barrier. *Angew Chem Int Ed* 1997; 36:24-41.
- Ambudkar SV, Dey S, Hrycyna CA, Ramachandra M, Pastan I and Gottesman MM. Biochemical, cellular, and pharmacological aspects of the multidrug transporter. *Pharmacol Toxicol* 1999; 36:361-98.
- Ambudkar SV, Kimchi-Sarfaty C, E Sauna Z and Gottesman MM. P-glycoprotein: from genomics to mechanism. *Oncogene* 2003; 22:7468-85.
- Ambudkar SV, Kim I-W and Sauna ZE. The power of the pump: Mechanisms of action of P-glycoprotein. *Eur J Pharm Sciences* 2006; 27:392-400.
- Ayrton A and Morgan P. Role of transport proteins in drug absorption distribution and excretion. *Xenobiotica* 2001; 31:469-97.
- Ballabh P, Braun A and Nedergaard M. The blood-brain barrier: an overview Structure, regulation and clinical implications. *Neurobiol Dis* 2004; 16:1-13.
- Ballinger JR, Bannerman J, Boxen I, Firby P, Hartman NG and Moore MJ. Technetium-99m-Tetrofosmin as a substrate for P-glycoprotein: *in vitro* studies in multidrug-resistant breast tumor cells. *J Nucl Med* 1996; 37:1578-82.
- Barbarics E, Kronauge JF, Cohen D, Davison A, Jones AG and Croop JM. Characterization of P-glycoprotein transport and inhibition *in vivo*. *Cancer Res* 1998; 58:276-83.
- Bart J, Groen HJM, Hendrikse NH, van der Graaf WTA, Vaalburg W and de Vriest EGE. The blood-brain barrier and oncology: new insights into function and modulation. *Canc Treat Rev* 2000; 26:449-62.
- Bauer B, Hartz AMS, Fricker G and Miller DS. Modulation of p-glycoprotein transport function at the blood-brain barrier. *Proc Soc Exp Biol Med* 2005; 1535:118-27.
- Beaulieu E, Demeule M, Ghitescu L and Beliveau R. P-glycoprotein is strongly expressed in the luminal membranes of the endothelium of blood vessels in the brain. *J Biochem* 1997; 326:539-44.
- Biegel D, Spencer DD and Pachter JS. Isolation and culture of human brain microvessel endothelial cells for the study of blood-brain barrier properties *in vitro*. *Brain Res* 1995; 692:183-9.
- Bodor N and Buchwald P. Recent advances in the brain targeting of neuropharmaceuticals by chemical delivery

- systems. *Adv Drug Deliv Rev* 1999; 36:229-54.
- Borst P, Schinkel AH. What have we learnt thus far from mice with disrupted P-glycoprotein genes? *Eur J Cancer* 1996; 32:985-90.
- Bosch I and Croop JM. P-glycoprotein structure and evolutionary homologies. *Cytotechnology* 1998; 27:1-30.
- Brightman MW and Reese TS. Junctions between intimately apposed cell membranes in the vertebrate brain. *J Cell Biol* 1969; 40:648-58.
- Brightman MW. Morphology of blood-brain interfaces. *Exp Eye Res* 1977; S1-25.
- Brinkmann U, Roots I and Eichelbaum M. Pharmacogenetics of the human drug-transporter gene MDR1: impact of polymorphisms on pharmacotherapy. 2001; 6:836-9.
- Chen C, Chin JE, Ueda K, Clark DP, Pastan I, Gottesman MM and Roninson IB. Internal Duplication and homology with bacterial transport proteins in the *mdr1* (P-glycoprotein) gene from multidrug-resistant human cells. *Cell* 1986; 47:381-9.
- Cordon-Cardo C, O'Brien JP, Casals D, Rittman-Grauer L, Biedler JL, Melamed MR and Bertino JR. Multidrug-resistance gene (P-glycoprotein) is expressed by endothelial cells at blood-brain barrier sites. *Proc Natl Acad Sci* 1989; 86:695-8.
- Croop JM, Gros P and Housman DE. Genetics of multidrug resistance. *J Clin Invest* 1988; 81:1303-9.
- Croop JM, Raymond M, Haber D, Devault A, Arceci RJ, Gros P and Housman DE. The three mouse multidrug resistance (*mdr*) genes are expressed in a tissue-specific manner in normal mouse tissues. *Mol Cell Biol* 1989; 9:1346-50.
- Dallas S, Miller DS and Bendayan R. Multidrug resistance-associated proteins: expression and function in the central nervous system. *Pharmacol Rev* 2006; 58:140-161.
- de Boer AG, van der Sandt ICJ and Gaillard PJ. The role of drug transporters at the blood-brain barrier. *Annu Rev Pharmacol Toxicol* 2003; 43:629-56.
- de Boer AG and Gaillard PJ. Drug targeting to the brain. *Ann Rev Pharmacol Toxicol* 2007; 47:323-55.
- Dean M, Hamon Y and Chimini G. The human ATP-binding cassette (ABC) transporter superfamily. *J Lipid Res* 2001; 42:1007-17.
- Devault A and Gros P. Two members of the mouse *mdr* gene family confer multidrug resistance with overlapping but distinct drug specificities. *Mol Cell Biol* 1990; 10:1652-63.
- Dey S, Ramachandra M, Pastan I, Gottesman MM and Ambudkar SV. Evidence for two nonidentical drug-interaction sites in the human P-glycoprotein. *Proc Natl Acad Sci USA* 1997; 94:10594-9.
- Ebinger M and Manfred U. ABC drug transporter at the blood-brain barrier. Effects on drug metabolism and drug response. *Eur Arch Psychiatry Clin Neurosci* 2006; 256:294-8.
- Elsinga PH, Hendrikse NH, Bart J, Vaalburg W and van Waarde A. PET studies on P-glycoprotein function in the blood-brain barrier: How is affects uptake and binding of drugs within the CNS. *Curr Pharm Des* 2004; 10:1493-1509.
- Elsinga PH, Hendrikse NH, Bart J, van Waarde A and Vaalburg W. Positron emission tomography studies on binding of central nervous system drugs and P-glycoprotein function in the rodent brain. *Mol Imaging Biol* 2005; 7:37-44.
- Endicott JA and Ling V. The biochemistry of P-glycoprotein-mediated multidrug resistance. *Annu Rev Biochem* 1989; 58:137-71.
- Fricke G and Miller DS. Modulation of drug transporters at the blood-brain barrier. *Pharmacology* 2004;

- 70:169-76.
- Gottesman MM and Pastan I. Biochemistry of multidrug resistance. *Annu Rev Biochem* 1993; 62:385-427.
- Gottesman MM, Pastan I and Ambudkar SV. P-glycoprotein and multidrug resistance. *Curr Opin Genet Dev* 1996; 6:610-7.
- Gottesman MM and Ambudkar SV. Overview: ABC transporters and human disease. *J Bioenerg Biomembr* 2001; 33:453-8.
- Gros P, Croop J and Housman D. Mammalian multidrug resistance gene: complete cDNA sequence indicates strong homology to bacterial transport proteins. *Cell* 1986; 47:371-80.
- Habgood MD, Begley DJ and Abbott NJ. Determinants of passive drugs entry into the central nervous system. *Cell Mol Neurobiol* 2000; 20:231-53.
- Hendrikse NH, Schinkel AH, de Vries EGE, Fluks E, van der Graaf WTA, Willemsen ATM et al. Complete in vivo reversal of P-glycoprotein pump function in the blood-brain barrier visualized with positron emission tomography. *Brit J Pharmacol* 1998; 124:1413-8.
- Hendrikse NH, Franssen EJF, van der Graaf WTA, Vaalburg W and de Vries EGE. Visualization of multidrug resistance in vivo. *Eur J Nucl Med* 1999; 25:283-93.
- Higgins CF and Linton KJ. The ATP switch model for ABC transporters *Nat Struct Mol Biol* 2004; 11:918-926.
- Hsu SIH, Lothstein L and Horwitz SB. Differential overexpression of three *mdr* gene family members in multidrug-resistant J774.2 mouse cells. *J Biol Chem* 1989; 264:12053-62.
- Huai-Yun H, Secrest TD, Mark SK, Carney D, Brandquist C, Elmquist WF and Miller WD. Expression of multidrug resistance-associated protein (MRP) in brain microvessel endothelial cells. *Biochem Biophys Res Commun* 1998; 243:816-20.
- Huisman MT, Smit JW and Schinkel AH. Significance of P-glycoprotein for the pharmacology and clinical use of HIV protease inhibitors. *Aids* 2000; 14:237-42.
- Juliano RL and Ling V. A surface glycoprotein modulating drug permeability in chinese hamster ovary cell mutants. *Biochimica et Biophysica Acta* 1976; 455:152-62.
- Kim RB, Fromn MF, Wandel C, Leake B, Wood AJJ, Roden DM and Wilkinson GR. The drug transporter P-glycoprotein limits oral absorption and brain entry of HIV-1 protease inhibitors. *J Clin Invest* 1998; 101:289-94.
- Kim RB, Leaks BF, Choo EF, Dresser GK, Kubba SV, Schwarz UI et al. Identification of functionally variant MDR1 alleles among European Americans and African Americans. *Clin Pharmacol Therap* 2001; 70:189-99.
- Kim RB. Transporters and drug discovery: why, when and how. *Mol Pharm* 2005; 3:26-32.
- Klein I, Sarkadi B and Váradi A. An inventory of the human ABC proteins. *Biochimica et Biophysica* 1999; 1461:237-62.
- Kortekaas R, Leenders KL, Van Oostrom JCH, Vaalburg W, Bart J, Willemsen ATM and Hendrikse NH. Blood-brain barrier dysfunction in parkinsonian midbrain in vivo. *Trans Am Neurol Assoc* 2005; 57:176-9.
- Kostakoglu I, Elahi N, Kıratlı P, Ruacan S, Sayek I, Baltalı E et al. Clinical validation of the influence of P-glycoprotein on technetium-99m-sestamibi uptake in malignant tumors. *J Nucl Med* 1997; 38:1003-8.
- Kwan P and Brodie MJ. Potential role of drug transporters in the pathogenesis of medically intractable epilepsy. *Epilepsia* 2005; 46:224-35.
- Lacan G, Plenevaux A, Rubins DJ, Way BM, Defraiteur C, Lemaire C et al. Cyclosporine, a P-glycoprotein modulator, increases [¹⁸F]MPPF uptake in rat brain and peripheral tissues: microPET and ex vivo studies.

- Eur J Nucl Med Mol Imaging 2008; 35:2256-66.
- Lam FC, Liu R, Lu P, Shapiro AB, Renoir JM, Sharom FJ and Reiner PB. β -amyloid efflux mediated by P-glycoprotein. J Neurochem 2001; 76:1121-8.
- Langford D. Altered P-glycoprotein expression. J Neuropathol Exp Neurol 2004; 63:1038-47.
- Lazarova N, Zoghbi SS, Hong J, Seneca N, Tuan E, Gladding RL et al. Synthesis and evaluation of [N-methyl- ^{11}C]N-Desmethyl-loperamide as a new and improved PET radiotracer for imaging P-gp function. J Med Chem 2008; 51:6034-43.
- Lee Y-J, Maeda J, Kusahara H, Okauchi T, Inaji M, Nagai Y, Obayashi S et al. In vivo evaluation of P-glycoprotein function at the blood-brain barrier in nonhuman primates using [^{11}C]verapamil. J Pharmacol Exp Ther 2006; 316:647-53.
- Levchenko A, Mehta BM, Lee JB, Humm JL, Augensen F, Squire O et al. Evaluation of ^{11}C -colchicine for PET imaging of multiple drug resistance. J Nucl Med 2000; 41:493-501.
- Levin AV. Relationship of octanol/water partition coefficient and molecular weight to rat brain capillary permeability. J Med Chem 1980; 23:682-4.
- Linnet K, Ejsing TB. A review on the impact of P-glycoprotein on the penetration of drugs into the brain. Focus on psychotropic drugs. Eur Neuropsychopharmacol 2008; 18:157-69.
- Löscher W and Potschka H. Role of drug efflux transporters in the brain for drug disposition and treatment of brain diseases. Prog Neurobiol 2005; 76:22-76.
- Löscher W. and Potschka H. Role of multidrug transporters in pharmacoresistance to antiepileptic drugs. J Pharmacol Exp Ther 2002; 301:7-14.
- Löscher W. Drug transporters in the epileptic brain. Epilepsia 2007; 48:8-13.
- Luna-Tortós C, Fedrowitz M and Löscher W. Several major antiepileptic drugs are substrates for human P-glycoprotein. Neuropharmacol 2005; 55:1364-75.
- Luurtsma G, Molthoff CFM, Windhorst JW, Smit H, Keizer R, Boellaard AA et al. (R)- and (S)-[^{11}C]Verapamil as PET-tracers for measuring P-glycoprotein function: in vitro and in vivo evaluation. Nucl Med Biol 2003; 30:747-51.
- Maeda K and Sugiyama Y. Impact of genetic polymorphisms of transporters on the pharmacokinetic, pharmacodynamic and toxicological properties of anionic drugs. Drug Metab Pharmacokinet 2008; 23:223-35.
- Mandalapu BP, Amato M and Stratmann HG. Technetium Tc 99m Sestamibi myocardial perfusion imaging. Chest 1999; 115:1684-94.
- Nobili S, Landini I, Gigliani B and Mini E. Pharmacological strategies for overcoming multidrug resistance. Curr Drug Targets 2006; 7:861-79.
- Oldendorf WH. The blood-brain barrier. Exp Eye Res 1977; S177-190.
- Pardridge WM. Drug delivery to the brain. J Cerebr Flow Metabol 1977; 17:713-31.
- Pardridge WM. CNS drug design based on principles of blood-brain barrier transport. J Neurochem 1998; 70:1781-92.
- Pardridge WM. Non-invasive drug delivery to the human brain using endogenous blood-brain barrier transport systems. PSTT 1999; 2:49-59.
- Pardridge WM. Drug and gene delivery to the brain: the vascular route. Neuron 2002; 36:555-8.
- Pardridge WM. Blood-brain barrier genomics and the use of endogenous transporters to cause drug penetration

- into the brain. *Curr Opin Drug Discov Devel* 2003; 6:683-91.
- Pardridge WM. Blood-brain barrier delivery. *Drug Discov Today* 2007; 12:54-61.
- Passchier J, van Waarde A, Doze P, Elsinga PH and Vaalburg W. Influence of P-glycoprotein on brain uptake of [¹⁸F]MPPF in rats. *Eur J Pharmacol* 2000; 407:273-80.
- Reese TS and Karnovsky MJ. Fine structural localization of a blood-brain barrier to exogenous peroxidase. *J Cell Biol* 1967; 34:207-17.
- Rubin LL and Staddon JM. The cell biology of the blood-brain barrier. *Annu Rev Neurosci* 1999; 22:11-28.
- Sauna ZE and Ambudkar SV. Characterization of the catalytic cycle of ATP hydrolysis by human P-glycoprotein. *J Biol Chem* 2001; 276:11653-61.
- Schinkel AH, Wagenaar E, Mol CAAM and Van Deemter Liesbeth. P-glycoprotein in the blood-brain barrier of mice influences the brain penetration and pharmacological activity of many drugs. *J Clin Invest* 1996; 97:2517-24.
- Schinkel AH. The physiological function of drug-transporting P-glycoproteins. *Semin Cancer Biol* 1997; 8:161-70.
- Schinkel AH. P-Glycoprotein, a gatekeeper in the blood-brain barrier. *Adv Drug Deliv Rev* 1999; 36:179-94.
- Schinkel AH and Jonker JW. Mammalian drug efflux transporters of the ATP binding cassette (ABC) family: an overview. *Adv Drug Disc Rev* 2003; 55:3-29.
- Seelig A. A general pattern for substrate recognition by P-glycoprotein. *Eur J Biochem* 1998; 251:252-61.
- Siddiqui A, Kerb R, Weale ME, Brinckmann U, Smith A, Goldstein DB et al. Association of multidrug resistance in epilepsy with a polymorphism in the drug-transporter gene ABCB1. *N Engl J Med* 2003; 348:1442-8.
- Sugawara I, Hamada H, Tsuruo T and Mori S. Specialized Localization of P-glycoprotein recognized by MRK 16 monoclonal antibody in endothelial cells of the brain and the spinal cord. *J Cancer Res* 1990; 81:727-30.
- Sun H, Dai H, Shaik N and Elmquist WF. Drug efflux transporters in the CNS. *Advanced Drug Discovery Reviews* 2003; 55:83-105.
- Syvänen S, Hooker A, Rahman O, Wilking H, Blomquist G, Långström B et al. Pharmacokinetics of P-glycoprotein inhibition in the rat blood-brain barrier. *J Pharm Sci* 2008;97:5386-400.
- Tan B, Piwcina-Worms D and Ratner L. Multidrugresistance transporters and modulation. *Curr Op Oncol* 2000; 12:450-8.
- Tanigawara Y. Role of P-glycoprotein in drug disposition. *Ther Drug Monit* 2000; 22:137-40.
- Taylor EM. The impact of efflux transporters in the brain on the development of drugs for CNS disorders. *Clin Pharmacokinet* 2002; 41:81-92.
- Thiebaut F, Tsuruo T, Hamada H, Gottesman MM, Pastan I and Willingham MC. Cellular localization of the multidrug-resistance gene product P-glycoprotein in normal human tissues. *Proc Natl Acad Sci USA* 1987; 84:7735-8.
- Thiebaut F, Tsuruo T, Hamada H, Gottesman MM, Pastan I and Willingham MC. Immunohistochemical localization in normal tissues of different epitopes in the multidrug transport protein p170: evidence for localization in brain capillaries and crossreactivity of one antibody with a muscle protein. *J Histochem Cytochem* 1989; 37:159-64.
- Turgut G, Bastemir M, Turgut S, Akm F, Kursunluoglu R, Kaptanoglu B. P-glycoprotein polymorphism in hypo- and hyper-thyroidism patients. *Mol Biol Rep* 2008; 35:693-8.

- Vaidyanathan G and Zalutsky MR. Imaging Drug Resistance with radiolabeled molecules. *Curr Pharm Des* 2004; 10:2965-79.
- van der Blik AM, Kooiman PM, Schneider C and Borst P. Sequence of *mdr3* cDNA encoding a human P-glycoprotein. *Gene* 1988; 71:401-11.
- Varma MVS, Ashokraj Y, Dey CS and Panchagnula. P-glycoprotein inhibitors and their screening: a perspective from bioavailability enhancement. *Pharmacol Res* 2003; 48:347-59.
- Vogelgesang S, Cascorbi I, Schroeder E, Pahnke J, Walker LC and Warzok RW. Deposition of Alzheimer's β -amyloid is inversely correlated with P-glycoprotein expression in the brains of elderly nondemented humans. *Pharmacogenetics* 2002; 12:535-41.
- Wang RB, Kuo CL, Lien LL and Lien EJ. Structure-activity relationships: analyses of p-glycoprotein substrates and inhibitors. *Journal of clinical Pharmacy and therapeutics* 2003; 28:203-28.
- Zhang Y, Schuetz DJ, Elmquist FW and Miller DW. Plasma membrane localization of multidrug resistance-associated protein homologs in brain capillary endothelial cells. *J Pharmacol Exp Ther* 2004; 311:449-55.
- Zoghbi SS, Liow J-SL, Yasuno F, Hong J, Tuan E, Lazarova N et al. ^{11}C -Loperamide and its *N*-desmethyl radiometabolite are avid substrates for brain permeability-glycoprotein efflux. *J Nucl Med* 2008; 49:649-56.

Chapter 3

Catecholamine system in the brain



Chapter 3

Catecholamine system in the brain

3.1. Catecholamine pathways in the brain

3.1.1. GENERAL INTRODUCTION

Catecholamines (dopamine, norepinephrine and epinephrine) are neurotransmitters named after their chemical structure. They contain a benzene ring with two hydroxyl groups (catechol) and a side chain of ethylamine or one of its derivatives. All catecholamines are synthesized starting from tyrosine, an amino acid synthesized out of phenylalanine or derived from food proteins.

Tyrosine accumulates in neurons by an active transport mechanism. There, it is converted to dihydroxyphenyl-alanine (DOPA) by the enzyme tyrosine hydroxylase. L-DOPA is then decarboxylated to dopamine which is stored in vesicles in the nerve terminals (Weiner, 1970) where it can be further oxidized to norepinephrine using dopamine- β -hydroxylase (Figure 3.1) (Goodall and Kirshner, 1958).

Both neurotransmitters are released in the synaps through a calcium-dependent process initiated by nerve impulse activity (Figure 3.1). The released neurotransmitters can now interact with dopamine and adrenoceptors, respectively. Termination of the signal occurs by reuptake in the presynaptic neuron using the dopamine and norepinephrine transporter or by enzymatic degradation of the neurotransmitter using the enzymes monoamine oxidase (MAO) and catecholamine-O-methyltransferase (COMT). Reuptake is the main mechanism responsible for inactivation (Kanner and Schuldiner, 1987; Schmitz et al., 2003). The recycled neurotransmitter can be restored in vesicles by vesicular

monoamine transporters or further metabolized by MAO or COMT. Extravesicular dopamine is metabolized to dihydroxyphenylacetic acid whereas extracellular dopamine is degraded to homovanillic acid. 3-Methoxy-4-hydroxyphenethylglycol is the major metabolite formed by degradation of norepinephrine (Maas and Landis, 1968; Peyrin and Dalmaz, 1975; Eisenhofer and Fineberg, 1993; Kopin, 1994).

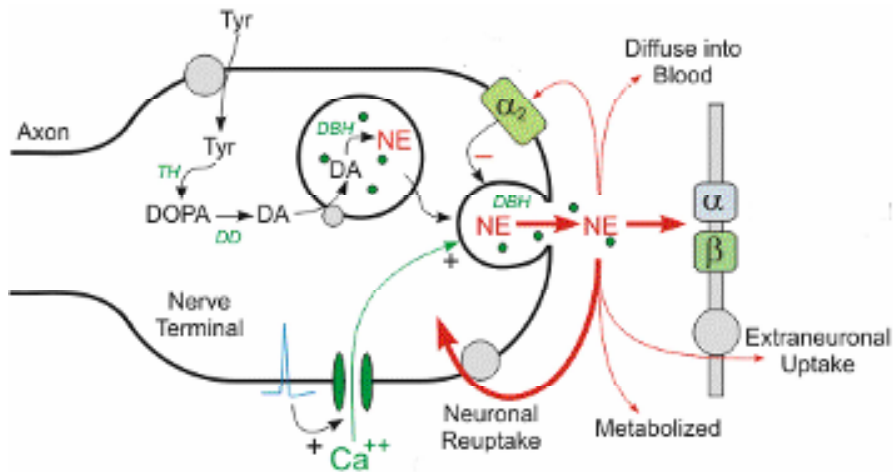


Figure 3.1 Schematic representation of noradrenergic synaptic signalling
(Klabunde, 2008)

DA = Dopamine; DD = DOPA decarboxylase; DOPA = dihydroxyphenyl-alanine;
DBH = dopamine- β -hydroxylase; NE = Norepinephrine; TH = tyrosine hydroxylase;
Tyr = tyrosine

The transporters responsible for inactivation of dopamine and norepinephrine as well as the enzyme MAO, will be further discussed.

3.1.2. NORADRENERGIC SYSTEM IN THE BRAIN

The major noradrenergic nucleus in the brain is the locus coeruleus. The locus coeruleus is the main source of the noradrenergic innervation in the hippocampus, thalamus, cerebellum as well as most cortical areas (Figure 3.2).

The lateral tegmental system, another group of noradrenergic cells, has its cells of origin located in discrete regions of the pons and medulla. These norepinephrine-containing cells innervates the hypothalamus and parts of the amygdale, but has also descending projections to the spinal cord (Nicholas et al., 1996; Aston-Jones, 2002).

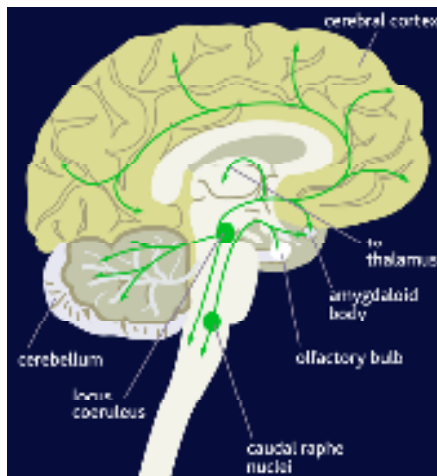


Figure 3.2 Noradrenergic pathways in the human brain (CNSforum.com)

Norepinephrine is involved in mood regulation, sleep regulation, memory, expression of behaviour and the general degree of alertness and arousal (Aston-Jones, 2002; Murchison et al., 2004). The actions of norepinephrine are carried out via the binding to the adrenergic receptors, a class of G-protein coupled receptors. There are two main groups of adrenergic receptors, α and β , which are further divided into α_{1A} , α_{1B} , α_{1D} , α_{2A} , α_{2B} , α_{2C} and β_1 , β_2 , β_3 . All receptors are G-protein coupled receptors and are localized post- or presynaptic (Nicholas et al., 1996; Docherty, 1998).

3.1.3. DOPAMINERGIC SYSTEM IN THE BRAIN

The dopaminergic neurons are classified into four main pathways (Figure 3.3) (For review see Reid, 1977; Moore and Bloom, 1978; Marsden, 2006). The

nigrostriatal pathway projects from the substantia nigra to the dorsal striatum. This pathway contains about 80 % of all dopaminergic innervations and is involved in the regulation of movements (Cousins and Salamone, 1996). The dopaminergic neurons involved in the mesolimbic and mesocortical pathways both originate in the ventral tegmental area. The mesolimbic pathway projects towards limbic areas such as nucleus accumbens and amygdala whereas the mesocortical pathway most densely projects to the prefrontal cortex. The mesolimbic system plays a role in emotional expression and motivation (Cabib et al., 1996). Memory, organization, attention and social behaviour are affected by the mesocortical pathway (Floresco and Magyar, 2006). Finally, the tuberoinfundibular pathway exists of a group of small neurons, signalling from the hypothalamus towards the pituitary gland. In this last pathway, dopamine inhibits prolactin release (Andrews and Grattan, 2004).

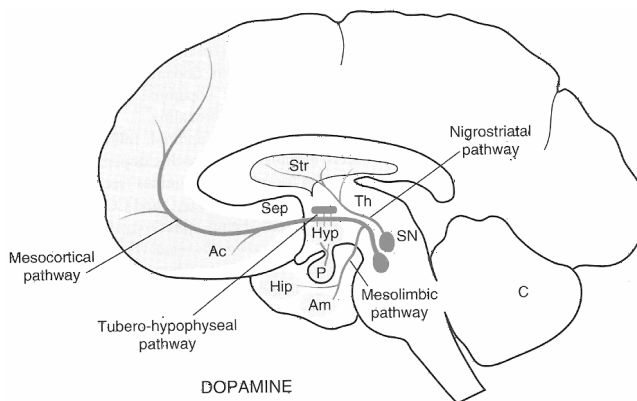


Figure 3.3 Dopaminergic pathways in the human brain (Rang et al., 1999)

Ac = nucleus accumbens; Am = amygdaloid nucleus; C = cerebellum; Hip = hippocampus; Hyp = hypothalamus; P = pituitary gland; Sep = septum; Str = corpus striatum; Th = thalamus; N = substantia nigra

The actions of dopamine are mediated by binding to specific membrane receptors, which belongs to the family of seven transmembrane domain G-protein coupled receptors. Two types of dopamine receptors, termed D₁ and D₂

were originally distinguished based on their biochemical and pharmacological properties. The D₁-like family includes the D₁ and D₅ receptors while the D₂-like receptors are further divided into D₂, D₃ and D₄. The most common receptors, D₁ and D₂, are involved in regulation of behaviour and are localized in striatum (D₁ and D₂), cortical regions (D₁ and D₂), amygdale (D₂), hippocampus (D₂) and thalamus (D₂). Presynaptically localized D₂ receptors are involved in the regulation of the biosynthesis and the release of dopamine (Jackson and Westlind-Danielsson, 1994, Marsden, 2006).

3.2. Catecholamine transporters

3.2.1. GENERAL INTRODUCTION

Synaptic signalling is primarily terminated by active transport of the neurotransmitter in neuronal cells by neurotransmitter transporters. Once inside the neuronal cell, neurotransmitters can be further transported into synaptic vesicles by vesicular carriers. These processes are responsible for the homeostasis of neurotransmitter pools within nerve endings. Both at the plasma and vesicular membranes, neurotransmitter influxes are directly coupled to transmembrane ion gradients which provide the energy for the retrotransport (Kanner and Schuldiner, 1987).

Neurotransmitter transporters can be classified in superfamilies, families, and subfamilies according to their primary structure and site of action. In particular, the latter criterion allows the distinction of two superfamilies: the plasma membrane transporters and the vesicular membrane transporters. The superfamily of plasma membrane transporters can be further divided into two families depending on their ionic dependence: the Na⁺/Cl⁻-dependent transporters and the Na⁺/K⁺-dependent transporters. Based on their substrate preferences, the Na⁺/Cl⁻-dependent transporters are classified into subfamilies among which the amino acid transporters and monoamine transporters (Masson

et al., 1999; Zahniser and Doolen, 2001). This thesis focuses on the dopamine transporter (DAT) and norepinephrine transporter (NET), both members of the monoamine transporter subfamily. The serotonin transporter (SERT) is the third transporter belonging to the monoamine transporters.

3.2.2. HISTORICAL BACKGROUND

The presence of an active transport system for the cellular uptake of norepinephrine at sympathetic nerve endings was suggested by studies on the tissue uptake and retention of [³H]-labelled norepinephrine administered to animals (Whitby et al., 1961; Hertting et al., 1961). Regional differences within the brain for the uptake of dopamine and norepinephrine indicated the existence of a separate mechanism for the neuronal reuptake of dopamine. Striatal synaptosomes showed a much higher affinity for uptake of dopamine than norepinephrine, whereas in other brain regions, the difference was less pronounced. There were no stereoselective preferences for uptake of D- and L-isomers of norepinephrine in the striatum, whereas in other regions, the L-isomer was the preferred substrate. This observation suggested that norepinephrine uptake in the striatum is mediated by DAT whereas in other regions, NET was abundant (Snyder and Coyle, 1969; Coyle and Snyder, 1969).

3.2.3. STRUCTURE, FUNCTION AND MECHANISM

Up to date, no X-ray crystallographic or high-resolution structural information is available for the topological assignments of the transporters. The identification of the cDNAs for the catecholamine transporters has contributed greatly to our understanding of the molecular structure and function of these important proteins (Amara and Kuhar, 1993).

The polytopic membrane proteins, DAT and NET show high homology (66 %) and share several structural features (Figure 3.4). They are both composed of 12

transmembrane domains (TMD), several similarly configured intracellular and extracellular loops with phosphorylation and glycosylation sites, and intracellular located amino- and carboxy-terminal residue. One large extracellular loop is positioned between TMD 3 and TMD 4 and contains a variable number of N-glycosylation sites (Giros and Caron., 1993). The presence of several intracellular sites for phosphorylation, suggests that second messengers may regulate transporter function and/or subcellular redistribution. Phosphorylation can occur by several enzymes with protein kinase A and C and calcium-modulin kinase II as the most important ones. TMD 1, 2 and 4 - 8 show the highest degree of sequence identity between DAT and NET. The conservation of sequence in these membrane-spanning domains argues for their functional importance in transport activity. The carboxy-terminal region, spanning from TMD 9 through the carboxy-terminal tail, seems to be responsible for the observed stereoselectivity and high affinity for their respective substrates (Giros et al., 1994; Buck and Amara, 1994 and 1995; Brüß et al., 1995; Hersch et al., 1997; Zahniser and Doolen, 2001).

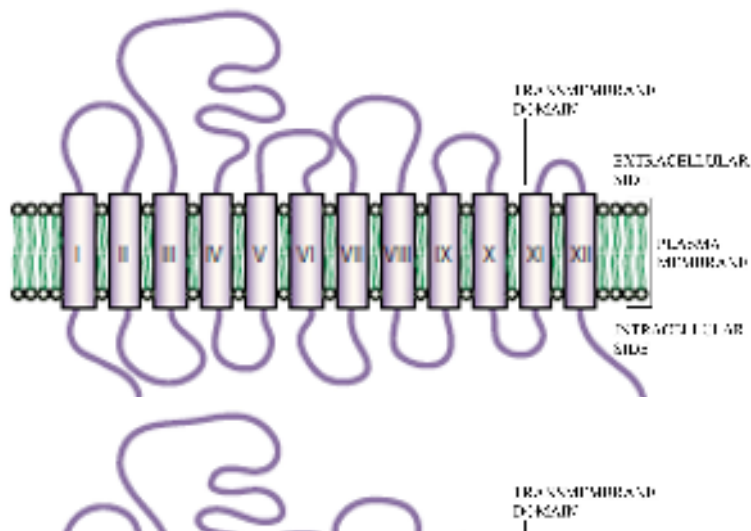


Figure 3.4 Topology of catecholamine transporters (Torres et al., 2003)

The observation that extracellular Na⁺ ions were a necessary requirement for substrate uptake provided one of the first insights into the transport mechanism. It is now well established that the mechanism by which transporter proteins mediate catecholamine uptake involves sequential binding and co-transport of Na⁺ and Cl⁻ ions. The driven force for transporter-mediated catecholamine uptake is the ion concentration gradient that is created and maintained by the plasma membrane Na⁺/K⁺ ATPase. In the case of DAT, two Na⁺ ions and one Cl⁻ ion are transported with the substrate, whereas NET co-transport its substrate with one Na⁺ ion and one Cl⁻ ion (Kanner and Schuldiner, 1987; Torres et al., 2003). A detailed description of the mechanism and regulation of transport is beyond the scope of this thesis but has extensively been discussed and reviewed by others (Rudnick and Clark, 1993; Sonders and Amara, 1996; Kavanaugh, 1998; Beckman and Quick, 1998; Torres, 2003; Meliaken, 2004; Blakely et al., 2005).

3.2.4. NOREPINEPHRINE TRANSPORTER

3.2.4.1. *Structure and localization*

Pacholzyk et al. (1991) identified the cDNA encoding for the human NET using an expression cloning strategy in COS cells. The NET cDNA was isolated from the SK-N-SH human neuroblastoma cell line on the basis of its ability to direct the transport of ¹²⁵I-labelled meta-iodobenzylguanidine, a norepinephrine analogue. The sequence of the NET cDNA predicts a protein of 617 amino acids weighing approximately 69 kDa. The human NET gene (SLC6A2) is located on chromosome 16q12.2, spans about 45 kb and consists of 14 exons (Gelernter et al., 1993; Porzgen et al., 1995). NET has 3 glycosylation sites on the second extracellular loop and also a few phosphorylation sites (Figure 3.5). A high affinity of NET for both dopamine and norepinephrine has been demonstrated whereas the affinity for epinephrine and the effectiveness of its transport is much lower (Moron et al., 2002; Bönisch and Bruss, 1994). As mentioned before, the

highest NET density is found in the locus coeruleus whereas striatum has negligible amounts of NET. Peripherally, NET is mainly localized in heart, lungs and smooth muscles (Raisman et al., 1982; Ressler and Nemeroff, 1999; Smith et al., 2006).

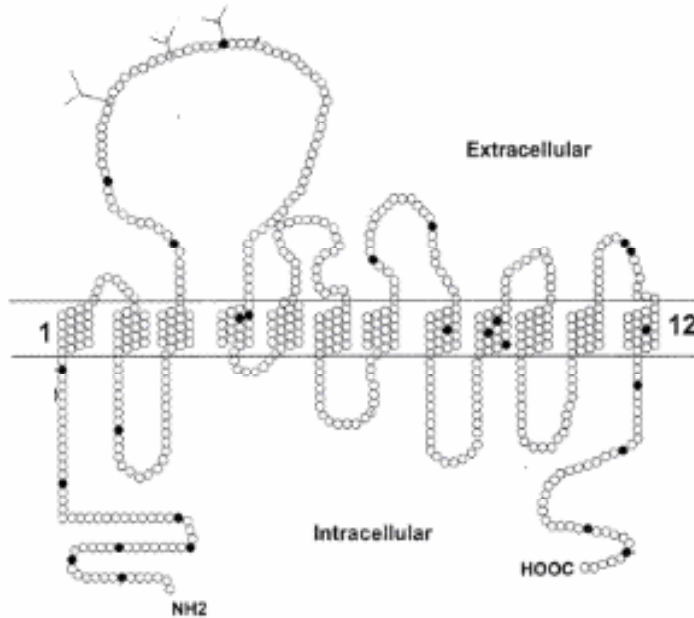


Figure 3.5 Topology of the rat norepinephrine transporter (Brüss et al., 1997)

Solid dots represent the 26 amino acid residues that are divergent in rat NET but are conserved in the human and bovine NETs.

3.2.4.2. *NET and human diseases*

Depression and anxiety disorders are common recurring disorders with a prevalence of 7 - 11 % (Ressler et al., 2007). The estimated annual cost of depression in the US alone was approximately 44 billion dollar in 1990 (Greenberg et al., 1993). More than 40 years of research through experimental models and in the clinical setting, have clearly indicated the importance of norepinephrine neurotransmission in the pathophysiology and subsequent treatment of affective and mood disorders such as major depression (For review

see Ressler and Nemeroff, 1999; Brunello et al., 2002). Given the importance of NET to noradrenergic transmission it is conceivable that regulation of the level of expression of NET gene in noradrenergic neurons may be a natural mechanism by which noradrenergic neurotransmission can be adjusted *in vivo* in response to physiological demands placed on this system. Evidence for such a mechanism was first provided by Lee et al. (1983), who demonstrated that NET is upregulated and downregulated in response to enhanced availability or depletion of norepinephrine, respectively. Thus, levels of NET appear to be regulated in order to maintain 'normal' concentrations of norepinephrine in the noradrenergic synapses (Lee et al., 1983). Klimek et al. (1997) demonstrated a reduced NET density in the locus coeruleus measured by a lower [³H]nisoxetine binding to NET in brain tissues collected post-mortem from subjects diagnosed with major depression (Klimek et al., 1997). Variations in the genes encoding for NET could be involved in predisposing individuals to psychiatric disorders. Linkage analysis for depression and other psychiatric disorders and the genetic variations of the NET gene displayed contradictory findings (For review see Hahn and Blakely, 2007). A few studies demonstrate positive association between the NET gene and psychiatric disorders (Urwin et al., 2002; Inoue et al., 2004; Ryu et al., 2004; Sun et al., 2008) while others show no association at all (Hadley et al., 1995; Owen et al., 1999; Sand et al., 2002; Zill et al., 2002).

The basis for the treatment of depression is to moderate the levels of neurotransmitters. Several classes of drugs have been identified and used as antidepressants (for Review see Leonard, 1999). Reboxetine (Figure 3.6) is the first potent, selective and specific norepinephrine reuptake inhibitor. Two chiral centres are present in reboxetine. However, due to the regio- and stereo-specificity of the key reactions used for its synthesis, only two diastereomers are present in reboxetine; it is a racemic mixture of *RR*- and *SS*-2-[α -(2-ethoxyphenoxy)benzyl]morpholine methanesulphonate (Melloni et al., 1984). Extensive research indicated that reboxetine is a clinically active, efficacious and well-tolerated antidepressant. Since 1997, reboxetine is on the market with

different trade names including Edronax[®], Norebox[®] and Vestra[®] and so on (Dostert et al., 1997; Holm and Spencer, 199; Wong et al., 2000).

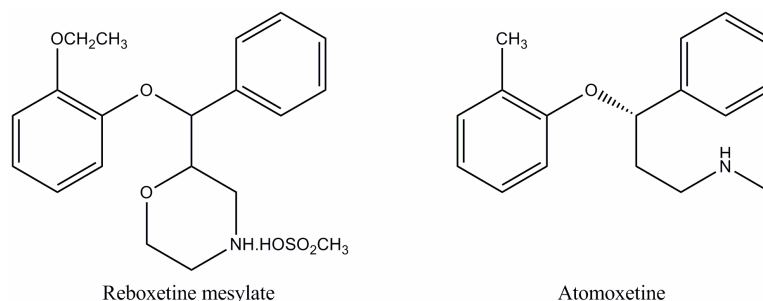


Figure 3.6 Chemical structures of Reboxetine mesylate and Atomoxetine

Atomoxetine (Figure 3.6), also known as (-)-*N*-methyl- γ -(2-methylphenoxy) benzenepropanamine, is another selective and potent inhibitor of norepinephrine reuptake (Wong et al., 1982). It is currently on the market as Strattera[®] for the treatment of attention deficit hyperactivity disorder (ADHD). ADHD is the most common neurobehavioural disorder of childhood and affects about 5 - 10 % of school-aged children. ADHD is characterized by inattention, hyperactivity and impulsivity. Until a few years ago, only stimulants have been approved for the treatment for ADHD. Although these agents have shown efficacy, they also have some limitations including a 10 - 30 % failure rate, intolerance, abuse liability and adverse effects such as insomnia and anxiety. Atomoxetine is the first non stimulant indicated for the management of ADHD. Over the last 7 years its pharmacokinetics, pharmacodynamics and clinical efficacy has well been established (Bymaster et al., 2002; Mattiuz et al., 2003; Corman et al., 2004; Sauer et al., 2005).

3.2.4.3. *Imaging of NET*

Because of the low density of NET in brain, radioligands should be highly selective and specific. Imaging of the NET has lagged behind due to the lack of

selective NET radioligands that give a high signal to noise ratio. Some potent NET reuptake inhibitors that have been labelled for *in vitro* or *in vivo* mapping of brain NET are discussed briefly.

Desipramine, a well-known tricyclic antidepressant, is a highly potent and selective inhibitor of NET. Tritium-labelled desipramine has been used for *in vitro* autoradiographic studies of NET in the human brain post mortem (Gross-Isseroff et al., 1988; Bäckström and Marcusson, 1990). Van Dort et al. (1997) reported the radiosynthesis of desipramine and its 2-hydroxy metabolite with ^{11}C but the *in vivo* evaluation was not included. [^{11}C]desipramine has been evaluated *in vivo* by Schou et al. (2005). An almost complete homogenous brain uptake was displayed, indicating that [^{11}C]desipramine has a high non-specific binding and is subsequently not suitable for imaging NET (Schou et al., 2005).

Although nisoxetine is very selective for NET *in vitro*, [^{11}C]nisoxetine exhibits very high levels of nonspecific binding *in vivo*, making it practically unsuitable for PET (Haka et al., 1989; Ding et al., 2005). An iodinated analogue of nisoxetine with promising *in vitro* properties has been developed (Chumpradit et al., 1992; Kiyono et al., 2003; Kung et al., 2004). Unfortunately, (R)-[^{125}I]2-iodonisoxetine also failed the *in vivo* tests; it displayed high nonspecific binding resulting in a high background uptake (Kiyono et al., 2004; Kung et al., 2004).

Evaluation of [^{11}C]talopram, [^{11}C]talsupram, [^{11}C]oxaprotiline and [^{11}C]lortalamine demonstrated lack of selective NET binding *in vivo*, even though their *in vitro* potentials were promising (McConathy et al., 2004; Ding et al., 2005; Schou et al., 2005).

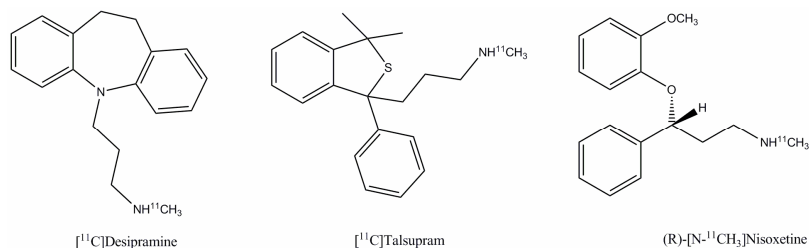


Figure 3.7 Structure of NET radioligands

Recently, ^{11}C and ^{18}F labelled analogues of reboxetine (Figure 3.8) have been synthesized and evaluated as PET radioligands in rodents, monkeys and humans. *In vivo* evaluation of (*S,S*)- ^{11}C -methylreboxetine (MeNER) displayed a regional distribution consistent with the known distribution of NET. Blocking studies in mice demonstrated the selectivity towards NET. Further evaluation of (*S,S*)- ^{11}C MeNER in nonhuman primates and human brain showed that no equilibrium was used during the PET measurement. This together with a somewhat noisy final signal at later time points lead to the preparation and evaluation of radiofluorinated analogues to extend the PET scanning time (Schou et al., 2003; Wilson et al., 2003; Ding et al., 2003; Severance et al., 2007). Its ^{18}F fluoromethyl analogue, (*S,S*)- ^{18}F FMeNER, displayed not only significant uptake in the NET-rich regions but also showed a high bone uptake due to *in vivo* defluorination. With the intention of reducing the *in vivo* defluorination, the di-deuterated analogue, (*S,S*)- ^{18}F FMeNER- D_2 was developed. PET studies indicated that the extent of defluorination was significantly reduced while the selectivity and affinity towards NET was retained (Schou et al., 2004; Seneca et al., 2005; Lin et al., 2005). These data encourage further PET studies using (*S,S*)- ^{18}F FMeNER- D_2 in humans (Schou et al., 2005; Arakawa et al., 2008, Takano et al., 2008).

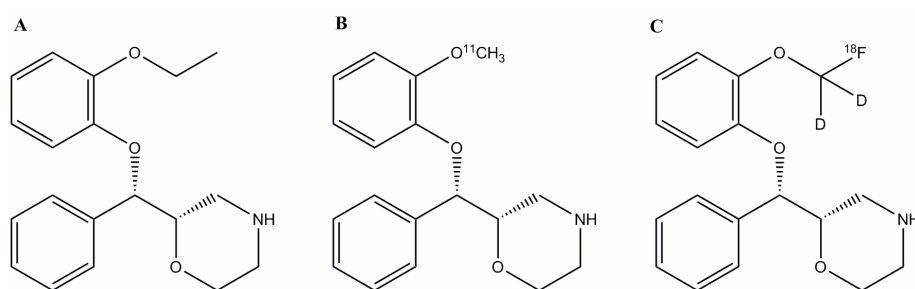


Figure 3.8 Structures of (*S,S*)-reboxetine (A), (*S,S*)- ^{11}C MeNER (B) and (*S,S*)- ^{18}F FMeNER- D_2 (C)

3.2.5. DOPAMINE TRANSPORTER

3.2.5.1. *Structure and localization*

Human DAT cDNA's were first isolated using highly homologous rat DNA or human NET cDNA sequences. The human DAT gene (SLC6A3) was mapped to chromosome 5p15.3. The organization of the entire gene has been reported. It spans about 65 kb of the human genome and consists of 15 exons separated by 14 introns (Giros et al., 1992; Kawari et al., 1997; Bannon et al., 2001). Transcription and translation of SLC6A3 results in an 80 kDa large transmembrane protein consisting of 620 amino acids (Figure 3.9).

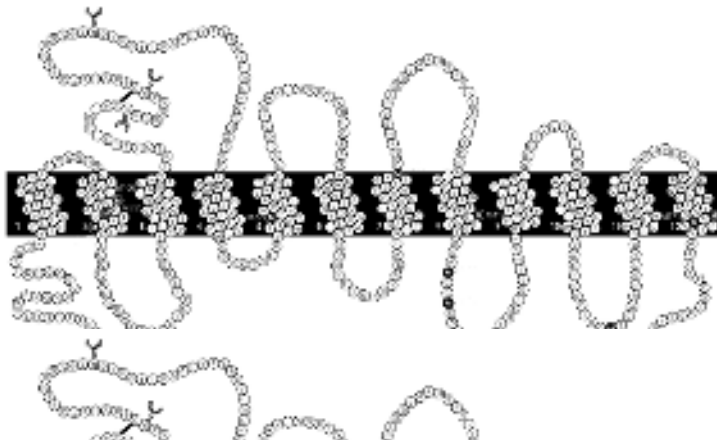


Figure 3.9 Sequence and Topology of the human dopamine transporter (Giros and Caron, 1993)

Cysteines 180 and 189 in the second extracellular loop are disulfide bonded. Asparagine residues 181, 188, and 205 in the second extracellular loop are linked with glycosyl groups. Methionine residues are indicated as black circles with white letters.

DAT is predominantly present in the brain although it is also found in the periphery. In the brain, DAT co-localizes with markers for tyrosine hydroxylase and dopamine D₂ receptors. Striatum has the highest DAT density whereas cerebellum is almost negligible of DAT (Chen and Reith, 2000; Uhl, 2003; Piccini,

2003). Peripheral organs expressing DAT are the lungs, the gastro-intestinal system (Mitsuma et al., 1998; Mezey et al., 1999) and the pancreas (Mezey et al., 1996). DAT mediates uptake of dopamine and is an inefficient transporter of norepinephrine (Giros et al., 1992).

3.2.5.2. *Psychostimulants and DAT*

Addiction to psychoactive drugs continues to be one of the most significant medical, social, and economic problems facing society. Drug addiction has been considered as a brain disorder characterized by compulsive drug-seeking behaviour and uncontrollable use of the drug. The major dysfunction and dysregulation associated with addictive disorders involves the brain's natural reward system. It has been shown that drugs interact with regions of the brain where dopaminergic terminals are abundant, specifically the mesolimbic pathway (Koob and Bloom, 1988; Wise, 1996; Koob, 2000; Pierce and Kumaresan, 2006). Cocaine and amphetamine, including methamphetamine and methylenedioxymethamphetamine (ecstasy) are powerful central nervous system stimulants which are widely abused (for review see Howell and Kimmel, 2008). Currently, no effective pharmacotherapy for psychostimulant abuse has demonstrated efficacy for long-term use. Both drugs increase the extracellular levels of monoamines. Although cocaine and amphetamines affect all three monoamine concentrations, the rewarding, reinforcing and stimulating effects are believed to depend primarily on its interaction with DAT (Ritz et al., 1987; Giros et al., 1996; Amara and Sonders, 1998; Carboni et al., 2001; Elliott and Beveridge, 2005).

Cocaine, a naturally occurring molecule that can be isolated from *Erythroxylon coca*, exerts its action by blocking dopamine reuptake, thereby increasing the concentration of dopamine in the synapse, which then causes overstimulation of dopamine receptors (Figure 3.10) (Witkin et al., 1991; Kuhar and Boja, 1991; Volkow et al., 1997; Geracitano et al., 2006).

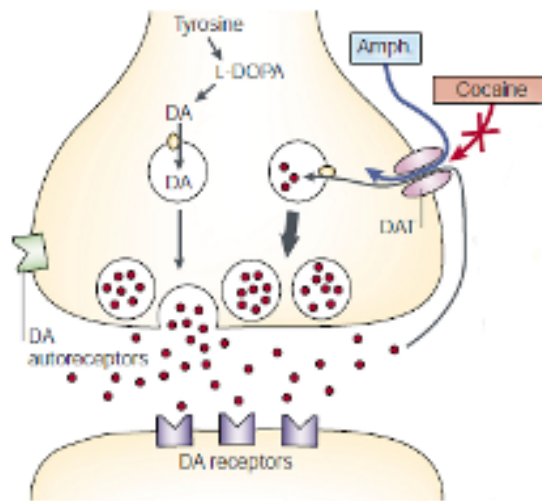


Figure 3.10 Influence of drugs on the function of DAT (Torres et al., 2003)

Amph = amphetamine; DA = dopamine; DAT = dopamine transporter; L-DOPA = L-dihydroxyphenyl-alanine

Amphetamine is a substrate-type releaser (Figure 3.10) (For review see Fleckenstein et al., 2007). It binds to the transporter protein and is subsequently transported into the cytoplasm of the nerve terminals. Extracellular transmitter concentrations are elevated by a two-pronged mechanism: (1) the amphetamines promote efflux of transmitter by a process of transporter-mediated exchange and (2) they increase cytoplasmic levels of transmitter by disrupting storage of transmitters in vesicles. This latter action increases the pool of neurotransmitters available for release by transporter-mediated exchange (Kahlig and Galli, 2003; Rothman and Baumann, 2003; Geracitano et al., 2006). It is important to emphasize that a number of synthetic stimulants, including amphetamines are useful medication in the treatment of ADHD, narcolepsy and obesity. The same drug can thus be a therapeutic entity or an abused substance depending upon the context in which the drug is administered. Methamphetamine for example is widely abused for its ability to increase wakefulness and physical activity and decrease appetite (Rothman and Baumann, 2003).

3.2.5.3. *Role of DAT in human disorders*

Parkinson's disease (PD), ADHD and schizophrenia each have abnormal dopamine function in addition to many other disabling features (Bannon, 2005). As mentioned before, ADHD is mainly treated with psychostimulants. These psychostimulants, for example methylphenidate (Rilatine®) exhibit their function by inhibiting the reuptake of dopamine. Several genetic findings indicated that specific alleles of the DAT gene seemed to be associated with ADHD (Cook et al., 1995; Gill et al., 1997). The results of different studies on the up- or downregulation of DAT in ADHD are inconsistent. Higher DAT density in the striatum have been reported (Krause et al., 2000; Cheon et al., 2003) as well as DAT decrements (Volkow et al., 2007; Hesse et al., 2009) and unchanged DAT density (van Dyck et al., 2002).

Idiopathic PD is a progressive neurodegenerative disorder which manifests itself by bradykinesia in combination with rigidity, tremor and postural instability (Gelb et al., 1999). PD affects approximately 0.2 % of the population and the prevalence increases with age. To date, PD remains an incurable disease. The available treatments are able to offer only symptomatic relief for patients. The drugs used to treat PD either boost the levels of dopamine in the brain or mimic the effects of dopamine. L-DOPA is the key compound in the treatment of PD, acting as a precursor of dopamine (for review see Schapira, 2007; Singh et al., 2007). The disease is neuropathologically characterized by the presence of Lewy bodies and by degeneration of dopamine-containing neurons in the ventral mesencephalon with loss of their nerve terminals in the basal ganglia structures, especially in the striatum (Stoof et al., 1999; Singh et al., 2007).

PD diagnosis is based on clinical symptoms and the presence of Lewy bodies (Gelb et al., 1999). The clinical symptoms however are manifested when already 50 – 80 % of the nigrostriatal neurons are lost. Clinical diagnosis fails to identify individuals before such a significant loss of dopamine neurons is reached. Lewy bodies also occur in patients suffering from other diseases like Alzheimer disease

and ataxia telangiectasia. Taken together, clinical diagnostic criteria are not always sufficient to make a confident, early diagnosis of PD. PD is also characterized by loss of dopamine neurons. Since DAT is exclusively localized on dopamine synthesizing neurons, it is a good marker for the integrity of these neurons. Over the last decade, radiotracers suitable for DAT imaging have been proposed as possible diagnostic tools and for monitoring the treatment of patients with PD (Figure 3.11). The high sensitivity and specificity of SPECT and PET (semi)quantitative images makes DAT imaging, at present, the best biomarker for evaluating dopamine neuron loss, which is responsible for most of the motor symptoms in PD patients (Stoof et al., 1999; Poewe and Scherfler, 2003; Shih et al., 2006).

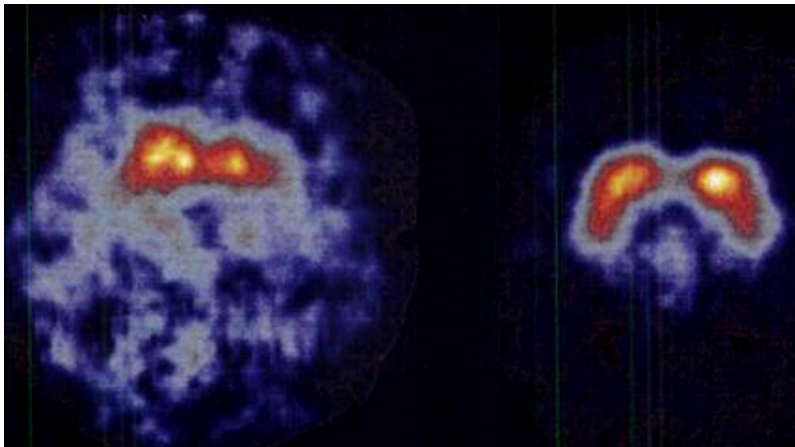


Figure 3.11 SPECT axial images in healthy control (right) and Parkinson's disease patient (left) (Seibyl et al., 1998)

Subjects were injected with 333 MBq (9 mCi) [^{123}I]FP-CIT. Tracer uptake showed a marked reduction in Parkinson's disease patient with greater abnormality in putamen.

3.2.5.4. *Imaging of DAT*

Several radioligands of different chemical classes have been developed for the visualization of DAT (for review see Guilloteau and Chalon, 2005; Volkow et al., 1996; Elsinga et al., 2006). A limitation of many of these radioligands is their lack

of selectivity towards DAT. They mostly have also high affinity for one of the other monoamine transporters.

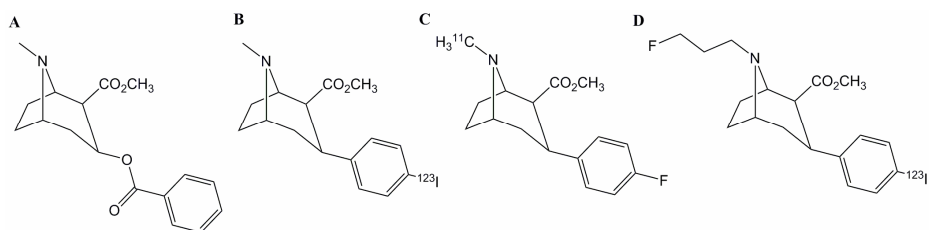


Figure 3.12 Structure of cocaine (A), [¹²³I]β-CIT (B), [¹¹C]β-CFT (C) and [¹²³I]FP-CIT (D)

The first DAT radioligand developed for PET was [¹¹C]nomifensine. Although it has favourable kinetics, [¹¹C]nomifensine is unsuitable as a tracer for DAT due to its high affinity binding at the NET (Aquilonius et al., 1987). The radiolabelling of cocaine with [¹¹C] initiated development of many promising labelled cocaine derivatives (Figure 3.12). [¹¹C]cocaine itself is not suitable due to high binding to SERT and NET in addition to low specific-to-nonspecific binding ratio and its very fast kinetics (Fowler et al., 1989; Volkow et al., 1996). The cocaine analogue [¹²³I]β-CIT also known as [¹²³I]RTI-55 has high affinity for DAT and a high specific-to-nonspecific binding. The major drawbacks of [¹²³I]β-CIT are its low selectivity towards DAT and rather slow kinetics. Striatal activity increases for 15 to 20 hours after bolus injection of the tracer. Consequently, SPECT measurements with [¹²³I]β-CIT in the human brain usually requires a delay of 24 hours between injection and imaging (Boja et al., 1992; Brucke et al., 1993; Laruelle et al., 1994). Consequently, PET measurements with [¹¹C]RTI-55 must be conducted far from equilibrium (Farde et al., 1994). [¹¹C]β-CFT better known as [¹¹C]WIN 35,428, also does not achieve a maximum value of striatal binding within the time constraints of PET experiments (Wong et al., 1993). Because of the high affinity of [¹¹C]β-CFT, Laakso et al. (1998) recommended an ¹⁸F labelled analogue, [¹⁸F]β-CFT, enabling prolonged PET-scanning since striatal binding

peaked at 225 min p.i. (Laakso et al., 1998). However, from a practical point of view, such a long scanning protocol is not desirable for clinical studies. Therefore, numerous compounds have been investigated to improve selectivity and obtain accurate kinetics. Among those, [^{11}C]PE2I (Halldin et al., 2003; Shetty et al., 2007), [^{18}F]FECNT (Goodman et al., 2000; Deterding et al., 2001; Davis et al., 2003) and [^{123}I]FP-CIT (Booij et al., 1997 and 1998) showed favourable brain kinetics although their selectivity towards DAT is still not optimal. [^{123}I]FP-CIT is since 2000 commercially available in Europe by the name DatSCANTM and is used for diagnosis of PD (Vlaar et al., 2008; Booij and Kemp, 2008).

Furthermore, useful [$^{99\text{m}}\text{Tc}$] labelled tropane analogues have been described such as [$^{99\text{m}}\text{Tc}$]TRODAT-1 (Kung et al., 1996; Hwang et al., 2002) and [$^{99\text{m}}\text{Tc}$]TropaBAT (Cleyhens et al., 2005; Kieffer et al., 2006).

Although most radioligands for DAT imaging are tropane derivatives ligands, GBR 13119 has also proven to be a good lead compound. Several derivatives have been prepared and displayed good *in vitro* properties (Kimura et al., 2003; Boos et al., 2006; Rothman et al., 2008). Radiolabelling of these derivatives could result in new improved radiotracers for DAT.

3.3. Monoamine oxidase

3.3.1. GENERAL INTRODUCTION

The enzyme monoamine oxidase (MAO) was discovered 80 years ago in beef liver as tyramine oxidase (Hare, 1928). Almost 10 years later, it was established that epinephrine, norepinephrine and dopamine were also substrates for this enzyme and it was renamed monoamine oxidase. MAO (EC 1.4.3.4.) is a flavin-containing (Kearney et al., 1971) mitochondrial membrane-bound protein (Schnaitman et al., 1967) which catalyzes the oxidative degradation of biogenic and xenobiotic amines to their corresponding aldehydes by the production of hydrogen peroxide and ammonia (Dostert et al., 1989; Tipton et al., 2004). MAO

(For review see Weyler et al., 1990) exists as two isoforms in many tissues of humans and other mammals, termed MAO-A and MAO-B. The two isoforms are distinguished by their substrate preference and by selective inhibitors, as well as by their physical properties (Housley et al., 1976; Schoepp and Azzaro, 1981). In general, it has been suggested that in the CNS intraneural MAO protect neurons from exogenous amines, terminate the actions of amine neurotransmitters, and regulate the contents of intracellular amine stores (Youdim et al., 2006).

3.3.2. EXPRESSION AND STRUCTURE

MAO-A and MAO-B (Figure 3.13) are different gene products with molecular weights of about 59.7 and 58.8 kDa respectively and a 70 % degree of homology in their amino acid sequence is present. Both genes are located on the X chromosome (Xp11.23), each comprising 15 exons with identical intron - exon organization (Lan et al., 1989; Bach et al., 1988; Shih, 1991).

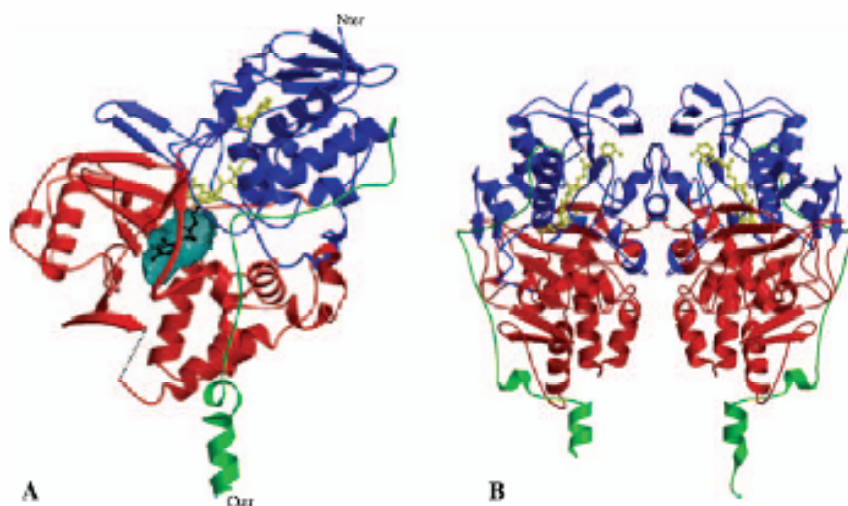


Figure 3.13 Crystal structures of human MAO-A (A) and human MAO-B (B)
(Edmondson et al., 2007)

The flavin binding domain is labelled in blue, red denotes the substrate binding domain and green denotes the membrane binding domain

The X-ray crystal structure of human MAO-B was first reported by Binda et al. (2002). The subsequent successes in the crystallization and structural elucidation of human MAO-A has provided insights into the structure and mechanism of both enzymes, allowing a detailed comparison of the active sites of both enzymes (De Colibus et al., 2005). Both proteins are predominantly located in the outer membrane of mitochondria, to which they are anchored by the C-terminal domain (Rebrin et al., 2001).

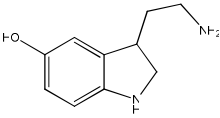
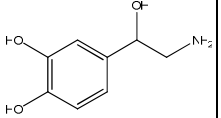
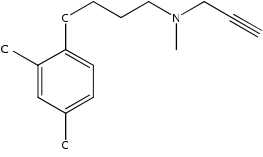
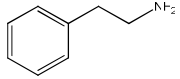
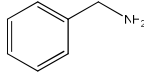
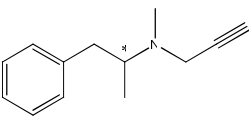
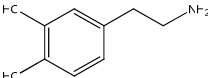
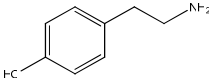
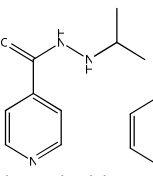
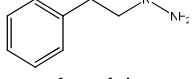
MAO is present in most mammalian tissues but the two isoforms occur with different ratios in different organs of different species (Shih et al., 1999; Inoue et al., 1999). In humans, MAO-B predominates in the brain, heart, kidneys and spleen, while MAO-A is most abundant in the lungs and duodenum. The highest levels of MAO activity were observed in liver and the spleen displayed the lowest MAO activity among the tissues investigated (Rodríguez et al., 2001; Saura et al., 1992; Saura et al., 1996a). There are regional differences in MAO activity in the brain. In the human brain, the basal ganglia and hypothalamus show the highest levels of activity, whereas low levels of activity are observed in the cerebellum and neocortex (Youdim et al., 2006). MAO-A is predominantly found in the locus coeruleus and the highest concentration of MAO-B is found in the raphe nuclei. (Jahng et al., 1997; Saura et al., 1996b; Willoughby et al., 1988). While the human brain profoundly express MAO-B, rat brain has higher concentrations of MAO-A.

3.3.3. SUBSTRATES AND INHIBITORS

The two isoforms are distinguished by their substrate preference and by different selective inhibitors. As shown in Table 3.1, MAO-A catalyses the oxidation of serotonin, epinephrine and norepinephrine preferentially, whereas MAO-B is active towards benzylamine and 2-phenethylamine. Dopamine, tryptamine and tyramine are oxidized by both isoforms in most species. Irrespective of tissue-

and species-based differences in substrate specificity, the two isoenzymes are best distinguished based on pharmacological criteria: MAO-A is selectively inhibited by low doses clorgyline, whereas MAO-B is blocked by low doses of L-deprenyl. Clorgyline as well as L-deprenyl form a covalent bond with the enzyme, indicating they are both irreversible inhibitors (Doster et al., 1989; Youdim et al., 2006). L-deprenyl with the combination of L-DOPA has been widely used in the treatment of PD (Birkmayer, 1983).

Table 3.1 Structures of MAO substrates/inhibitors

	Substrates		Inhibitors
MAO-A			
	serotonin	norepinephrine	Clorgyline
MAO-B			
	phenylethylamine	benzylamine	L-deprenyl
MAO-A and MAO-B			
	dopamine	tyramine	iproniazid
			
			phenelzine

Since the two isoforms of MAO share 70 % sequence identity, they show similar susceptibility to some inhibitors such as iproniazid, phenelzine and tranylcypromine (Riederer et al., 2004). Iproniazid, a drug used to treat tuberculosis (Ornstein, 1958), was found to produce mood elevation in patients and was subsequently discovered to be a MAO inhibitor useful in the treatment of depression. An undesirable and sometimes lethal side effect of MAO non-selective inhibitors was the so-called “cheese reaction”. This refers to the

hypertensive crisis in individuals who were taking non selective irreversible MAO inhibitors together with food that contain large quantities tyramine. Tyramine is normally broken down by MAO in the digestive organs. However when MAO is inhibited, tyramine levels are elevated causing dangerous surges in blood pressure (Crane, 1956; Anderson et al., 1993).

3.3.4. PHYSIOLOGICAL ROLE IN HEALTH AND DISEASE

MAO regulates concentrations of important neurotransmitters in the brain, as well as protects the body by oxidizing xenobiotics and dietary amines in peripheral tissues which could act as false neurotransmitters. MAO is involved in a wide range of neurological diseases, psychiatric disorders and behavioural traits (Shih and Thompson, 1999; Kebir et al., 2009, Bortolato et al., 2008; Meyer et al., 2006).

MAO-A knock-out mice have elevated brain levels of serotonin, causing a distinct behavioural syndrome, including enhanced aggression. This observation in MAO-A knock-out mice is in accordance with the abnormal aggression reported in males from a Dutch family with a complete MAO-A deficiency due to a point deletion in the gene encoding MAO-A (Brunner et al., 1993). Recent studies showed that the low MAO-A genotype was associated with antisocial behaviour and high self-reported trait aggression with children exposure to maltreatment. Alia-Klein et al. (2008) reported that a 15 % reduction in brain MAO-A activity is associated with elevated trait aggression.

PD is related with an elevated MAO-B activity in the substantia nigra, causing an increased oxidation of dopamine and subsequently higher levels of toxic H_2O_2 . This leads to the degradation of dopamine-synthesizing neurons (Shih et al., 1999).

MAO-B converts 1-methyl-4-phenyl-1,2,3,6-tetrahydropyridine (MPTP) to the toxic metabolite 1-methyl-4-phenylpyridinium (MPP⁺) which selectively destroys nigrostriatal neurons. The neurodegeneration induced by MPTP is similar to the neuronal damage in PD and is prevented by the MAO-B inhibitor L-deprenyl. Thus, MAO-B is also involved in the pathogenesis of MPTP-induced Parkinsonism (Shih et al., 1999).

Several lines of evidence suggest a link between cigarette smoke and MAO inhibition. Cigarette smokers have reduced levels of MAO-A and B (Fowler et al., 1996; Berlin et al., 1995). Likewise, the activities of MAO-A and MAO-B are decreased in animals exposed to cigarette smoke. The mechanism underlying this reduced MAO activity has not yet been elucidated. Although nicotine is the main pharmacologically active compound in tobacco, it is not the cause of the reduced MAO activity. Characterization of the compounds in tobacco smoke that inhibit MAO activity is still in progress (Lewis et al., 2007).

MAO may also be involved in alcoholism because lower levels of MAO-B activity are present in alcoholics. Furthermore, MAO-A mutations may underlie the susceptibility of individuals to alcoholism (shih et al., 1999).

3.3.5. IMAGING OF MAO

Given the pharmacological role of MAO and their importance in psychiatric and neurological diseases as well as in addiction, PET and SPECT are valuable tools for the non-invasive *in vivo* study of these enzymes. Studies in humans are of special value because species variability in MAO subtype distribution limits the relevance of animal measurements. Only a few compounds have been proposed as MAO-radiotracers. The first developed radiotracers for MAO were the selective irreversible MAO inhibitors clorgyline and L-deprenyl labelled with ¹¹C. Since both radiotracers are covalently bound to MAO-A or MAO-B, they visualize MAO by the suicide inactivator approach (MacGregor et al., 1985;

Fowler et al., 1987; Arnett et al., 1987; Lammertsma et al., 1991). The drawback of [^{11}C]clorgyline is that it displays an unexplained species difference. In contrast to results in humans clorgyline was not retained in baboon brain (Fowler et al., 2001). A number of different classes of selective, reversible inhibitors of MAO-A and MAO-B have been proposed as MAO-radiotracers. Derivatives of the harmine alkaloids have been labelled with ^{11}C and evaluated in the monkey brain for the assessment for MAO-A. [^{11}C]harmine (Figure 3.14), [^{11}C]methylharmine, [^{11}C]harmaline and [^{11}C]brofarmin were compared and only [^{11}C]harmine and [^{11}C]methylharmine had kinetic patterns in monkey brain that are compatible with a binding to MAO-A. [^{11}C]harmine however is extremely metabolized in plasma making absolute quantification difficult (Bergstrom et al., 1997a and 1997b). [^{11}C]befloxatone (Figure 3.14) shows good characteristics for imaging brain MAO-A but it is synthesized via a cyclization reaction with [^{11}C]phosgene which is toxic and rather rare available (Dolle et al., 2003; Bottlaender et al., 2003).

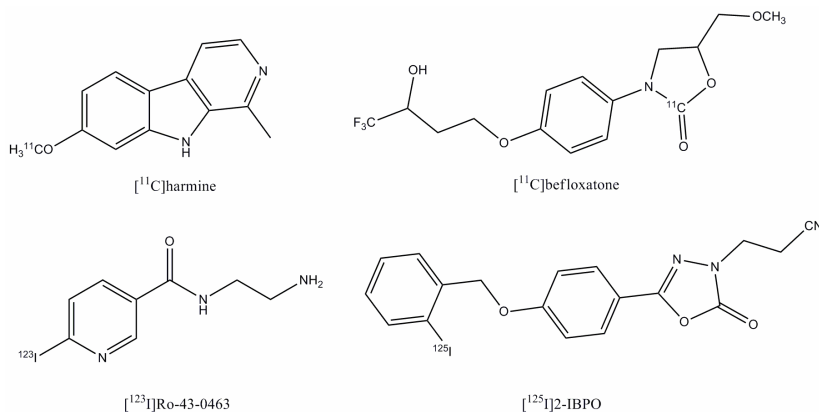


Figure 3.14 Structure of radiotracers for MAO-A and MAO-B

Examples of MAO-B tracers are [^{11}C]SL25.1188 (Bramoullé et al., 2007), [^{125}I]2-IBPO (Figure 3.14) (Hirata et al., 2002) and [^{123}I]Ro-43-0463 (Figure 3.14) (Beer et al., 1995). For review on MAO imaging see Fowler et al. (2002; 2005).

3.4. References

- Alia-Klein N, Goldstein RZ, Kriplani A, Logan J, Tomasi D, Williams B, et al. Brain monoamine oxidase A activity predicts trait aggression. *J Neurosci* 2008; 28:S099-S104.
- Amara SG and Kuhar MJ. Neurotransmitter transporters: Recent progress. *Annu Rev Neurosci* 1993;16:73-93.
- Amara SG and Sonders MS. Neurotransmitter transporters as molecular targets for addictive drugs. *Drug Alcohol Depend* 1998; 51:87-96.
- Anderson MC, Hasan F, McCrodden JM and Tipton KF. Monoamine oxidase inhibitors and the cheese effect. *Neurochem Res* 1993; 18:1145-9.
- Andrews ZB and Grattan DR. The roles of dopamine and the neurointermediate lobe of the pituitary in the regulation of prolactin secretion during late pregnancy in rats. *J Neuroendocrinology* 2004; 16:859-65.
- Aquilonius SM, Bergstrom K, Eckernas SA, Hartvig P, Leenders KL, Lundquist H et al. In vivo evaluation of striatal dopamine reuptake sites using ¹¹C-nomifensine and positron emission tomography. *Acta Neurol Scand* 1987; 76:283-7.
- Arakawa R, Okumura M, Ito H, Seki C, Takahashi H, Takano H et al. Quantitative analysis of norepinephrine transporter in the human brain using pet with (S,S)-¹⁸F-FMeNER-D₂. *J Nuc Med* 2008; 49:1270-6.
- Arnett CD, Fowler JS, MacGregor RR, Schlyer DJ, Wolf AP, Langstrom B and Halldin C. Turnover of brain monoamine oxidase measured in vivo by positron emission tomography using L-[¹¹C]deprenyl. *J Neurochem* 1987; 49:522-7.
- Aston-Jones G. Neuropsychopharmacology: The fifth generation of progress 2002 Chapter 4.
- Bach AW, Lan NC, Johnson DL, Abell CW, Bembenek ME et al. cDAN cloning of human liver monoamine oxidase A and B: molecular basis of differences in enzymatic properties. *Proc Natl acad Sci USA* 1988; 85:4934-8.
- Bäckström IT and Marcusson JO. High- and low-affinity [³H]desipramine-binding sites in human post-mortem brain tissue. *Neuropsychobiol* 1990; 23:68-73.
- Bannon MJ, Michelhaugh SK, Wang J and Sacchetti P. The human dopamine transporter gene: gene organization, transcriptional regulation, and potential involvement in neuropsychiatric disorders. *Eur Neuropsychopharmacol* 2001; 11:449-55.
- Bannon MJ. The dopamine transporter: role in neurotoxicity and human disease. *Toxicol Appl Pharmacol* 2005; 204: 355-60.
- Beckman ML and Quick MW. Neurotransmitter transporters: regulators of function and functional regulation. *J Membrane Biol* 1998; 164:1-10.
- Beer HF, Pressetti I, Frey LD, Hasler PH and Schubiger PA. 123I-labeling and evaluation of RO 43-0463, a SPECT tracer for MAO-B imaging. *Nucl Med Biol* 1995; 22:929-936.
- Bergström M, Westerberg G and Langström B. 11C-harmine as a tracer for monoamine oxidase A (MAO-A): in vitro and in vivo studies. *Nuc Med Biol* 1997a; 24:287-293.
- Bergström M, Westerberg G, Kihlberg T and Langström B. Synthesis of some c-labelled MAO-A inhibitors and their in vivo uptake kinetics in rhesus monkey brain. *Nuc Med Biol* 1997b; 24:381-388.
- Berlin I, Said S, Spreux-Varoquaux O, Olivares R, Launay J-M and Puech AJ. Monoamine oxidase A and B activities in heavy smokers. *Biol Psychiatry* 1995; 38:756-61.

- Binda C, Newton-Vinson P, Hubalek F, Edmondson DE and Mattevi A. Structure of human monoamine oxidase B, a drug target for the treatment of neurological disorders. *Nat Struct Biol* 2002; 9:22-26.
- Birkmayer W. Deprenyl (selegiline) in the treatment of Parkinson's disease. *Acta Neurol Scand* 1983; suppl 95:103-6.
- Blakely RD, DeFelice LJ and Galli A. Biogenic amine neurotransmitter transporters: just when you thought you knew them. *Physiology* 2005; 20:225-31.
- Boja JW, Mitchell WM, Patel A, Kopajtic TA, Carroll FI, Lewin AH et al. High-affinity binding of [¹²⁵I]RTI-55 to dopamine and serotonin transporters in rat brain. *Synapse* 1992; 12:27-36.
- Bönisch H and Brüss M. The norepinephrine transporter of the neuronal plasma membrane. *Ann N Y Acad Sci* 1994; 733:193-202.
- Booij J, Andringa G, Rijks LJM, Vermeulen J, De Bruin K, Boer JG et al. [¹²³I]FP-CIT binds to the dopamine transporter as assessed by biodistribution studies in rats and SPECT studies in MPTP-lesioned monkeys. *Synapse* 1997; 27:183-90.
- Booij J, Sokole EB, Stabin MG, Janssen AGM, de Bruin K and van Royen EA. Human biodistribution and dosimetry of [¹²³I]FP-CIT: a potent radioligand for imaging of dopamine transporters. *Eur J Nucl Med* 1998; 25:24-30.
- Booij J and Kemp P. Dopamine transporter imaging with [¹²³I]FP-CIT: potential effect of drugs. *Eur J Nucl Med Mol Imaging* 2008; 35:424-38.
- Boos TL, Greiner E, Calhoun WJ, Priszano TE, Nightingale B, Dersch, CM, Rothman, RB, Jacobson, AE, Rice, KC. Structure-activity relationships of substituted *N*-benzyl piperidines in the GBR series: Synthesis of 4-(2-(bis(4-fluorophenyl)methoxy)ethyl)-1-(2-trifluoromethylbenzyl)piperidine, an allosteric modulator of the serotonin transporter *Bioorg Med Chem* 2006; 14:3967-73.
- Bortolato M, Chen K and Shih JC. Monoamine oxidase inactivation: From pathophysiology to therapeutics. *Adv Drug Deliv Rev* 2008;60:1527-33.
- Bottlaender M, Dollé F, Guenther I, Roumenov D, Fuseau C, Bramouille Y, et al. Mapping the cerebral monoamine oxidase type a: Positron emission tomography characterization of the reversible selective inhibitor [11C] bexlofexone. *J Pharm Exp Therap* 2008; 305:467-473.
- Bramouillé Y, Puech F, Saba W, Valette H, Bottlaender M, George P and Dollé F. Radiosynthesis of (S)-5-methoxymethyl-3-[6-(4,4,4-trifluorobutoxy)benzo[d]isoxazol-3-yl]oxazolidin-2[11C]one ([11C]SL25.1188), a novel radioligand for imaging monoamine oxidase-B with PET. *J Labelled Comp Radiopharm* 2008; 51:153-158.
- Brücke T, Kornhuber J, Angelberger P, Asenbaum S, Frassine H and Podreka I. SPECT imaging of dopamine and serotonin transporters with [¹²³I]β-CIT. Binding kinetics in the human brain. *J Neural Transm* 1993; 94:137-46.
- Brunello N, Mendlewicz J, Kasper S, Leonard B, Montgomery S, Nelson JC, Paykel E, Versiani M and Racagni G. The role of noradrenaline and selective noradrenaline reuptake inhibition in depression. *Eur Neuropsychopharmacol* 2002;12:461-475
- Brunner HG, Nelen M, Breakefield O, Ropers HH and van Oost BA. Abnormal behaviour associated with a point mutation in the structural gene for monoamine oxidase A. *Science* 1993; 262:578-80.
- Brüss M, Hammermann R, Brimijoin S and Bönisch H. Antipeptide antibodies confirm the topology of the human norepinephrine transporter. *J Biol Chem* 1995; 270:9197-201.

- Buck KJ and Amara SG. Chimeric dopamine-norepinephrine transporters delineate structural domains influencing selectivity for catecholamines and 1-methyl-4-phenylpyridinium. *Proc Natl Acad Sci USA* 1994; 91:12584-8.
- Buck KJ and Amara SG. Structural domains of catecholamine transporter chimeras involved in selective inhibition by antidepressants and psychomotor stimulants. *Mol Pharmacol* 1995; 48:1030-7.
- Bymaster FP, M.S., Katner JS, B.S., Nelson DL, Hemrick-Luecke S, Threlkeld PG et al. Atomoxetine increases extracellular levels of norepinephrine and dopamine in prefrontal cortex of rat: a potential mechanism for efficacy in attention deficit/hyperactivity disorder. *Neuropsychopharmacology* 2002; 27:699-711.
- Cabib S and Puglisi-Allegra S. Stress, depression and the mesolimbic dopamine system. *Psychopharmacology* 1996; 128:331-342.
- Chen N and Reith MEA. Structure and function of the dopamine transporter. *Eur J Pharmacol* 2000; 405:329-39.
- Cheon KA, Ryu YH, Kim YK, Namkoong K, Kim CH and Lee DJ. Dopamine transporter density in the basal ganglia assessed with [¹²³I]IPT SPET in children with attention deficit hyperactivity disorder. *Eur J Nucl Med* 2003; 30:306-11.
- Chumpradit S, Kung M, Panyachotipun C, Prapansiri V, Foulon C, Brooks BP et al. Iodinated tomoxetine derivatives as selective ligands for serotonin and norepinephrine uptake sites. *J Med Chem* 1992; 35:4492-7.
- Cleynhens BJ, de Groot TJ, Vanbilloen HP, Kieffer D, Mortelmans L, Bormans G et al. Technetium-99m labelled integrated tropane-BAT as a potential dopamine transporter tracer. *Bioorg Med Chem* 2005; 13:1053-8.
- Cook EH, Stein MA, Krasowski MD, Cox NJ, Olkon DM, Kieffer JE et al. Association of attention-deficit disorder and the dopamine transporter gene. *Am J Hum Genet* 1995; 56:993-8.
- Corman SL, Fedutes BA and Culley CM. Atomoxetine: the first nonstimulant for the management of attention-deficit/hyperactivity disorder. *Am J Health-Syst Pharm* 2004; 61:2391-9.
- Cousins MS and Salamone JD. Involvement of ventrolateral striatal dopamine in movement initiation and execution: a microdialysis and behavioural investigation. *Neuroscience* 1996; 70:849-59.
- Coyle JT and Snyder SH. Catecholamine uptake by synaptosomes in homogenates of rat brain: stereospecificity in different areas. *J Pharmacol Exp Ther* 1969; 176:221-231.
- Crane GE. The Psychiatric side-effects of iproniazid. *Am J Psychiatry* 1956; 112:494-501.
- Davis MR, Votaw JR, Bremner D, Byas-Smith MG, Faber TL, Voll RL et al. Initial human PET imaging studies with the dopamine transporter ligand ¹⁸F-FECNT. *J Nucl Med* 2003; 44:855-61.
- De Colibus L, Li M, Binda C, Lustig A, Edmondson DE and Mattevi A. Three-dimensional structure of human monoamine oxidase A (MAO A): Relation to the structures of rat MAO A and human MAO B. *Proc Natl Acad Sci U S A* 2005; 102:12684-9.
- Deterding TA, Votaw JR, Wang CK, Eshima D, Eshima L, Keil R et al. Biodistribution and radiation dosimetry of the dopamine transporter ligand [¹⁸F]FECNT. *J Nucl Med* 2001; 42:376-81.
- Ding Y, Lin K, Logan J, Benveniste H and Carter P. Comparative evaluation of positron emission tomography radiotracers for imaging the norepinephrine transporter: (S,S) and (R,R) enantiomers of reboxetine analogs ([¹¹C]methylreboxetine, 3-Cl-[¹¹C]methylreboxetine and [¹⁸F]fluororeboxetine), (R)-[¹¹C]nisoxetine, [¹¹C]oxaprotiline and [¹¹C]lortalamine. *J Neurochem* 2005; 94:337-51.
- Ding Y, Lin K and Logan J. PET imaging of norepinephrine transporters. *Curr Pharm Des* 2006; 12:3831-45.

- Ding Y, Lin K, Garza V, Carter P, Alexoff D, Logan J, Shea C, Xu Y and King P. Evaluation of a new norepinephrine transporter PET ligand in baboons, both in brain and peripheral organs. *Synapse* 2008; 50:345-52.
- Docherty JR. Subtypes of functional α_1 - and α_1 -adrenoreceptors. *Eur J Pharmacol* 1998; 361:1-15.
- Dolle F, Valette H, Bramouille Y, Guenther I, Fuseau C, Coulon C et al. Synthesis and in vivo imaging properties of [¹¹C]befloxatone: a novel highly potent positron emission tomography ligand for monoamine oxidase-A. *Bioorg Med Chem Lett* 2003; 13:1771-5.
- Dostert PL, Strolin-Benedetti M, Tipton KF. Interactions of monoamine oxidase with substrates and inhibitors. *Med Res Rev* 1989; 9:45-89.
- Dostert P, Benedetti MS and Poggesi I. Review of the pharmacokinetics and metabolism of reboxetine, a selective noradrenaline reuptake inhibitor. *Eur Neuropsychopharmacol* 1997; 7:23-35.
- Edmondson DE, DeColibus L, Binda C, Li M and Mattevi A. New insights into the structures and functions of human monoamine oxidases A and B. *J Neurol Transm* 2007; 114:703-5.
- Eisenhofer G and Finberg JPM. Different metabolism of norepinephrine and epinephrine by catechol-O-methyltransferase and monoamine oxidase in rats. *J Pharmacol Exp Ther* 1993; 268:1242-50.
- Elliott JM and Beveridge TJR. Psychostimulants and monoamine transporters: upsetting the balance. *Curr Opin Pharmacol* 2005; 5:94-100.
- Elsinga PH, Hatano K, Ishiwata K. PET tracers for the dopaminergic system. *Curr Med Chem* 2006; 13:2139-53.
- Farde L, Halldin C, Muller L, Suhara T, Karlsson P and Hall H. PET study of [¹¹C] β -CIT binding to monoamine transporters in the monkey and human brain. *Synapse* 1994; 16:93-103.
- Fleckenstein AE, Volz TJ, Riddle EL, Gibb JW and Hanson GR. New insights into the mechanism of action of amphetamines. *Annu Rev Pharmacol Toxicol* 2007; 47:681-98.
- Floresco SB and Magyar O. Mesocortical dopamine modulation of executive functions: beyond working memory. *Psychopharmacology* 2006; 188:567-85.
- Fowler JS, MacGregor RR, Wolf AP, Arnett CD, Dewey SL, Schlyer D et al. Mapping human brain monoamine oxidase A and B with ¹¹C-labeled suicide inactivators and PET. *Reports* 1987: 481-5.
- Fowler JS, Volkow ND, Wolf AP, Dewey SL, Schlyer DJ, Macgregor RR et al. Mapping cocaine binding sites in human and baboon brain in vivo. *Synapse* 1989; 4:371-7.
- Fowler JS, Volkow ND, Wang G-J, Pappas N, Logan J, Shea C et al. Brain monoamine oxidase a inhibition in cigarette smokers. *Proc Natl Acad Sci* 1996; 93:14065-9.
- Fowler JS, Ding Y-S, Logan J, MacGregor RR, Shea C, Garza V et al. Species differences in [¹¹C]clorgyline binding in brain. *Nuc Med Biol* 2001; 28:779-85.
- Fowler JS, Logan J, Volkow ND, Wang GJ, MacGregor RR and Ding YS. Monoamine oxidase: radiotracer development and human studies. *Methods* 2002; 27:263-277.
- Fowler JS, Logan J, Volkow ND, Wang GJ. Translational neuroimaging: positron emission tomography studies of monoamine oxidase. *Mol Imaging Biol* 2005; 7:377-387.
- Gelb DJ, Oliver E and Gilman S. Diagnostic criteria for Parkinson disease. *Arch Neurol* 1999; 56:33-9.
- Gelernter J, Kruger S, Pakstis AJ, Pacholczyk T, Sparkes RS, Kidd KK and Amara S. Assignment of the norepinephrine transporter protein (NET1) locus to chromosome 16. *Genomics* 1993; 18:690-2.

- Geracitano R, Federici M, Bernardi G and Mercuri NB. On the effects of psychostimulants, antidepressants, and the antiparkinsonian drug levodopa on dopamine neurons. *Ann NY Acad Sci* 2006; 1074:320-9.
- Gill M, Daly G, Heron S, Hawi Z and Fitzgerald M. Confirmation of association between attention deficit hyperactivity disorder and a dopamine transporter polymorphism. *Mol Psychiatry* 1997; 2:311-3.
- Giros B, Mestikawy SE, Godinot N, Zheng K, Han H, Yang-Feng T et al. Cloning, pharmacological characterization, and chromosome assignment of the human dopamine transporter. *Mol Pharmacol* 1992; 42:383-90.
- Giros B and Caron MG. Molecular characterization of the dopamine transporter. *Trends Pharmacol Sci* 1993;14:43-9.
- Giros B, Wang Y-M, Suter S, McLeskey SB, Pifl C and Caron MG. Delineation of discrete domains for substrate, cocaine, and tricyclic antidepressant interactions using chimeric dopamine-norepinephrine transporters. *J Biol Chem* 1994; 269:15985-8.
- Giros B, Jaber M, Jones SR, Wightman RM and Caron MG. Hyperlocomotion and indifference to cocaine and amphetamine in mice lacking the dopamine transporter. *Nature* 1996; 379:606-12.
- Goodall McC and Kirshner N. Biosynthesis of epinephrine and norepinephrine by sympathetic nerves and ganglia. *Circulation* 1958; 17:366-71.
- Goodman MM, Kilts CD, Keil R, Shi B, Martarello L, Xing D et al. ¹⁸F-labeled FECNT: a selective radioligand for PET imaging of brain dopamine transporters. *Nucl Med Biol* 2000; 27:1-12.
- Greenberg PE, Stiglin LE, Finkelstein SN and Berndt ER. The economic burden of depression in 1990. *J Clin Psychiatry* 1993; 54:405-18.
- Gross-Isseroff R, Israeli M and Biegon A. Autoradiographic analysis of [³H]desmethylimipramine binding in the human brain post-mortem. *Brain Research* 1988; 456:120-6.
- Guilloteau D and Chalon S. PET and SPECT exploration of central monoaminergic transporters for the development of new drugs and treatments in brain disorders. *Curr Pharm Des* 2005; 11:3237-45.
- Hadley D, Hoff M, Holik J, Reimherr F, Wender P, Coon H et al. Manic-depression and the norepinephrine transporter gene. *Hum Hered* 1995; 45:165-8.
- Hahn MK and Blakely RD. The functional impact of SLC6 transporter genetic variation. *Annu Rev Pharmacol Toxicol* 2007; 41:401-41.
- Haka Ms and Kilbourn MR. Synthesis and regional mouse brain distribution of [¹¹C]nisoxetine, a norepinephrine uptake inhibitor. *Nucl Med Biol* 1989; 16:771-4.
- Halldin C, Erixon-Lindroth N, Pauli S, Chou Y-H, Okubo Y, Karlsson P et al. [¹¹C]PE2I: a highly selective radioligand for PET examination of the dopamine transporter in monkey and human brain. *Eur J Nucl Med Mol Imaging* 2003; 30:1220-30.
- Hare MLC. Tyramine oxidase. A new enzyme system in the liver. *Biochem J* 1928; 22:968-79.
- Herrting G, Axelrod J, Kopin IJ and Whitby LG. Lack of uptake of catecholamines after chronic denervation of sympathetic nerves. *Nature* 1961;189:66.
- Hersch SM, Yi H, Heilman CJ, Edwards RH and Levey AI. Subcellular localization and molecular topology of the dopamine transporter in the striatum and substantia nigra. *J Comp Neurol* 1997; 388:211-27.
- Hesse S, Ballaschke O, Barthel H and Sabri O. Dopamine transporter imaging in adult patients with attention-deficit/hyperactivity disorder. *Psychiatry Res* 2009; 171:120-8.

- Hirata M, Magata Y, Ohmomo Y, Saji H, Murakami K, Takagaki T et al. Evaluation of radioiodinated iodoclogyline as a SPECT radiopharmaceutical for MAO-A in the brain. *Nuc Med Biol* 1995; 22:175-80.
- Hirata M, Kagawa S, Yoshimoto M and Ohmomo Y. Synthesis and characterization of radioiodinated MD-230254: A new ligand for potential imaging of monoamine oxidase B activity by single photon emission computed tomography. *Chem Pharm Bull* 2002; 50:609-614.
- Holm KJ and Spencer CM. Reboxetine, a review of its use in depression. *CNS Drugs* 1999; 12:65-83.
- Housley MD and Tipton KF. Multiple forms of monoamine oxidase: fact and artefact. *Life Sciences* 1976; 19:467-78.
- Howell LL and Kimmel HL. Monoamine transporters and psychostimulant addiction. *Biochem Pharmacol* 2008; 75:196-217.
- Hwang JJ, Liao MH, Yen TC, Wey SP, Lin KJ, Pan WHT et al. Biodistribution study of [^{99m}Tc] TRODAT-1 alone or combined with other dopaminergic drugs in mice with macroautradiography. *Appl Radiat Isot* 2002; 57:35-42.
- Inoue H, Castagnoli K, Van Der Schyf C, Mabic S, Igarashi K and Castagnoli N. Species-dependent differences in monoamine oxidase A and B-catalyzed oxidation of various C4 substituted 1-methyl-4-phenyl-1,2,3,6-tetrahydropyridinyl derivatives. *J Pharm Exp* 1999; 291:856-64.
- Inoue K, Itoh K, Yoshida K, Shimizu T and Suzuki T. Positive association between T-182C polymorphism in the norepinephrine transporter gene and susceptibility to major depressive disorder in a Japanese population. *Neuropsychobiology* 2004; 50:301-4.
- Jackson DM and Westlind-Danielsson A. Dopamine receptors: molecular biology, biochemistry and behavioural aspects. *Pharmac Ther* 1994; 64:291-369.
- Jahng JW, Houpt TA, Wessel TC, Chen K, Shih JC and Joh TH. Localization of monoamine oxidase A and B mRNA in the rat brain by in situ hybridization. *Synapse* 1997; 25:30-6.
- Kahlig KM and Galli A. Regulation of dopamine transporter function and plasma membrane expression by dopamine, amphetamine, and cocaine. *Eur J Pharmacol* 2003; 479:153-8.
- Kanner IB and Schuldiner S. Mechanism of transport and storage of neurotransmitters. *Crit Rev Biochem* 1987; 22:1-38.
- Kavanaugh MP. Neurotransmitter transport: Models in flux. *Proc Natl Acad Sci USA* 1998; 95:12737-8.
- Kawari T, Kawakami H, Yamamuri Y and Nakamura S. Structure and organization of the gene encoding human dopamine transporter. *Gene* 1997; 195:11-8.
- Kearney EB, Salach JI, Walker WH, Seng RL, Kenney W, Zeszotek E et al. The covalently-bound flavin of hepatic monoamine oxidase. *Eur J Biochem* 1971; 24:321-7.
- Kebir O, Tabbane K, Sengupta S and Joobar R. Candidate genes and neuropsychological phenotypes in children with ADHD: review of association studies. *J Psychiatry Neurosci* 2009;34:88-101.
- Kieffer DM, Vanbilloen HP, Cleynhens BJ, Terwinghe CY, Mortelmans L, Bormans GM et al. Biological evaluation of a technetium-99m-labeled integrated tropane-BAT and its piperidine congener as potential dopamine transporter imaging agents. *Nucl Med Biol* 2006; 33:125-133.
- Kimura M, Masuda T, Yamada K, Mitani M, Kubota N, Kwakatsu N et al. Novel Diphenylalkyl Piperazine Derivatives with High Affinities for the Dopamine Transporter. *Bioorg Med Chem* 2003; 11:3953-63.
- Kiyono Y, Kanegawa N, Kawashima H, Fujiwara H, Iida Y, Nishimura H and Saji H. A new norepinephrine transporter imaging agent for cardiac sympathetic nervous function imaging: radioiodinated (R)-N-methyl-3-

- (2-iodophenoxy)-3-phenylpropanamine. *J Med Chem* 2003; 30:697-706.
- Kiyono Y, Kanegawa N, Kawashima H, Kitamura Y, Iida Y and Saji H. Evaluation of radioiodinated (R)-N-methyl-3-(2-iodophenoxy)-3-phenylpropanamine as a ligand for brain norepinephrine transporter imaging. *Nuc Med Biol* 2004; 31:147-53.
- Klabunde RE. www.cvpharmacology.com 2008.
- Klimek V, Stockmeier C, Overholser J, Meltzer HY, Kalka S, Dille G and Ordway GA. Reduced levels of norepinephrine transporters in the locus coeruleus in major depression. *J Neurosci* 1997; 17:8451-58.
- Koob GF and Bloom FE. Cellular and molecular mechanisms of drug dependence. *Science* 1988; 242:715-23.
- Koob G. *Drug Addiction. Neurobiol Dis* 2000; 7:543-5.
- Kopin IJ. Monoamine oxidase and catecholamine metabolism. *J Neural Transm* 1994; 41:57-67.
- Krause KH, Dresel SH, Krause J, Kung HF and Tatsch K. Increased striatal dopamine transporter in adult patients with attention deficit hyperactivity disorder: effects of methylphenidate as measured by single photon emission computed tomography. *Neurosci Lett* 2000; 285:107-10.
- Kuhar MJ and Boja JW. The dopamine hypothesis of the reinforcing properties of cocaine. *TINS* 1991; 14:299-302.
- Kung HF, Kim H-J, Kung M-P, Meegalla SK, Plössl K and Lee H-K. Imaging of dopamine transporters in humans with technetium-99m TRODAT-1. *Eur J Nucl Med* 1996; 23:1527-30.
- Kung M, Choi S, Hou C, Zhuang Z, Foulon C, Kung H. Selective binding of 2-[¹²⁵I]iodo-nisoxetine to norepinephrine transporters in the brain. *Nuc Med Biol* 2004; 31:533-41.
- Laakso A, Bergman J, Haaparanta M, Vilkinan H, Solin O and Hietala J. [¹⁸F]CFT ([¹⁸F]WIN 35,428), a radioligand to study the dopamine transporter with PET: Characterization in human subjects. *Synapse* 1998; 28:244-50.
- Lammertsma AA, Banch CJ, Price GW, Cremer JE, Luthra SK, Turton D et al. Measurement of cerebral monoamine oxidase B activity using L-[¹⁴C]deprenyl and dynamic positron emission tomography. *J Cereb Blood Flow Metab* 1991; 11:545-56.
- Lan NC, Chen C and Shih JC. Expression of functional human monoamine oxidase A and B cDNAs in mammalian cells. *J Neurochem* 1989; 52:1652-4.
- Laruelle M, Wallace E, Seibyl JP, Baldwin RM, Zea-Ponce Y, Zoghbi SS et al. Graphical, kinetic, and equilibrium analyses of in vivo [¹²³I]β-CIT binding to dopamine transporters in healthy human subjects. *J Cereb Blood Flow Metab* 1994; 14:982-94.
- Lee C-M, Javitch JA and Snyder SH. Recognition sites for norepinephrine uptake: regulation by neurotransmitter. *Science* 1983;220:626-9.
- Leonard BE. Neuropharmacology of antidepressants that modify central noradrenergic and serotonergic function: a short review. *Hum Psychopharmacol Clin Exp* 1999; 14:75-81.
- Lewis A, Miller JH and Lea RA. Monoamine oxidase and tobacco dependence. *Neurotoxicology* 2007; 28:182-95.
- Lin K, Ding Y, Kim S and Kil K. Synthesis, enantiometric resolution, F-18 labeling and biodistribution of reboxetine analogs: promising radioligands for imaging the norepinephrine transporter with positron emission tomography *Nucl Med Biol* 2005; 32:415-22.
- Maas JW and Landis DH. *In vivo* studies of the metabolism of norepinephrine in the central nervous system. *J Pharmacol Exp Ther* 1968; 163:147-62.

- MacGregor RR, Halldin C, Fowler JS, Wolf Af, Arnett CD, Langstrom B and Alexoff D. Selective, irreversible *in vivo* binding of [¹¹C]clorgyline and [¹¹C]-L-deprenyl in mice: potential for measurement of functional monoamine oxidase activity in brain using positron emission tomography. *Biochem Pharmacol* 1985; 34:3207-10.
- Marsden CA. Dopamine: the rewarding years. *British Journal of Pharmacology* 2006; 147:S136-44.
- Masson J, Hamon CS and Mestikawy SE. Neurotransmitter transporters in the central nervous system. *Pharm Rev* 1999; 51:439-64.
- Mattiuz EL, Ponsler GD, Barbuch RJ, Wood PG, Mullen JH, Shugert RL et al. Disposition and metabolic fate of atomoxetine hydrochloride pharmacokinetics, metabolism, and excretion in the fischer 344 rat and beagle dog. *J Pharmacol Exp Ther* 2003; 31:88-97.
- McConathy J, Owens M, Kilts C, Malveaux E, Camp V, Votaw J, Nemeroff C and Goodman M. Synthesis and biological evaluation of [¹¹C]talopram and [¹¹C]talsupram: candidate pet ligands for norepinephrine transporter. *Nucl Med Biol* 2004;31:705-718.
- Meliakén HE. Neurotransmitter transporter trafficking: endocytosis, recycling, and regulation. *Pharmacol Ther* 2004;104:17-27.
- Melloni P, Carniel G, Torre AD, Bonsignori A, Buonamici M et al. Potential antidepressant agents. α -Aryloxy-benzyl derivatives of ethanolamine and morpholine. *Eur J Med Chem* 1984; 19:235-42.
- Meyer JH, Ginovart N, Boovariwala A, Segrati S, Hussey D, Garcia A et al. Elevated monoamine oxidase A levels in the brain. *Arch Gen Psychiatry* 2006; 63:1209-16.
- Mezey E, Eisenhofer G, Harta G, Hansson S, Gould L, Hunyady B et al. A novel nonneuronal catecholaminergic system: exocrine pancreas synthesizes and releases dopamine. *Proc Natl Acad Sci USA* 1996; 93:10377-82.
- Mezey E, Eisenhofer G, Hansson S, Harta G, Hoffman BJ, Gallatz K et al. Non-neuronal dopamine in the gastrointestinal system 1999; 26:S14-S22.
- Mitsuma T, Rhue N, Hirroka Y, Kayama M, Wago T, Mori Y et al. Distribution of dopamine transporter in the rat: an immunohistochemical study. *Endocr Regul* 1998; 32:71-5.
- Moore RY and Bloom FE. Central catecholamine neuron systems: anatomy and physiology of the dopamine systems. *Annu Rev Neurosci* 1978; 1:129-69.
- Moron JA, Brockington A, Wise RA, Rocha BA and Hope BT. Dopamine uptake through the norepinephrine transporter in brain regions with low levels of the dopamine transporter: evidence from knock-out mouse lines. *J Neurosci* 2002; 22:389-95.
- Mukherjee J and Yang ZJ. Development of *N*-[3-(2',4'-dichlorophenoxy)-2-¹⁸F-fluoropropyl]-*N*-methylpropargylamine (¹⁸F-fluoroclogyline) as a potential PET radiotracer for monoamine oxidase A. *Nucl Med Biol* 1999; 26:619-25.
- Murchison CF, Zhang X-Y, Zhang W-P, Ouyang M, Lee A and Thomas SA. A distinct role for norepinephrine in memory retrieval. *Cell* 2004; 117:131-143.
- Nicholas AP, Hökfelt T and Pieribone VA. The distribution and significance of CNS adrenoreceptors examined with *in situ* hybridization. *Trends Pharmacol Sci* 1996;17:245-55.
- Ornstein GG. Iproniazid in pulmonary tuberculosis. *Dis Nerv Syst* 1958:545.
- Owen D, Du L, Bakish D, Lapierre YD and Hrdina PD. Norepinephrine transporter gene polymorphism is not associated with susceptibility to major depression. *Psychiatry Res* 1999; 87:1-5.

- Pacholzyk T, Blakely RD and Amara SG. Expression cloning of a cocaine- and antidepressant-sensitive human noradrenaline transporter. *Nature* 1991; 350:350-4.
- Peyrin L and Dalmaz Y. Peripheral secretion and inactivation of catecholamines – epinephrine, norepinephrine and dopamine. *J Physiol* 1975; 70:353-433.
- Piccini PP. Dopamine transporter: basic aspects and neuroimaging. *Mov Disord* 2003; 18:S3-S8.
- Poewe W and Scherfler C. Role of dopamine transporter imaging in investigation of parkinsonian syndromes in routine clinical practice. *Mov Disord* 2003; 18:S16-S21.
- Porzgen P, Bonisch H and Bruss M. Molecular cloning and organization of the coding region of the human norepinephrine transporter. *Biochem Biophys Res Comm* 1995; 215:1145-50.
- Raisman R, Sette M, Pimoule C, Briley M and Langer SZ. High-affinity [³H]desipramine binding in the peripheral and central nervous system: a specific site associated with the neuronal uptake of noradrenaline. *Eur J Pharmacol* 1982; 78:345-51.
- Rebrin I, Geha RM, Chen K and Shih JC. Effects of carboxyl-terminal truncations on the activity and solubility of human monoamine oxidase B. *J Biol Chem* 2001; 276:29499-506.
- Reid JL. Dopaminergic pathways and their pathophysiological significance. *Clin Sci Mol Med* 1977; 53:303-6.
- Ressler KJ and Nemeroff CB. Role of norepinephrine in the pathophysiology and treatment of mood disorders. *Biol Psychiatry* 1999; 46:1219-1233.
- Ressler RC, Merikangas KR and Wang PS. Prevalence, comorbidity, and service utilization for mood disorders in the United States at the beginning of the twenty-first century. *Annu Rev Clin Psychol* 2007; 3:137-58.
- Riederer P, Lachenmayer L and Laux G. Clinical application of MAO-inhibitors. *Curr Med Chem* 2004; 11:2033-43.
- Ritz MC, Lamb RJ, Goldberg SR and Kuhar MJ. Cocaine receptors on dopamine transporters are related to self-administration of cocaine. *Science* 1988; 237:1219-23.
- Rodríguez MJ, Saura J, Billett EE, Finch CC and Mahy N. Cellular localization of monoamine oxidase A and B in human tissues outside of the central nervous system. *Cell Tissue Res* 2001; 304:215-20.
- Rothman RB and Baumann MH. Monoamine transporters and psychostimulant drugs. *Eur J Pharmacol* 2003; 479: 23-40.
- Rothman RB, Baumann MH, Prisinzani TE, Newman AM. Dopamine transport inhibitors based on GBR12909 and benzotropine as potential medications to treat cocaine addiction. *Biochem Pharmacol* 2008; 75:2-16.
- Rudnick G and Clark J. From synapse to vesicle: the reuptake and storage of biogenic amine neurotransmitters. *Biochimica et Biophysica Acta* 1993; 1144:249-63.
- Ryu S, Lee S, Lee H, Cha J, Ham B, Han C, et al. Association between norepinephrine transporter gene polymorphism and major depression. *Neuropsychobiology* 2004; 49:174-7.
- Sand PG, Mori T, Godau C, Stöber G, Flachenecker P, Franke P, et al. Norepinephrine transporter gene (NET) variants in patients with panic disorder. *Neurosci Lett* 2002; 333:41-4.
- Sauer JM, Ring BJ and Witcher JW. Clinical pharmacokinetics of atomoxetine. *Clin Pharmacokinet* 2005; 44:571-90.
- Saura J, Kettler R, Da Prada M and Richards JG. Quantitative enzyme radioautography with ³H-Ro 41-1049 and ³H-Ro 19-6327 *in vitro*: localization and abundance of MAO-a and MAO-B in rat CNS, peripheral organs, and human brain. *J Neurosci* 1992; 12:1977-99.

- Saura J, van den Berg NB, Vila M, Bombi JA and Mahy N. Localization of monoamine oxidases in human peripheral tissues. *Life Sci* 1996a; 59:1341-9.
- Saura J, Bleuel Z, Ulrich J, Mendelowitsch A, Chen K, Shih JC et al. Molecular neuroanatomy of human monoamine oxidases A and B revealed by quantitative enzyme radioautography and in situ hybridization histochemistry. *Neuroscience* 1996b; 70:755-74.
- Schapira AHV. Treatment options in the modern management of Parkinson disease. *Arch Neurol* 2007; 64:1083-8.
- Schmitz Y, Benoit-Marand M, Gonon F and Sulzer D. Presynaptic regulation of dopaminergic neurotransmission. *J Neurochem* 2003; 87:273-289.
- Schnaitman C, Erwin VG and Greenawalt WJ. The submitochondrial localization of monoamine oxidase an enzymatic marker for the outer membrane of rat liver mitochondria. *J Cell Biol* 1967; 32:719-35.
- Schoepp DD and Azzaro AJ. Specificity of endogenous substrates for types A and B monoamine oxidase in rat striatum. *J Neurochem* 1981; 36:2025-31.
- Schou M, Halldin C, Pike V, Mozley P, Dobson D, Innis R, Farde L and Hall H. Post-mortem human brain autoradiography of the norepinephrine transporter using (S,S)-[¹⁸F]FMeNER-D₂. *European neuropsychopharmacology* 2005; 15:517-20.
- Schou M, Halldin C, Sovago J, Pike VW, Gulyás B, Mozley PD et al. Specific in vivo binding to the norepinephrine transporter demonstrated with the PET radioligand, (S,S)-[¹¹C]MeNER. *Nucl Med Biol* 2003; 30:707-14.
- Schou M, Halldin C, Sóvágó J, Pike V, Hall H, Gulyás B et al. Pet evaluation of novel radiofluorinated reboxetine analogs as norepinephrine transporter probes in the monkey brain. *Synapse* 2004; 53:57-67.
- Schou M, Sóvágó J, Pike V, Gulyás B, Bogeso K, Farde L and Halldin C. Synthesis and positron emission tomography evaluation of three norepinephrine transporter radioligands: [C-11]desipramine, [C-11]talopram and [C-11]talsupram. *Mol Imaging Biol* 2005;8:1-8.
- Seibyl JP, Marek K, Sheff K, Zoghbi S, Baldwin RM, Charney DS et al. Iodine-123-β-CIT and iodine-123-FPCIT SPECT measurement of dopamine transporters in healthy subjects and Parkinson's patients. *J Nucl Med* 1998; 39:1500-8.
- Seneca N, Andree B, Sjöholm N, Schou M, Pauli S, Mozley D et al. Whole-body biodistribution, radiation dosimetry estimates for the pet norepinephrine transporter probe (S,S)-[¹⁸F]FMeNER-D₂ in non-human primates. *Nucl Med Comm* 2005; 26:695-700.
- Severance A, Milak M, Kumar JS, Prabhakaran J, Majo V, Simpson N et al. In vivo assessment of [¹¹C]MRB as a prospective pet ligand for imaging the norepinephrine transporter. *Eur J Nucl Med Mol Imaging* 2007; 34:688-93.
- Shetty HU, Zoghbi SS, Liow JS, Ichise M, Hong J, Musachio JL et al. Identification and regional distribution in rat brain of radiometabolites of the dopamine transporter PET radioligand [¹¹C]PE2I. *Eur J Nucl Med Mol Imaging* 2007; 34:667-78.
- Shih JC. Molecular basis of human MAO A and B. *Neuropsychopharmacology* 1991; 4:1-7.
- Shih JC and Thompson RF. Monoamine oxidase in neuropsychiatry and behaviour. *Am J Hum Genet* 1999;65:593-8.
- Shih JC, Chen K and Ridd MJ. Monoamine oxidase: From genes to behaviour. *Annu Rev Neurosci* 1999; 22:197-217.

- Shih MC, Hoexter MQ, Andrade LAF, Bressan RA. Parkinson's disease and dopamine transporter neuroimaging – a critical review. *Sao Paulo Med J* 2006; 123:168-175.
- Singh N, Pillay Vand Choonara YE. Advances in the treatment of Parkinson's disease. *Prog Neurobiol* 2007; 81:29-41.
- Smith HR, Beveridge TJR and Porrino LJ. Distribution of norepinephrine transporters in the non-human primate brain. *Neuroscience* 2006; 138:703-14.
- Snyder SH and Coyle JT. Regional differences in H³-norepinephrine and H³-dopamine uptake into rat brain homogenates. *J Pharmacol Exp Ther* 1968;165:78-86.
- Sonders MS and Amara SG. Channels in transporters. *Curr Opin Neurobiol* 1996; 6:294-302.
- Stoof JC, Winogrodzka A, van Muiswinkel FL, Wolters EC, Voorn P, Groenewegen HJ et al. Leads for development of neuroprotective treatment in Parkinson's disease and brain imaging methods for estimating treatment efficacy. *Eur J Pharmacol* 1999; 375:75-86.
- Sun N, Cu Y, Wang Y, Duan H, Wang S, Ren Y, et al. The combined effect of norepinephrine transporter gene and negative life events in major depression of chinese han population. *J Neural Transm* 2008; 115:1681-6.
- Takano A, Halldin C, Varrone A, Karlsson P, Sjöholm N, Stubbs J et al. Biodistribution and radiation dosimetry of norepinephrine transporter radioligand (S,S)-[¹⁸F]-FMeNER-D₂: a human whole-body pet study. *Eur J Nucl Med Mol Imaging* 2008;35:630-6.
- Tipton KF, Boyce S, O'Sullivan J, Davey GP and Healy J. Monoamine oxidase: certainties and uncertainties. *Curr Med Chem* 2004;11:1965-82.
- Torres GE, Gainetdinov RR and Caron MG. Plasma membrane monoamine transporters: structure, regulation and function. *Nature Reviews* 2003; 4:13-25.
- Torres GE. The dopamine transporter proteome. *J Neurochem* 2006; 97:3-10.
- Uhl GR. Dopamine transporter: basic science and human variation of a key molecule for dopaminergic function, locomotion, and parkinsonism. *Mov Disord* 2003; 18:S71-S80.
- Urwin RE, Bennetts B, Wilcken B, Lampropoulos B, Beumont P, Clarke S, et al. Anorexia nervosa (restrictive subtype) is associated with a polymorphism in the novel norepinephrine transporter gene promoter polymorphic region. *Mol Psychiatry* 2002; 7:652-7.
- Van Dort M, Kim J, Thuczek L and Wieland D. Synthesis of ¹¹C-labeled desipramine and its metabolite 2-hydroxydesipramine: potential radiotracers for pet studies of the norepinephrine transporter. *Nucl Med Biol* 1997; 24:707-11.
- van Dyck CH, Quinlan DM, Cretella LM, Staley JK, Malison RT, Baldwin RM et al. Unaltered dopamine transporter availability in adult attention deficit hyperactivity disorder. *Am J Psychiatry* 2002; 159:309-12.
- Vlaar AMM, de Nijs T, Kessels AGH, Vreeling FW, Winogrodzka A, Mess WH et al. Diagnostic value of ¹²³I-Ioflupane and ¹²³I-Iodobenzamide SPECT scans in 248 patients with Parkinsonian syndromes. *Eur Neurol* 2008; 59:258-66.
- Volkow ND, Fowler JS, Gatley J, Logan J, Wang G, Ding Y, Dewey S. PET evaluation of the dopamine system of the human brain *J Nuc Med* 1996; 37:1242-56.
- Volkow ND, Wang GJ, Fischman MW, Foltin RW, Fowler JS, Abumrad NN et al. Relationship between subjective effects of cocaine and dopamine transporter occupancy. *Nature* 1997; 386:827-30.
- Volkow ND, Wang GJ, Newcorn J, Fowler JS, Telang F, Solanto MV et al. Brain dopamine transporter levels in treatment and drug naive adults with ADHD. *Neuroimage* 2007; 34:1182-90.

- Weiner N. Regulation of norepinephrine biosynthesis. 1970; 273-290.
- Weyler W, Hsu Y-PP and Breakefield XO. Biochemistry and genetics of monoamine oxidase. *Pharmac Ther* 1990;47:391-417.
- Whitby LG, Axelrod J and Weil-Malherbe H. The fate of H³-norepinephrine in animals. 1961;132:193-201.
- Willoughby J, Glover V and Sandler M. Histochemical localisation of monoamine oxidase A and B in rat brain. *J Neural Transm* 1988; 74:29-42.
- Wilson A, Johnson D, Mozley D, Hussey D, Ginovart N, Nobrega J, Garcia A, Meyer J and Houle S. Synthesis and in vivo evaluation of novel radiotracers for the in vivo imaging of the norepinephrine transporter. *Nucl Med Biol* 2003; 30:85-92.
- Wise RA. Neurobiology of addiction. *Curr Opin Neurobiol* 1996; 6:243-51.
- Witkin JM, Nichols DE, Terry P and Katz JL. Behavioral effects of selective dopaminergic compounds in rats discriminating cocaine injections. *J Pharm Exp Therap* 1990; 257:706-13.
- Wong DT, Threlkeld PG, Best KL and Bymaster FP. A new inhibitor of norepinephrine uptake devoid of affinity for receptors in rat brain. *J Pharmacol Exp Ther* 1982; 22:61-5.
- Wong DF, Yung B, Dannals RF, Shaya EK, Ravert HT, Chen CA et al. In vivo imaging of baboon and human dopamine transporters by positron emission tomography using [¹¹C]WIN 35,428. *Synapse* 1993; 15:130-42.
- Wong E HF, Sonder MS, Amara SG, Tinholt PM, Piercey M FP, Hoffmann WP et al. Reboxetine: a pharmacologically potent, selective, and specific norepinephrine reuptake inhibitor. *Biol Psychiatry* 2000; 47:818-29.
- Youdim MBH, Edmondson D and Tipton KF. The therapeutic potential of monoamine oxidase inhibitors. *Nature Reviews* 2006; 7:295-309.
- Zahniser NR and Doolen S. Chronic and acute regulation of Na⁺/Cl⁻-dependent neurotransmitter transporters: drugs, substrates, presynaptic receptors and signalling systems. *Pharm Therap* 2001; 92:21-55.
- Zill P, Engel R, Baghai TC, Juckel G, Frodl T, Siecheneder-Müller F et al. Identification of a naturally occurring polymorphism in the promoter region of norepinephrine transporter and analysis in major depression. *Neuropsychopharmacology* 2002; 26:489-93.

Scope and Aims



SCOPE AND AIMS

SCOPE

Psychiatric disorders are highly prevalent and have important personal, social and economic impacts. An estimated 26.2 % of Americans aged 18 and older suffer from a diagnosable mental disorder in a given year. The most common mental disorders in adults in the United States are major depression and anxiety disorders, both of which affect up to 10 % of the adult population each year (Voshol et al., 2003). Psychiatrists face many problems during the assessment and differential diagnosis for individuals with mental disorders. Simplify the diagnosis from a better understanding of the neurobiological basis of brain disorders would increase the diagnostic validity, reliability and precision (Barnhill, 2008). Medical imaging technique can map structural and functional changes in the brain and thus are unique tools for clinical researchers to elucidate and understand the pathophysiology of neuropsychiatric disorders.

SPECT and PET are non-invasive imaging techniques in which radiotracers are used to study biochemical and physiological functions in the living brain. *In vivo* brain mapping with PET or SPECT can be of great importance in drug development as well as in the effective diagnosis, treatment and management of neurological and psychiatric disorders and substance abuse. Therefore, the development of new and more specific and selective radiotracers is of great importance in neuroimaging (Gee, 2003).

Monoamine transporters and enzymes that cause degradation of the monoamines (for example MAO) are responsible for the homeostasis of neurotransmitter pools at the nerve endings and control the duration and intensity of neurotransmitter action. The transporters and enzymes are main actors of the

neuronal communication, being therefore involved in the physiology and diseases of the CNS. Distribution, density, and activity of these transporters and enzymes in the brain can be visualized by using specific radioligands and SPECT and PET imaging. Further studies of the molecular mechanisms of the various transmitter systems can improve our understanding of complex brain functions and can provide more insight into the causes and consequences of neurological and psychiatric disease interaction (Wong and Brasic, 2001; Guilloteau and Chalon, 2005).

A prerequisite of efficient drug treatment of CNS disorders is that sufficient amounts of the drug enter the brain. Active transport by P-gp has a major impact on drug resistance to psychotropic drugs, affects the pharmacokinetics of many drugs and can be inhibited by the administration of modulators or competitive substrates (Linnet and Ejsing, 2008). Moreover, changes or abnormalities in P-gp expression and function are involved in the etiology and pathogenesis of several neurological diseases (Rapposelli et al., 2009). PET and SPECT can be applied to evaluate the efficacy of candidate P-gp-modulators *in vivo* and to investigate the effect of P-gp on the brain uptake of new psychotropic drugs. In addition, visualization of P-gp in the normal brain and during various pathologic conditions could be of great value to elucidate the relationship between P-gp function/expression and neuronal and neuropsychiatric disorders.

AIMS

As discussed above, an accurate and selective PET or SPECT tracer provides a useful clinical tool for the diagnosis and treatment of psychiatric and neurological disorders. Therefore, the aim of this thesis was the development of novel radiotracers for two distinct brain elements being the monoamine system and the P-gp transporter. The first objective was the design of radiotracers for, NET

(**Chapter 5**), MAO (**Chapter 6**) and DAT (**Chapter 7**) which are all responsible for neurotransmitter inactivation in the monoamine system. By the discovery that the radiotracer designed in Chapter 7 is modulated by P-gp, the focus of this thesis was redirected towards imaging of the P-gp transporter (**Chapter 8 and 9**).

Since no valuable SPECT radiotracer for visualization of the norepinephrine transporter is available, we will synthesize and subsequently label a reboxetine analogue with ^{123}I . The radiotracer will be evaluated *in vivo* in a biodistribution study in mice to determine brain uptake (**Chapter 5**).

The objective of **Chapter 6** is to label a suitable reversible inhibitor for mapping MAO-A *in vivo* with PET. We will select appropriate candidates from the literature. The chosen molecules will be radiolabelled with ^{14}C and evaluated *in vivo* in a biodistribution study in mice. The selectivity of the radiotracers for MAO-A will be assessed in a blocking study in mice and imaging studies in rats. Stability of the tracers will be determined *in vivo* in mice.

In a following part, we will develop a SPECT tracer that is more selective towards DAT compared to the existing radiotracers for DAT imaging. FMIP was picked out a report by Boos et al. (2006) based on its nanomolar affinity for the dopamine transporter and good selectivity over the other monoamine transporters. FMIP and the precursor molecule for the ^{123}I labelling will be synthesized. The potency of [^{123}I]-FMIP to visualize the dopamine transporter *in vivo* will be investigated in a biodistribution study in mice, a blocking study in mice and a regional brain distribution study in rats. Stability of the tracer will be assessed *in vitro* as well as *in vivo*. These studies are described in **Chapter 7**.

All reported radiotracers for the P-gp transporter are aimed to visualize P-gp function but not the expression of P-gp and they all have at least one limitation. Moreover, no iodinated SPECT tracer has been reported so far. In the last part of this thesis, we will label and evaluate a SPECT (**Chapter 8**) and a PET (**Chapter 9**) radiotracer for imaging P-gp function or expression.

The potential SPECT tracer, [^{123}I]-FMIP will be evaluated *in vivo* in a biodistribution study in wild-type and P-gp knock-out mice. The influence of CsA, a P-gp modulator, on the tissue distribution of the ^{123}I labelled tracer in wild-type and P-gp knock-out mice will be determined. The metabolic profile will be evaluated in wild-type mice with and without CsA pretreatment as well as in P-gp knock-out mice. [^{123}I]-FMIP will be further evaluated in a μSPECT study. These studies are described in **Chapter 8**.

Additionally, we will label an *in vitro* characterized substrate of the P-gp pump, with ^{11}C and evaluate this tracer *in vivo* in a biodistribution study in wild-type and P-gp knock-out mice. The influence of CsA and the unlabeled molecule on the biodistribution profile of the radiotracer will be explored. The stability of the tracer will be investigated *in vivo* in wild-type mice with and without CsA pretreatment as well as in P-gp knock-out mice (**Chapter 9**).

References

- Barnhill LJ. The diagnosis and treatment of individuals with mental illness and developmental disabilities: an overview. *Psychiatr Q* 2008; 79:157-70.
- Gee AD. Neuropharmacology and drug development. *Br Med Bull* 2003; 65:169-77.
- Guilloteau D and Chalon S. PET and SPECT exploration of central monoaminergic transporters for the development of new drugs and treatments in brain disorders. *Curr Pharm Des* 2005; 11:3237-45.
- Linnet K, Ejsing TB. A review on the impact of P-glycoprotein on the penetration of drugs into the brain. Focus on psychotropic drugs. *Eur Neuropsychopharmacol* 2008; 18:157-69.
- Rapposelli S, Digiacomo M and Balsamo A. P-gp transporter and its role in neurodegenerative diseases. *Curr Topics in Med Chem* 2009; 9:209-17.
- Voshol H, Glucksman MJ and van Oostrum J. Proteomics in the discovery of new therapeutic targets for psychiatric disease. *Curr Mol Med* 2003; 3:447-58.
- Wong DF and Brasic JR. In vivo imaging of neurotransmitter systems in neuropsychiatry. *Clin Neurosci Res* 2001; 1:35-45.

Chapter 4

Materials and Methods



Chapter 4

Materials and Methods

4.1. General

All solvents and chemicals were purchased from Acros (Geel, Belgium) or Sigma-Aldrich (Bornem, Belgium) unless otherwise mentioned and were used without further purification. HPLC solvents were purchased from Chemlab NV (Belgium). Cyclosporin A (Sandimmune®) was obtained from Novartis Pharma (250 mg/5 mL, Vilvoorde, Belgium).

No carrier added (n.c.a.) [¹²³I] sodium iodide (in 0.05 M NaOH) was purchased from GE Healthcare (Cygne, The Netherlands).

Unless otherwise mentioned, the HPLC system used consisted of a Waters 515 HPLC pump, a Waters 2487 UV detector (Waters, Milford, USA), a Ludlum model 2200 scaler ratemeter equipped with a Geiger Müller tube (Ludlum Measurements Inc., Sweetwater, USA), and a Shimadzu C-RSA chromatopac data analyser. Absorption units full scale were set at 0.0001 and wave length was set at 254 nm, unless otherwise mentioned. The columns, mobile phases and flow rates used are indicated in the chapters.

Radioactivity was counted with an automated gamma-ray spectrometer equipped with five 1x1 inch NaI(Tl) crystals (Cobra Autogamma, Packard Canberra) or with a Capintec dose calibrator (CRC-15R, Ramsey, USA).

4.2. Animals

All animal studies were conducted following the principles of laboratory animal care and the Belgian Law on the protection of animals. The performed experiments were approved by the local Ethics Committee of Ghent University.

All wild type mice (FVB and NMRI) and rats (Sprague-Dawley) were purchased from Bioservices or Charles River. The *mdr1a* (-/-) mice were obtained from Taconic (Hudson, USA).

The *mdr1a* (-/-) mouse strain was developed in the laboratory of Dr. Alfred Schinkel from the Netherlands Cancer Institute. Taconic maintained the colony. The *mdr1a* (-/-) mouse strain was healthy and fertile and did not display clear physiological abnormalities or a decreased life span. Mice homozygous for a disruption of the *mdr1a* gene have completely lost all detectable P-gp in brain capillaries. Also P-gp density in gut epithelium is dramatically decreased. They displayed an increase in *mdr1b* RNA in liver and kidney, probably to compensate for the loss of excretory capacity caused by the *mdr1a* disruption (Schinkel et al., 1994; 1997). Since *mdr1a* (-/-) mice were made on a FVB background, the wild type mice used as control group were FVB mice.

4.3. Carbon-11 as radionuclide

4.3.1. GENERAL

Decay of ^{11}C to the stable nuclei ^{11}B occurs for the most part by positron emission (99.8 % by β^+ emission, 0.19 % by electron capture). The maximum kinetic energy of the positron is 0.96 MeV and the mean kinetic energy is 0.385 MeV. A theoretical specific activity of $3.4 \cdot 10^5 \text{ GBq}/\mu\text{mol}$ ($9.2 \cdot 10^3 \text{ Ci}/\mu\text{mol}$) can be obtained for ^{11}C . The short half-life of ^{11}C (20.4 min) demands a fast production of the precursor molecule as well as the radiotracer itself. The several

steps that must be completed to obtain a radiotracer labelled with ^{11}C are depicted in Figure 4.1.

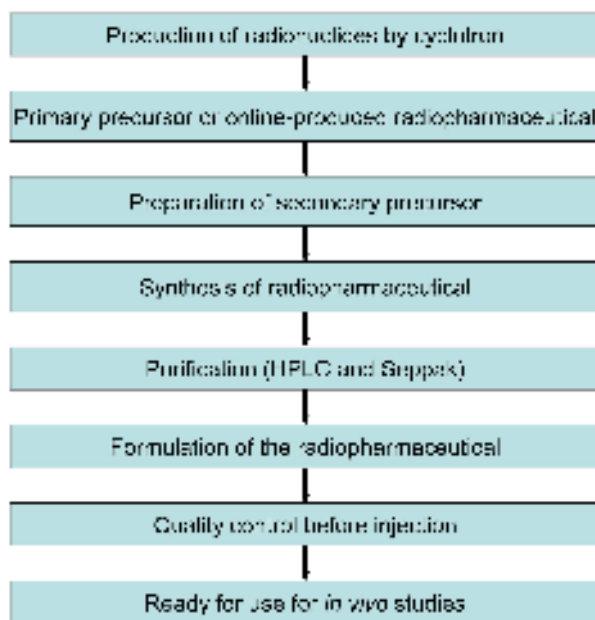


Figure 4.1 Major steps in routine preparation of PET radiopharmaceuticals

The development of a rapid labelling synthesis is often highly dependent on the availability of suitable labelled precursors. For ^{11}C -chemistry, the most used primary precursors are $^{11}\text{CO}_2$ and $^{11}\text{CH}_4$. Regarding secondary precursors, $[^{11}\text{C}]$ methyl triflate and $[^{11}\text{C}]$ methyl iodide are widely used as alkylating agents for the introduction of ^{11}C into organic molecules (Stöcklin and Pike, 1993). In this dissertation $^{11}\text{CH}_4$ is used as primary precursor for the synthesis of $^{11}\text{CH}_3\text{I}$, which is used as such.

4.3.2. PRODUCTION OF $^{11}\text{CH}_4$

$^{11}\text{CH}_4$ was produced in a Cyclone 18 twin cyclotron (IBA, Ghent, Belgium) via the $^{14}\text{N}(p,\alpha)^{11}\text{C}$ reaction induced by irradiation of N_2 gas containing 5 % H_2 with a proton beam (18 MeV, 14 μA) for 20 min.

4.3.3. SYNTHESIS OF $^{11}\text{CH}_3\text{I}$

$^{11}\text{CH}_4$ was transferred from the cyclotron target to a home made synthesis module housed in a hot cell. $^{11}\text{CH}_4$ was trapped on a loop filled with Porapak N (divinylbenzene/vinyl pyrrolidone polymer) that was cooled in liquid argon. Once all $^{11}\text{CH}_4$ was released from the target, the loop was flushed with helium to remove N_2/H_2 and allowed to warm to room temperature. The $^{11}\text{CH}_4$ was swept off the loop with a helium flow and mixed with I_2 vapours at 50°C , after which the mixture was passed through an oven heated to 600°C to yield $^{11}\text{CH}_3\text{I}$. After the reaction, the remaining iodine and produced hydrogen iodide were trapped in ascarite, while $^{11}\text{CH}_3\text{I}$ was collected on a Porapak N trap at room temperature. The unreacted $^{11}\text{CH}_4$ was further circulated until no more $^{11}\text{CH}_3\text{I}$ was produced. $^{11}\text{CH}_3\text{I}$ was released from the Porapak N trap by heating the trap to 120°C .

4.4. Iodine-123 as radionuclide

4.4.1. GENERAL

Iodine-123 decays by electron capture; mainly (83 %) emitting γ -rays with an energy of 159 keV, which makes it a very suitable isotope for diagnostic SPECT imaging. ^{123}I has a theoretical maximum specific activity of 8.769 TBq/ μmol (237 Ci/ μmol).

4.4.2. NUCLEOPHILIC IODINATION

Several distinct mechanisms are possible for nucleophilic iodination depending on the substrate, the leaving group and the reaction conditions. The iodide anion serves as the nucleophile. One possible method is the copper-assisted halogen exchange. Given the relatively low reactivity of nucleophilic aromatic halogen substitution, a copper salt or metal is used as catalyst. For this reaction type, a

wide variety of reaction conditions can be employed. For a detailed review of possible reaction methods and mechanisms see Coenen et al. (2006).

4.4.3. ELECTROPHILIC IODINATION

Electrophilic iodination is a process in which formally a positively charged iodine (I^+) attacks a system with high electron density such as an aromatic ring. As a result a covalent carbon-iodine bond is formed with loss of a positively charged leaving group. The radioiodide can be oxidized *in situ* using chloramine T (Figure 4.2). Under certain conditions, chloramine T can release hypochlorite, which oxidises iodide under formation of an iodonium ion. The reaction is terminated by adding the antioxidant sodium metabisulfite.

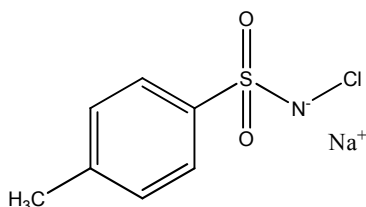


Figure 4.2 Chloramine T

4.5. Experimental procedures

4.5.1. SPECIFIC ACTIVITY

The specific activity of a tracer can be defined as the amount of radioactivity present per mole of product. Specific activity is usually expressed as Ci/ μ mol or GBq/ μ mol.

Tracer amount was determined by HPLC. Tracer activity was determined by Capintec readings. The mass of tracer was calculated by the use of a calibration curve of reference compound. In the case no detectable carrier UV-signal could

be obtained, the detection limit for the compound was used for the calculation of the minimum specific activity.

4.5.2. LOG $D_{7.4}$

The log $D_{7.4}$ value gives an indication about the BBB permeability. The log partition coefficient was measured according to the shake flask method (Wilson et al., 2001; Waterhouse, 2003). An aliquot (10 – 20 μL) of the tracer (185 - 370 kBq (5 - 10 μCi) for ^{123}I tracers and 1.9 - 3.7 MBq (50 - 100 μCi) for ^{11}C tracers) was added to a test tube containing 3 mL n-octanol and 3 mL phosphate buffered saline (PBS) (0.01 M, pH 7.4). The mixture was vigorously shaken by hand for 1 min, vortexed for 2 min and centrifuged for 3 min at 3000 g. 0.5 mL of both phases was taken and placed in separate vials, taking care to avoid cross contamination between the phases. The remaining aqueous phase was discarded and 2.5 mL fresh PBS (0.01 M, pH 7.4) was added to the test tube. The procedure was repeated three more times to give four vials of each phase for measuring radioactivity. The partition coefficient was calculated as [radioactivity in n-octanol (cpm)/radioactivity in phosphate buffer (cpm)].

4.5.3. METABOLITE STUDIES

Activity was injected through a tail vein and the mice were sacrificed at different time points post injection (p.i.). Blood and whole brain were isolated. Blood was collected into a vacutest tube containing 3.6 mg K_3EDTA and was centrifuged at 4000 g for 6 min to separate plasma. 200 μL plasma was mixed with 800 μL CH_3CN whereas the whole brain was mixed with 1.5 mL CH_3CN . Both samples were vortexed for 30 sec and centrifuged at 3000 g for 3 min. Pellet and supernatant were separated and counted for radioactivity. An aliquot (500 μL) of the supernatant obtained from the plasma and brain homogenates was subjected

to HPLC analysis. The HPLC eluate was collected in 0.5 min fractions and their radioactivity was measured.

To determine the recovery as well as the stability of the radiotracer during workup and analysis, control experiments ($n=3$) were done using plasma and brain spiked with authentic radiotracer (2 MBq (54 μ Ci) or 37 kBq (1 μ Ci) for ^{11}C and ^{123}I respectively). Sample workup was done as described above. Results are expressed as percentages of the total activity \pm standard deviation (SD).

4.6. References

- Coenen HH, Mertens J and Maziere B. Radioiodination reactions for radiopharmaceuticals. Published by Springer in 2006.
- Schinkel AH, Smit JJM, van Tellingen O, Beijnen JH, Wagenaar E, van Deemter L et al. Disruption of the mouse *mdr1a* P-glycoprotein gene leads to a deficiency in the blood-brain barrier and to increases sensitivity to drugs. *Cell* 1994; 77:491-502.
- Schinkel AH. The physiological function of drug-transporting P-glycoproteins. *Semin Cancer Biol* 1997; 8:161-70.
- Schinkel AH, Mayer U, Wagenaar E, Mol CAAM, Van Deemter L, Smit JJM et al. Normal viability and altered pharmacokinetics in mice lacking *mdr1*-type (drug-transporting) P-glycoproteins. *Proc Natl Acad Sci USA* 1997; 94:4028-33.
- Stöcklin G and Pike VW. Radiopharmaceuticals for Positron Emission Tomography – Methodological aspects. Kluwer Academic Publishers 1993; 24.
- Waterhouse RN. Determination of lipophilicity and its use as a predictor of blood-brain barrier penetration of molecular agents. *Mol Imaging Biol* 2003; 5:376-389.
- Wilson AA, Garcia A, DaSilva JN, Houle S. An admonition when measuring the lipophilicity of radiotracers using counting techniques. *Appl Rad Isot* 2001; 54:203-8.

Chapter 5

Synthesis and preliminary *in vivo*
evaluation of [¹²³I]-(*S,S*)-IPBM for
mapping the norepinephrine transporter



Chapter 5

Synthesis and preliminary *in vivo* evaluation of [¹²³I]-(*S,S*)-IPBM for mapping NET

5.1. Abstract

Aim: Abnormalities in brain NET have been implicated in the pathophysiology of various neuropsychiatric diseases and neurodegenerative disorders. A selective radioligand for mapping NET could further probe the link between NET and these disorders. This study reports the development and preliminary evaluation of (*S,S*)-2-[α -(2-[¹²³I]-iodophenoxy)benzyl]morpholine ([¹²³I]-(*S,S*)-IPBM).

Methods: Precursor and reference compounds were synthesized by a stereoselective nine-step synthetic procedure. Enantiomeric purity was investigated using NMR spectroscopy. [¹²³I]-(*S,S*)-IPBM was obtained by electrophilic iododestannylation followed by reduction. A biodistribution study was performed in male NMRI mice.

Results: The precursor was prepared in an overall chemical yield of 8 % with an enantiomeric excess of > 95 %. Radiosynthesis afforded [¹²³I]-(*S,S*)-IPBM with a radiochemical purity of > 98 % and a specific activity of > 148 GBq/ μ mol. Biodistribution studies demonstrated high brain uptake (4.62 ± 0.66 % ID/g at 1 min p.i.) followed by efficient wash-out (0.55 ± 0.17 % ID/g at 180 min p.i.).

Conclusion: [¹²³I]-(*S,S*)-IPBM displayed an excellent brain-blood distribution. Since [¹²³I]-(*S,S*)-IPBM was reported by others at the moment we performed our biodistribution studies, we did not conduct any further evaluation. Regarding their results, the choice to develop [¹²³I]-(*S,S*)-IPBM as a radiotracer for NET was an excellent suggestion.

5.2. Introduction

The norepinephrine transporter (NET), which is located at the pre-synaptic terminal of noradrenergic neurons, belongs to the superfamily of the Na⁺/Cl⁻ dependent neurotransmitter transporters (Masson et al., 1999). The principal physiological role of NET is to regulate the noradrenergic neurotransmission by re-uptake of norepinephrine into the presynaptic neuron. Abnormalities in brain NET have been implicated in the pathophysiology of various neuropsychiatric diseases and neurodegenerative disorders including mood disorders (Ressler and Nemeroff, 1999), ADHD (Biederman and Spencer, 1999), depression (Klimek et al., 1997) and Alzheimer's disease (Tejani-Butt et al., 1993). A selective radioligand able to image and quantify NET density with PET or SPECT would provide more insight in the role of noradrenergic mechanisms in these disorders. At the start of this thesis, no suitable radioligand for SPECT imaging had been designed so far, directing our focus to the development of a selective radioiodinated NET radioligand. Due to the low density and widespread distribution of NET-binding sites in the brain, the design of a suitable NET radioligand is very challenging.

Although nisoxetine is selective for NET *in vitro*, [¹¹C]nisoxetine exhibits a very high level of non-specific binding *in vivo* (Haka et al., 1989). An iodinated analogue of nisoxetine was developed and it displayed superior *in vitro* properties compared to nisoxetine. Just as [¹¹C]nisoxetine, (*R*)-[¹²⁵I]2-iodonisosoxetine displayed high non-specific binding *in vivo* resulting in a high background uptake (Kiyono et al., 2004; Kung et al., 2004). Reboxetine is a more potent and selective inhibitor of NET and is on the market as an antidepressant (Edronax®). The (*S,S*) enantiomer of reboxetine is approximately 24 times more potent than the (*R,R*) enantiomer (Benedetti et al., 1995). Replacement of the methoxy moiety of nisoxetine by iodine resulted in enhanced *in vitro* properties. Since reboxetine structurally resembles nisoxetine, it was suggested that the same effect would be observed when substituting the ethoxy group of reboxetine by iodine. This idea

prompted us to the development and preliminary evaluation of [^{123}I]-(*S,S*)-2-[α -(2-iodophenoxy)benzyl]morpholine ([^{123}I]-(*S,S*)-IPBM) (Figure 5.1).

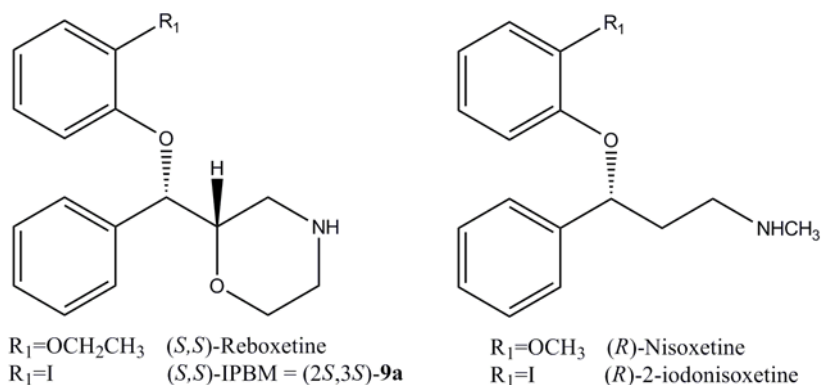


Figure 5.1 Chemical structures of Reboxetine and Nisoxetine analogues

5.3. Materials & Methods

5.3.1. ORGANIC SYNTHESIS

^1H NMR spectra were recorded on a Varian 300 MHz FT-NMR spectrometer (Laboratory for Medicinal chemistry, Ghent University, Belgium). Chemical shifts were recorded in ppm (δ) relative to an internal tetramethylsilane (TMS) standard in either deuterated DMSO or CDCl_3 . J (Hz) assignments of ^1H resonance coupling were done. Mass spectrometry was performed on a Waters Micromass ZMD mass spectrometer with an electrospray ionization (ESI) probe. Samples were dissolved in $\text{MeOH} - \text{H}_2\text{O} - \text{HCOOH}$ (50 – 50 – 0.1) and recorded in the positive (MH $^+$) mode.

(2*S*,3*S*)-phenylglycidol was purchased from Speedchemical Co. LTD (Shanghai, China). All other chemicals were obtained from Acros (Geel, Belgium) or Sigma-Aldrich (Bornem, Belgium). Organic reactions were performed under nitrogen atmosphere using anhydrous solvents and were monitored by normal phase thin layer chromatography (TLC) by UV detection at 254 nm (TLC, Polygram SIL

G/UV254, 200 μm, Machery-Nagel, Germany). Purification of organic compounds was achieved with column chromatography on silica gel (70-230 mesh, 60Å, Sigma-Aldrich, Belgium). Solvent systems are indicated in the text. For mixed solvent systems, ratios are given with respect to volumes

5.3.1.1. Cold reference compound synthesis

(*S,S*)-IPBM or (2*S,3S*)-**9a** was synthesized based on the synthetic procedure outlined by Melloni et al. (1985). Since (*R,R*) and (*S,S*) enantiomers were synthesized in the same manner, only the preparation of the (*S,S*) enantiomers is described

(2*S,3R*)/(2*R,3S*)-1,2-dihydroxy-3-(2-bromophenoxy)-3-phenylpropane (1a)

A mixture of 2-iodophenol (6.6 g, 30 mmol), methyltributylammonium chloride (0.6 mL) and 0.05 M NaOH (30 mL) was stirred at 70°C for 2 h. (2*R,3R*)-phenylglycidol (1.5 g, 10 mmol, dissolved in 50 mL H₂O) was added drop-wise and the resulting mixture was heated for another 3 h. The reaction mixture was cooled to room temperature, added to ice-cold NaOH (1 M, 30 mL) and extracted with CH₂Cl₂ (3 x 50 mL). The organic layer was washed with 1 M NaOH (100 mL), water (100 mL) and brine (100 mL) and dried over Na₂SO₄. The solvent was removed under reduced pressure to give viscous oil. The crude product was purified by column chromatography (eluent: ethyl acetate/hexane 30/70) to yield 9.5 mmol of (2*R,3S*)-**1a** (95 %).

¹H NMR (DMSO): δ 3.70-3.55 (m, 2H, R-CH₂-OH), 3.8 (m, 1H, R₂-CH-OH), 4.65 (t, 1H, *J* = 5.6, R-CH₂-OH), 4.95 (d, 1H, *J* = 5.6, R₂-CH-OH), 5.32 (d, 1H, *J* = 6.2, Ar-O-CH-R), 7.74-6.58 (m, 9H, Ar-H). ESI-MS: calcd MW for C₁₅H₁₅O₃I: 370, found 393 [M + Na⁺].

(2*S*,3*R*)/(2*R*,3*S*)-2-hydroxy-3-(2-iodophenoxy)-1-(*t*-butyldimethylsilyloxy)-3-phenylpropane (2a)

tert-Butyldimethylsilyl chloride (1.6 g, 10.6 mmol) dissolved in 5 mL DMF was added drop-wise to an ice-cold solution of (2*R*,3*S*)-**1a** (3.5 g, 9.5 mmol) and imidazole (1.6 g, 23.8 mmol) in DMF (8 mL). After stirring for 80 min at 0°C, the reaction mixture was added to a separatory funnel containing 100 mL water and 100 mL ethyl acetate. After extraction, the organic layer was dried over Na₂SO₄ and evaporated to give a crude oil, which was used without further purification.

(2*S*,3*R*)/(2*R*,3*S*)-3-(2-iodophenoxy)-2-mesyloxy-1-(*t*-butyldimethylsilyloxy)-3-phenylpropane (3a)

A mixture of crude (2*R*,3*S*)-**2a** (9.5 mmol), Et₃N (1.95 mL, 14 mmol) and ethyl acetate (15 mL) was stirred at 0°C. Methanesulfonyl chloride (0.882 mL, 11.4 mmol) was dissolved in ethyl acetate (5 mL) and added to the reaction mixture over 30 min. Afterwards, the mixture was stirred for an additional 2 h at 0°C. The organic layer was washed with water, dried over Na₂SO₄ and evaporated. The resulting crude oil, (2*R*,3*S*)-**3a**, was used without further purification.

(2*S*,3*R*)/(2*R*,3*S*)-3-(2-iodophenoxy)-2-mesyloxy-3-phenyl-1-propanol (4a)

A solution of crude (2*R*,3*S*)-**3a** (9.5 mmol), THF (30 mL) and 1 M tetrabutylammonium fluoride solution in THF (15 mL) was stirred for 30 min at room temperature. The reaction was quenched with water (5 mL). The layers were separated and the aqueous layer was extracted with CH₂Cl₂. The combined organic extract was washed with brine (2 x 100 mL), dried over Na₂SO₄, and the solvent removed under reduced pressure to afford a crude residue. The residue was purified with column chromatography (eluent: 30 % ethyl acetate/hexane) to yield 8.7 mmol (92 % over the three steps) (2*R*,3*S*)-**4a**.

¹H NMR (CDCl₃): δ 2.7 (s, 3H, S-CH₃), 4.02 (dd, 1H, *J* = 3.0, 12.6, R-CH₂-OH), 4.23 (dd, 1H, *J* = 5.4, 12.6, R-CH₂-OH), 4.88 (m, 1H, R₂-CH-OMs), 5.5 (d, 1H, *J* = 5.7, Ar-O-CH-R), 7.7 - 6.5 (m, 9H, Ar-H). ESI-MS: calcd MW for C₁₆H₁₇O₅SI: 448, found 449 [M + H⁺].

(2*R*,3*R*)/(2*S*,3*S*)-1,2-epoxy-3-(2-iodophenoxy)-3-phenylpropane (5a)

A solution of the mesylate (2*R*,3*S*)-**4a** (3.9 g, 8.7 mmol), toluene (20 mL), 4 M NaOH (20 mL) and methyltributylammonium chloride (2.45 mL, 10 μmol) was stirred vigorously for 2 h at room temperature. The solution was diluted with water (50 mL) and the product was extracted into CH₂Cl₂ (3 x 50 mL). The organic layer was dried over Na₂SO₄, evaporated under reduced pressure followed by purification of the product using column chromatography to afford (2*S*,3*S*)-**5a** (5 mmol, 57 %).

¹H NMR (CDCl₃): δ 2.81 (m, 2H, R-O-CH₂-CH-R), 3.48 (m, 1H, Ar-O-CH-CH-R), 4.95 (d, 1H, *J* = 6.0, Ar-O-CH-R), 7.8-6.6 (m, 9H, Ar-H). ESI-MS: calcd MW for C₁₅H₁₃O₂I: 352, found 353 [M + H⁺].

(2*R*,3*R*)/(2*S*,3*S*)-1-amino-2-hydroxy-3-(2-iodophenoxy)-3-phenylpropane (6a)

A solution of (2*S*,3*S*)-**5a** (1.76 g, 5 mmol) in MeOH (35 mL) and 30 % NH₄OH (20 mL) was stirred overnight. The solution was diluted with saturated NaHCO₃ and extracted with CH₂Cl₂. After filtering over Na₂SO₄, CH₂Cl₂ was removed under reduced pressure. Purification with column chromatography (5:95 MeOH:CH₂Cl₂) yielded (2*S*,3*S*)-**6a** (3.6 mmol, 72 %).

¹H NMR (DMSO): δ 2.38 (dd, 1H, *J* = 8.1, 12.6, R-CH₂-NH₂), 2.58 (dd, 1H, *J* = 3.9, 12.9, R-CH₂-NH₂), 3.88 (m, 1H, R-CH-OH), 5.42 (d, 1H, *J* = 5.7, Ar-O-CH-R), 7.8 - 6.61 (m, 9H, Ar-H). ESI-MS: calcd MW for C₁₅H₁₆NO₂I: 369, found 370 [M + H⁺].

(2*R*,3*R*)/(2*S*,3*S*)-1-chloroacetylamino-2-hydroxy-3-(2-iodophenoxy)-3-phenylpropane (7a)

The amine (*2S,3S*)-**6a** (1.3 g, 3.6 mmol) was dissolved in CH₂Cl₂ (16 mL) and Et₃N (0.626 mL, 4.5 mmol). The solution was kept at -10°C and chloroacetyl chloride (0.318 mL, 4 mmol) dissolved in CH₂Cl₂ (7 mL) was added slowly followed by stirring for 1 h. The solution was quenched with water and subsequently extracted with ethyl acetate. The combined ethyl acetate portion was dried over Na₂SO₄, and the solvent was removed under reduced pressure to afford a crude oil. The crude product was purified by column chromatography (eluent 35:65 ethyl acetate:hexane) to give 2.9 mmol (81 %) of (*2S,3S*)-**7a**.

¹H NMR (DMSO): δ 2.9 - 3 (ddd, 1H, *J* = 5.4, 8.4, 13.2, R-NH-CH₂-R), 3.25 - 3.45 (ddd, 1H, *J* = 3.9, 6.0, 13.5, R-NH-CH₂-R), 3.95 (m, 1H, R-CH-OH), 4.03 (s, 2H, R-CH₂-Cl), 5.42 (d, 1H, *J* = 5.1, Ar-O-CH-R), 7.72-6.60 (m, 9H, Ar-H), 8.12 (t, 1H, R-NH-R). ESI-MS: calcd MW for C₁₇H₁₇NO₃Cl: 445, found 468 [M + Na⁺].

(2*R*,3*R*)/(2*S*,3*S*)-2-[α-(2-iodophenoxy)benzyl]morpholine-5-one (8a)

A solution of (*2S,3S*)-**7a** (1.3 g, 2.9 mmol) in *t*-butanol (4 mL) and CH₂Cl₂ (9 mL) was added drop-wise over 1 h to a solution of potassium *t*-butoxide (0.52 g, 4.6 mmol) in *t*-butanol (12 mL). The mixture was stirred for one more hour, neutralized with 10 % HCl and extracted with CH₂Cl₂. The organic layer was then dried over Na₂SO₄, and evaporated. The crude product was purified by column chromatography (eluent 50:50 ethyl acetate:hexane) to yield (*2S,3S*)-**8a** (2.3 mmol, 79 %).

¹H NMR (DMSO): δ 2.78 (dt, 1H, *J* = 3.9, 12.0, R-NH-CH₂-R), 3.25 (t, 1H, *J* = 11.7, R-NH-CH₂-R), 3.97 (d, 1H, *J* = 12.3, R-O-CH₂-R), 4.05 (d, 1H, *J* = 12.6, R-O-CH₂-R), 4.15 (ddd, 1H, *J* = 3.3, 6.0, 10.5, R-CH-CH₂-NH-R), 5.61 (d, 1H, *J* =

5.1, Ar-O-CH-R), 7.72 - 6.56 (m, 9H, Ar-H), 7.92 (d, 1H, R-NH-R). ESI-MS: calcd MW for C₁₇H₁₆NO₃I: 409, found 448 [M + K⁺].

(2*R*,3*R*)/(2*S*,3*S*)-2-[α -(2-iodophenoxy)benzyl]morpholine (9a)

A mixture of (2*S*,3*S*)-**8a** (0.94 g, 2.3 mmol) and BH₃ (12 mL of a 1 M solution in THF) in THF (30 mL) was stirred for 2 h at room temperature. The mixture was added to acetic acid (50 % in water, 20 mL) and THF was evaporated. Potassium carbonate was added until a pH of 9 was reached and the resulting solution was extracted with CH₂Cl₂. The combined CH₂Cl₂ fractions were dried over Na₂SO₄, concentrated under reduced pressure and then purified by column chromatography (eluent 15:85 ethyl acetate:hexane) to yield (2*S*,3*S*)-**9a**, also termed (*S,S*)-IPBM (0.7 mmol, 30 %) as a colourless oil.

¹H NMR (CDCl₃): δ 2.45 (m, 1H, R-O-CH₂-CH₂-R), 2.61 (m, 1H, R-O-CH₂-CH₂-R), 3.04 (m, 2H, R-O-CH₂-R), 3.58 (m, 1H, R-CH-CH₂-NH-R), 3.90 (ddd, 1H, *J* = 2.1, 5.1, 11.4, R-CH-CH₂-NH-R), 4.00 (dd, 1H, *J* = 3.6, 5.4, R-CH-CH₂-NH-R), 5.17 (d, 1H, *J* = 5.1, Ar-O-CH-R), 7.43-6.59 (m, 9H, Ar-H). ESI-MS: calcd MW for C₁₇H₁₈NO₂I: 395, found 396 [M + H⁺].

5.3.1.2. *Precursor synthesis*

(2*S*,3*S*)-**9b** was synthesized in the same manner as (2*S*,3*S*)-**9a**, using 2-bromophenol as a starting material instead of 2-iodophenol.

(2*S*,3*R*)/(2*R*,3*S*)-1,2-dihydroxy-3-(2-bromophenoxy)-3-phenyl-propane (1b)

A mixture of 2-bromophenol (3.5 mL, 30 mmol), methyltributylammonium chloride (0.6 mL) and 0.05 M NaOH (30 mL) was stirred at 70°C for 2 h. (2*R*,3*R*)-phenylglycidol (1.5 g, 10 mmol dissolved in 50 mL H₂O) was added drop-wise and the resulting mixture was heated for another 3 h. The reaction

mixture was cooled to room temperature, added to ice-cold NaOH (1 M, 30 mL) and extracted with CH₂Cl₂ (3 x 50 mL). The organic layer was washed with 1 M NaOH (100 mL), water (100 mL) and brine (100 mL), dried over Na₂SO₄, and the solvent was removed under reduced pressure to afford a viscous oil. The crude product was purified by column chromatography (eluent: ethyl acetate/hexane 30/70) to give 9 mmol of (*2R,3S*)-**1b** (90 %).

¹H NMR (DMSO): δ 3.70-3.55 (m, 2H, R-CH₂-OH), 3.78 (m, 1H, R₂-CH-OH), 4.65 (t, 1H, *J* = 5.6, R-CH₂-OH), 4.94 (d, 1H, *J* = 5.6, R₂-CH-OH), 5.32 (d, 1H, *J* = 6.2, Ar-O-CH-R), 7.56-6.8 (m, 9H, Ar-H). ESI-MS: calcd MW for C₁₅H₁₅O₃Br: 323, found 346 [M + Na⁺].

(*2S,3R*)/(*2R,3S*)-2-hydroxy-3-(2-bromophenoxy)-1-(*t*-butyldimethylsilyloxy)-3-phenylpropane (2b**)**

tert-Butyldimethylsilyl chloride (1.6 g, 10.6 mmol) dissolved in 5 mL DMF, was added drop-wise to an ice-cold solution of (*2R,3S*)-**1b** (2.9 g, 9 mmol) and imidazole (1.5 g, 22.1 mmol) in DMF (8 mL). After stirring for 80 min at 0°C, the reaction mixture was added to a separatory funnel containing 100 mL water and 100 mL ethyl acetate. After extraction, the organic layer was dried over Na₂SO₄ and evaporated to afford a crude oil, which was used without further purification.

(*2S,3R*)/(*2R,3S*)-3-(2-bromophenoxy)-2-mesyloxy-1-(*t*-butyldimethylsilyloxy)-3-phenylpropane (3b**)**

A mixture of crude (*2R,3S*)-**2b** (9 mmol), Et₃N (1.9 mL, 13.7 mmol) and ethyl acetate (11 mL) was stirred at 0°C. Methanesulfonyl chloride (0.831 mL, 10.7 mmol) was dissolved in ethyl acetate (5 mL) and added to the reaction mixture over 30 min. Afterwards, the mixture was stirred for an additional 2 h at 0°C. The organic layer was washed with water, dried over Na₂SO₄ and evaporated. The resulting crude oil, (*2R,3S*)-**3b**, was used without further purification.

(2*S*,3*R*)/(2*R*,3*S*)-3-(2-bromophenoxy)-2-mesyloxy-3-phenyl-1-propanol (4b)

A solution of crude (2*R*,3*S*)-**3b** (9 mmol), THF (27 mL) and 1 M tetrabutylammonium fluoride solution in THF (14.7 mL) was stirred for 30 min at room temperature. The reaction was quenched with water (5 mL). The layers were separated and the aqueous layer was extracted with CH₂Cl₂. The combined organic extract was washed with brine (2 x 100 mL), dried over Na₂SO₄, and the solvent was removed under reduced pressure to offer a crude residue. The residue was purified with column chromatography (eluent: 30 % ethyl acetate/hexane) to yield 8 mmol (89 % over the three steps) (2*R*,3*S*)-**4b**.

¹H NMR (CDCl₃): δ 2.65 (s, 3H, S-CH₃), 4.02 (dd, 1H, *J* = 3.0, 12.6, R-CH₂-OH), 4.22 (dd, 1H, *J* = 5.4, 12.6, R-CH₂-OH), 4.88 (m, 1H, R₂-CH-OMs), 5.50 (d, 1H, *J* = 5.7, Ar-O-CH-R), 7.46 - 6.62 (m, 9H, Ar-H). ESI-MS: calcd MW for C₁₆H₁₇O₅SBr: 401, found 402 [M + H⁺].

(2*R*,3*R*)/(2*S*,3*S*)-1,2-epoxy-3-(2-bromophenoxy)-3-phenylpropane (5b)

A solution of the mesylate (2*R*,3*S*)-**4b** (3.2 g, 8 mmol), toluene (18.6 mL), 4 M NaOH (18.6 mL) and methyltributylammonium chloride (2.26 mL, 9 μmol) was stirred vigorously for 2 h at room temperature. The solution was diluted with water (50 mL) and the product was extracted into CH₂Cl₂ (3 x 50 mL). The organic layer was dried over Na₂SO₄, evaporated under reduced pressure followed by purification of the product using column chromatography to afford (2*S*,3*S*)-**5b** (5.5 mmol, 69 %).

¹H NMR (CDCl₃): δ 2.81 (m, 2H, R-O-CH₂-CH-R), 3.48 (m, 1H, Ar-O-CH-CH-R), 4.95 (d, 1H, *J* = 6, Ar-O-CH-R), 7.46 - 6.62 (m, 9H, Ar-H). ESI-MS: calcd MW for C₁₅H₁₃O₂Br: 305, found 328 [M + Na⁺].

(2*R*,3*R*)/(2*S*,3*S*)-1-amino-2-hydroxy-3-(2-bromophenoxy)-3-phenylpropane (6b)

A solution of (*2S,3S*)-**5b** (1.7 g, 5.5 mmol) in MeOH (35 mL) and 30 % NH₄OH (24 mL) was stirred overnight. The solution was diluted with saturated NaHCO₃ and extracted with CH₂Cl₂. After filtering over Na₂SO₄, CH₂Cl₂ was removed under reduced pressure. Purification with column chromatography (5:95 MeOH:CH₂Cl₂) yielded (*2S,3S*)-**6b** (3.7 mmol, 67 %).

¹H NMR (DMSO): δ 2.31 (dd, 1H, *J* = 8.1, 12.6, R-CH₂-NH₂), 2.61 (dd, 1H, *J* = 3.9, 12.9, R-CH₂-NH₂), 3.79 (m, 1H, R-CH-OH), 5.05 (bs, 2H, NH₂), 5.42 (d, 1H, *J* = 5.7, Ar-O-CH-R), 7.56 - 6.75 (m, 9H, Ar-H). ESI-MS: calcd MW for C₁₅H₁₆O₂NBr: 322, found 323 [M + H⁺].

(2*R*,3*R*)/(2*S*,3*S*)-1-chloroacetyl-amino-2-hydroxy-3-(2-bromophenoxy)-3-phenylpropane (7b)

The amine (*2S,3S*)-**6b** (1.2 g, 3.7 mmol) was dissolved in CH₂Cl₂ (16 mL) and Et₃N (0.626 mL, 4.5 mmol). The solution was kept at -10°C and chloroacetyl chloride (0.318 mL, 4 mmol) dissolved in CH₂Cl₂ (7 mL) was added slowly followed by stirring for 1 h. The solution was quenched with water and subsequently extracted with ethyl acetate. The combined ethyl acetate portion was dried over Na₂SO₄, and the solvent was removed under reduced pressure to afford a crude oil. The crude product was purified by column chromatography (eluent 35:65 ethyl acetate:hexane) to give 2.7 mmol (73 %) of (*2S,3S*)-**7b**.

¹H NMR (DMSO): δ 2.87 – 2.94 (ddd, 1H, *J* = 5.4, 8.4, 13.2, R-NH-CH₂-R), 3.25 – 3.45 (ddd, 1H, *J* = 3.9, 6.0, 13.5, R-NH-CH₂-R), 3.95 (m, 1H, R-CH-OH), 4.03 (s, 2H, R-CH₂-Cl), 5.42 (d, 1H, *J* = 5.1, Ar-O-CH-R), 7.56 - 6.74 (m, 9H, Ar-H), 8.12 (t, 1H, R-NH-R). ESI-MS: calcd MW for C₁₇H₁₇O₃NCIBr: 398, found 421 [M + Na⁺].

(2*R*,3*R*)/(2*S*,3*S*)-2-[α -(2-bromophenoxy)benzyl]morpholine-5-one (8b**)**

A solution of (2*S*,3*S*)-**7b** (1.1 g, 2.7 mmol) in *t*-butanol (3.5 mL) and CH₂Cl₂ (8.6 mL) was added drop-wise over 1 h to a solution of potassium *t*-butoxide (482 mg, 4.3 mmol) in *t*-butanol (10.8 mL). The mixture was then stirred for one more hour, neutralized with 10 % HCl and extracted with CH₂Cl₂. The organic layer was then dried over Na₂SO₄, and evaporated. The crude product was purified by column chromatography (eluent 50:50 ethyl acetate:hexane) to yield compound (2*S*,3*S*)-**8b** (2.1 mmol, 78 %).

¹H NMR (DMSO): δ 2.78 (dt, 1H, $J = 3.9, 12.3$, R-NH-CH₂-R), 3.25 (t, 1H, $J = 11.7$, R-NH-CH₂-R), 3.97 (d, 1H, $J = 12.3$, R-O-CH₂-R), 4.05 (d, 1H, $J = 12.6$, R-O-CH₂-R), 4.15 (ddd, 1H, $J = 3.3, 6.0, 10.5$, R-CH-CH₂-NH-R), 5.61 (d, 1H, $J = 5.1$, Ar-O-CH-R), 7.54 - 6.74 (m, 9H, Ar-H), 7.92 (d, 1H, R-NH-R). ESI-MS: calcd MW for C₁₇H₁₆O₃NBr: 362, found 401 [M + K⁺].

(2*R*,3*R*)/(2*S*,3*S*)-2-[α -(2-bromophenoxy)benzyl]morpholine (9b**)**

A mixture of (2*S*,3*S*)-**8b** (0.76 g, 2.1 mmol) and 1 M BH₃ solution in THF (11 mL) in THF (30 mL) was stirred for 2 h at room temperature. The mixture was added to acetic acid (50 % in water, 20 mL) and THF was evaporated. Potassium carbonate was added until pH of 9 was reached and the resulting solution was extracted with CH₂Cl₂. The combined CH₂Cl₂ fractions were dried over Na₂SO₄, concentrated under reduced pressure and then purified by column chromatography (eluent 15:85 ethyl acetate:hexane) to give (2*S*,3*S*)-**9b** (0.8 mmol, 38 %) as a colourless oil.

¹H NMR (CDCl₃): δ 2.52 (m, 1H, R-O-CH₂-CH₂-R), 2.68 (m, 1H, R-O-CH₂-CH₂-R), 3.14 (m, 2H, R-O-CH₂-R), 3.68 (td, 1H, $J = 2.1, 12.6$, R-CH-CH₂-NH-R), 3.90 (ddd, 1H, $J = 2.1, 5.1, 11.4$, R-CH-CH₂-NH-R), 4.08 (dd, 1H, $J = 3.6, 5.4$, R-CH-CH₂-NH-R), 5.25 (d, 1H, $J = 5.1$, Ar-O-CH-R), 7.52 - 6.68 (m, 9H, Ar-H). ESI-MS: calcd MW for C₁₇H₁₈O₂NBr: 348, found 349 [M + H⁺].

(2*R*,3*R*)/(2*S*,3*S*)-2-[α -(2-trimethylstannanephenoxy)benzyl]morpholine-5-one (10)

0.06 mmol (2*S*,3*S*)-**8b** (23 mg), hexamethyldistannane (37 μ L, 0.18 mmol), and a catalytic amount of tetrakis(triphenylphosphine)palladium were dissolved in 5 mL toluene. The mixture was shielded from light and refluxed overnight. The reaction mixture was filtered and the solvent was evaporated under reduced pressure. Purification of the crude product with preparative TLC (eluent 90:10 ethyl acetate:hexane) afforded (2*S*,3*S*)-**10** (0.021 mmol, 35 %) as a yellow oil.

¹H NMR (DMSO): δ 0.27 (s, 9H, 3*Sn-CH₃) 2.78 (m, 1H, R-NH-CH₂-R), 3.25 (m, 1H, R-NH-CH₂-R), 4.18-3.98 (m, 3H, R-CH-O-CH₂-R), 5.61 (d, 1H, *J* = 5.4, Ar-O-CH-R), 7.49 - 6.85 (m, 9H, Ar-H). ESI-MS: calcd MW for C₂₀H₂₅O₃NSn: 445, found 446 [M + H⁺].

5.3.2. ENANTIOMERIC PURITY

The enantiomeric purity of the precursor was evaluated using a Bruker DRX500 300 Mhz NMR spectrometer (Department of Organic Chemistry, Ghent University, Belgium). Chemical shifts were recorded in ppm (δ) relative to an internal TMS standard in CDCl₃. To control enantiomeric purity, 1 equivalent chiral shift reagents, europium tris[3-(heptafluoropropylhydroxymethylene)-(-)-camphorate] (Eu(hfc)₃) was added to the NMR sample.

5.3.3. RADIOCHEMISTRY

[¹²³I]-(*S,S*)-IPBM was obtained in two steps. First, an electrophilic iododestannylation on the trimethylstannylprecursor (2*S*,3*S*)-**10** was accomplished. In the following step, [¹²³I]-2*S*,3*S*)-**8a** was reduced to yield [¹²³I]-(*S,S*)-IPBM.

The precursor (*2S,3S*)-**10** (200 µg, 0.45 µmol) was dissolved in absolute ethanol (50 µL). Chloramine-T (1.0 µmol, 15 µL of a 20 mg/ml aqueous solution), n.c.a. [¹²³I]NaI (dissolved in 0.05 M NaOH, 5 – 10 µL, 37 - 185 MBq), and glacial acetic acid (5 µL) were added. The radiolabelling proceeded for 10 min at room temperature. The reaction was quenched by the addition of sodium metabisulfite (1.6 µmol, 15 µL of a 20 mg/ml aqueous solution). After the solution was evaporated under nitrogen stream, 100 µL THF and 50 µL BH₃ (1 M solution in THF) were added to the ice-cold reaction vessel. The mixture was allowed to react during 40 min at room temperature. HPLC mobile phase was added (100 µL CH₃CN:H₂O:HCOOH 55:45:0.1) and the mixture was injected onto a RP C₁₈ HPLC column (Alltima, 250 mm * 4.6 mm, 5 µm) for purification at a flow rate of 1 mL/min. The fraction corresponding to [¹²³I]-(*S,S*)-IPBM (T_r = 21 min) was collected, diluted with sterile water and concentrated on an activated C₁₈ Sep-pak cartridge (Alltech Maxi-Clean Prevail C₁₈). [¹²³I]-(*S,S*)-IPBM was eluted from the Sep-pak column with 1 mL EtOH. Finally the EtOH was diluted with physiological saline to obtain an injectable solution (< 10 % (v:v) EtOH).

5.3.4. QUALITY CONTROL

The radioanalytical data were obtained by injecting 100 µL test solution on an analytical RP-HPLC (Alltima C₁₈, 250 mm x 4.6 mm, 5 µm) using 55:45:0.1 (v:v) - CH₃CN:H₂O:HCOOH as mobile phase at a flow rate of 1 mL/min. Radiochemical purity and identity was determined by co-injection of an aliquot of [¹²³I]-(*S,S*)-IPBM with authentic cold reference product.

A calibration curve between 10 x 10⁻³ µM and 0.1 x 10⁻³ µM and subsequently a more detailed calibration curve between 0.6 x 10⁻³ µM and 0.1 x 10⁻³ µM was determined. Log D_{7.4} was determined according to the method described in Chapter 4.

5.3.5. BIODISTRIBUTION STUDY

Male NMRI mice of 5 - 7 weeks old, weighing 22 - 26 g were injected in a tail vein with 200 μ L 8:92 (v:v) - EtOH:physiological saline containing approximately 185 kBq (5 μ Ci) [¹²³I]-(*S,S*)-IPBM. The mice were awake during the injection. At various time points p.i. mice ($n=3$ for each time point) were sacrificed under isoflurane anaesthesia and dissected. Blood, urine and organs were removed, weighed and counted for radioactivity in a gamma counter. To remove adhering blood, all organs were rinsed with water prior to weighing and counting. For calculation of the injected dose, five aliquots of the injection solution were weighed and counted for activity. Results are decay corrected and expressed as a percentage of the injected dose per gram of tissue (% ID/g) \pm SD.

5.4. Results & Discussion

5.4.1. ORGANIC SYNTHESIS

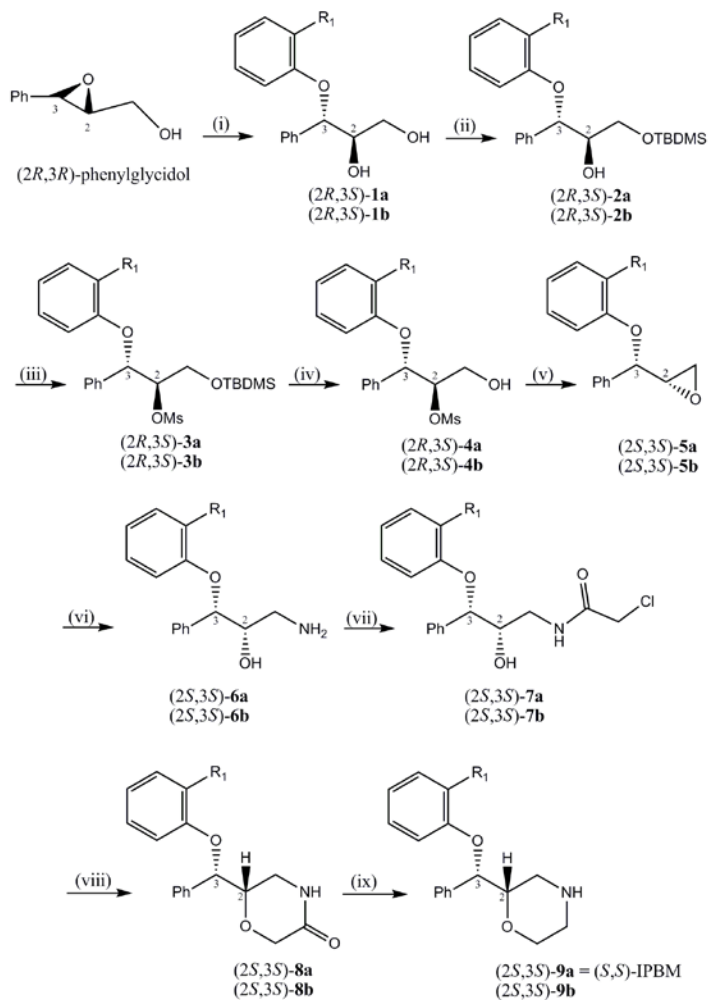


Figure 5.2 Synthesis of halogenated reboxetine analogues

a $\text{R}_1=\text{I}$; **b** $\text{R}_1=\text{Br}$ Reagents: (i) 2-halogenated phenol, aq. NaOH; (ii) *t*-butyldimethylsilyl chloride, DMF, imidazole; (iii) methanesulfonyl chloride, Et_3N , ethyl acetate; (iv) tetrabutylammonium chloride, THF; (v) aq. NaOH, toluene; (vi) 30 % NH_4OH , MeOH; (vii) chloroacetylchloride, Et_3N , CH_2Cl_2 ; (viii) potassium *t*-butoxide, *t*-butanol; (ix) BH_3 , THF

The same procedure by which we were able to synthesize (*S,S*)-IPBM, was also applied to synthesize (*R,R*)-IPBM, (*2S,3S*)-**9b** and (*2R,3R*)-**9b** (Figure 5.2).

The key stereogenic centers of (*S,S*)-IPBM were created by regioselective ring opening with 2-iodophenol of the enantiomerically pure starting compound, (*2R,3R*)-phenylglycidol. The resulting diol, (*2R,3S*)-**1a** was isolated in a 95 % yield. The primary hydroxyl group of (*2R,3S*)-**1a** was selectively protected with a trimethylsilyl group to give (*2R,3S*)-**2a**. Compound (*2R,3S*)-**4a** (yield of 92 %) was prepared by reaction of the secondary hydroxyl group of **2a** with methanesulfonyl chloride, followed by removal of the trimethylsilyl group with tetrabutylammonium fluoride. Treatment of (*2R,3S*)-**4a** with NaOH in toluene afforded the epoxide (*2S,3S*)-**5a** in 57 % yield. This reaction occurred via an S_N2 mechanism resulting in inversion of configuration at the chiral C2 carbon. Consequently the configuration changed from (*2R,3S*) to (*2S,3S*). The reaction of (*2S,3S*)-**5a** with NH₄OH in MeOH yielded the amino alcohol (*2S,3S*)-**6a** (72 %). Compound (*2S,3S*)-**6a** was then transformed into the final morpholine in three steps. Treatment of (*2S,3S*)-**6a** with chloroacetyl chloride to give compound (*2S,3S*)-**7a** (81 % yield) was followed by cyclization with potassium *t*-butyl oxide. The resulting morpholinone (*2S,3S*)-**8a** (79 % yield) was then reduced to give (*2S,3S*)-**9a** in a 30 % yield by the use of BH₃. Several reducing agents were tested but most of them tended to dehalogenate the phenyl group as well. (*2S,3S*)-**9a** was synthesized in an overall chemical yield of 7 % whereas (*2S,3S*)-**9b** was obtained with a 8 % overall chemical yield. The low general chemical yields are a result of the low yield in the final step. Excluding the last step the overall chemical yields were 23 % and 21 % for (*2S,3S*)-**9a** and (*2S,3S*)-**9b**, respectively.

5.4.2. ENANTIOMERIC PURITY

The optical rotation of both (*2S,3S*)-**9b** and (*2R,3R*)-**9b** was determined: (*2S,3S*)-**9b** [α]_D = -65.6° (c = 1.25, MeOH) and (*2R,3R*)-**9b** [α]_D = +72.8° (c = 0.95, MeOH). The enantiomeric purity was assessed by NMR analysis with and

without the addition of chiral shift reagent. Addition of Eu(hfc)₃ to the samples resulted in a shift of 0.2 ppm of the signal at 5.25. This indicated that the samples have an enantiomeric excess of more than 95 %.

5.4.3. RADIOCHEMISTRY

Since radiosynthesis accomplished by an iodine-bromine exchange reaction is often difficult to purify, we choose to produce [¹²³I]-(*S,S*)-IPBM by electrophilic substitution. Unfortunately we were not able to replace the bromine of (*2S,3S*)-**9b** by a tributylstannyl group or trimethylstannyl group. Alternatively, [¹²³I]-(*S,S*)-IPBM was synthesized in two steps starting from (*2S,3S*)-**10**. The tributylstannyl precursor (*2S,3S*)-**10** was synthesized in a 35 % yield. Radioiodination of (*2S,3S*)-**10**, yielded [¹²³I]-(*2S,3S*)-**8a** which was immediately reduced to give [¹²³I]-(*S,S*)-IPBM. The radiochemical yield was approximately 10 %.

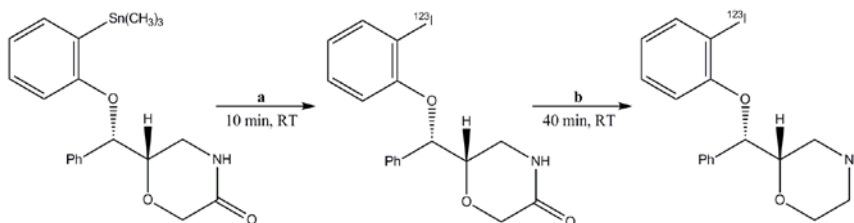


Figure 5.3 Radiosynthesis of [¹²³I]-(*S,S*)-IPBM

a EtOH, chloramine-T, glacial acetic acid, n.c.a. Na¹²³I **b** THF, BH₃ (1 M in THF)

5.4.4. QUALITY CONTROL AND LOG D_{7.4}

Co-injection of the obtained radiotracer and cold reference compound illustrated similar retention times for [¹²³I]-(*S,S*)-IPBM and (*S,S*)-IPBM, confirming the identity of the radiotracer. Radiochemical purity was > 98 %. Since no UV-signal was observed for the amount [¹²³I]-(*S,S*)-IPBM synthesized, the detection limit was applied for calculation of the specific activity. Using the described

radioanalytical method, the detection limit for [¹²³I]-(*S,S*)-IPBM was 0.25×10^{-3} μM . Specific activity appeared to be at least 148 GBq/ μmol (4 Ci/ μmol).

An ideal log $D_{7.4}$ value for brain radiotracers is between 1.5 and 3.5 (Waterhouse, 2003). The determined log octanol/PBS partition coefficient was found to be 1.9 ± 0.05 %, which is suitable for brain penetration.

5.4.5. BIODISTRIBUTION STUDY

Results of the biodistribution study are shown in Table 5.1. [¹²³I]-(*S,S*)-IPBM displayed an excellent brain uptake (4.62 ± 0.66 % ID/g at 1 min p.i.) followed by a good wash-out (0.55 ± 0.17 % ID/g at 180 min p.i.) At each time point, brain activity remained higher than radioactivity uptake in blood (Figure 5.4).

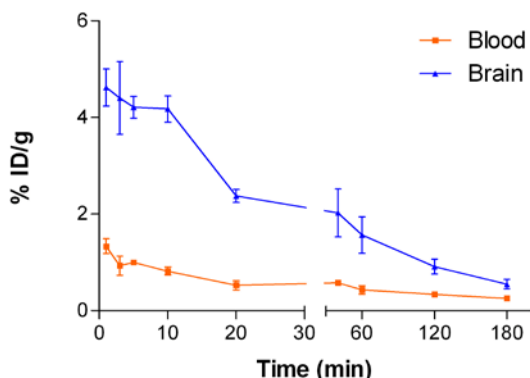


Figure 5.4 Blood-brain distribution of [¹²³I]-(*S,S*)-IPBM in NMRI mice

Values are expressed as % ID/g \pm SD ($n=3$)

Other organs with high tracer uptake were heart (12.65 ± 2.43 % ID/g at 1 min p.i.) and lungs (69.21 ± 8.02 % ID/g at 1 min p.i.). Radioactivity uptake in liver increased until 20 min p.i. and then declined. High uptake was seen in small (10.53 ± 3.84 % ID/g at 180 min p.i.) and large intestines (14.90 ± 5.53 % ID/g at 180 min p.i.), suggesting biliary clearance of [¹²³I]-(*S,S*)-IPBM. High kidney (10.91 ± 1.07 % ID/g at 5 min p.i.) and urine (data not shown) radioactivity uptake, show that urinary clearance of [¹²³I]-(*S,S*)-IPBM also occurred.

Table 5.1 Tissue uptake of radioactivity in male NMRI mice at various time points following i.v. administration [¹²³I]-(S,S)-IPBM

	Time (min)								
	1	3	5	10	20	40	60	120	180
Blood	1.33 ± 0.26	0.93 ± 0.34	1.00 ± 0.04	0.82 ± 0.14	0.53 ± 0.17	0.58 ± 0.06	0.43 ± 0.15	0.34 ± 0.07	0.26 ± 0.08
Brain	4.62 ± 0.66	4.40 ± 1.30	4.21 ± 0.40	4.17 ± 0.47	2.37 ± 0.23	2.03 ± 0.87	1.57 ± 0.65	0.91 ± 0.26	0.55 ± 0.17
Heart	12.65 ± 2.53	7.80 ± 3.08	5.61 ± 0.56	4.23 ± 0.82	3.53 ± 1.07	2.01 ± 0.62	1.70 ± 0.38	0.84 ± 0.04	0.66 ± 0.06
Lungs	69.21 ± 8.02	60.48 ± 16.26	51.80 ± 8.53	42.72 ± 5.45	34.57 ± 21.39	11.65 ± 2.61	10.29 ± 3.75	3.62 ± 1.52	3.29 ± 0.93
Stomach	2.53 ± 1.21	2.60 ± 0.98	2.50 ± 0.71	2.31 ± 1.11	2.47 ± 1.28	1.63 ± 0.80	1.29 ± 0.46	1.53 ± 0.69	2.53 ± 1.22
Spleen	1.98 ± 0.90	2.48 ± 0.84	3.32 ± 0.58	3.69 ± 0.88	4.61 ± 1.01	2.71 ± 0.85	2.90 ± 1.84	2.39 ± 2.64	1.50 ± 1.72
Liver	2.57 ± 1.08	2.96 ± 0.87	3.82 ± 0.20	3.46 ± 1.96	5.85 ± 2.97	3.53 ± 1.52	2.70 ± 0.86	2.30 ± 1.91	2.60 ± 1.42
Kidneys	10.81 ± 4.23	9.62 ± 3.56	10.91 ± 1.07	9.86 ± 3.17	10.92 ± 2.26	6.06 ± 1.55	4.10 ± 0.99	2.83 ± 0.94	1.88 ± 0.75
Small intestine	1.57 ± 0.38	1.39 ± 0.45	1.50 ± 0.17	3.81 ± 1.26	10.80 ± 4.17	11.18 ± 2.86	18.74 ± 1.06	6.90 ± 1.26	10.53 ± 3.84
Large intestine	0.88 ± 0.23	0.80 ± 0.06	0.91 ± 0.08	0.92 ± 0.15	0.74 ± 0.20	0.54 ± 0.18	4.01 ± 3.98	12.54 ± 6.09	14.90 ± 5.53
Pancreas	2.70 ± 2.64	4.67 ± 1.63	4.99 ± 0.29	3.78 ± 1.06	3.33 ± 1.08	1.58 ± 0.28	1.24 ± 0.09	0.88 ± 0.22	0.39 ± 0.07
Muscle	1.29 ± 0.45	1.38 ± 0.21	1.93 ± 0.51	1.54 ± 0.04	1.38 ± 0.29	0.80 ± 0.18	0.65 ± 0.08	0.34 ± 0.05	0.27 ± 0.07
Fat	0.70 ± 0.21	0.89 ± 0.31	1.04 ± 0.32	1.34 ± 0.66	1.43 ± 0.55	0.92 ± 0.41	0.66 ± 0.24	0.80 ± 0.44	0.37 ± 0.14

Values are expressed as % ID/g ± SD (n=3)

5.5. Conclusion

As an effort to develop a potential SPECT imaging agent for brain NET, an iodinated reboxetine derivate, [^{123}I]-(*S,S*)-IPBM, was synthesized. Both the precursor and cold reference compound were prepared stereoselectively by a nine-step synthetic procedure. NMR analysis with $\text{Eu}(\text{hfc})_3$ as chiral shift reagent showed an enantiomeric excess of 95 % using the described stereoselective procedure. [^{123}I]-(*S,S*)-IPBM was obtained by radioiodination of (*2S,3S*)-**10**, followed by reduction with a radiochemical purity of > 98 % and a specific activity of at least 148 GBq/ μmol (4 Ci/ μmol). *In vivo* evaluation showed a rapid and marked accumulation in the brain. The radioactivity in blood was cleared rapidly, and the brain to blood ratio, an essential factor for brain imaging, was high.

Unfortunately, at the time we performed our biodistribution study, a report about the synthesis and evaluation of the same compound, [$^{123/125}\text{I}$]-(*S,S*)-IPBM was published (Kanegawa et al., 2006). Only a few months later, an article concerning an *in vivo* evaluation of [^{123}I]-(*S,S*)-IPBM in primates was published (Tamagnan et al., 2007). Since [$^{123/125}\text{I}$]-(*S,S*)-IPBM was described by others, we performed no further attempts to increase the radiochemical yield and did not conduct additional *in vivo* studies.

Kanegawa et al. radiosynthesized [^{125}I]-(*S,S*)-IPBM by bromine-iodine exchange. They reported a yield of 65 % but they gave no information about the obtained specific activity and chemical purity. They performed a biodistribution study in Sprague-Dawley rats using [^{125}I]-(*S,S*)-IPBM. The accumulation of radioactivity was greater in NET-rich regions, such as the thalamus and cortex, than in the striatum, a NET-poor region (Tejani-Butt, 1992). The ratio of radioactivity in other brain regions to that in the striatum was highest at 180 min p.i. *Ex vivo* autoradiographic analyses demonstrated the highest level of radioactivity in the locus coeruleus and anteroventricular thalamic nucleus, which are known to be

rich in NET. The NET-selective agent nisoxetine reduced the accumulation of radioactivity in the NET-rich regions to that of the striatum whereas fluoxetine, a selective agent for the serotonin transporter, and GBR12909, a DAT-selective agent did not affect the accumulation of [^{125}I]-(*S,S*)-IPBM. Additionally, a SPECT study in a marmoset with [^{123}I]-(*S,S*)-IPBM exhibited a regional localization consistent with the known densities of NET and [^{123}I]-(*S,S*)-IPBM accumulation could be displaced by treatment with nisoxetine (Kanegawa et al., 2005).

Tamagnan et al. applied the electrophilic substitution method to yield [^{123}I]-(*S,S*)-IPBM but no information concerning their radiochemical yield and specific activity was added. They performed a dynamic SPECT imaging study in an adult female baboon. Regional brain tracer uptake is consistent with the distribution of NET in the baboon brain, with the highest uptake in locus coeruleus and thalamus, and lowest uptake in cerebellum and striatum. To assess the pharmacological specificity, reboxetine was injected which resulted in a reduction of radioactivity in all brain regions with the most pronounced reduction in NET-rich regions. In contrast, displacement with citalopram or methylphenidate did not show any displacement of [^{123}I]-(*S,S*)-IPBM (Tamagnan et al., 2007).

The lack of data in their study makes it unfeasible to compare the different synthetic and radiosynthetic procedures whereas the *in vivo* data can not be compared due to differences in the experimental design.

Regarding the results of Tamagnan et al. (2007) and Kanegawa et al. (2006), we can state that the choice to develop [^{123}I]-(*S,S*)-IPBM as radiotracer for NET was an excellent suggestion.

5.6. References

- Benedetti Ms, Frigerio E, Tocchetti P, Brianceschi G, Caselli M, Pellizzoni C et al. Stereoselective and species-dependent kinetics of reboxetine in mouse and rats. *Chirality* 1995; 7:285-9.
- Biederman J and Spencer T. Attention-deficit/hyperactivity disorder (ADHD) as a noradrenergic disorder. *Biol*

- Psychiatry 1999; 46:1234-42.
- Haka Ms and Kilbourn MR. Synthesis and regional mouse brain distribution of [¹¹C]nisoxetine, a norepinephrine uptake inhibitor. Nucl Med Biol 1989; 16:771-4.
- Kanegawa N, Kiyono Y, Kimura H, Sugita T, Kajiyama S, Kawashima H et al. Synthesis and evaluation of radioiodinated (S,S)-2-(alpha-(2-iodophenoxy)benzyl)morpholine for imaging brain norepinephrine transporter. Eur J Nucl Med Mol Imaging 2006; 33:639-47.
- Kiyono Y, Kanegawa N, Kawashima H, Fujiwara H, Iida Y, Nishimura H and Saji H. A new norepinephrine transporter imaging agent for cardiac sympathetic nervous function imaging: radioiodinated (R)-N-methyl-3-(2-iodophenoxy)-3-phenylpropanamine. J Med Chem 2003; 30: 697-706.
- Klimek V, Stockmeier C, Overholser J, Meltzer HY, Kalka S, Dille G and Ordway GA. Reduced levels of norepinephrine transporters in the locus coeruleus in major depression. J Neurosci 1997; 17:8451-58.
- Kung M, Choi S, Hou C, Zhuang Z, Foulon C, Kung H. Selective binding of 2-[¹²⁵I]iodo-nisoxetine to norepinephrine transporters in the brain. Nuc Med Biol 2004; 31:533-41.
- Lin K, Ding Y, Kim S and Kil K. Synthesis, enantiometric resolution, F-18 labeling and biodistribution of reboxetine analogs: promising radioligands for imaging the norepinephrine transporter with positron emission tomography Nucl Med Biol 2005; 32:415-22.
- Masson J, Hamon CS and Mestikawy SE. Neurotransmitter transporters in the central nervous system. Pharm Rev 1999; 51:439-64.
- Melloni P, Torre D, Lazzari E, Mazzini G and Meroni M. Configurational studies on 2-[alpha-(2-ethoxyphenoxy)benzyl]morpholine FCE 20124. Tetrahedron 1985; 41:1393-9.
- Raisman R, Sette M, Pimoule C, Briley M and Langer SZ. High-affinity [³H]desipramine binding in the peripheral and central nervous system: a specific site associated with the neuronal uptake of noradrenaline. Eur J Pharmacol 1982; 78:345-51.
- Ressler KJ and Nemeroff CB. Role of norepinephrine in the pathophysiology and treatment of mood disorders. Biol Psychiatry 1999; 46:1219-1233
- Schou M, Halldin C, Sovago J, Pike VW, Gulyas B, Mozley PD et al. Specific in vivo binding to the norepinephrine transporter demonstrated with the PET radioligand, (S,S)-[¹¹C]MeNER. Nucl Med Biol 2003; 30:707-14.
- Schou M, Halldin C, S ov ag o J, Pike V, Hall H, Guly as B et al. Pet evaluation of novel radiofluorinated reboxetine analogs as norepinephrine transporter probes in the monkey brain. Synapse 2004; 53:57-67.
- Tamagnan GD, Brenner E, Alagille D, Staley JK, Haile C, Koren A et al. Development of SPECT imaging agents for the norepinephrine transporter: [¹²³I]NER. Bioorg Med Chem 2007; 17:533-7.
- Tejani-Butt SM. [³H]nisoxetine: a radioligand for quantitation of norepinephrine uptake sites by autoradiography or by homogenate binding. J Pharmacol Exp Ther 1992; 260:427-36.
- Tejani-Buut SM, Yang J and Zaffer H. Norepinephrine transporter sites are decreased in the locus coeruleus in Alzheimer's disease. Brain Res 1993; 631:147-50.
- Waterhouse RN. Determination of lipophilicity and its use as a predictor of blood-brain barrier penetration of molecular agents. Mol Imaging Biol 2003; 5:376-389.
- Wilson A, Johnson D, Mozley D, Hussey D, Ginovart N, Nobrega J, Garcia A, Meyer J and Houle S. Synthesis and in vivo evaluation of novel radiotracers for the in vivo imaging of the norepinephrine transporter. Nucl Med Biol 2003; 30:85-92.

Chapter 6

Radiosynthesis and *in vivo* evaluation of [¹¹C]-labelled pyrrole-2-carboxamide derivatives for MAO-A imaging



De Bruyne S.¹, La Regina G.², Staelens S.³, wyffels L.¹, Deleye S.³, Silvestri R.², De Vos F.¹

Nuclear Medicine and Biology, accepted for publication

¹ Laboratory for Radiopharmacy, Ghent University, Harelbekestraat 72, 9000 Ghent, Belgium

² Dipartimento di Chimica e Tecnologie del Farmaco, Sapienza University of Rome, P.le Aldo Moro 5, 00185 Roma - Italy

³ IBITECH-Medisip, Ghent University-IBBT, De Pintelaan 185, 9000 Ghent, Belgium

Chapter 6

Radiosynthesis and *in vivo* evaluation of [¹¹C]-labelled pyrrole-2-carboxamide derivatives for MAO-A imaging

6.1. Abstract

Aim: The search for new PET ligands for MAO-A with optimal properties is justified by the lack of an ideal ligand and the observation that fluctuations in MAO-A functionality are associated with human diseases. This study reports the radiolabelling of [¹¹C]-labelled 1*H*-pyrrole-2-carboxamide derivatives, RS 2315 and RS 2360, and the characterization of their *in vivo* properties.

Methods: The radiolabelling of [¹¹C]-RS 2315 and [¹¹C]-RS 2360 was accomplished by methylation of the amide precursors with ¹¹CH₃I. Biodistribution, blocking and metabolite studies of both tracers were performed in NMRI mice. Finally, a PET study in Sprague-Dawley rats was performed for [¹¹C]-RS 2360.

Results: Both tracers were obtained in a radiochemical yield of approximately 30 % with radiochemical purity of > 98 %. Biodistribution studies showed high brain uptake followed by rapid brain clearance for both radiotracers. In the brain, [¹¹C]-RS 2360 was more stable than [¹¹C]-RS 2315. Blocking studies in mice could not demonstrate specificity of [¹¹C]-RS 2315 towards MAO-A or B. The blocking and imaging study with [¹¹C]-RS 2360 on the other hand indicated specific binding at MAO-A at the earliest time points.

Conclusion: These results indicate that [¹¹C]-RS 2315 is not suitable for mapping MAO-A *in vivo* and that further research is necessary to investigate the potential of [¹¹C]-RS 2360 in MAO-A imaging.

6.2. Introduction

Because of the ability of MAO to catabolise neurotransmitters, MAO is involved in several psychiatric and neurological disorders (Meyer et al., 2006; Heafield and Williams, 1992) as well as in behaviour (Shih and Thompson, 1999; Alia-Klein et al., 2008; Brunner et al., 1993) and tobacco addiction (Fowler et al., 1996; Berlin et al., 1995). A very efficient non-invasive method to study enzymes *in vivo* is visualization with PET. There are only a few PET tracers for MAO-A designed and they all have their own drawbacks. The first developed radiotracer, [¹¹C]clorgyline, displayed an unexplained species difference (Fowler et al., 2001; Bergström et al., 1997). In contrast to results in humans, clorgyline was not retained in baboon brain. Another MAO-A tracer, [¹¹C]befloxatone is synthesized with [¹¹C]phosgene which is toxic and is rather rare available (Dolle et al., 2003). The drawback of [¹¹C]harmine is its extensive metabolism in plasma with only 10 % intact product at 10 min p.i. (Bergström et al., 1997).

The search for new ligands with optimal properties is justified by the lack of an ideal ligand and the observation that fluctuations in MAO-A functionality are associated with human diseases and tobacco addiction.

A series of new pyrrole derivatives have been synthesized and evaluated for their MAO-A and -B inhibitory activity and selectivity (La Regina et al., 2007). Out of this new class of MAO inhibitors we selected the most potent inhibitors for MAO-A: *N*-(phenethyl)-*N*-methyl-1*H*-pyrrole-2-carboxamide (RS 2315) and (*R*)-*N*-(α -cyclohexylethyl)-*N*-methyl-1*H*-pyrrole-2-carboxamide (RS 2360) (Figure 6.1). Their K_i values are 7 nM and 1.7 nM for MAO-A and 12 nM and 30 nM for MAO-B, for RS 2315 and RS 2360, respectively (La Regina et al., 2007).

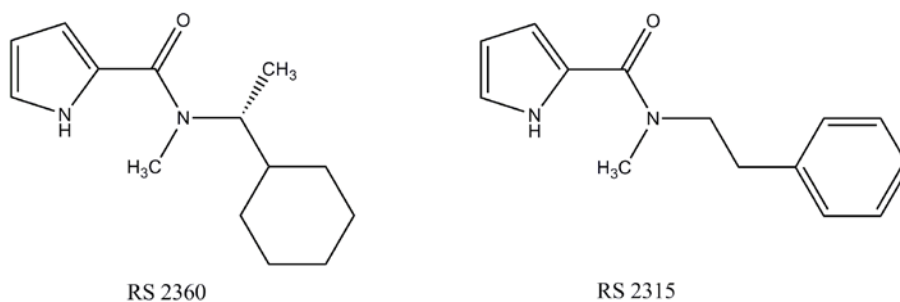


Figure 6.1 Chemical structures of RS 2360 and RS 2315

The present study reports the radiolabelling and purification of ¹¹C labelled RS 2315 and RS 2360. Their partition coefficient is determined. Specific activity and radiochemical purity are reported. [¹¹C]-RS 2315 and [¹¹C]-RS 2360 are both evaluated *in vivo*. First, a biodistribution study in NMRI mice is performed to assess their ability to cross the blood-brain barrier. A blocking study is conducted to investigate their *in vivo* selectivity and specificity. Possible metabolism of [¹¹C]-RS 2315 and [¹¹C]-RS 2360 is verified by analyzing mouse blood and brain samples on HPLC. Finally, a PET study in Sprague-Dawley rats is performed for the most promising radiotracer.

6.3. Materials & Methods

6.3.1. GENERAL

The starting compounds *N*-(phenethyl)-1*H*-pyrrole-2-carboxamide (RS 2115) and (*R*)-*N*-(α -cyclohexylethyl)-1*H*-pyrrole-2-carboxamide (RS 2226) as well as the cold reference compounds RS 2315 and RS 2360 for this study were kindly provided by Dipartimento di Chimica e Tecnologie del Farmaco, Sapienza University of Rome, Italy (La Regina et al., 2007).

6.3.2. RADIOCHEMISTRY

The alkylating reagent [¹¹C]methyl iodide was prepared from [¹¹C]methane by gas-phase iodination. The production of both ¹¹CH₄ and ¹¹CH₃I is described in Chapter 4.

6.3.2.1. [¹¹C]-RS 2315

A solution of 3 μmol precursor RS 2115 in DMSO/DMF (189 μL/60 μL) and 1 μL tetrabutylammonium hydroxide (TBAH) was added to a reaction vessel and the mixture was cooled in an ice bath. A stream of helium containing the alkylating agent ¹¹CH₃I was bubbled through the reaction mixture until maximum of ¹¹C activity was trapped. The reaction mixture was heated in an oil bath at 65°C for 10 min and subsequently diluted with 200 μL HPLC eluent and purified with semipreparative C₁₈ HPLC (Econosphere, 10 μm, 10 mm x 250 mm; Grace Davison Discovery Sciences, Lokeren, Belgium) using a smartline UV detector 2500 (Knauer, Berlin, Germany) set at 254 nm. Radiodetection occurred by a solar-blind P.I.N. photodiode. Elution was carried out at 6 mL/min flow rate with 45 % (v/v) CH₃CN in 0.02 M sodium acetate buffer (pH 4.5) as mobile phase. The fraction containing [¹¹C]-RS 2315 was collected into a vessel with 40 mL sterile water and loaded on a C₁₈ Sep-pak (Alltech Maxi-clean SPE Prevail C₁₈, previously activated with 1 mL EtOH and 5 mL sterile water). After the cartridge was washed with 5 mL sterile water, the desired product, [¹¹C]-RS 2315, was eluted with 1 mL EtOH. For biodistribution and blocking studies the EtOH fraction was diluted with 10 mL physiological saline. For metabolite analysis, EtOH was evaporated to dryness and the residue was redissolved in an adequate amount of EtOH/physiological saline (8/92 - v/v).

6.3.2.2. [¹¹C]-RS 2360

The same procedure as described for [¹¹C]-RS 2315, with minor modifications was applied to synthesize [¹¹C]-RS 2360.

[¹¹C]-RS 2360 was prepared by methylation with ¹¹CH₃I of the normethyl derivative RS 2226 (3 μmol) in DMF/DMSO (60 μL/188 μL) for 7 min at 70°C using 1.5 μL TBAH. Purification was accomplished using CH₃CN/H₂O/HCOOH (50/50/0.1 – v/v/v) as mobile phase at a flow rate of 6 mL/min. The collected HPLC fraction containing [¹¹C]-RS 2360 (T_r 8.5 min) was diluted with 40 mL 0.01 M PBS before loading onto a Sep-pak column (Alltech Maxi-clean SPE Prevail C₁₈, previously activated with 1 mL EtOH and 5 mL sterile water). After the cartridge was washed with 5 mL sterile water, the desired product, [¹¹C]-RS 2360, was eluted with 1 mL EtOH. For biodistribution and blocking studies the EtOH fraction was diluted with 10 mL physiological saline. For metabolite and imaging studies, EtOH was evaporated to dryness and the residue was redissolved in an adequate amount of EtOH/physiological saline (8/92 - v/v).

6.3.3. IN VITRO CHARACTERIZATION

Quality control consisted of the determination of radiochemical purity and specific activity, calculated by analytical HPLC assay using a Gracesmart C₁₈ column (5 μm, 4.6 mm x 250 mm; Grace Davison Discovery Sciences, Lokeren, Belgium) at a flow rate of 1 mL/min. The eluents were the same as described for the purification.

A calibration curve of unlabelled reference compound (0.02 μM – 1 μM) was made and controlled for its accuracy and reproducibility. Specific activities were decay corrected back to the end of purification.

Co-injection on analytical HPLC of the final end product and cold reference compound was performed to confirm the identity of the obtained radiotracer. Log $D_{7.4}$ was determined according to the method described in Chapter 4.

6.3.4. BIODISTRIBUTION STUDIES

The biodistribution of [¹¹C]-RS 2315 and [¹¹C]-RS 2360 was studied in male NMRI mice (approximately 25 g and 6 weeks old). Awake mice ($n=3$ at each time point) were injected in a tail vein with approximately 200 μ L containing 7.5 – 11 MBq (0.2 – 0.3 mCi) [¹¹C]-RS 2315 or [¹¹C]-RS 2360. At 1, 10, 30 and 60 min p.i. mice were euthanized and dissected. Blood, urine and organs were weighed and counted for radioactivity. All organs were rinsed with water prior to weighing and counting. For calculation of the injected dose, five aliquots of the injection solution were weighed and counted for activity. Results are decay-corrected and expressed as % ID/g \pm SD.

6.3.5. BLOCKING STUDIES

Blocking studies were carried out with preinjection of 100 μ L clorgyline hydrochloride (MAO-A inhibitor) or *R*-(-)-deprenyl hydrochloride (MAO-B inhibitor) i.v. both in a dose of 10 mg/kg (Arnett et al., 1987; Fowler et al., 2001; Hirata et al., 2002; Jensen et al., 2008). 9 ± 1 MBq (243 ± 27 μ Ci) ¹¹C tracer (100 μ L) was injected 30 min later via a tail vein. The mice ($n=3$ at each time point) were awake during the injections. The mice were sacrificed and dissected at 1, 10 and 30 min after ¹¹C tracer injection. Blood, urine and organs were weighed and counted for radioactivity. All organs were rinsed with water prior to weighing and counting. For calculation of the injected dose, five aliquots of the injection solution were weighed and counted for activity. Results are decay-corrected and expressed % ID/g \pm SD. Statistical analysis was performed using one-sided, unpaired student's *t*-test. Only p-values < 0.05 are considered significant.

6.3.6. METABOLITE ANALYSIS

The *in vivo* metabolic stability of [¹¹C]-RS 2315 and [¹¹C]-RS 2360 in plasma and brain was studied in male NMRI mice. 22 – 37 MBq (0.59 - 1 mCi) of [¹¹C]-RS 2315 or [¹¹C]-RS 2360 dissolved in 200 µL was injected through a tail vein and the mice ($n=3$ for each time point) were sacrificed at 1, 10 or 30 min p.i. Sample workup was done as described in Chapter 4. HPLC analysis was performed using the same conditions as used for purification (see 6.3.2).

6.3.7. IMAGING STUDY

Additional *in vivo* tests with [¹¹C]-RS 2360 were performed using microPET imaging technology. Awake Sprague-Dawley rats ($n=4$ for each treatment group) were injected with physiological saline, clorgyline hydrochloride (10 mg/kg) or (R)-(-)-deprenyl hydrochloride (10 mg/kg) 30 min prior to their microPET scan. The latter acquisitions are performed using the Gamma Medica Ideas labPET 8, a state-of-the-art microPET device existing of $2 \times 2 \times 10$ mm³ LYSO/LGSO scintillators in a 8-pixel, quad-APD detector module arrangement. This system is capable of delivering 1 mm spatial resolution in rodents at a sensitivity of 4 % thereby covering a field-of-view of 10 cm transaxially by 8 cm axially.

All animals were injected with 35 – 40 MBq (0.95 - 1.08 mCi) [¹¹C]-RS 2360 on the camera bed at the start of a dynamic acquisition. Frames of 4 x 0.5 min, 3 x 1 min, and 1 x 5 min were accordingly sequentially recorded. The resulting data were reconstructed using 30 iterations of the Maximum Likelihood Expectation Maximization algorithm in 160 x 160 x 63 images of 0.5 mm x 0.5 mm x 1.175 mm voxel size. An a posteriori three-dimensional Gaussian filter of 2 x 2 x 2 mm was applied to all frames. Statistical analysis was performed using one-sided, unpaired student's *t*-test. Only p-values < 0.05 are considered significant. Images were analysed with PMOD whereby volumes of interest (VOIs) were drawn on the brain region (Figure 6.2) and the background region (Figure 6.3) of each

animal. Since the selection of the background region is critical, we delineated the background VOI on the last frame of 5 min acquisition. In this way, noise is eliminated and a robust reference value is obtained to normalize brain uptake for injected activity in all other frames on an individual animal basis. We selected the background region so that no specific muscle activity was present.

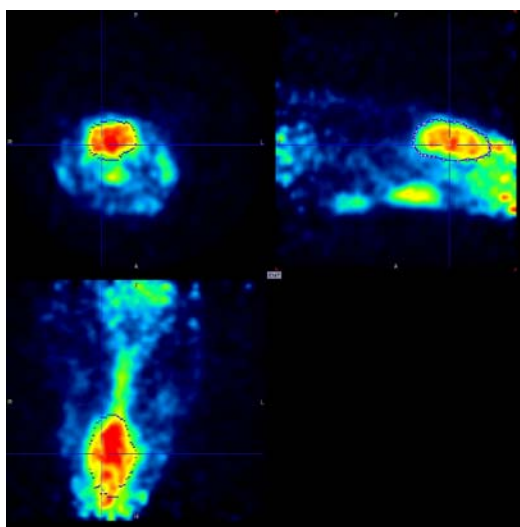


Figure 6.2 Example VOI for the brain region

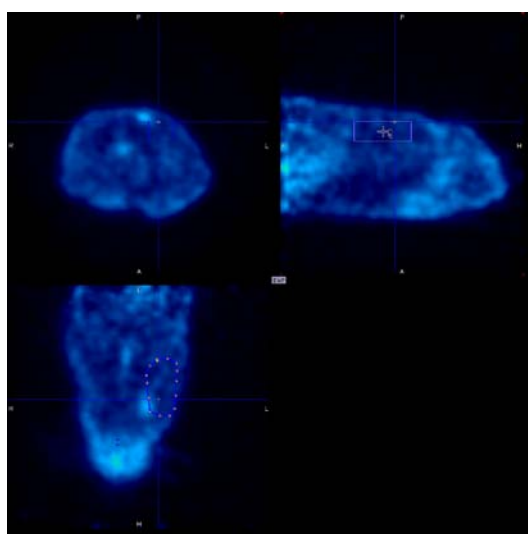


Figure 6.3 Example VOI for the background region

6.4. Results & Discussion

6.4.1. RADIOSYNTHESIS

The synthesis of radioligands [¹¹C]-RS 2315 and [¹¹C]-RS 2360 is shown in Figure 6.4. Their respective amide precursors were labelled with ¹¹CH₃I prepared from ¹¹CH₄, in the presence of TBAH as a base through N-[¹¹C]methylation and isolated by semipreparative HPLC.

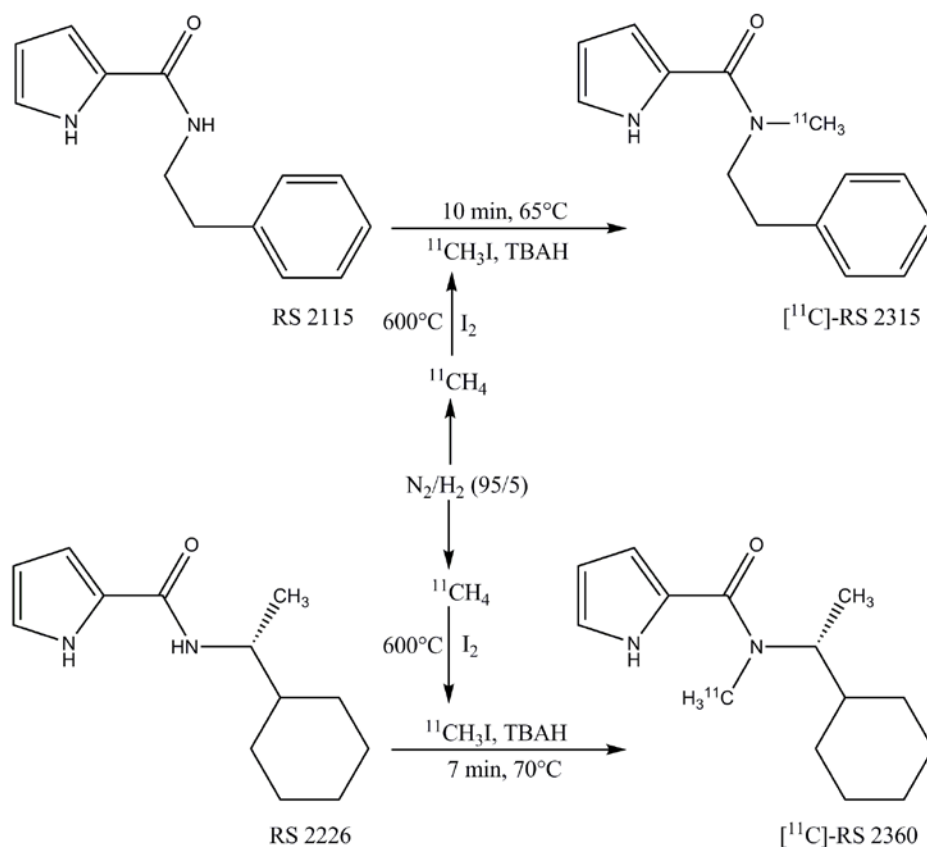


Figure 6.4 Radiosynthesis of [¹¹C]-RS 2315 and [¹¹C]-RS 2360

6.4.1.1. [¹¹C]-RS 2315

A typical UV- and radio-chromatogram for a [¹¹C]-RS 2315 synthesis purification run is shown in Figure 6.5.

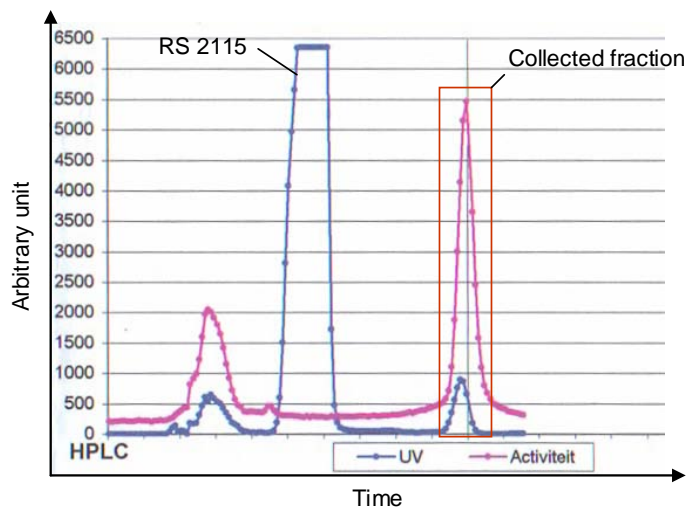


Figure 6.5 UV (blue) and radio-chromatogram (pink) of a typical [¹¹C]-RS 2315 purification

[¹¹C]-RS 2315 elutes with a retention time of 10 min. Extraction efficiency of the Sep-pak column was calculated to be $82 \pm 8 \%$ ($n=6$). Based on the amount ¹¹CH₃I added to the reaction vial, the radiochemical yield was $28 \pm 4 \%$ ($n=6$). The total synthesis, from the end of ¹¹CH₃I delivery to reaction vessel to delivery for *in vivo* studies was completed in 35 min.

6.4.1.2. [¹¹C]-RS 2360

The overall synthesis, purification (Figure 6.6) and formulation time to obtain [¹¹C]-RS 2360 was 30 min. In a typical experiment, target tracer [¹¹C]-RS 2360 was provided in a radiochemical yield of $30 \pm 6 \%$ ($n=6$), decay-corrected to start of

the reaction, based on the amount ¹¹CH₃I added. Almost all activity was released from the Sep-pak column ($93 \pm 4\%$ ($n=6$)).

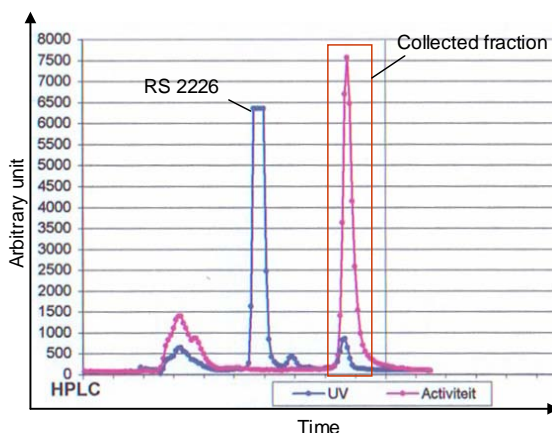


Figure 6.6 UV (blue) and radio-chromatogram (pink) of a typical synthesis purification of [¹¹C]-RS 2360

6.4.2. IN VITRO CHARACTERIZATION

6.4.2.1. *Quality control, specific activity and stability*

The identity of both tracers was confirmed by co-elution with authentic reference compound after co-injection on HPLC. Calculation of specific activity resulted in a range from 25 – 92 GBq/ μ mol (0.68 – 2.49 Ci/ μ mol) for [¹¹C]-RS 2315 ($n=6$) and 41 – 106 GBq/ μ mol (1.11 – 2.87 Ci/ μ mol) for [¹¹C]-RS 2360 ($n=6$). Radiochemical purity of the tracer recovered at the end of the experiment was > 98 % for both radiotracers. [¹¹C]-RS 2315 and [¹¹C]-RS 2360 remained stable during the time span of the experiments.

6.4.2.2. *Log D_{7.4}*

We determined log D_{7.4} as an indicator for lipophilicity and blood-brain-permeability. Octanol – buffer partition coefficient measurements gave a log D_{7.4}

of 1.65 ± 0.19 for [¹¹C]-RS 2315, slightly higher than the log D_{7.4} of [¹¹C]-RS 2360 (1.48 ± 0.04). The higher log D_{7.4} value of [¹¹C]-RS 2315 is in accordance with what we can predict from the replacement of cyclohexane by a benzene ring. Both values are suitable for brain penetration (Waterhouse, 2003).

6.4.3. BIODISTRIBUTION STUDIES

Following i.v. injection of [¹¹C]-RS 2315 into NMRI mice, the time course of radioactivity was determined in several tissues (Figure 6.7). High initial uptake in heart, lungs, pancreas and kidneys (5.52 ± 0.41 % ID/g, 5.96 ± 1.11 % ID/g, 5.19 ± 1.63 % ID/g and 6.81 ± 3.23 % ID/g, respectively at 1 min p.i.) was observed but except for the kidneys (8.34 ± 1.09 % ID/g at 60 min p.i.), the studied organs did not show any retention of [¹¹C]-RS 2315. In the liver, the activity peaked at 9.09 ± 0.97 % ID/g at 10 min p.i. and decreased over time. The activity in intestines had the highest increase between 10 min p.i. (4.36 ± 1.68 % ID/g) and 30 min p.i. (10.62 ± 2.81 % ID/g), indicating hepatobiliary clearance. Urinary clearance was also observed (data not shown).

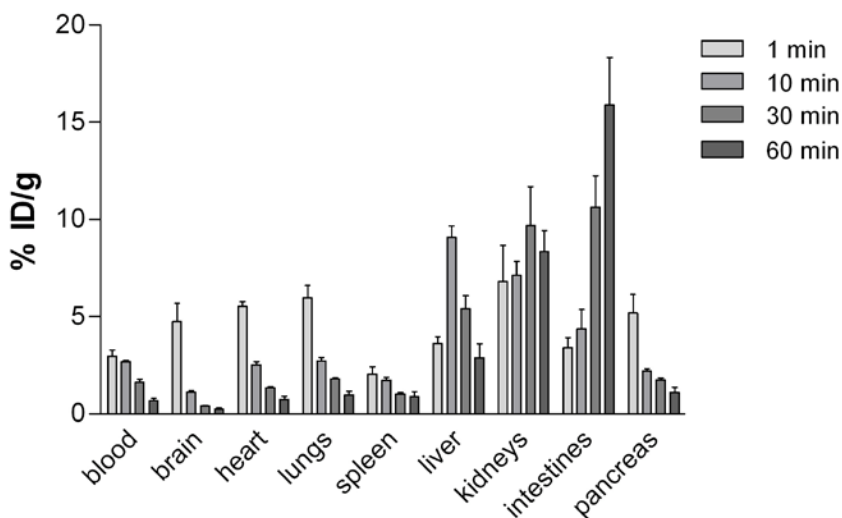


Figure 6.7 Tissue distribution of [¹¹C]-RS 2315 in male NMRI mice

Values are expressed as % ID/g \pm SD ($n=3$)

The blood-brain distribution of both [¹¹C]-RS 2315 and [¹¹C]-RS 2360 is shown in Figure 6.8. [¹¹C]-RS 2315 entered the brain quickly and was rapidly cleared (from 4.75 ± 1.62 % ID/g at 1 min p.i. to 0.24 ± 0.07 % ID/g at 60 min p.i.). [¹¹C]-RS 2360 displayed a rapid and high brain uptake of 7.08 ± 0.95 % ID/g at 1 min p.i., indicating a good penetration of the radiotracer into the brain. This high brain uptake was followed by an efficient wash-out (0.51 ± 0.06 % ID/g at 30 min p.i.).

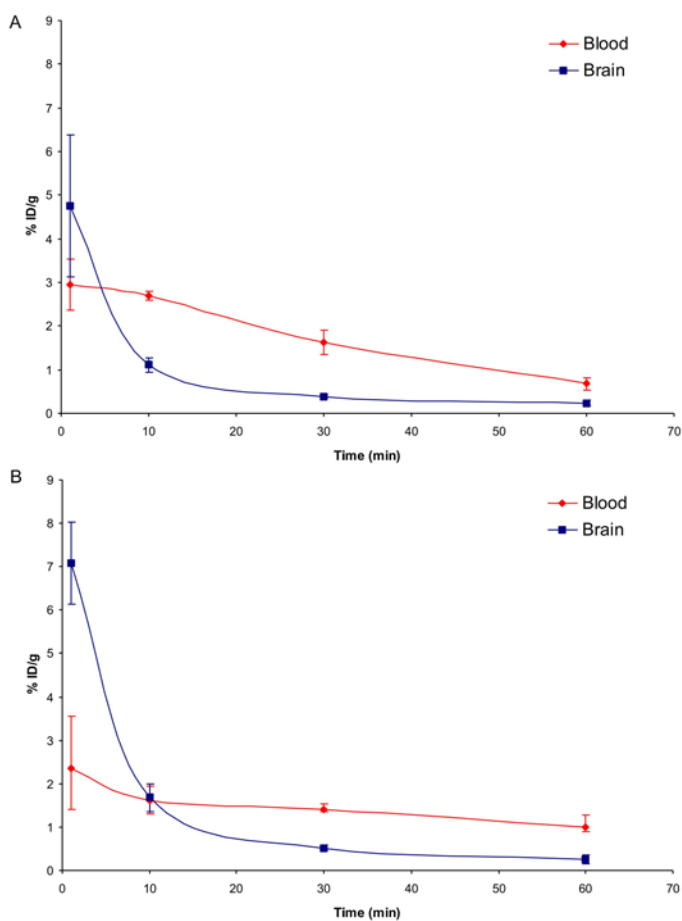


Figure 6.8 Blood-brain distribution of [¹¹C]-RS 2315 (A) and [¹¹C]-RS 2360 (B) in male NMRI mice

Values are expressed as % ID/g \pm SD ($n=3$)

Figure 6.9 summarizes the tissue time-course distribution of [¹¹C]-RS 2360 in male NMRI mice. The lungs, heart and pancreas showed high initial uptake (respectively, 23.62 ± 4.22 % ID/g, 11.51 ± 0.93 % ID/g and 3.93 ± 1.78 % ID/g at 1 min p.i.) followed by a fast wash-out (6.01 ± 2.28 % ID/g, 1.75 ± 0.16 % ID/g and 1.66 ± 0.37 % ID/g at 30 min p.i.). As for [¹¹C]-RS 2315, the uptake in the liver was also increased at 10 min after injection (7.45 ± 0.35 % ID/g) after which it decreased (4.24 ± 0.99 % ID/g at 60 min p.i.). Clearance of radioactivity occurred by both the hepatobiliary and urinary pathway (data not shown).

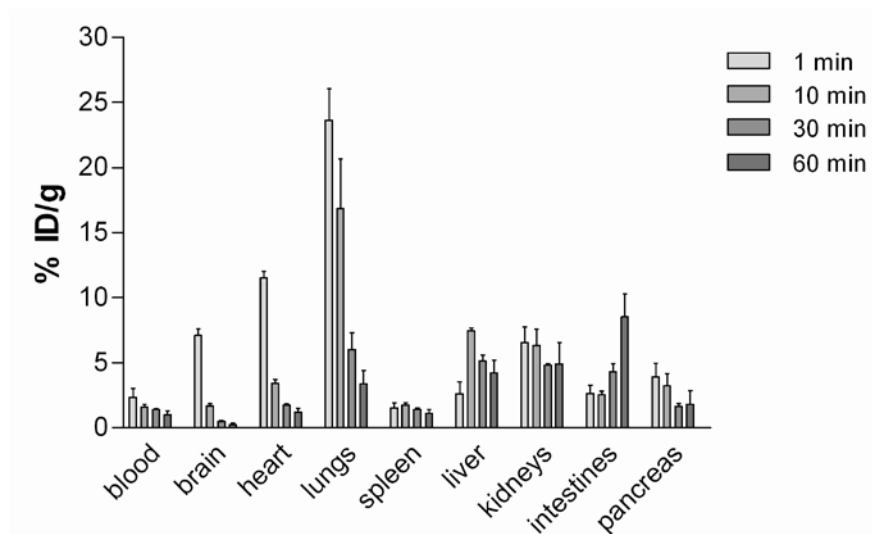


Figure 6.9 Tissue distribution of [¹¹C]-RS 2360 in male NMRI mice
Values are expressed as % ID/g \pm SD ($n=3$)

6.4.4. BLOCKING STUDIES

In vivo selectivity and specificity of both radiotracers was examined by pre-injection of clorgyline hydrochloride (MAO-A inhibitor) and R(-)-deprenyl hydrochloride (MAO-B inhibitor). Uptake of radioactivity in brain (Figure 6.10) and peripheral organs was measured at 1, 10 and 30 min after injection. of the ¹¹C tracer.

[¹¹C]-RS 2315 brain uptake could not be decreased by administrating clorgyline or R(-)-deprenyl. Surprisingly, a significantly higher brain uptake is observed at 30 min p.i. both after MAO-A and MAO-B inhibition. The effect on the brain/blood ratio however is not significant. A raise in brain uptake also occurred at 1 min p.i. but since the blood activity increased as well, the brain/blood ratio was not affected. Peripherally, an increased liver uptake is observed at 1 min p.i. both after clorgyline (from 3.63 ± 0.56 % ID/g to 7.15 ± 3.02 % ID/g) and after R(-)-deprenyl (from 3.63 ± 0.56 % ID/g to 7.81 ± 0.73 % ID/g) pretreatment. At 10 and 30 min p.i., a raise in intestinal activity (from 4.36 ± 1.68 % ID/g to 7.84 ± 3.21 % ID/g after clorgyline pretreatment and to 5.74 ± 0.73 % ID/g after R(-)-deprenyl pretreatment at 10 min p.i.) is seen, suggesting an enhanced hepatobiliary clearance after administration of clorgyline and R(-)-deprenyl. This peripheral redistribution after pretreatment with clorgyline and R(-)-deprenyl could be the reason of the observed higher brain uptake. Another possible hypothesis for the higher brain uptake is that clorgyline or R(-)-deprenyl administration caused a shift in metabolism pattern.

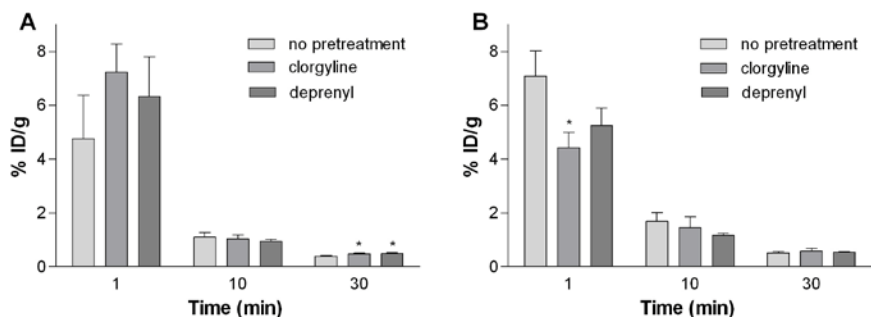


Figure 6.10 Brain uptake of [¹¹C]-RS 2315 (A) and [¹¹C]-RS 2360 (B) in control mice and in mice pretreated with clorgyline or (R)-(-)-deprenyl

Values are expressed as % ID/g \pm SD ($n=3$), * $p < 0.05$, student's *t*-test

At 1 min p.i., pretreatment with clorgyline resulted in a significant decrease in brain uptake of [¹¹C]-RS 2360 ($p = 0.02$). (R)-(-)-deprenyl administration also

lowered brain uptake but this decrease was not significant. This effect is in accordance with what we would expect from the *in vitro* properties ($K_i = 1.7$ nM for MAO-A and $K_i = 30$ nM for MAO-B). At 10 and 30 min p.i however, no effect of clorgyline or R-(-)-deprenyl pre-administration could be observed. In the peripheral organs, no clear effect of blocking MAO-A or MAO-B could be distinguished (data not shown).

6.4.5. METABOLITE ANALYSIS

Control experiments with spiked plasma and brain revealed extraction efficiencies of 96 ± 1 % for plasma and 93 % for brain samples for [¹¹C]-RS 2315 and 93 ± 6 % for plasma and 85 ± 6 % for brain samples for [¹¹C]-RS 2360, respectively. Plasma and brain obtained from mice at 1, 10 and 30 min p.i. were analyzed by RP-HPLC to investigate the metabolism pattern of [¹¹C]-RS 2315 and [¹¹C]-RS 2360 (Table 6.1).

Table 6.1 Metabolic profile of [¹¹C]-RS 2315 and [¹¹C]-RS 2360 in NMRI mice

Tissue	Time	Retention time on RP-HPLC		
		2.5 min	4.5 min	10 min
Plasma [¹¹ C]-RS-2315	1 min			> 96 %
	10 min	55 ± 5 %	24 ± 5 %	21 ± 2 %
	30 min	83 ± 1 %	8 %	9 ± 2 %
Brain [¹¹ C]-RS-2315	1 min			> 99 %
	10 min	10 ± 1 %	28 ± 4 %	62 ± 3 %
	30 min	28 ± 5 %	19 ± 3 %	53 ± 7 %
Plasma [¹¹ C]-RS-2360	1 min			> 99 %
	10 min	64 ± 10 %	8 %	29 ± 10 %
	30 min	75 ± 5 %	5 ± 1 %	21 ± 5 %
Brain [¹¹ C]-RS 2360	1 min			> 99 %
	10 min	10 ± 3 %	10 ± 1 %	81 ± 4 %
	30 min	27 ± 4 %	8 %	66 ± 4 %

Values are expressed as percent of total radioactivity ± SD ($n=3$)

RP-HPLC analysis of mouse plasma showed that [¹¹C]-RS 2315 (Figure 6.11) was rapidly metabolized with only 21 ± 2 % parent compound remaining at 10 min p.i. All detected metabolites were more polar than the original radiotracer. The percentage of radioactivity in mouse brain extracts derived from unmetabolized [¹¹C]-RS 2315 was > 99 % at 1 min p.i., 62 ± 3 % at 10 min p.i. and 53 ± 7 % at 30 min p.i. respectively.

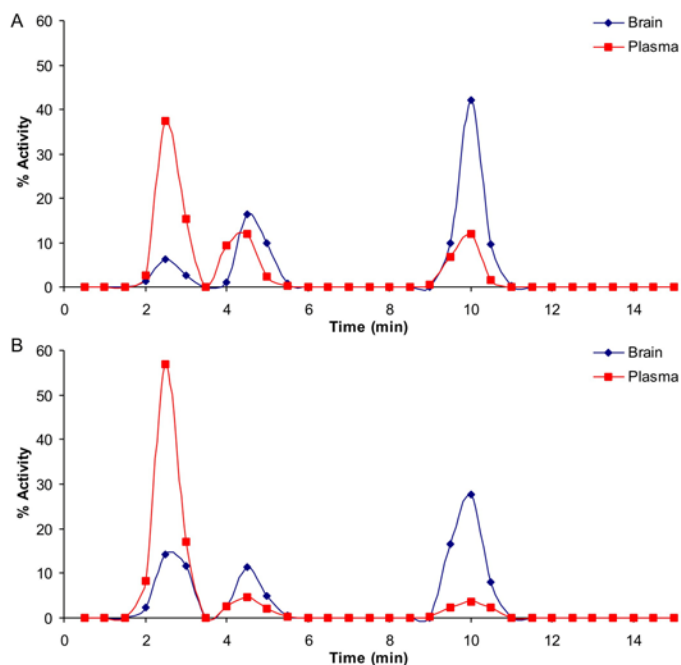


Figure 6.11 Metabolite chromatogram of [¹¹C]-RS 2315 at 10 min (A) and 30 min (B) p.i.

Values are the mean of three experiments and are expressed as percent of total activity

The relative percentage of intact [¹¹C]-RS 2360 (Figure 6.12) in plasma as a function of time after injection was 29 ± 10 % at 10 min p.i and 21 ± 5 % at 30 min p.i. HPLC analysis of the brain samples showed that 81 ± 4 % and 66 ± 4 % of the radioactivity existed of unchanged [¹¹C]-RS 2360 at 10 and 30 min p.i. respectively. At 1 min p.i., no degradation products were found in plasma neither in brain.

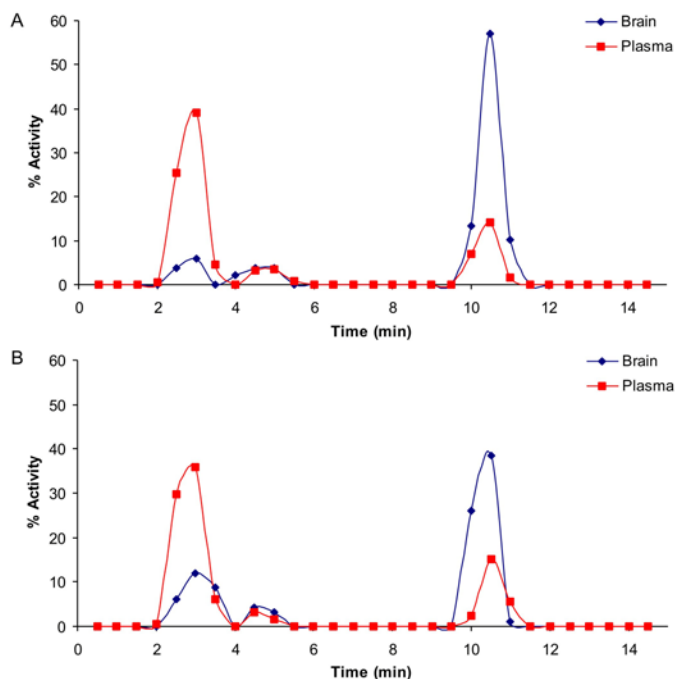


Figure 6.12 Metabolite chromatogram of [¹¹C]-RS 2360 at 10 min (A) and 30 min (B) p.i.

Values are the mean of three experiments and are expressed as percent of total activity

At all time points examined, the extent of metabolism was higher for [¹¹C]-RS 2315 than for [¹¹C]-RS 2360. It seems quite likely that the hydrophilic degradation fragments with the retention time of 2.5 min were methanol, formaldehyde or formic acid; which were formed after demethylation of the radiotracer. The metabolite at 4.5 min could be the result of the breaking of the amide bond. In the case of [¹¹C]-RS 2360, the metabolite could also be caused by hydroxylation on the phenyl group.

6.4.6. PET SCANS

The results shown in Figure 6.13 illustrate that for [¹¹C]-RS 2360 an overall significant inhibition by clorgyline of 30 % can be concluded when compared to

injection of physiological saline ($p = 0.006$). An inhibition of 16 % by R(-)-deprenyl is noticeable, albeit not significant ($p = 0.07$). These observations indicated that [¹¹C]-RS 2360 is more selective towards MAO-A than to MAO-B which is in accordance with the *in vitro* determined K_i values. When we investigate the influence of clorgyline pretreatment at each time frame separately, a significant inhibition is observed at the first 5 time frames but not at the latter three time frames. R(-)-deprenyl administration caused no significant inhibition of brain uptake at any of the separate time frames. These observations are in accordance with those of the blocking study. The impossibility to show specificity towards MAO-A at the latter time points could be due to the extensive metabolism of [¹¹C]-RS 2360.

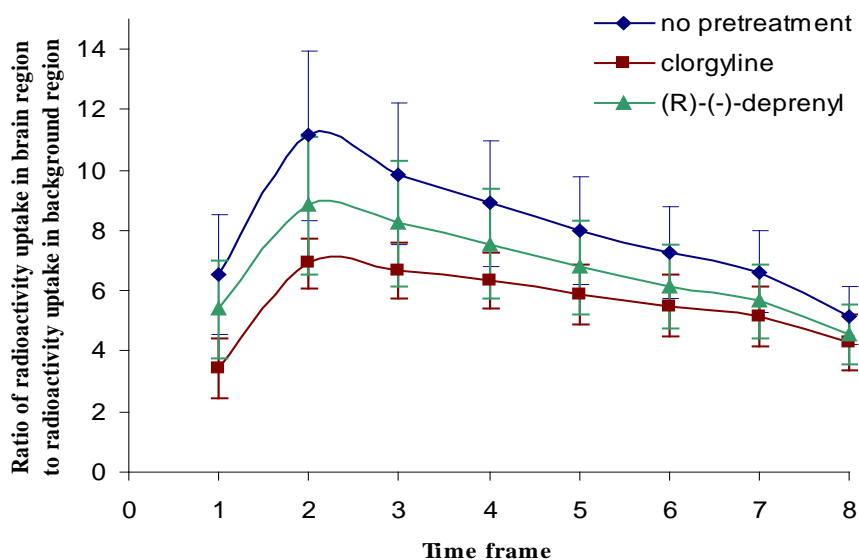


Figure 6.13 Results for the PET imaging experiments

Values are the mean of four experiments

6.5. Conclusion

The radiosynthesis of both radiotracers was achieved by nucleophilic substitution of the desmethyl precursor with ¹¹CH₃I in the presence of TBAH. After HPLC

purification, the radiochemical yields were $28 \pm 4 \%$ and $30 \pm 6 \%$ for [¹¹C]-RS 2315 and [¹¹C]-RS 2360, respectively and radiochemical purity appeared $> 98 \%$ for both radiotracers. The authenticity of the tracers was determined by co-elution with the non-radioactive reference compound. Specific activity ranged from 25 – 92 GBq/ μ mol (0.68 – 2.49 Ci/ μ mol) for [¹¹C]-RS 2315 and 41 – 106 GBq/ μ mol (1.11 – 2.87 Ci/ μ mol) for [¹¹C]-RS 2360. For the duration of the experiments, [¹¹C]-RS 2315 as well as [¹¹C]-RS 2360 remained stable. The determined log $D_{7.4}$ of 1.65 ± 0.19 for [¹¹C]-RS 2315 was slightly higher than the log $D_{7.4}$ of [¹¹C]-RS 2360 (1.48 ± 0.04) as expected when comparing the chemical structures. Both values are suitable for brain penetration.

Upon intravenous administration, high initial levels of activity were observed in mouse brain indicating an excellent passage through the BBB of both [¹¹C]-RS 2315 and [¹¹C]-RS 2360. The brain activity diminished very quickly and at 10 min p.i. for [¹¹C]-RS 2315 and 30 min p.i. for [¹¹C]-RS 2360 brain activity did no longer exceeded blood activity. Metabolism studies revealed that at 1 min p.i. almost no degradation occurred neither in plasma or brain. At 10 and 30 min p.i., [¹¹C]-RS 2315 and [¹¹C]-RS 2360 were extensively metabolized in plasma and remained more stable in brain. At all time points examined, the extent of metabolism was greater for [¹¹C]-RS 2315 than for [¹¹C]-RS 2360. The blocking study failed to proof specificity of [¹¹C]-RS 2315 at all time points. [¹¹C]-RS 2360 showed specificity towards MAO-A at 1 min p.i. At 10 and 30 min p.i. however, no effect of clorgyline pretreatment could be observed. The absence of selectivity at the later time points might be explained by the appearance of metabolites in the brain. Administration of *R*-(-)-deprenyl had no significant effect on the brain uptake of [¹¹C]-RS 2360. In the imaging study with [¹¹C]-RS 2360, administration of *R*-(-)-deprenyl caused a decreased brain uptake although this effect is not significant. Clorgyline pretreatment on the other hand, showed an overall significant reduced uptake of [¹¹C]-RS 2360 indicating specific binding at MAO-A. These observations indicate that [¹¹C]-RS 2360 is more selective towards

MAO-A than to MAO-B which is in accordance with the *in vitro* determined K_i values.

Based on these results, we can conclude that [¹¹C]-RS 2315 is not suitable for visualization of MAO-A *in vivo*. [¹¹C]-RS 2360 on the other hand might have potential for mapping MAO-A when PET scan is performed directly after injection of the tracer. Further studies are necessary to evaluate the potential role of [¹¹C]-RS 2360 in MAO-A imaging in humans. It is possible that the metabolism pattern in humans is different from that obtained in rodents. Therefore it is useful to compare the metabolism pattern of [¹¹C]-RS 2360 in whole rodent blood spiked with [¹¹C]-RS 2360 with the metabolism in whole human blood spiked with [¹¹C]-RS 2360 to have an initial notion about the difference in metabolism in humans and rodents. A slower metabolism in humans could result in improved selectivity at later time points.

6.6. References

- Alia-Klein N, Goldstein RZ, Kriplani A, Logan J, Tomasi D, Williams B et al. Brain monoamine oxidase A activity predicts trait aggression. *J Neurosci* 2008; 28:5099-104.
- Arnett CD, Fowler JS, MacGregor RR, Schlyer DJ, Wolf AP, Langstrom B and Halldin C. Turnover of brain monoamine oxidase measured *in vivo* by positron emission tomography using L-[¹¹C]deprenyl. *J Neurochem* 1987; 49:522-7.
- Bergstrom M., Westerberg G. and Langstrom B. ¹¹C –Harmin as a tracer for monoamine oxidase A (MAO-A): *in vitro* and *in Vivo* studies. *Nuc Med Biol* 1997; 24:287-93.
- Bergstrom M., Westerberg G., Kihlberg T. and Langstrom B. Synthesis of some ¹¹C-labelled MAO-A inhibitors and their *in vivo* uptake kinetics in rhesus monkey brain. *Nuc Med Biol* 1997; 24:381-8.
- Berlin I, Said S, Spreux-Varoquaux O, Olivares R, Launay J-M and Puech AJ. Monoamine oxidase A and B activities in heavy smokers. *Biol Psychiatry* 1995; 38:756-61.
- Brunner HG, Nelen M, Breakefield XO, Ropers HH and van Oost BA. Abnormal behaviour associated with a point mutation in the structural gene for monoamine oxidase A. *Science* 1993; 262:578-80.
- Dolle F, Valette H, Bramouille Y, Guenther I, Fuseau C, Coulon C et al. Synthesis and *in vivo* imaging properties of [¹¹C]Befloxadone: a novel highly potent positron emission tomography ligand for mono-amine oxidase-A. *Bioorg Med Chem* 2003; 13:1771-5.
- Fowler JS, Volkow ND, Wang G-J, Pappas N, Logan J, Shea C et al. Brain monoamine oxidase A inhibition in cigarette smokers. *Proc Natl Acad Sci USA* 1996; 93:14065-9.

- Fowler S.J., Ding Y-S., Logan J., MacGregor R.R., Shea C. et al. Species differences in [¹¹C]clorgyline binding in brain. *Nucl Med Biology* 2001; 28:779-85.
- Heafield MTE and Williams AC. Parkinson's disease: clinical and therapeutics effects. *Current opinion in neurology and neurosurgery* 1992; 5:288-294.
- Hirata M, Kagawa S, Yoshimoto M and Ohmomo Y. Synthesis and characterization of radioiodinated MD-230254: A new ligand for potential imaging of monoamine oxidase B activity by single photon emission computed tomography. *Chem Pharm Bull* 2002; 50:609-614.
- Jensen SB, Di Santo R, Olsen AK, Pedersen K, Costi R, Cirilli R and Cumming P. Synthesis and cerebral uptake of 1-(1-[¹¹C]methyl-1*H*-pyrrol-2-yl)-2-phenyl-2-(1-pyrrolidinyl)ethanone, a novel tracer for positron emission tomography studies of monoamine oxidase type A. *J Med Chem* 2008; 51:1617-22.
- La regina G, Silvestri R, Artico M, Lavecchia A, Novellino E, Befani E et al. New pyrrole inhibitors of monoamine oxidase: synthesis, biological evaluation, and structural determinants of MAO-A and MAO-B selectivity. *J Med Chem* 2007; 50:922-931.
- Meyer JH, Ginovart N, Boovariwala A, Sagrati S, Hussey D, Garcia A et al. Elevated monoamine oxidase A levels in the brain. *Arch Gen Psychiatry* 2006; 63:1209-16.
- Shih JC and Thompson RF. Monoamine oxidase in neuropsychiatry and behaviour. *Am J Human Genet* 1999; 65:593-8.
- Waterhouse RN. Determination of lipophilicity and its use as a predictor of blood-brain barrier penetration of molecular agents. *Mol Imaging Biol* 2003; 5:376-389.

Chapter 7

Synthesis, radiosynthesis and *in vivo* evaluation of [¹²³I]-FMIP for imaging the dopamine transporter



De Bruyne S.^a, Boos T.L.^b, wyffels L.^a, Goeman J.L.^c, Rice K.C.^b, De Vos F.^a
Journal of Labelled Compounds and Radiopharmaceuticals **2009**; 52 (8): 304-311.

^a Laboratory for Radiopharmacy, Ghent University, Harelbekestraat 72, 9000 Ghent, Belgium

^b Chemical Biology Research Branch, National Institute on Drug Abuse and National Institute on Alcohol Abuse and Alcoholism, National Institutes of Health, Bethesda, MD, USA

^c Department of Organic Chemistry, Ghent University, Krijgslaan 281 S4, 9000 Ghent, Belgium

Chapter 7

Synthesis, radiosynthesis and *in vivo* evaluation of [¹²³I]-FMIP for imaging the dopamine transporter

7.1. Abstract

Aim: 4-(2-(Bis(4-fluorophenyl)methoxy)ethyl)-1-(4-iodobenzyl)piperidine (FMIP) has nanomolar affinity for DAT and better selectivity over the other monoamine transporters compared to the already existing ligands for DAT imaging with SPECT. The aim of this study was to synthesize and evaluate the usefulness of [¹²³I]-FMIP as an *in vivo* tracer for DAT.

Methods: [¹²³I]-FMIP was synthesized by electrophilic destannylation. Biodistribution, blocking and metabolite studies of [¹²³I]-FMIP were performed in male NMRI mice whereas a more detailed brain dissection was done in male Sprague-Dawley rats.

Results: The tributylstannyl precursor was synthesized with an overall yield of approximately 25 %. The mean radiochemical yield of [¹²³I]-FMIP was 40 ± 10 % and after purification, the radiochemical purity appeared to be > 98 %. The specific activity of the compound was at least 667 GBq/ μ mol. Biodistribution studies showed brain uptake of 0.96 ± 0.53 % ID/g at 0.5 min p.i. and 0.26 ± 0.02 % ID/g at 180 min p.i. High blood activity was observed at all time points. Blocking studies indicated no selectivity of [¹²³I]-FMIP towards DAT. A metabolite study demonstrated that in brain, over 80 % was present as intact [¹²³I]-FMIP at 60 min p.i. In rats, regional brain distribution of [¹²³I]-FMIP was not in agreement with DAT localization demonstrating lack of selectivity towards DAT.

Conclusion: These results indicate that [¹²³I]-FMIP is not suitable for mapping DAT *in vivo*.

7.2. Introduction

It has been demonstrated that DAT neuroimaging is useful in PD diagnosis, providing information on the integrity of the dopaminergic neurotransmission system *in vivo* (Poewe and Sherfler, 2003; Dhawan and Eidelberg, 2001; Shih et al., 2006). Because of the crucial role of DAT in the etiology of PD as well as other neurological disorders and addiction, several DAT ligands have been developed for *in vivo* SPECT imaging (Volkow et al., 1996; Elsinga et al., 2006). These ligands all share the same problem of being not selective towards SERT. The commercially available [¹²³I]-FP-CIT (DaTSCAN, GE Healthcare, Little Chalfont, UK) has a K_i value of 3.5 nM for DAT, 0.11 nM for SERT and 63 nM for NET, indicating lack of selectivity for DAT (Neumeyer et al., 1991; 1996; Scheffel et al., 1997). Other drawbacks of [¹²³I]FP-CIT are the lack of good *in vivo* kinetics and the formation of 4 labelled metabolites in plasma (Bergstrom et al., 1996; Emond et al., 1997). Another investigated DAT radioligand, [¹²³I]PE2I, has K_i values of 17 nM, 500 nM and over 1000 nM, for DAT, SERT and NET respectively so a SERT/DAT selectivity of 29 was calculated. Another disadvantage of [¹²³I]PE2I is *in vivo* deiodination of the iodo vinyl group (Guilloteau et al., 1997). These shortcomings indicate that there is still a need for selective radioligands for DAT.

A study by Boos et al. (2006) has concentrated on the development of novel analogues of 1-(2-(bis(4-fluorophenyl)methoxy)ethyl)-4-(3-phenylpropyl)piperazine (GBR 12909). GBR 12909 (Figure 7.1) is a high affinity, selective, long-lasting inhibitor of dopamine reuptake and a noncompetitive blocker of DAT in rats (van der Zee et al., 1980; Rothman et al., 1991). The newly developed analogues were pharmacologically evaluated to identify ligands with varying transporter affinity and selectivity.

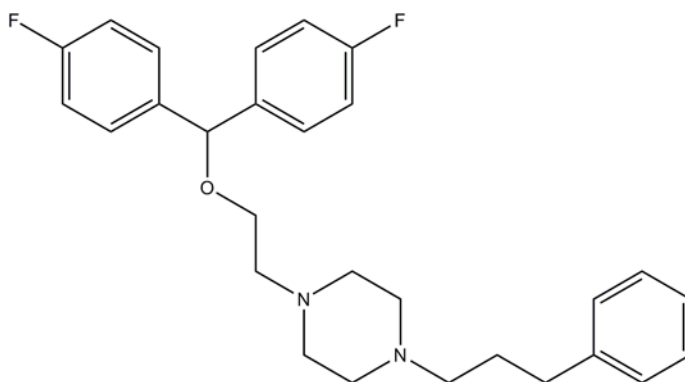


Figure 7.1 Structure of GBR 12909

For the compound investigated in this study, 4-(2-(bis(4-fluorophenyl)methoxy)ethyl)-1-(4-iodobenzyl)piperidine (FMIP), they reported K_i values of 1.9 nM for DAT, 205 nM for SERT and 4110 nM for NET. These values indicate that FMIP has good *in vitro* selectivity over the other monoamine transporters (108 for SERT/DAT and 2163 for NET/DAT). Compared to [¹²³I]FP CIT and [¹²³I]PE2I, the *in vitro* properties of FMIP are promising. We therefore evaluated the potential of [¹²³I]-FMIP as a suitable tracer for DAT *in vivo* (Figure 7.2).

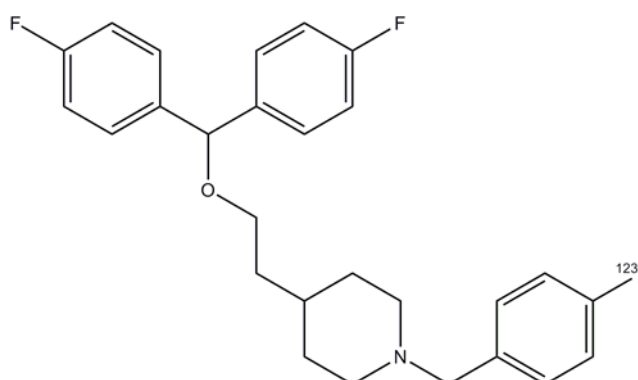


Figure 7.2 Structure of [¹²³I]-FMIP

In this Chapter we present the synthesis of the precursor and reference molecule. The radiosynthesis of [¹²³I]-FMIP, along with its purification, quality control, log D_{7.4}, stability and specific activity is reported. [¹²³I]-FMIP is evaluated *in vivo* in NMRI mice. Metabolic assays are performed on blood and brain of NMRI mice. The selectivity of [¹²³I]-FMIP towards DAT is investigated by a regional brain distribution in Sprague-Dawley rats and a blocking study in NMRI mice.

7.3. Materials & Methods

7.3.1. ORGANIC SYNTHESIS

The starting material, 4-(2-(bis(4-fluorophenyl)methoxy)ethyl)piperidine (**1**), was described and synthesized by Boos et al. (2006). All melting points (m.p.) were determined on a Thomas–Hoover melting point apparatus and are uncorrected. The ¹H NMR spectra were recorded on a Varian XL-300 instrument with DMSO-*d*₆ as solvent, δ values were recorded in ppm (TMS as internal standard), *J* (Hz) assignments of ¹H resonance coupling were done. Electron ionization (EI) mass spectra were obtained using a VG-Micro Mass 7070F mass spectrometer. TLC was performed on 250 mm Analtech GHLF silica gel plates. Visualization was accomplished under UV at 254 nm. Elemental analyses were performed by Atlantic Microlabs, Inc. (Norcross, GA).

7.3.1.1. (4-(2-(Bis(4-fluorophenyl)methoxy)ethyl)piperidin-1-yl)(4-hydroxyphenyl)-methanone (**2**)

A solution of 4-hydroxybenzoic acid (2.0 g, 14.5 mmol) and *N*-hydroxybenzotriazole (1.9 g, 13.3 mmol) in CH₂Cl₂ (200 mL) was stirred for 15 min, prior to the addition of 4-(2-(bis(4-fluorophenyl)methoxy)ethyl)piperidine (**1**) (4.0 g, 12.1 mmol) and 1-ethyl-3-(3'-dimethylaminopropyl)carbodiimide hydrochloride (5.1 g, 26.6 mmol). The solution was stirred for 96 h after which the

solvent was removed under reduced pressure. The semi-solid was dissolved in ethyl acetate (250 mL) and the organic layer was washed with 1 M HCl (250 mL), 10 % potassium carbonate (250 mL), and brine (250 mL). The organic layer was dried over anhydrous Na₂SO₄ and the solvent was removed under reduced pressure. TLC analysis (9:1 (v:v) – CHCl₃:MeOH) identified a small amount of unreacted starting material not removed in the acid washing. Flash chromatography provided two compounds that co-migrated in the 9:1 (v:v) – CHCl₃:MeOH solvent system. Both compounds were dried under high vacuum and underwent alane reduction without further purification.

7.3.1.2. 4-((4-(2-(Bis(4-fluorophenyl)methoxy)ethyl)piperidin-1-yl)methyl)phenol (**3**)

To a flame dried flask, lithium aluminiumhydride (1.3 g, 33 mmol) was added and cooled to 0°C under argon. THF (10 mL) was added drop-wise while stirring. Upon the completion of the addition of THF, sulphuric acid (1.1 g, 17 mmol) in THF (10 mL) was added drop-wise. The solution was stirred at 0°C for 45 min. To the ice-cold solution was added **2** (3.0 g, 6.6 mmol) in THF (10 mL). The solution was stirred for an additional 15 min at 0°C, then allowed to warm to room temperature and stirred for 2 h. 10 % NaOH (200 mL) and ethyl acetate (75 mL) were added to the solution. The layers were separated and the aqueous layer was further extracted with ethyl acetate (2 x 75 mL). The organic extracts were combined and washed with H₂O (200 mL) and brine (200 mL). The organic layer was dried over anhydrous Na₂SO₄ and the solvent was removed under reduced pressure to yield **3** as a solid. TLC analysis identified a small quantity of starting material. The solid was dissolved in ether and 1.1 equivalent of oxalic acid was added. 2.6 g (5.9 mmol) of **3** as the oxalate salt was obtained. The yield of the reaction was 89 %.

¹H NMR (DMSO-d₆, 300 MHz): δ 6.7 - 7.4 (m, 12H, ar); 5.5 (s, 1H, CH-O); 3.8 (bs, 2H, CH₂NH); 3.0-3.4 (m, 4H); 2.5-2.9 (m, 3H); 1.3-1.7 (m, 6H). HRMS (EI) calcd for C₂₇H₃₀F₂NO₂ *m/z*, 438.2245; found 438.2243. Anal. calcd for

C₂₇H₂₉F₂NO₂·0.5 C₂H₂O₄: C, 69.69; H, 6.27; N, 2.90. Found: C, 69.17; H, 6.21; N, 2.88. m.p. 198-199.5°C. R_f = 0.53 (9:1-CHCl₃:MeOH).

7.3.1.3. *4-((4-(2-(Bis(4-fluorophenyl)methoxy)ethyl)piperidin-1-yl)methyl)phenyltrifluoromethanesulfonate (4)*

N-Phenyltrifluoromethanesulfonimide (1.4 g, 3.8 mmol), **3** (1.3 g, 3.0 mmol) and *N,N*-diisopropylethylamine (1.0 mL, 6.0 mmol) were combined in CH₂Cl₂ (20 mL) and stirred under argon, overnight. To the solution was added H₂O (50 mL) and CH₂Cl₂ (50 mL). The organic layer was separated and subsequently washed with a 10 % NaHCO₃ solution, H₂O (50 mL) and brine (50 mL). The organic layer was dried over anhydrous Na₂SO₄ and the solvent was removed under reduced pressure. After chromatography on silica gel using 9:1 (v:v) - CHCl₃:MeOH as solvent system, **4** was obtained as a clear oil 1.5 g (2.6 mmol). The yield of the reaction was 87 %.

¹H NMR (DMSO-*d*₆, 300 MHz): δ 7.0 - 7.4 (m, 12H, ar); 5.5 (s, 1H, CH-O); 4.0 (s, 2H, CH₂NH); 3.2-3.4 (m, 4H); 3.1 (m, 2H); 1.2-1.7 (m, 7H). HRMS (EI) calcd for C₂₈H₂₉F₂NO₄S *m/z* 570.1737; found 570.1738. Anal. calcd for C₂₈H₂₉F₂NO₄S·2 H₂O: C, 55.53; H, 5.32; N, 2.31. Found: C, 55.71; H, 5.27; N, 2.31.

7.3.1.4. *4-(2-(Bis(4-fluorophenyl)methoxy)ethyl)-1-(4-(tributylstannyl)benzyl)piperidine (5)*

1.1 g (1.9 mmol) of **4** was dissolved in anhydrous dioxane (15 mL) and to the solution was added bis(tributyltin) (1.5 g, 2.5 mmol). Under argon, lithium chloride (0.2 g, 5.7 mmol), tetrakis(triphenylphosphine)palladium (0.7 g, 0.06 mmol) and a catalytic amount of 2,6-di(*tert*)-butyl-4-methylphenol were added. The solution was heated to reflux and stirred overnight. The reaction was quenched upon the addition of ethyl acetate (50 mL) and a 10 % aqueous NaOH solution (50 mL). The organic layer was filtered through a pad of celite. The filtrate was washed with H₂O (50 mL) and brine (50 mL). The organic layer was dried over anhydrous

Na₂SO₄. Chromatography with 7:3 (v:v) - hexane:ethyl acetate as solvent system provided 0.46 g (0.6 mmol) of **5** as a chromatographically pure, clear oil. The reaction yield was 68 %.

¹H NMR (DMSO-d₆, 300 MHz): δ 7.1 - 7.4 (m, 12H, ar); 5.5 (s, 1H, CH-O); 3.3-3.4 (m, 8H); 0.8-1.5(m, 30H). HRMS (EI) calcd for C₃₉H₅₆F₂NOSn *m/z*, 712.3352; found 710.3344. Anal. calcd for C₃₉H₅₅F₂NOSn·0.5 H₂O: C, 65.09; H, 7.84; N, 1.95. Found: C, 64.83; H, 7.81; N, 1.95.

7.3.1.5. 4-(2-(Bis(4-fluorophenyl)methoxy)ethyl)-1-(4-iodobenzyl)piperidine (FMIP)

To a solution of **1** (0.5 g, 1.4 mmol) and potassium carbonate (0.6 g, 4.2 mmol) in DMF (15 mL) was added a catalytic amount of NaI and 4-iodobenzyl bromide (0.5 g, 1.5 mmol). The solution was stirred overnight. TLC analysis identified no remaining starting material and the solution was poured into H₂O (200 mL) and extracted with ethyl acetate (3 x 100 mL). The combined extracts were washed with H₂O (2 x 200 mL) and brine (200 mL). The organic layer was dried over anhydrous Na₂SO₄ and the solvent was removed under reduced pressure. The resulting oil was dissolved in EtOH (50 mL) and 1.1 equivalent of oxalic acid in EtOH was added. Upon cooling, crystals were formed and an additional recrystallization provided 0.4 g (0.7 mmol) of a FMIP oxalate as white solid. The reaction proceeded with a yield of 50 %.

¹H NMR (DMSO-d₆, 300 MHz): δ 7.1 - 7.8 (m, 12H, ar); 5.5 (s, 1H, CH-O); 4.0 (bs, 2H, CH₂NH); 3.1-3.5 (m, 4H); 2.5-2.7 (m, 3H); 1.2-1.8 (m, 6H). HRMS (ESI) calcd for C₂₇H₂₉IF₂NO *m/z*, 548.1262; found 548.1264. Anal. calcd for C₂₇H₂₈IF₂NO·C₂H₂O₄: C, 54.64; H, 4.74; N, 2.20. Found: C, 54.37; H, 4.95; N, 2.18. m.p. 157-158 °C.

7.3.2. RADIOCHEMISTRY

[¹²³I]-4-(2-(Bis(4-fluorophenyl)methoxy)ethyl)-1-(4-iodobenzyl)piperidine ([¹²³I]-FMIP) was prepared by electrophilic radioiododestannylation of **5**. Briefly, EtOH (50 μ L), glacial acetic acid (8 μ L), chloramine-T (1.0 μ mol, 300 μ g in 15 μ L deionized H₂O) and n.c.a. [¹²³I]NaI (37 MBq in 10 μ L 0.05 M NaOH) were added to a reaction vial containing **5** (200 μ g, 0.281 mmol). The mixture was allowed to react for 10 min at ambient temperature. The reaction was quenched by adding sodium metabisulfite (1.6 μ mol, 300 μ g in 15 μ L deionized H₂O). Purification was performed by HPLC on a Apollo C₁₈ column (250 mm x 4.6 mm, 5 μ m) using 90:10:0.1 (v:v) - MeOH:H₂O:NH₄OH as solvent system at a flow rate of 1 mL/min. [¹²³I]-FMIP eluted with a retention time of 24-25 min. The collected fraction was diluted with sterile water and concentrated on an activated C₁₈ Sep-pak cartridge (Alltech Maxi-Clean Prevail C18). [¹²³I]-FMIP was eluted from the Sep-pak with 1 ml EtOH. Finally the EtOH was diluted with isotonic saline to obtain an injectable solution (< 10 % (v:v) EtOH).

7.3.3. IN VITRO CHARACTERIZATION

The radioanalytical data were obtained by injection of 100 μ L test solution on a RP analytical HPLC (Alltima C₁₈, 250 mm x 4.6 mm, 5 μ m) using 91:9:0.1 (v:v) - MeOH:H₂O:NH₄OH as mobile phase at a 1 mL/min flow rate.

Radiochemical purity and identity were determined by co-injection of an aliquot of [¹²³I]-FMIP (after Sep-pak purification) with authentic cold reference product (FMIP).

To test the *in vitro* stability, [¹²³I]-FMIP was maintained in 0.01 M PBS (pH 7.4) and in the injection solution, at room temperature. After 24 h, [¹²³I]-FMIP was analyzed by HPLC.

For calculating specific activity, a calibration curve between 10 x 10⁻³ μ M and 0.1 x 10⁻³ μ M and subsequently a more detailed calibration curve between 0.5 x 10⁻³ μ M

and $0.1 \times 10^{-3} \mu\text{M}$ was obtained. Log $D_{7.4}$ was determined according to the method described in Chapter 4.

7.3.4. BIODISTRIBUTION STUDY

Male NMRI mice of 4 - 6 weeks old, weighing 22 - 30 g were injected in a tail vein with 200 μL 8:92 (v:v) - EtOH:physiological saline containing approximately 185 kBq (5 μCi) of [¹²³I]-FMIP. The mice were awake during the injection. At various time points p.i. mice ($n=3$ for each time point) were sacrificed under isoflurane anaesthesia and dissected. Blood, urine and organs were removed, weighed and counted for radioactivity in a gamma counter. To remove adhering blood, all organs were rinsed with water prior to weighing and counting. For calculation of the injected dose, five aliquots of the injection solution were weighed and counted for activity. Results are decay corrected and expressed as % ID/g \pm SD.

7.3.5. REGIONAL BRAIN DISTRIBUTION STUDY

Male rats (250 - 300 g, Sprague-Dawley) were injected in a tail vein with 7.4 MBq (200 μCi) of [¹²³I]-FMIP dissolved in 300 μL 8:92 (v:v) - EtOH:physiological saline. The rats were awake during the injection. At 10, 30, 60, 180 or 360 min, animals ($n=3$ for each time point) were sacrificed by i.v. injection of T61. Blood was taken and the brain was removed and dissected. Blood samples and the different brain parts were weighed and counted for radioactivity with a gamma counter. For calculation of the injected dose, five aliquots of the injection solution were weighed and counted for activity. Results are decay corrected and are expressed as % ID/g \pm SD.

7.3.6. BLOCKING STUDY

To determine the specific tissue uptake of the labelled compound, blocking studies were performed in male NMRI mice of 4 - 6 weeks old, weighing approximately 25 g. Prior to tracer injection, mice received a tail vein injection of 150 μ l (95:5 – physiological saline:EtOH) containing a selective ligand (5 mg/kg) for respectively the DAT (GBR 12909), SERT (citalopram) or NET (reboxetine mesylate). The control group received a tail vein injection of 150 μ l (95:5 – physiological saline:EtOH) without ligand. After 20 min, the mice were injected with approximately 185 kBq (5 μ Ci) of [¹²³I]-FMIP dissolved in 100 μ l EtOH:physiological saline solution (8:92). The mice were awake during the injections. The animals ($n=3$ for each time point) were sacrificed at 2, 5, 60 or 180 min p.i. All tissues were treated as previously described. For calculation of the injected dose, five aliquots of the injection solution were weighed and counted for activity. The concentration of radioactivity in tissues is decay-corrected and expressed as % ID/g \pm SD. Statistical analysis was performed using one-sided, unpaired student's *t*-test. Only p-values < 0.05 are considered significant.

7.3.7. PLASMA BINDING

Plasma protein binding was determined according to literature procedures (Gandelman et al., 1994; Fowler et al., 2007). In brief, a known amount of radiotracer (37 kBq (1 μ Ci)) was added to 500 μ L mouse plasma and the mixture was incubated for 10 min at room temperature. Three aliquots (30 μ L) of spiked plasma were counted for radioactivity. The remaining plasma was transferred onto a Centrifree device with a nominal molecular weight limit of 30 kDa (Amicon inc, Millipore) and centrifuged for 15 min at 4000 g. The top part of the Centrifree tube was discarded, and 3 aliquots (30 μ L) of the solution remaining in the bottom cup (unbound fraction) were counted for radioactivity. The plasma protein binding

was determined by calculating the free fraction as the ratio of the counts of filtered aliquot to the counts of non-centrifuged aliquot.

7.3.8. METABOLITE ANALYSIS

200 µL 92:8 (v:v) - Isotonic saline:EtOH containing 1.85 - 3.7 MBq (50 – 100 µCi) [¹²³I]-FMIP was injected in a tail vein of awake male NMRI mice (5 - 7 weeks old, weighing 25 - 30 g). At 10 or 60 min p.i., the mice ($n=3$ for each time point) were sacrificed and blood and brain were taken and treated as described in Chapter 4. HPLC analysis was performed using a RP C₁₈ HPLC column (Econosphere C₁₈ 250 mm x 10 mm, 10 µm) attached to a precolumn (Alltima C₁₈ 33 mm x 7 mm, 10 µm) with 91:9:0.1 (v:v) methanol:H₂O:NH₄OH as solvent system at a flow rate of 6 mL/min.

7.3.9. BLOOD-BRAIN BARRIER TRANSPORT INHIBITION STUDY

To investigate if the low brain uptake of [¹²³I]-FMIP is due to P-gp interference, a biodistribution study with pretreatment of the mice with CsA was performed. A 50 mg/kg dose and a 30 min time period between CsA and tracer injection has been reported to inhibit the efflux action of P-gp pumps in rodent brain (Ishiwata et al., 2007). Male NMRI mice with a body mass of approximately 25 g ($n=3$ for each time point) were i.v. injected with either 50 mg/kg CsA (test group) or the same volume of physiological saline (control group). After 30 min, [¹²³I]-FMIP (185 kBq (5 µCi), 150 µL) was injected via a tail vein. The mice were awake during the injections. The mice were sacrificed and dissected at 2, 60 or 180 min p.i. of [¹²³I]-FMIP. Blood and organs were weighed and counted for radioactivity. TO remove adhering blood, all organs were rinsed with water prior to weighing and counting. For calculation of the injected dose, five aliquots of the injection solution were weighed and counted for activity. Results are decay-corrected and expressed as %

ID/g \pm SD. Statistical analysis was performed using one-sided, unpaired student's *t*-test. Only p-values < 0.05 are considered significant.

7.3.10. REGIONAL BRAIN DISTRIBUTION AFTER CSA PRETREATMENT

Male rats (250 - 300 g, Sprague-Dawley) were injected in a tail vein with 7.4 MBq (200 μ Ci) of [¹²³I]-FMIP dissolved in 300 μ L 8:92 (v:v) – EtOH:physiological saline. 30 min prior to tracer injection, a solution of 50 mg/kg CsA (test group) or physiological saline (control group) was administered intravenously. At 30, 60, 180 and 360 min after [¹²³I]-FMIP injection, animals ($n=3$ for each time point) were sacrificed by intravenous injection of T61. Blood was taken and the brain was removed and dissected. Blood samples and the different brain parts were weighed and counted for radioactivity with a gamma counter. For calculation of the injected dose, five aliquots of the injection solution were weighed and counted for activity. Radioactivity is decay corrected and results are expressed as % ID/g \pm SD. Statistical analyses were performed using the one-side unpaired student's *t* test. A p-value < 0.05 is interpreted as statistically significant.

7.4. Results & Discussion

7.4.1. ORGANIC SYNTHESIS

As mentioned in Chapter 4, iodination can be accomplished by electrophilic as well as nucleophilic substitution. Several attempts to produce [¹²³I]-FMIP by nucleophilic substitution failed due to the unefficient radiochemical yield. In order to radiosynthesize [¹²³I]-FMIP by electrophilic substitution, the synthesis of the tributylstannyl precursor was necessary.

7.4.1.1. Precursor synthesis

The precursor molecule was synthesized in four steps as is depicted in Figure 7.3. The starting material **1** was prepared by Boos et al. (2006).

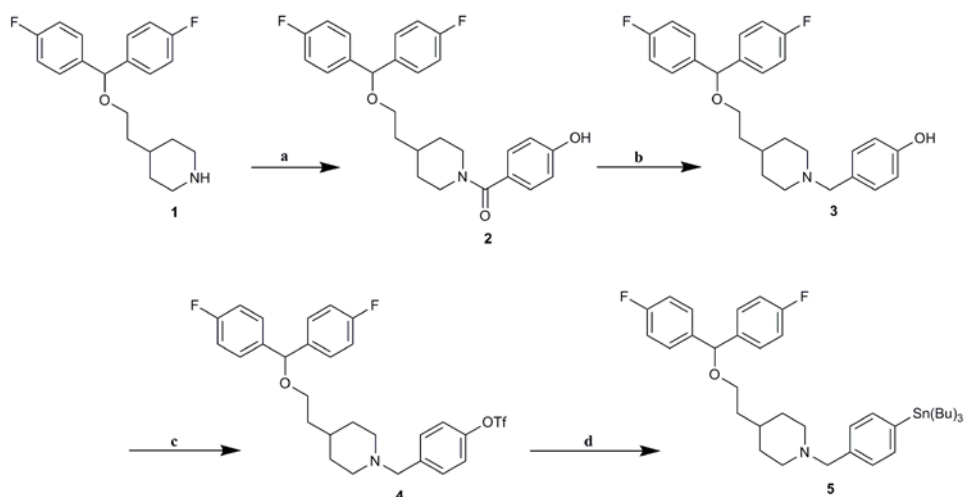


Figure 7.3 Synthesis of the tributylstannyl precursor **5**

Reagents: (a) 4-hydroxybenzoic acid, *N*-hydroxybenzotriazole, 1-ethyl-3-(3'-dimethylaminopropyl)carbodiimide, CH₂Cl₂; (b) lithiumaluminiumhydride, sulphuric acid, THF; (c) *N*-phenyltrifluoromethanesulfonamide, *N,N*-diisopropylethylamine, CH₂Cl₂; (d) bis(tributyltin), tetrakis(triphenylphosphine)palladium, lithium chloride, dioxane

The most direct route to the tributylstannyl precursor is generally a palladium catalyzed stannylation using hexabutylstannane and tetrakis(triphenylphosphine)-palladium where a bromine-atom is replaced by a tributylstannyl group. Several attempts to synthesize **5** by this route were unsuccessful, requiring another route. It was found that the triflate analogue was a suitable substrate for the Stille coupling. In this way, the tributylstannyl precursor **5** was synthesized starting from **1** through the triflate intermediate in an overall yield of 25 %. First, the secondary cyclic amine **1** was coupled with 4-hydroxybenzoic acid, resulting in **2** which was used without further purification. Reduction of **2** yielded the tertiary amine **3** (89

%). The hydroxyl function of **3** was converted into the triflate (87 %), making it a better leaving group. Finally, the precursor molecule was obtained by replacing the triflate by tributylstannyl using bis(tributylstannane) (68 %).

7.4.1.2. Synthesis of FMIP

Nucleophilic substitution of **1** yielded the cold iodinated product FMIP in a yield of 50 % (Figure 7.4). FMIP is required as reference compound in HPLC analysis.

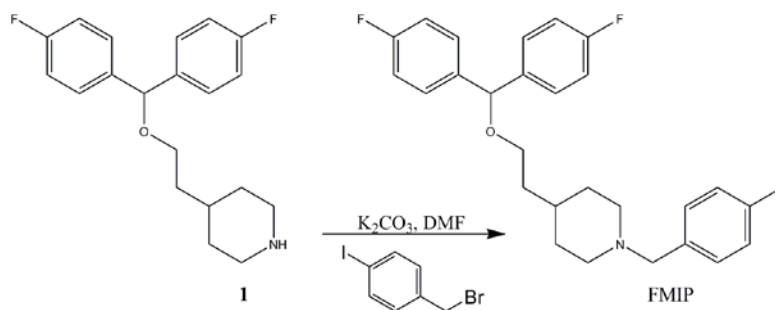


Figure 7.4 Synthesis of 4-(2-(bis(4-fluorophenyl)methoxy)ethyl)-1-(4-iodobenzyl)piperidine

7.4.2. RADIOSYNTHESIS

[^{123}I]-FMIP was obtained in a radiochemical yield of 40 ± 10 % by electrophilic iododestannylation of the tributylstannyl precursor **5** (Figure 7.5).

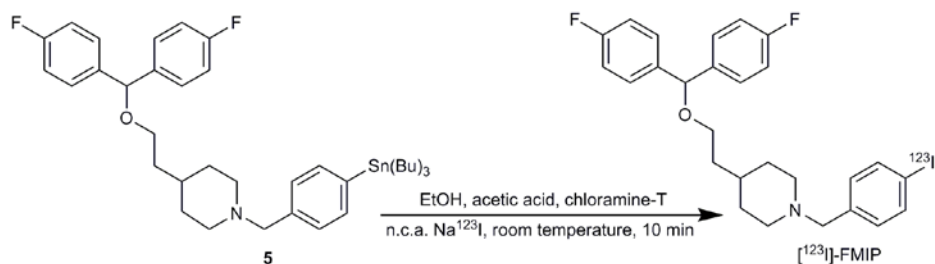


Figure 7.5 Radiosynthesis of [^{123}I]-FMIP

7.4.3. IN VITRO CHARACTERIZATION

The radiolabelled compound [¹²³I]-FMIP was co-injected with the cold compound. Similar retention times were observed for [¹²³I]-FMIP and FMIP, confirming the identity of the synthesized product (Figure 7.6). The average radiochemical purity of [¹²³I]-FMIP was found to be > 98 %. After 24 h, the radiochemical purity of [¹²³I]-FMIP remained higher than 95 % both in PBS buffer and in the injection solution.

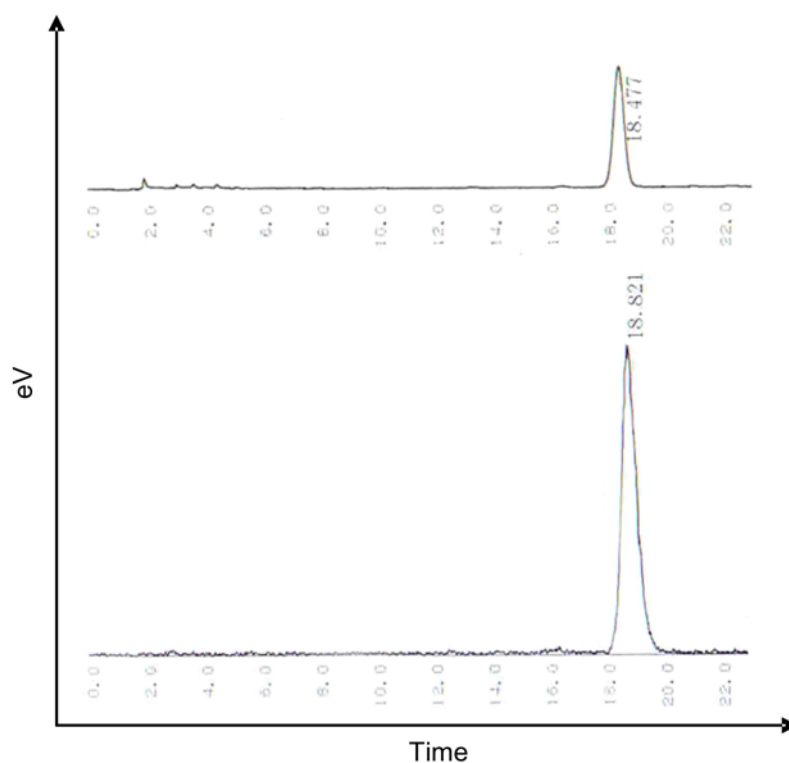


Figure 7.6 HPLC chromatogram of [¹²³I]-FMIP and FMIP co-injection

The upper part of the figure shows the UV-chromatogram, the radiochromatogram is shown in the lower part.

Since no UV-signal was observed for the amount of [¹²³I]-FMIP synthesized, the detection limit was used for calculation of the specific activity. Using the described

radioanalytical method, the detection limit for [¹²³I]-FMIP was 1.5×10^{-6} M. Specific activity appeared to be at least 667 GBq/ μ mol (18 Ci/ μ mol).

An ideal log $D_{7.4}$ value for brain radiotracers is between 1.5 and 3.5 (Waterhouse, 2003). The determined log octanol/PBS partition coefficient was found to be 1.42 ± 0.12 , which is suitable for brain penetration.

7.4.4. BIODISTRIBUTION STUDY

Results of the biodistribution study are shown in Table 7.1. Radioactivity concentrations for [¹²³I]-FMIP in blood and brain of NMRI mice are shown in Figure 7.7. Uptake of the tracer in mouse brain was demonstrated with a maximum value of 0.96 ± 0.53 % ID/g in brain at 0.5 min p.i. The tracer was rapidly cleared out of the blood. At all time points, blood activity remained higher than brain activity.

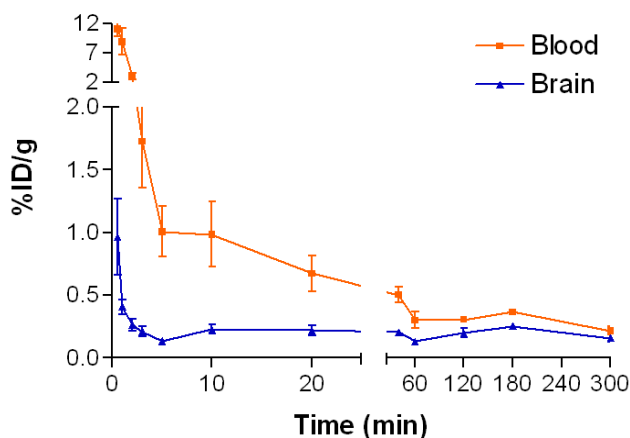


Figure 7.7 Blood-brain distribution of [¹²³I]-FMIP in male NMRI mice

Values are expressed as % ID/g \pm SD ($n=3$)

Other organs with high tracer uptake were heart (11.14 ± 3.79 % ID/g at 0.5 min p.i.) and lungs (43.27 ± 15.46 % ID/g at 0.5 min p.i.). The heart and lungs are the

first organs that are passed by the blood flow after intravenous injection of the radiotracer in the blood. The radioactivity uptake in these organs is therefore probably a reflection of the blood pool radioactivity. Since radioactivity uptake in stomach is low (1.33 ± 0.55 % ID/g at 0.5 min p.i.) and does not change between the various time points (1.06 ± 0.08 % ID/g at 180 min p.i.), [¹²³I]-FMIP is probably not sensitive to dehalogenation *in vivo*.

High uptake was seen in liver (11.43 ± 4.53 % ID/g at 20 min p.i.), kidneys (4.91 ± 2.14 %ID/g at 0.5 min p.i.) and urine (data not shown) and uptake in the intestines was low, suggesting mainly urinary and no biliary clearance of [¹²³I]-FMIP during the investigated timeframe.

Table 7.1 Tissue uptake of radioactivity in male NMRI mice at various time points following i.v. administration [¹²³I]-FMIP

	Time (min)											
	0.5	1	2	3	5	10	20	40	60	120	180	300
Blood	11.14 ± 2.28	8.95 ± 3.97	3.02 ± 0.96	1.73 ± 0.65	1.01 ± 0.35	0.99 ± 0.45	0.67 ± 0.24	0.50 ± 0.11	0.30 ± 0.11	0.31 ± 0.01	0.37 ± 0.02	0.22 ± 0.05
Brain	0.96 ± 0.53	0.41 ± 0.11	0.26 ± 0.08	0.21 ± 0.07	0.14 ± 0.02	0.23 ± 0.07	0.22 ± 0.07	0.21 ± 0.04	0.13 ± 0.04	0.20 ± 0.06	0.26 ± 0.02	0.16 ± 0.06
Heart	11.14 ± 3.79	5.48 ± 1.29	4.91 ± 0.59	4.54 ± 2.12	3.20 ± 1.22	5.01 ± 1.36	4.24 ± 1.01	2.35 ± 0.72	1.15 ± 0.36	0.96 ± 0.23	1.06 ± 0.14	0.71 ± 0.23
Lungs	43.27 ± 15.46	20.03 ± 1.3	14.32 ± 1.54	17.51 ± 8.73	11.80 ± 3.42	13.37 ± 6.75	9.12 ± 7.17	5.70 ± 1.44	3.87 ± 1.35	3.66 ± 1.13	3.73 ± 0.51	2.23 ± 1.03
Stomach	1.33 ± 0.55	0.81 ± 0.17	0.83 ± 0.25	1.11 ± 0.47	0.50 ± 0.12	0.94 ± 0.29	0.85 ± 0.02	1.65 ± 1.15	0.61 ± 0.28	0.67 ± 0.27	1.06 ± 0.08	0.88 ± 0.52
Spleen	3.23 ± 1.45	2.42 ± 0.56	3.85 ± 1.78	6.34 ± 3.87	4.23 ± 1.43	6.61 ± 0.69	5.99 ± 1.36	3.84 ± 1.66	1.85 ± 0.82	2.08 ± 0.5	2.46 ± 0.84	1.77 ± 0.74
Liver	4.91 ± 2.97	3.53 ± 0.86	5.04 ± 1.06	5.17 ± 2.04	3.99 ± 1.17	9.03 ± 1.8	11.43 ± 4.53	10.09 ± 2.76	8.10 ± 4.27	10.30 ± 3.02	14.20 ± 4.35	8.70 ± 4.28
Kidneys	4.91 ± 2.14	3.67 ± 0.85	3.61 ± 1.05	3.97 ± 1.91	2.76 ± 0.87	4.65 ± 0.3	4.46 ± 1.04	3.55 ± 1.11	2.53 ± 1.35	2.88 ± 0.79	3.00 ± 0.86	2.09 ± 0.86
Small intestine	0.68 ± 0.28	0.49 ± 0.06	0.53 ± 0.2	0.65 ± 0.21	0.35 ± 0.06	0.74 ± 0.12	0.71 ± 0.21	0.69 ± 0.03	0.48 ± 0.24	0.80 ± 0.15	1.20 ± 0.13	0.91 ± 0.49
Large intestine	0.37 ± 0.16	0.25 ± 0.03	0.24 ± 0.07	0.29 ± 0.12	0.16 ± 0.05	0.38 ± 0.11	0.28 ± 0.11	0.31 ± 0.06	0.20 ± 0.09	0.36 ± 0.11	0.63 ± 0.22	0.69 ± 0.28
Bladder	1.25 ± 0.65	0.73 ± 0.08	0.64 ± 0.1	0.68 ± 0.28	0.63 ± 0.28	0.82 ± 0.15	0.85 ± 0.04	1.01 ± 0.32	0.95 ± 0.34	1.34 ± 0.73	1.64 ± 0.54	0.93 ± 0.15
Pancreas	1.54 ± 0.55	1.05 ± 0.25	1.08 ± 0.21	1.45 ± 0.96	0.1 ± 0.98	1.54 ± 0.18	1.5 ± 0.33	1.19 ± 0.73	1.05 ± 0.42	1.68 ± 0.28	2.4 ± 0.34	2.54 ± 1.14
Muscle	0.91 ± 0.28	0.57 ± 0.13	0.75 ± 0.09	0.84 ± 0.15	0.66 ± 0.19	1.30 ± 0.58	0.88 ± 0.07	0.88 ± 0.21	0.61 ± 0.26	0.65 ± 0.17	0.75 ± 0.03	0.38 ± 0.11
Fat	0.93 ± 0.15	0.85 ± 0.62	0.85 ± 0.34	4.27 ± 5.57	0.72 ± 0.43	0.81 ± 0.38	0.76 ± 0.27	1.12 ± 0.77	1.10 ± 0.56	1.25 ± 0.11	2.03 ± 0.34	0.93 ± 0.51

Values are expressed as % ID/g of tissue ± SD (*n*=3)

7.4.5. REGIONAL BRAIN DISTRIBUTION STUDY

The uptake of radioactivity in various rat brain regions as a function of time following intravenous administration of [¹²³I]-FMIP is shown in Table 7.2.

Table 7.2 Tissue uptake of radioactivity in different brain regions in rats at various time points following i.v. administration of [¹²³I]-FMIP

	Time (min)				
	10	30	60	180	360
Blood	0.086 ± 0.060	0.089 ± 0.097	0.123 ± 0.084	0.116 ± 0.049	0.087 ± 0.094
Striatum	0.022 ± 0.016	0.013 ± 0.012	0.036 ± 0.031	0.053 ± 0.038	0.016 ± 0.012
Cerebellum	0.013 ± 0.007	0.024 ± 0.019	0.042 ± 0.051	0.029 ± 0.025	0.026 ± 0.012
Frontal cortex	0.013 ± 0.008	0.009 ± 0.011	0.036 ± 0.041	0.027 ± 0.035	0.015 ± 0.011
Occipital cortex	0.018 ± 0.009	0.027 ± 0.033	0.043 ± 0.063	0.015 ± 0.007	0.018 ± 0.016
Temporal cortex	0.015 ± 0.008	0.010 ± 0.013	0.017 ± 0.013	0.019 ± 0.012	0.021 ± 0.025
Parietal cortex	0.015 ± 0.010	0.019 ± 0.024	0.037 ± 0.039	0.026 ± 0.028	0.010 ± 0.007
Hippocampus	0.015 ± 0.008	0.077 ± 0.065	0.007 ± 0.008	0.049 ± 0.058	0.027 ± 0.018
Hypothalamus	0.014 ± 0.006	0.023 ± 0.026	0.030 ± 0.020	0.027 ± 0.013	0.010 ± 0.011
Thalamus	0.003 ± 0.003	0.015 ± 0.013	0.016 ± 0.021	0.026 ± 0.006	0.013 ± 0.012
Pons & medulla	0.022 ± 0.011	0.023 ± 0.019	0.064 ± 0.050	0.073 ± 0.055	0.038 ± 0.032
Total brain	0.017 ± 0.010	0.020 ± 0.010	0.042 ± 0.035	0.052 ± 0.036	0.032 ± 0.026

Values are expressed as % ID/g of tissue ± SD ($n=3$)

In the brain, DAT is predominantly localized in the striatum. The cerebellum seems to receive negligible dopaminergic innervation (Kaufman et al., 1991; Ciliax et al., 1995). The regional distribution of [¹²³I]-FMIP in the rat brain was almost homogenous, which is not consistent with this current knowledge of DAT localization. The uptake in the striatum was not higher compared to the uptake in the other brain regions. No difference in radioactivity uptake was observed between the striatum (0.053 ± 0.038 % ID/g at 180 min p.i.) and the reference region (cerebellum (0.029 ± 0.025 % ID/g at 180 min p.i.)) suggesting that no specific binding of [¹²³I]-FMIP to DAT is accomplished.

7.4.6. BLOCKING STUDY

The inability to show specific binding in the striatum could be due to the overall low brain uptake. This leads to high relative standard errors that could possibly influence the outcome of the study. DAT is not only present in the brain but is also found in several peripheral organs. Therefore, the specificity for DAT peripherally should also be investigated. For these reasons a blocking study with selective ligands for the monoamine transporters was performed in mice.

Results of the blocking study on the blood and brain uptake of [¹²³I]-FMIP are shown in Table 7.3. No differences in radioactivity uptake are observed between the four treatment regimens at none of the selected time points.

Table 7.3 Tissue uptake of radioactivity of [¹²³I]-FMIP after injection of physiological saline (control), GBR 12909 (A), citalopram (B) or reboxetine mesylate (C)

		Time (min)			
		2	5	60	180
Control group	Blood	1.35 ± 0.42	0.77 ± 0.32	0.28 ± 0.20	0.54 ± 0.37
	Brain	0.11 ± 0.04	0.11 ± 0.05	0.08 ± 0.04	0.13 ± 0.08
Test group A	Blood	1.30 ± 0.63	0.45 ± 0.03	0.40 ± 0.23	0.21 ± 0.03
	Brain	0.13 ± 0.03	0.07 ± 0.03	0.11 ± 0.02	0.11 ± 0.04
Test group B	Blood	0.90 ± 0.31	0.44 ± 0.20	0.10 ± 0.04	0.12 ± 0.04
	Brain	0.13 ± 0.07	0.16 ± 0.05	0.09 ± 0.03	0.15 ± 0.09
Test group C	Blood	1.55 ± 1.00	0.63 ± 0.37	0.17 ± 0.08	0.11 ± 0.04
	Brain	0.22 ± 0.14	0.12 ± 0.05	0.11 ± 0.05	0.09 ± 0.05

Values are expressed as % ID/g of tissue ± SD (*n*=3)

Outside the central nervous system, localization of DAT is found in the gastrointestinal tract, stomach, pancreas (Mezey et al., 1999) and kidneys (Lee,

1993). Therefore uptake of [¹²³I]-FMIP in peripheral organs was also measured (data not shown) and no influence of pretreatment with GBR 12909, citalopram or reboxetine mesylate could be demonstrated. These results suggest that no specific binding of [¹²³I]-FMIP to DAT is accomplished.

7.4.7. PLASMA PROTEIN BINDING AND METABOLITE ANALYSIS

Determination of plasma protein binding revealed that 96 ± 2 % of [¹²³I]-FMIP was bound to plasma proteins. Control experiments with spiked plasma and brain revealed an extraction efficiency of 76 ± 4 % for plasma and 82 ± 7 % for brain samples. These extraction efficiencies indicate that the binding of [¹²³I]-FMIP to plasma proteins is reversible. HPLC analysis of the spiked samples showed that all extracted radioactivity complies with [¹²³I]-FMIP, so no degradation of [¹²³I]-FMIP occurred during the extraction procedure.

Metabolite analysis of plasma demonstrated that at 10 min p.i. 70 ± 4 % and at 60 min p.i. 55 ± 5 % of intact [¹²³I]-FMIP is remaining (Figure 7.8). [¹²³I]-FMIP eluted at 18.5 min. Degradation products in plasma were iodide-123 (17 ± 11 % at 10 min p.i. and 37 ± 2 % at 60 min p.i.) and a lipophilic compound with a retention time of 15.5 min that eluted just before the parent compound (12 ± 7 % at 10 min p.i. and 8 ± 6 % at 60 min p.i.). This compound will probably have a structure close to the parent compound and is most likely caused by a hydroxylation on a phenyl group or defluorination of the phenyl ring.

In the brain, percentages of intact [¹²³I]-FMIP were 82 ± 11 % at 10 min p.i. and 83 ± 7 % at 60 min p.i. (Figure 7.8). The detected metabolites were iodide-123 (9 ± 3 % at 10 min p.i. and 13 ± 3 % at 60 min p.i.) and another hydrophilic degradation product with a retention time of 5 min (10 ± 8 % at 10 min p.i. and 4 ± 5 % at 60 min p.i.). This metabolite is possibly the result of *N*-dealkylation.

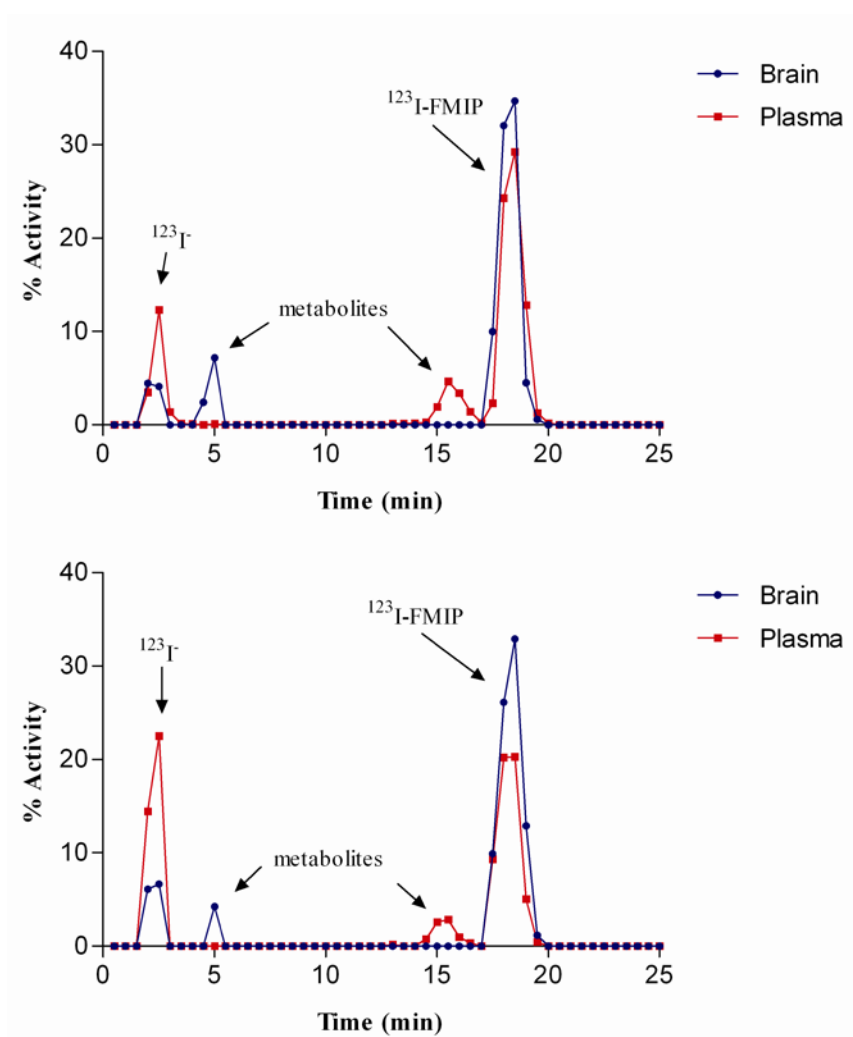


Figure 7.8 Metabolite analysis at 10 min p.i. (above) and 60 min p.i. (below) of brain and plasma samples from mice

Values are the mean of three experiments and are expressed as percent of total activity

These values indicate that the tracer shows a relative good *in vivo* metabolic profile. Radioactivity in brain was mainly (> 80 %) present as intact [^{123}I]-FMIP at the two time points. Besides the presence of free iodide, only 1 metabolite was found in plasma and another, more hydrophilic one in brain.

7.4.8. BLOOD-BRAIN BARRIER TRANSPORT INHIBITION STUDY

P-gp is an efflux pump for a wide range of xenobiotics at the BBB. Hence, P-gp can be a severe obstacle for the accumulation of drugs into the brain. The efflux action of P-gp pumps can be reduced by so-called modulators of which CsA is an example.

Table 7.4 Blood-brain distribution of [¹²³I]-FMIP

	Control group ^a			Test group ^b		
	2 min	60 min	180 min	2 min	60 min	180 min
Blood	1.35 ± 0.42	0.28 ± 0.20	0.54 ± 0.37	2.7 ± 1.15	0.39 ± 0.29	0.50 ± 0.24
Brain	0.11 ± 0.04	0.08 ± 0.04	0.13 ± 0.08	0.45 ± 0.14	0.42 ± 0.13	0.70 ± 0.25
Brain/Blood	0.08 ± 0.01	0.35 ± 0.16	0.33 ± 0.18	0.18 ± 0.06	1.32 ± 0.47	1.48 ± 0.27

^a pretreatment with physiological saline

^b pretreatment with CsA

Values are expressed as % ID/g ± SD (*n*=3). Values in bold: *p* < 0.05 (Student's *t* test, one-sided, compared with control)

Pretreatment of mice with CsA indicated a significantly higher brain uptake compared to the control group (*p* = 0.02 at all time points). Blood values were not affected by CsA pretreatment (*p* = 0.09 at 2 min p.i.; *p* = 0.32 at 1 h p.i.; *p* = 0.45 at 3 h p.i.). CsA treatment increased both the brain uptake (4.2 – 5.1 – 5.2 fold) and subsequently the brain-to-blood ratio. These findings are a possible explanation for the low brain accumulation of [¹²³I]-FMIP. Further research to validate the usefulness of [¹²³I]-FMIP as a SPECT tracer for P-gp pumps *in vivo* is reported in Chapter 8.

7.4.9. REGIONAL BRAIN DISTRIBUTION AFTER CSA PRETREATMENT

We wanted to investigate if CsA also raises brain radioactivity in rats and if this increased brain uptake is homogenous or limited to DAT rich regions. If the

increased brain radioactivity is homogenous, it will be pointed out that [¹²³I]-FMIP is not selective towards DAT *in vivo*.

CsA administration resulted in a significantly higher brain uptake at 30 min ($p = 0.036$), 180 min ($p = 0.003$) and 360 min ($p = 0.014$) p.i. compared to control group. At 60 min p.i. an increase in brain uptake was also observed although this increase was not significant. Blood activity was not affected by pretreatment with CsA. Unfortunately, the increased brain radioactivity was homogenous and not restricted to DAT rich regions (Figure 7.9). Radioactivity uptake increased in both striatum and cerebellum. These findings direct us to conclude that the non-ability to prove DAT selectivity in brain was not due to the low brain uptake of [¹²³I]-FMIP but due to its lack of selectivity towards DAT in brain.

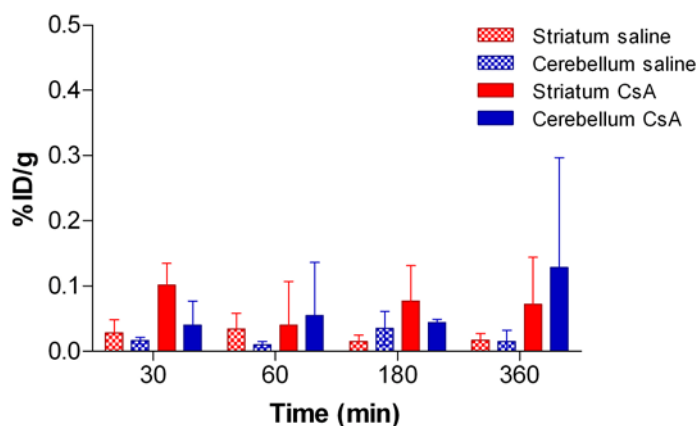


Figure 7.9 Tissue uptake of [¹²³I]-FMIP with CsA or physiological saline pretreatment

Values are expressed as % ID/g \pm SD ($n=3$)

7.5. Conclusion

The preparation and purification of the precursor molecule, as well as the reference compound were accomplished with sufficient yields and without any significant problems. The radiosynthesis of [¹²³I]-FMIP was achieved by electrophilic destannylation. Using a one-pot synthetic procedure, [¹²³I]-FMIP was

prepared in a 40 ± 10 % yield and with good specific activity. After purification, the radiochemical purity appeared to be higher than 98 %. The authenticity of the tracer was determined by co-elution with the nonradioactive reference compound. *In vitro*, [¹²³I]-FMIP remained stable for at least 24 h. The determined log $D_{7.4}$ was 1.42 ± 0.12 %, which is suitable for brain penetration.

Upon intravenous administration, low levels of activity were observed in mouse brain indicating low blood-brain penetration of [¹²³I]-FMIP. At none of the selected time points, radioactivity concentration in the brain exceeded blood activity. A possible reason for the low brain uptake of [¹²³I]-FMIP is the contribution of P-gp pumps or other multidrug resistance protein transporters in the brain distribution of [¹²³I]-FMIP. A significant increase in brain uptake (4.2 – 5.2 fold) of [¹²³I]-FMIP was observed after CsA administration compared to the control group indicating [¹²³I]-FMIP is transported by the P-gp pumps out of the brain. The effect of P-gp modulation on the biodistribution of [¹²³I]-FMIP will be further explored and reported in Chapter 8. In rat brain, the regional distribution of DAT was not reflected in the radioactivity distribution. A blocking study also failed to proof selectivity of [¹²³I]-FMIP towards DAT. Even more, [¹²³I]-FMIP did not display selectivity towards one of the monoamine transporters.

Although FMIP is selective for DAT *in vitro*, it did not display the expected selective distribution *in vivo* in brain neither peripheral. A possible reason can be the selectivity of FMIP towards other receptors. *In vitro*, FMIP was only tested for its affinity to the monoamine transporters. Sigma receptors are a class of receptors distributed uniformly in the brain (Bouchard P and Quirion R, 1997). This distribution is in accordance with the observed homogenous brain uptake. A blocking study with selective inhibitors for this class of receptors should be performed to proof this assumption. Based on these results, one can conclude that [¹²³I]-FMIP is not suitable as radioligand for *in vivo* SPECT visualization of DAT.

7.6. References

- Bergström KI, Halldin C, Lundkvist C, Swahn C-G, Akerman KK, Kuikka JT et al., Characterization of C-11 or I-123 labelled β -CIT-FP and β -CIT-FE metabolism measured in monkey and human plasma. Identification of two labelled metabolites with HPLC. *Hum Psychopharmacol* 1996; 11:483-90.
- Boos TL, Greiner E, Calhoun WJ, Priszczano TE, Nightingale B, Dersch CM. et al., Structure–activity relationships of substituted *N*-benzyl piperidines in the GBR series: Synthesis of 4-(2-(bis(4-fluorophenyl)methoxy)ethyl)-1-(2-(trifluoromethylbenzyl)piperidine, an allosteric modulator of the serotonin transporter *Bioorg Med Chem* 2006; 14:3967-73.
- Bouchard P and Quirion R. [³H]1,3-Di(2-tosyl)guanidine and [³H](+)pentazocine binding sites in the rat brain: autoradiographic visualization of the putative σ_1 and σ_2 receptor subtypes. *Neuroscience* 1997; 76:467–77
- Ciliax BJ, Heilman C, Demchysyn LL, Pristupa ZB, Ince E, Hersch SM et al. The dopamine transporter: immunochemical characterization and localization in brain. *J Neurosci* 1995; 15:1714-1723.
- Dhawan V, Eidelberg D. SPECT imaging in Parkinson's disease. *Adv Neurol* 2001; 86 : 205-13.
- Donnan GA, Kaczmarczyk SJ, Paxinos G, Chilco PJ, Kalnins RM, Woodhouse DG, et al. Distribution of catecholamine uptake sites in human brain as determined by quantitative [³H]mazindol autoradiography. *J Comp Neurol* 1991; 304:419-34.
- Elsinga PH, Hatano K, Ishiwata K. PET tracers for the dopaminergic system. *Curr Med Chem* 2006; 13:2139-53.
- Emond P, Garreau L, Chalon S, Boazi M, Caillet M, Bricard J, et al. Synthesis and ligand binding of nortropine derivatives: *N*-substituted 2 β -carbomethoxy-3 β -(4'-iodophenyl)nortropine and *N*-(3-iodoprop-(2E)-enyl)-2 β -carbomethoxy-3 β -(3',4'-disubstitutedphenyl)nortropine. New high-affinity and selective compounds for the dopamine transporter. *J Med Chem* 1997; 40:1366-72.
- Fowler JS, Kroll C, Ferrieri R, Alexoff D, Logan J, Dewey SL et al. PET studies of *d*-methamphetamine pharmacokinetics in primates: comparison with *l*-methamphetamine and (-)-cocaine. *J Nuc Med* 2007; 48:1724-32.
- Gandelman MS, Baldwin RM, Zoghbi SS, Zea-Ponce Y, Innis RB. Evaluation of ultrafiltration for the free fraction determination of single photon emission computerized tomography (SPECT) radiotracers: β -CIT, IBF and iomazenil. *J Pharm Sci* 1994; 83:1014–1019.
- Guilloteau D, Emond P, Baulieu J-L, Garreau L, Frangin Y, Pourcelot L et al., Exploration of the dopamine transporter: *in vitro* and *in vivo* characterization of a high-affinity and high-specificity iodinated tropane derivative (E)-*N*-(3-iodoprop-2-enyl)-2 β -carbomethoxy-3 β -(4'-methylphenyl)nortropine (PE2I). *Nucl Med Biol* 1998; 25:331-7.
- Ishiwata K, Kawamura K, Yanai K, Hendrikse NH. *In vivo* evaluation of P-glycoprotein modulation of 8 PET radioligands used clinically. *J Nuc Med* 2007; 48:81-7.
- Kaufman MJ, Spelman RD, Madras BK. Distribution of cocaine recognition sites in monkey brain: I. *In vitro* autoradiography with [³H]CFT. *Synapse* 1991; 9:177-87.
- Lee MR. Dopamine and the kidney: ten years on. *Clin Sci* 1993;84:357-75.
- Mezey E, Eisenhoger G, Hansson S, Harta G, Hoffman BJ, Gallatz K, et al. Non-neuronal dopamine in the gastrointestinal system. *Clin Exp Pharmacol Physiol* 1999; 26:S14-S22.

- Neumeayer JL, Tamagnan G, Wang s, Gao Y, Milius RA, kula NS et al., N-Substituted analogues of 2 β -carbomethoxy-3 β -(4'-iodophenyl)tropane (β -CIT) with selective affinity to dopamine and serotonin transporters in rat forebrain. *J Med Chem* 1996; 39:543-8.
- Neumeayer JL, Wang S, Milius RA, Baldwin RM, Zea-Ponce Y, Baldwin RM, et al. [¹²³I]-2 β -carbomethoxy-3 β -(4-iodophenyl)tropane: High-affinity SPECT radiotracer of monoamine reuptake sites in brain. *J Med Chem* 1991; 34:3144-6.
- Poewe W, Sherfler C. Role of dopamine transporter imaging in investigation of parkinsonian syndromes in routine clinical practice. *Mov Disord* 2003; 18:S16-S21.
- Rothman RB, Mele A, Reid AA, Akunne HC, Greig N, Thurkauf BR et al. GBR12909 antagonizes the ability of cocaine to elevate extracellular levels of dopamine. *Pharmacol Biochem Behav* 1991; 40:387-97.
- Scheffel U, Lever JR, Abraham P, Parham KR, Mathews WB, Kopajtic T, et al. N-Substituted phenyltropanes as *in vivo* binding ligands for rapid imaging studies of the dopamine transporter. *Synapse* 1997; 25:345-9.
- Shih MC, Hoexter MQ, Andrade LAF, Bressan RA. Parkinson's disease and dopamine transporter neuroimaging – a critical review. *Sao Paulo Med J* 2006; 123:168-175.
- Van der Zee P, Koger HS, Goojtes J and Hesper W. Aryl 1,4-dialk(en)ylpiperazines as selective and very potent inhibitors of dopamine uptake. *Eur J Med Chem* 1980; 15:363-70.
- Volkow ND, Fowler JS, Gatley J, Logan J, Wang G, Ding Y, Dewey S. PET evaluation of the dopamine system of the human brain *J Nuc Med* 1996; 37:1242-56.
- Waterhouse RN. Determination of lipophilicity and its use as a predictor of blood-brain barrier penetration of molecular agents. *Mol Imaging Biol* 2003; 5:376-389.

Chapter 8

In vivo evaluation of [¹²³I]-FMIP for imaging the P-glycoprotein transporter



De Bruyne S.¹, wyffels L.¹, Boos T.L.², Staelens S.³, Deleye S.³, Rice K.C.², De Vos F.¹

Nuclear Medicine and Biology, submitted

¹ Laboratory for Radiopharmacy, Ghent University, Harelbekestraat 72, 9000 Ghent, Belgium

² Chemical Biology Research Branch, National Institute on Drug Abuse and National Institute on Alcohol Abuse and Alcoholism, National Institutes of Health, Bethesda, MD, USA

³ IBITECH-Medisip, Ghent University-IBBT, De Pintelaan 185, 9000 Ghent, Belgium

Chapter 8

In vivo evaluation of [¹²³I]-FMIP for imaging the P-glycoprotein transporter

8.1. Abstract

Aim: P-gp is an energy-dependent drug efflux transporter that contributes to the efflux of a wide range of xenobiotics at the BBB playing a role in drug-resistance or therapy failure. In this study, we evaluated [¹²³I]-FMIP as a novel SPECT tracer for imaging of P-gp at the brain *in vivo*.

Methods: The tissue distribution and brain uptake as well as the metabolic profile of [¹²³I]-FMIP in wild-type and *mdr1a* (-/-) mice after pretreatment with physiological saline or CsA (50 mg/kg) was investigated. The influence of increasing doses CsA on brain uptake of [¹²³I]-FMIP was explored. μ SPECT images of mice brain were obtained for different treatment strategies.

Results: Modulation of P-gp with CsA as well as *mdr1a* gene depletion results in a significant increase in cerebral uptake of [¹²³I]-FMIP with only a minor effect on blood activity. [¹²³I]-FMIP is quite stable *in vivo* with > 80 % intact [¹²³I]-FMIP in brain at 60 min p.i. in the different treatment regiments. A dose-dependent sigmoidal increase in brain uptake of [¹²³I]-FMIP with increasing doses of CsA was observed. *In vivo* ROI-based SPECT measurements correlated well with the observations of the biodistribution studies.

Conclusion: These findings indicate that [¹²³I]-FMIP is an effective SPECT tracer for imaging P-gp at the BBB.

8.2. Introduction

P-gp is an energy-dependent drug efflux transporter that contributes to the efflux of a wide range of xenobiotics at the BBB. Hence, P-gp can play a major role in drug-resistance or therapy failure (Schinkel et al., 1996; Linnet and Ejsing, 2008). Apart from its role in the central nervous system, P-gp is overexpressed in tumors and therefore implicated in the resistance to chemotherapeutics and in the pathogenesis of cancer (Gottesman and Pastan, 1993; Gottesman et al., 2002).

Imaging of P-gp function and expression with PET or SPECT could be of great importance in drug development and medicine. Non-invasive monitoring of P-gp could be applied to elucidate the role of P-gp in several human diseases and to evaluate the efficacy of new P-gp modulators. Several PET tracers have already been evaluated for P-gp modulation among which [¹¹C]verapamil (Hendrikse et al., 1998; Lee et al., 2006) and [¹¹C]N-desmethyl-loperamide (Lazarova et al., 2008). The only reported SPECT radioligands for P-gp are [^{99m}Tc]sestamibi (Kostakoglu et al., 1997; Ballinger et al., 1995) and [^{99m}Tc]tetrofosmin (Ballinger et al., 1996). However, [^{99m}Tc]sestamibi and [^{99m}Tc]tetrofosmin are not only substrates for P-gp but are also involved in efflux mediated by multidrug resistance-associated protein and are not suitable for P-gp imaging in the brain (Hendrikse et al., 1997; Barbarics et al., 1998; Ballinger et al., 1996). To date, no iodinated SPECT ligands for P-gp functionality imaging have been published.

This study describes the *in vivo* evaluation of [¹²³I]-FMIP, a possible P-gp tracer. [¹²³I]-FMIP was originally designed as a tracer for the dopamine transporter but did not display the anticipated *in vivo* behaviour. Brain uptake was only minor which lead to the hypothesis that [¹²³I]-FMIP might be a substrate for the P-gp transporter (Chapter 7). Therefore we investigated the influence of P-gp blocking with CsA as well as the influence of gene depletion on the biodistribution and brain penetration of [¹²³I]-FMIP. A dose-response study is performed to assess the impact of increasing CsA dose on the brain uptake of [¹²³I]-FMIP. The influence of CsA pretreatment and *mdr1a* gene depletion on the metabolism of

[¹²³I]-FMIP is investigated. Finally, a multipinhole μ SPECT study of the brain uptake of [¹²³I]-FMIP is performed using the Milabs U-SPECT-II in wild-type mice (with and without CsA administration) and in P-gp knock-out mice (*mdr1a* (-/-) mice).

8.3. Materials & Methods

8.3.1. BIODISTRIBUTION STUDIES IN MICE

The biodistribution of [¹²³I]-FMIP was studied in male wild-type (=FVB) mice and *mdr1a* (-/-) mice of 5 – 7 weeks weighing 20 – 25 g. Wild-type mice and *mdr1a* (-/-) mice were divided into two groups. One group received an injection of CsA in a 50 mg/kg dose. The second group received the same volume physiological saline as control. After 30 min, approximately 185 kBq (5 μ Ci) [¹²³I]-FMIP was injected intravenously and mice ($n=3$ for each group and each time point) were sacrificed at 1, 10, 30, 60 or 180 min after [¹²³I]-FMIP injection. Organs and tissues were removed and weighed. To remove adhering blood, all organs were rinsed with water prior to weighing and counting. For calculation of the injected dose, five aliquots of the injection solution were weighed and counted for activity. The radioactivity was measured using an automated gamma-counter. Radioactivity concentrations were decay-corrected and results are expressed as % ID/g \pm SD. Statistical analysis was performed using a one-sided, unpaired student's *t*-test. Only *p* values < 0.05 are considered significant.

8.3.2. DOSE ESCALATION STUDY

Adult male NMRI mice weighing 22 – 28 g were injected in a tail vein with increasing amounts of CsA. The dosages used were 10, 20, 25, 30, 40, 50 and 60 mg/kg. Due to the toxicity of CsA, higher doses CsA are not recommended. Side effects that can occur are nephrotoxicity, pancreatitis, liver toxicity,

gastrointestinal tract dysfunctions and edemia. These undesired effects of CsA were not problematic since CsA was administrated just before the radiotracer and the animals were terminated afterwards.

[¹²³I]-FMIP (185 kBq (5 µCi)) was administrated intravenously 30 min after CsA injection. The mice were awake during the injections. The mice (*n*=3 for each dosage) were sacrificed at 40 min p.i. of [¹²³I]-FMIP. Three control animals receiving physiological saline were subjected to the same protocol. Blood and organs were removed, weighed and counted for radioactivity in an automated gamma counter. All organs were rinsed with water prior to weighing and counting. For calculation of the injected dose, five aliquots of the injection solution were weighed and counted for activity. Decay-corrected results are expressed as % ID/g ± SD.

Using Graphpad, a dose-response curve was fitted by a sigmoidal curve that is described by the four parameter logistic equation:

$$y = y_0 + (y_{\max} - y_0) / (1 + 10^{-(\log EC_{50} - x) * n})$$

y is the response, *x* is the logarithm of concentration, EC₅₀ the half-maximum effect dose and *n* the Hill coefficient.

8.3.3. METABOLITE ANALYSIS

The metabolic pattern of [¹²³I]-FMIP and the influence of CsA pretreatment, as well as the influence of depletion of the *mdr1a* gene were investigated.

Male FVB (wild-type) or *mdr1a* (-/-) mice (approximately 6 weeks old and 25 g) were injected with CsA (50 mg/kg) or physiological saline 30 min prior to the administration of 1.85 – 3.7 MBq (50 – 100 µCi) [¹²³I]-FMIP. The mice were awake during the injections. At 10 min (*n*=3) and 60 min (*n*=3) p.i., the mice were sacrificed and blood and brain were removed and processed as described in Chapter 4. HPLC analysis was performed on a RP C₁₈ HPLC column (Alltima C₁₈ 250 mm × 10 mm, 10 µm) using 91:9:0.1 (v:v) MeOH:H₂O:NH₄OH as solvent system at a flow rate of 6 mL/min.

8.3.4. U-SPECT SCAN

Mice were divided into three groups ($n=3$ for each group). The first group, test group A, was injected with 50 mg/kg CsA 30 min before tracer injection, whereas the control group and test group B received physiological saline instead of CsA. In test group A and the control group, wild-type (FVB) mice were used. Test group B on the other hand, consisted of *mdr1a* (-/-) mice.

Dynamic scanning in 12 frames of 5 minutes was performed at 30 min p.i. of [¹²³I]-FMIP using the Milabs U-SPECT-II (Milabs, Utrecht, The Netherlands). This μ SPECT scanner is equipped with collimators consisting of a tungsten cylinder with 5 rings of 15 pinhole apertures of 0.6 mm diameter. All pinholes focused on a single volume in the center of the tube. For imaging mice brain, the animal bed was translated in 3 dimensions using an XYZ stage into 12 different bed positions. This aforementioned combination enabled a multiple-position acquisition and dynamic imaging at a time scale of a few minutes. Mice were injected with 11.1 MBq (0.3 mCi) [¹²³I]-FMIP and anesthetized throughout the μ SPECT scan by inhalation of 1.5 % isoflurane. The 20 % photopeak was centered at 159 keV and a double 10 % energy window correction at 135 keV and 190 keV was applied. The data were reconstructed on 0.375 voxels by 3 iterations of 16 OSEM subsets. The images were postfiltered by a Gaussian postfilter of 1.125 mm and color scales were normalized. A cylindrical brain ROI of 25 mm³ (4 mm diameter and 2 mm height) was drawn on the brain for further analysis. Statistical analysis was performed using a one-sided, unpaired student's *t*-test. Only p-values < 0.05 are considered significant.

8.4. Results & Discussion

8.4.1. RADIOCHEMISTRY

[¹²³I]-FMIP was prepared in a 40 ± 10 % radiochemical yield, as previously described (Figure 8.1). The specific activity was > 667 GBq/ μ mol (18 Ci/ μ mol) and radiochemical purity appeared to be higher than 98 % (see Chapter 7). [¹²³I]-FMIP was formulated in a 8:92 (v:v) - EtOH:physiological saline solution for *in vivo* studies.

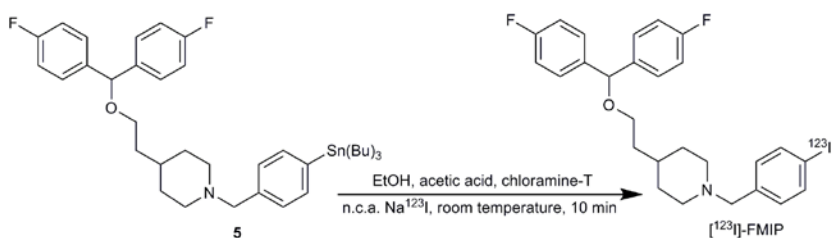


Figure 8.1 Radiosynthesis of [¹²³I]-FMIP

8.4.2. BIODISTRIBUTION STUDIES

Figure 8.2 shows the tissue distribution of radioactivity uptake after intravenous injection of 185 kBq (5 μ Ci) [¹²³I]-FMIP in wild-type and *mdr1a* knock-out mice with physiological saline or CsA pre-administration.

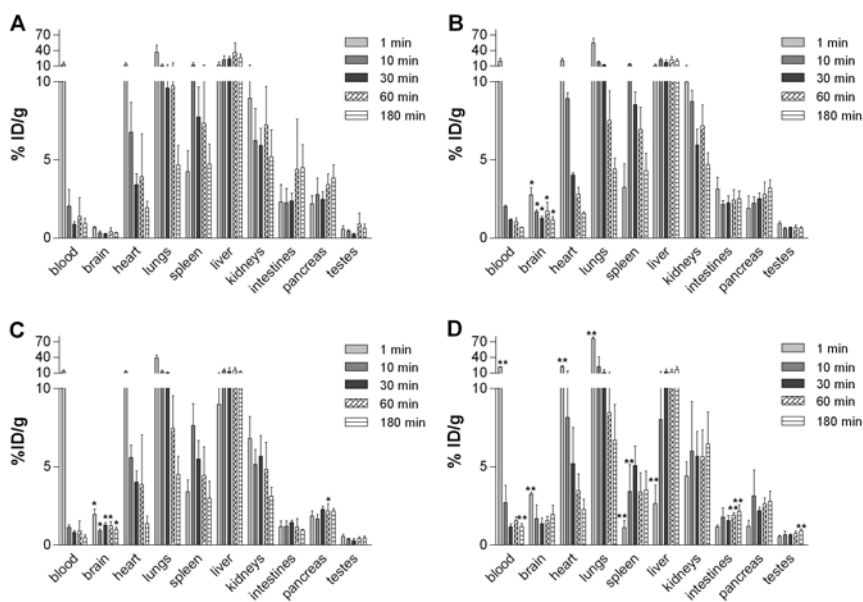


Figure 8.2 Tissue distribution of [¹²³I]-FMIP in wild-type and *mdr1a* knock-out mice with saline or CsA pre-administration

Values are mean of three experiments, ^A pretreatment with saline in wild-type mice, ^B pretreatment with CsA in wild-type mice, ^C pretreatment with saline in *mdr1a* (-/-) mice, ^D pretreatment with CsA in *mdr1a* (-/-) mice * $P < 0.05$ (student's *t* test) compared to group A ** $P < 0.05$ (student's *t* test) compared to group C

8.4.2.1. Biodistribution study in wild-type mice

The brain uptake was low at each time point investigated (0.67 ± 0.15 % ID/g at 1 min p.i. and 0.41 ± 0.24 % ID/g at 60 min p.i.). Although [¹²³I]-FMIP was rapidly cleared out of the blood, blood activity remained higher than brain activity at all time points (Figure 8.2). At 60 min p.i., the highest tracer uptake was observed in the liver with 36.38 ± 18.12 % ID/g (Figure 8.2). Other peripheral organs with high tracer uptake at 60 min p.i. were lungs (9.74 ± 6.01 % ID/g), kidneys (7.23 ± 2.46 % ID/g) and spleen (7.34 ± 4.90 % ID/g).

8.4.2.2. Influence of CsA pretreatment

Modulation of P-gp with 50 mg/kg CsA resulted in significant changes in cerebral uptake of [¹²³I]-FMIP at each time point investigated (Figure 8.3).

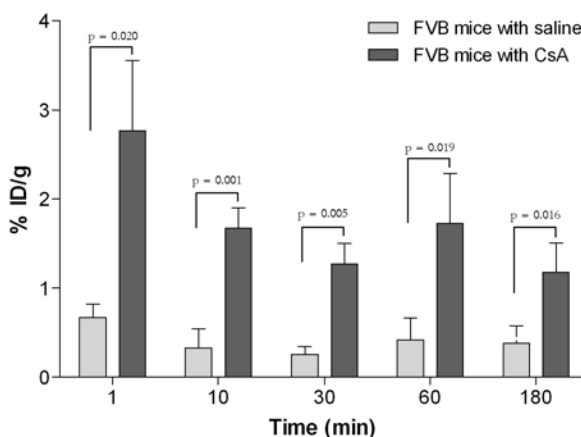


Figure 8.3 Brain distribution of [¹²³I]-FMIP in wild-type mice with saline and CsA pretreatment

Values are expressed as % ID/g \pm SD ($n=3$); p-values are calculated using the one-sided student's *t* test

Brain uptake raised 2.6 – 5.1 fold compared to mice without CsA pretreatment. At 10 min p.i. the highest raise was observed (5.09 ± 1.48). Since CsA pretreatment had no effect on blood activity, the brain/blood ratio was also significantly increased. At 60 and 180 min p.i. a slight decrease in intestinal uptake was observed after CsA pretreatment. This is possibly due to a slower excretion caused by P-gp modulation. Furthermore, no significant differences could be observed at any of the selected time points in the peripheral organs (Figure 8.2).

8.4.2.3. Influence of gene depletion

The influence of genetic disruption of P-gp in mice on brain radioactivity uptake is shown in Figure 8.4.

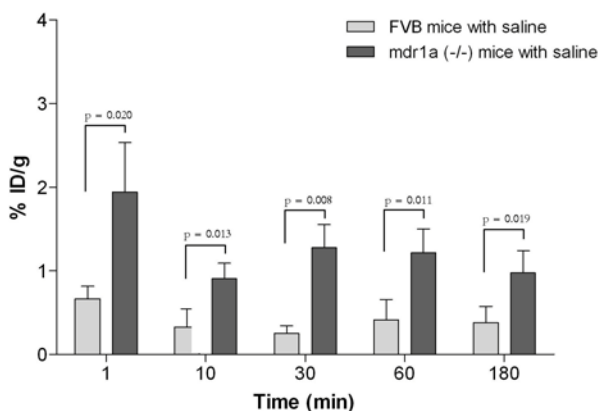


Figure 8.4 Brain distribution of [¹²³I]-FMIP in wild-type mice with saline and *mdr1a* (-/-) mice with saline pretreatment ($n=3$)

Values are expressed as % ID/g \pm SD ($n=3$); p-values are calculated using the one-sided student's *t* test

In *mdr1a* (-/-) mice, [¹²³I]-FMIP content was increased in the brain at all selected time points. Brain uptake raised 2.9 – 5.0 fold compared to wild-type mice with the highest increase at 30 min p.i. (4.95 ± 0.81). In contrast, no significant differences in [¹²³I]-FMIP levels in plasma were measured between the two types of mice at the chosen time points. Consequently, brain/blood ratios were significant higher in *mdr1a* (-/-) mice (except at 180 min p.i.). Although liver, kidneys and intestines displayed a decreased radioactivity uptake in the *mdr1a* (-/-) mice, this decrease was not significant. None of the peripheral organs displayed significant changes at any of the selected time points except the pancreas at 60 min p.i. (Figure 8.2).

8.4.2.4. Influence of CsA pretreatment in *mdr1a* (-/-) mice

Pretreatment of *mdr1a* (-/-) mice with CsA had no additional significant effect on brain activity except at the earliest time point (Figure 8.5). At 1 min p.i., not only brain but also blood uptake was increased resulting in similar brain/blood ratio.

Heart and lung uptake was significantly increased, an effect that is probably caused by the increased blood pool activity and not P-gp mediated. At 60 and 180 min p.i. a significant increase in intestinal uptake was observed after CsA pretreatment. This effect could be P-gp mediated but could also be the result of a shift in excretion after CsA administration. In conclusion, it can be stated that CsA administration in *mdr1a* (-/-) mice did not cause significant changes in the brain uptake of [¹²³I]-FMIP (Figure 8.5).

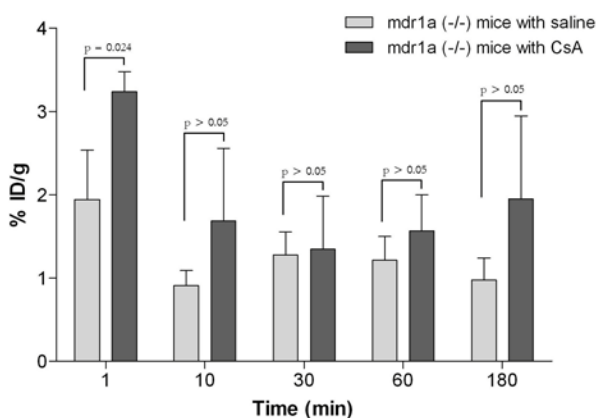


Figure 8.5 Brain distribution of [¹²³I]-FMIP in *mdr1a* (-/-) with saline and CsA pretreatment (*n*=3)

Values are expressed as % ID/g ± SD (*n*=3); p-values are calculated using the one-sided student's *t* test

8.4.3. DOSE ESCALATION STUDY

The effect of increasing doses CsA on the brain uptake and blood concentration of [¹²³I]-FMIP was investigated (Figure 8.6). The experiment showed a sigmoid relationship between the concentration of CsA administered and the uptake of [¹²³I]-FMIP in the brain. The EC₅₀ value was 24.48 ± 0.73 mg/kg. With a higher dose of CsA, a higher brain uptake was observed with stagnation from 30 mg/kg CsA. Between 30 mg/kg (0.61 ± 0.13 % ID/g) and 60 mg/kg (0.56 ± 0.23 % ID/g) CsA, there was no significant difference in brain uptake. The effect of CsA

administration on brain uptake was significant at each dosage used compared to the control group. Only a minor increase in blood activity was observed after administration of increasing doses of CsA. Blood uptake of radioactivity without CsA pretreatment was 0.29 ± 0.14 % ID/g and increased to 0.51 ± 0.06 % ID/g at the highest dose CsA used but the increase was not significant.

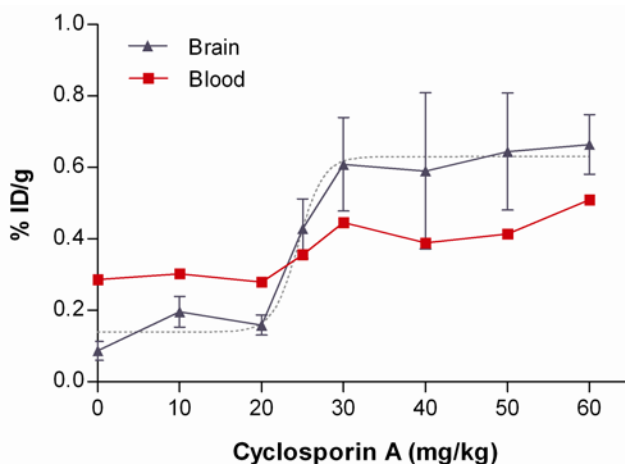


Figure 8.6 Effect of various doses CsA on brain uptake and blood activity of [¹²³I]-FMIP

Values are expressed as % ID/g \pm SD ($n=3$)

8.4.4. METABOLITE ANALYSIS

Table 8.1 summarizes the metabolic profile of [¹²³I]-FMIP. Metabolite analysis of plasma in wild-type mice demonstrated that at 10 min p.i. 70 ± 6 % and at 60 min p.i. 54 ± 8 % of intact [¹²³I]-FMIP is remaining (Figure 8.7). Degradation products in plasma were ¹²³I- (13 ± 1 % at 10 min p.i. and 39 ± 4 % at 60 min p.i.) and a lipophilic metabolite with a retention time of 9 min that elutes just before the parent compound (17 ± 7 % at 10 min p.i. and 8 ± 4 % at 60 min p.i.). This compound is believed to have a structure close to the parent compound and probably originates from a hydroxylation on a phenyl group or defluorination of a phenyl ring.

In brain, percentages of intact [¹²³I]-FMIP were 86 ± 2 % at 10 min p.i. and 85 ± 3 % at 60 min p.i. (Figure 8.7). The detected metabolites were iodide-123 (8 ± 2 % at 10 min p.i. and 12 ± 4 % at 60 min p.i.) and a hydrophilic degradation product with a retention time of 5.5 min (5 ± 1 % at 10 min p.i. and 4 ± 1 % at 60 min p.i.). This metabolite is possibly the result of *N*-dealkylation.

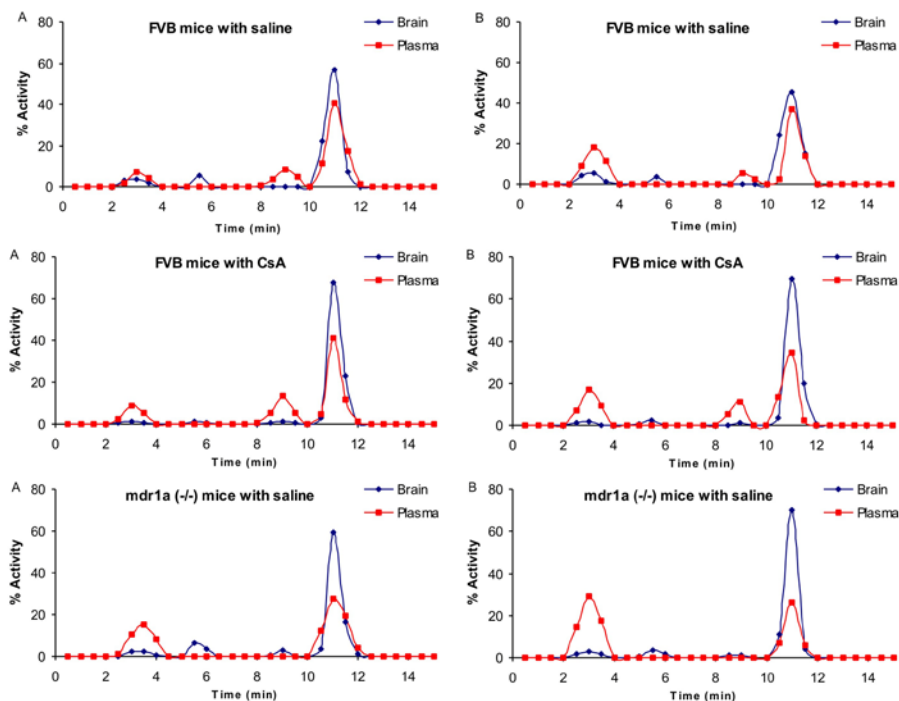


Figure 8.7 Metabolite chromatogram of [¹²³I]-FMIP in FVB and *mdr1a* (-/-) mice after saline and CsA pretreatment at 10 min p.i. (A) and 60 min p.i. (B) Values are the mean of three experiments and are expressed as percent of total activity

Pretreatment with CsA resulted in less degradation in the brain with 94 ± 3 % and 93 ± 5 % intact [¹²³I]-FMIP at 10 min and 60 min p.i., respectively. The formation of an extra metabolism product (2 ± 1 % at 10 min p.i. and 1 ± 1 % at 60 min p.i.) with the same retention time of that found in plasma was observed. In plasma, pretreatment with CsA caused an increase in metabolism of [¹²³I]-

FMIP at 10 min p.i. while at 60 min p.i. the fraction of [¹²³I]-FMIP remained unchanged.

Depletion of the *mdr1a* gene had no effect on the fraction of radioactivity present as [¹²³I]-FMIP in brain. Just as observed with CsA pretreatment, the same extra metabolism product was found ($3 \pm 3\%$ at 10 min p.i. and $2 \pm 0\%$ at 60 min p.i.). In plasma, on the other hand, a high increase in the fraction of iodide-123 was observed. At 60 min p.i., ¹²³I- was the only extracted degradation product.

Table 8.1 Metabolic profile of [¹²³I]-FMIP at 10 min and 60 min p.i.

	Tissue	Time (min)	Retention time on RP-HPLC			
			3 min ¹²³ I-	5.5 min	9 min	11 min [¹²³ I]-FMIP
Control ^a	Brain	10	8 ± 2	5 ± 1		86 ± 2
		60	12 ± 4	4 ± 1		85 ± 3
	Plasma	10	13 ± 1		17 ± 7	70 ± 6
		60	39 ± 4		8 ± 4	54 ± 8
Test A ^b	Brain	10	2 ± 2	2 ± 1	2 ± 1	94 ± 3
		60	3 ± 1	3 ± 3	1 ± 1	93 ± 5
	Plasma	10	17 ± 12		24 ± 19	59 ± 5
		60	33 ± 12		16 ± 2	51 ± 14
Test B ^c	Brain	10	5 ± 4	11 ± 8	3 ± 3	81 ± 10
		60	6 ± 3	6 ± 2	2 ± 0	86 ± 5
	Plasma	10	36 ± 11		3 ± 5	64 ± 12
		60	61 ± 8			39 ± 8

Values are expressed as percent of total activity ± SD (*n*=3)

^a pretreatment with saline in wild-type mice, ^b pretreatment with CsA (50 mg/kg) in wild-type mice, ^c pretreatment with saline in *mdr1a* (-/-) mice

8.4.5. U-SPECT SCAN

The μSPECT images obtained are shown in Figure 8.8. A low homogenous brain uptake was observed after injection of [¹²³I]-FMIP. As seen in Figure 8.8, almost

no activity was visible on the μ SPECT scan. Radioactivity uptake in brain, integrated over the full scan time of 60 min, was considerably higher after CsA pretreatment as well as in *mdr1a* (-/-) mice. In the experiment in which CsA had been preadministrated to block P-gp, radioactivity concentration was on average 3.94 ± 0.84 fold higher compared to the baseline experiment. The ratio of brain radioactivity in test group B to that in the control group was about 4.27 ± 1.20 times increased.

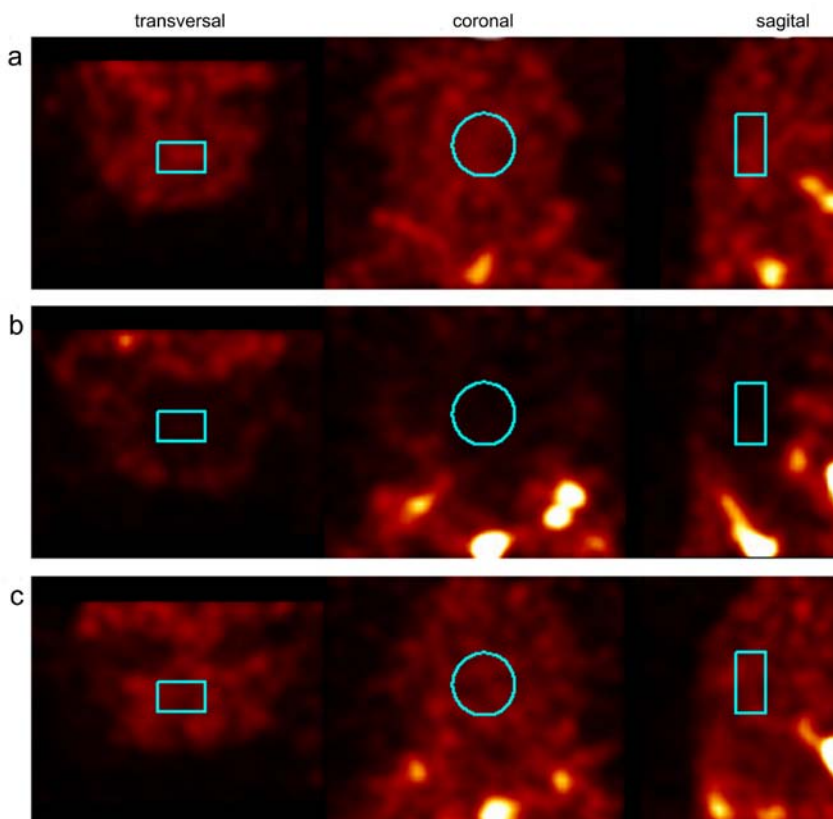


Figure 8.8 μ SPECT image of mice brain at 60 min p.i. of [¹²³I]-FMIP

ROI's were drawn around the middle of the brain, ^a pretreatment with CsA in wild-type mice, ^b pretreatment with saline in wild-type mice, ^c pretreatment with saline in *mdr1a* (-/-) mice

The regional distribution of [¹²³I]-FMIP in mice brain was homogenous in the control group as well as in test group A and test group B. The uptake in the

striatum was not higher compared to the uptake in the other brain regions, confirming the previous finding that no specific binding of [¹²³I]-FMIP to the dopamine transporter is accomplished (Chapter 7).

The correlation of the biodistribution studies with μ SPECT measurements are represented in table 8.2. ROI's were obtained at 30 min p.i. and at 60 min p.i. for an exact comparison with the values of the biodistribution studies. The increase in brain uptake after CsA pretreatment and in *mdr1a* (-/-) mice is slightly higher in biodistribution studies compared to measurements obtained from μ SPECT imaging (Table 8.2). In addition, the standard deviation is higher in the biodistribution studies. The low counts obtained when measuring the brain radioactivity in wild-type mice with saline pretreatment are a possible reason for these higher standard deviations. Another explanation can be the use of aliquots of the injection solution for calculation of the injected dose in the biodistribution study. These findings indicate not only the advantage of μ SPECT imaging in small animal studies but also that *in vivo* ROI-based SPECT measurements correlated with the observations of the biodistribution studies.

Table 8.2 Comparison of brain radioactivity uptake ratios of [¹²³I]-FMIP in the biodistribution study and μ SPECT imaging

	Experiment	30 min p.i.	60 min p.i.
Influence CsA ^a	biodistribution	4.92 ± 1.94	4.17 ± 2.79
	μ SPECT imaging	2.87 ± 0.83	3.04 ± 0.73
Influence gene depletion ^b	biodistribution	4.95 ± 2.03	2.92 ± 1.85
	μ SPECT imaging	2.24 ± 0.35	2.92 ± 0.56

Values are mean of three experiments ± SD, ^a brain uptake in wild-type mice pretreated with Cs A/brain uptake in wild-type mice pretreated with saline, ^b brain uptake in wild-type mice pretreated with saline/brain uptake in *mdr1a* (-/-) mice pretreated with saline

8.5. Conclusion

P-gp is among other localizations expressed in the BBB where it prevents accumulation of certain xenobiotics in the brain by an active transport

mechanism. Hence, P-gp can play a significant role in the resistance to CNS drugs (Schinkel et al., 1996; Linnert and Ejsing, 2008). P-gp has also been associated with several human disorders (Lam et al., 2001; Langford et al., 2004; Kwan and Brodie, 2005; Kortekaas et al., 2005; Turgut et al., 2008). Non-invasive monitoring of P-gp could be applied to elucidate the role of P-gp in these human diseases and to evaluate the efficacy of new P-gp modulators. Several tracers have already been evaluated for P-gp modulation but so far, no iodinated SPECT tracer for P-gp has been reported. Iodine-123 has a half-life of 13.2 h allowing a prolonged scanning time and consequently a longer follow-up of the radioactivity distribution is possible.

The aim of this study was to evaluate the usefulness of [¹²³I]-FMIP for SPECT imaging of the P-gp transporters in brain. The synthesis and radiosynthesis of [¹²³I]-FMIP were reported in Chapter 7.

The biodistribution studies revealed a 2.6 – 5.1 increase in brain uptake after blocking P-gp with CsA. The effect on blood activity was negligible indicating that the increased brain uptake is the result of a decreased tracer efflux and not due to an improved influx to the brain. Additional proof of P-gp involvement was obtained in the study with *mdr1a* (-/-) mice. In this study, we demonstrated a raise in brain radioactivity ranging from 2.9 – 5.0. No significant differences in other organs containing P-gp, like liver and kidneys, were observed. These finding corresponds with those reported in other studies (Hendrikse et al., 1998; Luurtsema et al., 2003) and can be explained by the unique barrier of the brain as well as the role of liver and kidneys in excretion and metabolism and experimental artefacts (bile ducts are not dissected apart from the liver).

[¹²³I]-FMIP shows a fairly stable *in vivo* metabolic profile. One labelled metabolite (*T_r* 9.5 min) is probably also a substrate for P-gp as the metabolite only occurs in the brain after CsA pretreatment and in *mdr1a* (-/-) mice. Radioactivity in brain was mainly (> 80 %) present as intact [¹²³I]-FMIP at the two time points in the three different treatment regimens.

A dose escalation study with increasing concentrations CsA revealed a sigmoidal dose-response relationship between the dose CsA administered and the brain uptake of [¹²³I]-FMIP. A log EC₅₀ value of 24.48 mg/kg was obtained. This study demonstrated that the blockade of [¹²³I]-FMIP efflux by P-gp is saturated and complete with a CsA dosage of 30 mg/kg. The dose with maximal tracer uptake and the EC₅₀ value are comparable with the values reported for other tracers. [¹¹C]Carvedilol for example reached maximum brain uptake at a dosage of 30 mg/kg (Elsinga et al., 2005). [¹¹C]Verapamil has a EC₅₀ value of 22.76 which is comparable with that of [¹²³I]-FMIP (Bart et al., 2003).

Comparison of biodistribution data with *in vivo* μSPECT observations shows a relative good correlation. With *mdr1a* (-/-) mice, the biodistribution study showed at 60 min p.i. a 2.92 ± 1.85 fold increase in brain uptake of [¹²³I]-FMIP, whereas μSPECT measurements revealed an 2.92 ± 0.56 fold increase. In biodistribution studies, pretreatment with CsA resulted in 4.17 ± 2.79 higher brain uptake which is in agreement with the 3.04 ± 0.73 increase obtained with μSPECT imaging. Using μSPECT measurements, the obtained standard errors were remarkably lower compared to those of the biodistribution studies. The use of a μSPECT device eliminates potential errors due to organ removal, weighing and gamma counting in a separate system. Furthermore, the injected dose is directly measured in contrast to the biodistribution studies where aliquots of the injection solution were employed to calculate the injected dose.

While the brain was visible as a black cavity when only [¹²³I]-FMIP was administered, CsA administration or the use of *mdr1a* (-/-) mice improved brain uptake of [¹²³I]-FMIP resulting in a better image of the brain. In all treatment regimens a homogenous brain distribution was observed, supporting the previous finding that [¹²³I]-FMIP is not suitable for mapping the dopamine transporter *in vivo*.

Brain uptake of [¹²³I]-FMIP is very low in wild-type mice with physiological saline pre-administration, consistent with the rapid action and high capacity of P-gp.

CsA pretreatment as well as *mdr1a* gene depletion resulted in increase (two- to five-fold) of cerebral uptake of [¹²³I]-FMIP in mice. The effect on blood activity and radioactivity concentration in other organs was negligible. These findings indicate that [¹²³I]-FMIP is a very promising radiotracer to visualize P-gp function at the BBB.

8.6. References

- Ballinger JR, Bannerman J, Boxen I, Firby P, Hartman NG and Moore MJ. Technetium-99m-Tetrofosmin as a substrate for P-glycoprotein: *in vitro* studies in multidrug-resistant breast tumor cells. *J Nucl Med* 1996; 37:1578-82.
- Ballinger JR, Hua HA, Berry BW, Firby P and Boxen I. ^{99m}Tc-sestamibi as an agent for imaging P-glycoprotein-mediated multi-drug resistance: *in vitro* and *in vivo* studies in a rat breast tumour cell line and its doxorubicin-resistant variant. *Nucl Med Comm* 1995; 16:253-7.
- Barbarics E, Kronauge JF, Cohen D, Davison A, Jones AG and Croop JM. Characterization of P-glycoprotein transport and inhibition *in vivo*. *Cancer Res* 1998; 58:276-82.
- Bart J, Willemsen ATM, Groen HJM, van der Graaf WTA, Wegman TD, Vaalburg W et al. Quantitative assessment of P-glycoprotein function in the rat blood-brain barrier by distribution volume of [¹¹C]Verapamil measured with PET. *Neuroimage* 2003; 20:1775-82.
- Elsinga PH, Hendrikse NH, Bart J, van Waarde A and Vaalburg W. Positron emission tomography studies on binding of central nervous system drugs and P-glycoprotein function in the rodent brain. *Mol Imaging Biol* 2005; 7:37-44.
- Gottesman MM and Pastan I. Biochemistry of multidrug resistance mediated by the multidrug transporter. *Annu Rev Biochem* 1993; 62:385-427.
- Gottesmann MM, Fojo T and Bates SE. Multidrug resistance in cancer: Role of ATP-dependent transporters. *Nat Rev Cancer* 2002; 2:48-58.
- Hendrikse NH, Franssen EJF, van der Graaf WTA, Meijer C, Piers DA, Vaalburg W, et al. Tc-99m-sestamibi is a substrate for P-glycoprotein and the multidrug resistance-associated protein. *Brit J Cancer* 1997; 77:353-8.
- Hendrikse NH, Schinkel AH, de Vries EGE, Fluks E, van der Graaf WTA, Willemsen ATM et al. Complete *in vivo* reversal of P-glycoprotein pump function in the blood-brain barrier visualized with positron emission tomography. *Br J Pharmacol* 1998; 124:1413-8.
- Kortekaas R, Leenders KL, van Oostrom JCH, Vaalburg W, Bart J, Willemsen ATM et al. Blood-brain barrier dysfunction in parkinsonian midbrain *in vivo*. *Ann Neurol* 2005; 57:176-9.
- Kostakoglu L, Elahi N, Kiratli P, Ruacan S, Sayek I, Baltali E et al. Clinical validation of the influence of P-glycoprotein on technetium-99m-sestamibi uptake in malignant tumors. *J Nucl Med* 1997; 38:1003-8.
- Kwan P and Brodie MJ. Potential role of drug transporters in the pathogenesis of medically intractable epilepsy. *Epilepsia* 2005; 46:224-35.

- Lam FC, Liu R, Lu P, Shapiro AB, Renoir J-M, Sharom FJ et al. B-amyloid efflux mediated by p-glycoprotein. *J Neurochem* 2001; 76:1121-8.
- Langford D, Grigorian A, Hurford R, Adame A, Ellis RJ, Hansen L et al. Altered P-glycoprotein expression in AIDS patients with HIV encephalitis. *J Neuropath Exp Neurol* 2004; 63:1038-46.
- Lazarova N, Zoghbi SS, Hong J, Seneca N, Tuan E, Gladding RL et al. Synthesis and evaluation of [¹¹C]N-Desmethyl-loperamide as a new and improved PET radiotracer for imaging P-gp function. *J Med Chem* 2008; 51:6034-43.
- Lee Y-J, Maeda J, Kusuhara H, Okauchi T, Inaji M, Nagai Y, Obayashi S et al. In vivo evaluation of P-glycoprotein function at the blood-brain barrier in nonhuman primates using [¹¹C]verapamil. *J Pharmacol Exp Ther* 2006; 316:647-53.
- Linnert K and Ejsing TB. A review on the impact of P-glycoprotein on the penetration of drugs into the brain. Focus on psychotropic drugs. *Eur Neuropsychopharmacol* 2008; 18:157-69.
- Luurtsema G, Molthoff CFM, Windhorst JW, Smit H, Keizer R, Boellaard AA et al. (R)- and (S)-[¹¹C]Verapamil as PET-tracers for measuring P-glycoprotein function: *in vitro* and *in vivo* evaluation. *Nuc Med Biol* 2003; 30:747-51.
- Schinkel AH, Smit JJM, van Tellingen O, Beijnen JH, Wagenaar E, Van Deemter L et al. Disruption of the mouse *mdr1a* P-glycoprotein gene leads to a deficiency in the blood-brain barrier and to increased sensitivity to drugs. *Cell* 1994; 77:491-502.
- Schinkel AH, Wagenaar E, Mol CAAM and van Deemter L. P-glycoprotein in the blood-brain barrier of mice influences the brain penetration and pharmacological activity of many drugs. *J Clin Invest* 1996; 97:2517-24.
- Turgut G, Bastemir M, Turgut S, Akin F, Kursunluoglu R and Kaptanoglu B. P-glycoprotein polymorphism in hypo- and hyper-thyroidism patients. *Mol Biol Rep* 2008; 35:693-8.

Chapter 9

Radiosynthesis and *in vivo* evaluation of [¹¹C]-MC80 for P-glycoprotein imaging



De Bruyne S.¹, wyffels L.¹, Moerman L.¹, Sambre J.³, Colabufo N.A.², Berardi F.²,
Perrone R.², De Vos F.¹

Nuclear Medicine and Biology, submitted

¹ Laboratory for Radiopharmacy, Ghent University, Harelbekestraat 72, 9000 Ghent, Belgium

² Dipartimento Farmaco-Chimico, Università degli Studi di Bari, via Orabona 4, 70125 Bari- Italy

³ Univeristy Hospital Gent, Cyclotron Department, De Pintelaan , 9000 Ghent, Belgium

Chapter 9

Radiosynthesis and *in vivo* evaluation of [¹¹C]- MC80 for P-glycoprotein imaging

9.1. Abstract

Aim: P-gp is an ATP-dependent efflux pump protecting the body against xenobiotics. We labelled an *in vitro* characterized substrate (MC80) of the P-gp pump with ¹¹C and evaluated this tracer *in vivo* for its potential to image P-gp function and expression.

Methods: MC80 was labelled using ¹¹CH₃I. Biodistribution studies were performed in male FVB or *mdr1a* (-/-) mice pretreated with physiological saline, CsA (50 mg/kg) or cold MC80 (15 mg/kg). The metabolic profile of [¹¹C]-MC80 was characterized.

Results: The radiochemical yield was 26 ± 5 % with a total synthesis time of 25 min. Cerebral uptake was increased in knock-out mice (1.5 – 2 fold) as well as after CsA pretreatment (1.3 – 2 fold). Administration of non-radioactive MC80 caused a reduced uptake in several organs including brain, pancreas and intestine. In brain, [¹¹C]-MC80 displayed an excellent metabolic profile (> 90 % intact at 30 min p.i.).

Conclusion: [¹¹C]-MC80 is modulated by and shows specific binding to P-gp. Since [¹¹C]-MC80 shows specific binding to target organs, this compound may be useful for P-gp imaging, especially in the intestines. This compound can also be a lead compound for the development of other novel radioligands for measuring the expression of P-gp in the brain.

9.2. Introduction

P-gp is an ATP-dependent efflux pump that is expressed in several normal tissues including liver, kidneys, intestine and brain (Thiebaut et al., 1987; Schinkel and Jonker, 2003). The function of this efflux pump is to protect the human body against xenobiotics. It prevents accumulation in the brain of a wide range of drugs (Schinkel et al., 1996; Linnet and Ejsing, 2008) including anti-epileptics (Luna-tortos et al., 2008), anti-HIV drugs (Kim et al., 1998) and antidepressants (Szabo et al., 1999). Overexpression of P-gp in tumors is implicated in the resistance to chemotherapeutics in some cancers (Gottesmann and Pastan, 1993; Gottesman et al., 2002). Besides its role in multidrug resistance, changes or abnormalities in P-gp expression and function are involved in the etiology and pathogenesis of several neurological diseases (Kwan and Brodie, 2005; Turgut et al., 2008; Kortekaas et al., 2005; Langford et al., 2004). A decreased P-gp function, for example, diminishes the clearance of amyloid plaques, increasing the vulnerability to Alzheimer disease (Lam et al., 2001; Vogelgesang et al., 2002).

Imaging of P-gp function and expression with PET or SPECT could be of great importance in drug development and medicine. Non-invasive monitoring of P-gp could be applied to elucidate the role of P-gp in several human diseases and to evaluate the efficacy of new P-gp modulators. Several tracers have already been evaluated for P-gp modulation among them [¹¹C]verapamil (Hendrikse et al., 1998; Lee et al., 2006), [¹¹C]N-desmethyl-loperamide (Lazarova et al., 2008; Zoghbi et al., 2008) and [^{99m}Tc]sestamibi (Kostakoglu et al., 1997; Ballinger et al., 1995). All these radiotracers have at least one limitation, including significant contamination with radiometabolites, difficulty in radiosynthesis or very low baseline brain uptake which makes it difficult to see minor changes in P-gp expression. Moreover, the reported radiotracers for P-gp are all aimed to visualize P-gp function but not the expression and quantification of P-gp.

In the search for a superior radiotracer to image P-gp function or expression, we evaluated [¹¹C]-6,7-dimethoxy-2-(6-methoxy-naphthalen-2-ylmethyl)-1,2,3,4-tetra-

hydroisoquinoline ([¹¹C]-MC80) for imaging P-gp function and expression. Recently, Colabufo et al. (2008) developed several 6,7-dimethoxytetrahydroisoquinoline derivatives as novel P-gp modulators. Their P-gp interacting mechanism and their potency towards P-gp was evaluated *in vitro* by combining three biological assays: [³H]vinblastine transport inhibition, apparent permeability determination and ATP-ase activation. From these assays, MC80 (Figure 9.1) can be hypothesized as a transported substrate with an interaction profile similar to CsA (Colabufo et al., 2008).

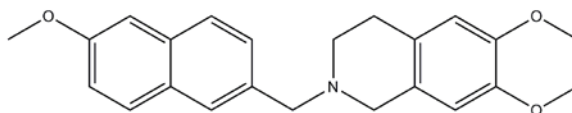


Figure 9.1 Chemical structure of MC80

This study describes the synthesis and purification of [¹¹C]-MC80. The development of a HPLC method for quantification is completed. Specific activity, radiochemical purity and log $D_{7.4}$ are reported. We also evaluated [¹¹C]-MC80 *in vivo* in mice. To investigate the P-gp modulation characteristics, [¹¹C]-MC80 is appraised in wild-type mice with or without CsA pretreatment in addition to P-gp knock-out mice. The metabolic profile of [¹¹C]-MC80 in all three treatment groups is determined. Finally, specific binding of [¹¹C]-MC80 is examined by pre-administration of cold MC80.

9.3. Materials & Methods

9.3.1. GENERAL

The precursor, 6,7-dimethoxy-2-(6-hydroxy-naphthalen-2-yl-methyl)-1,2,3,4-tetrahydroisoquinoline (MC90) as well as the cold reference compound, MC80, were kindly provided by the University of Bari, Dipartimento Farmaco-Chimico, Italy. MC80 was previously reported as compound 7h while MC90 was termed 7g.

MC80 was characterized as a transported substrate with an interaction profile similar to CsA (Colabufo et al., 2008).

[^{11}C]N-desmethyl-loperamide has been synthesized and evaluated by another PhD student of our lab. Those data are not reported in this thesis but are referred to when evaluating [^{11}C]-MC80.

9.3.2. RADIOCHEMISTRY

The alkylating reagent [^{11}C]methyl iodide was prepared from [^{11}C]methane by gas-phase iodination. The production of both $^{11}\text{CH}_4$ and $^{11}\text{CH}_3\text{I}$ is described in Chapter 4.

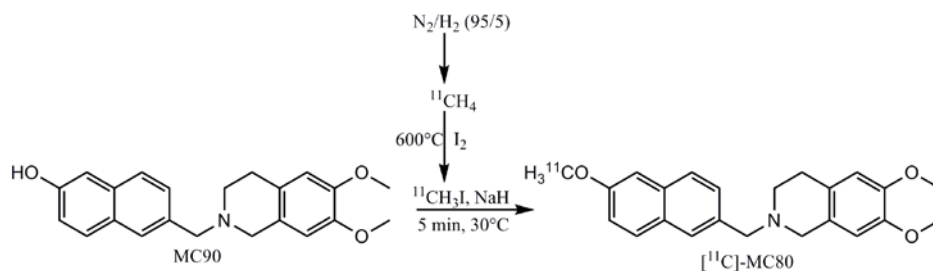


Figure 9.2 Radiosynthesis of [^{11}C]-MC80

The radiosynthesis of [^{11}C]-MC80 is shown in Figure 9.2. $^{11}\text{CH}_3\text{I}$ in carrier helium was bubbled into a sealed vial containing 3 μmol MC90 and 7 μL NaH (1 M in DMF) in DMF (243 μL). When the radioactivity in the reaction vial reached maximum activity levels, the reaction mixture was heated at 30°C for 5 min. Afterwards, the crude reaction mixture was diluted with eluent and injected onto a semipreparative C_{18} HPLC column (Econosphere, 10 μm , 10 mm x 250 mm, Grace Davison Discovery Sciences, Lokeren, Belgium) that was eluted at 6 mL/min with (80:20) MeOH:sodium acetate buffer (0.02 M, pH 5.5). The eluate was monitored for radioactivity (solar-blind P.I.N. photodiode) and UV absorbance (smartline UV detector 2500, Knauer, Berlin, Germany) at 254 nm. [^{11}C]-MC80 ($T_r = 9.3$ min) was collected in 30 mL PBS (pH 7.4, 0.01 M) and

loaded on a C₁₈ Sep-pak column (Alltech Maxi-clean SPE Prevail C₁₈, previously activated with 1 mL EtOH and 5 mL sterile water). After the cartridge has been washed with 5 mL sterile water, the desired product [¹¹C]-MC80 was eluted with 1 mL EtOH. For biodistribution studies, the EtOH fraction was diluted with 10 mL physiological saline. For metabolite analysis, EtOH was evaporated to dryness and the residue was redissolved in an adequate amount of EtOH/saline (8/92 - v/v).

9.3.3. IN VITRO CHARACTERIZATION

Quality control consisted of the determination of radiochemical purity and specific activity, calculated by analytical HPLC assay using a Gracesmart C₁₈ column (5 μm, 4.6 mm x 250 mm, Grace Davison Discovery Sciences, Lokeren, Belgium) at a flow rate of 1 mL/min. The mobile phase consisted of a mixture of 75 % MeOH and 25 % sodium acetate buffer (0.02 M, pH 5.5).

A calibration curve of unlabelled reference compound ($0.02 \times 10^{-3} \mu\text{M} - 1 \times 10^{-3} \mu\text{M}$) was determined and controlled for its accuracy and reproducibility. Additionally, the detection limit was determined. Specific activities were decay corrected to the end of purification. Log D_{7.4} was determined according to the method described in Chapter 4.

9.3.4. BIODISTRIBUTION STUDIES

Wild-type mice (FVB strain) or *mdr1a* knock-out mice of 5 – 7 weeks old weighing approximately 25 g were used. Mice ($n=3$ for each time point of each treatment group) were injected in a tail vein with about 150 μL EtOH:physiological saline (8:92) containing 4.5 MBq (122 μCi) [¹¹C]-MC80. Thirty minutes before administration of [¹¹C]-MC80, the mice were either treated with physiological saline or with CsA (50 mg/kg). The mice were awake during the injections. At various periods after injection of the radioligand, the animals

were sacrificed by cervical dislocation under isoflurane anaesthesia. Blood and urine were removed and organs were dissected. Tissues were weighed and counted for radioactivity using a gamma counter. To remove adhering blood, all organs were rinsed with water prior to weighing and counting. For calculation of the injected dose, five aliquots of the injection solution were weighed and counted for activity. Results are decay-corrected and expressed as % ID/g ± SD. Statistical analysis was performed using one-sided, unpaired student's *t*-test. Only p-values < 0.05 are considered significant.

Specific binding of [¹¹C]-MC80 was examined by pretreatment of FVB mice (*n*=3 for each time point) with 15 mg/kg non-radioactive MC80. At 30 and 60 min after [¹¹C]-MC80 injection, animals were killed and dissected. Tissues were treated as described above. Results are decay-corrected and expressed as % ID/g ± SD. Statistical analysis was performed using one-sided, unpaired student's *t*-test. Only p-values < 0.05 are considered significant.

9.3.5. METABOLITE ANALYSIS

200 µL 92:8 (v:v) – physiological saline:EtOH containing approximately 18.5 MBq (500 µCi) [¹¹C]-MC80 was injected in a tail vein of awake mice (5 - 7 weeks old, weighing 25 - 30 g). At 1, 10 and 30 min p.i., the mice were sacrificed and blood and brain were taken and treated as described in Chapter 4. HPLC analysis was performed using a RP C₁₈ HPLC column (Econosphere C₁₈ 250 mm x 10 mm, 10 µm) attached to a precolumn (Alltima C₁₈ 33 mm x 7 mm, 10 µm) with 80:20 (v:v) MeOH:sodium acetate buffer (0.02 M, pH 5.5) as solvent system at a flow rate of 6 mL/min. The same treatment regimens as for the biodistribution studies were investigated.

9.4. Results & Discussion

9.4.1. RADIOSYNTHESIS

[¹¹C]-MC80 was prepared with an overall decay-corrected yield of 26 ± 5 % ($n=6$). Extraction efficiency of the Sep-pak column was calculated to be 87 ± 3 % ($n=6$). The overall time of preparation was 25 min.

9.4.2. IN VITRO CHARACTERIZATION

9.4.2.1. *Quality control, specific activity and stability*

The identity of [¹¹C]-MC80 was confirmed by co-elution with MC80 after co-injection on HPLC. A radiochemical purity of more than 98 % was obtained. Specific activity was > 0.3 TBq/ μ mol (> 8.1 Ci/ μ mol). The [¹¹C]-MC80 formulation remained stable during the time span of the study.

9.4.2.2. *Log D_{7.4}*

The log D_{7.4} of [¹¹C]-MC80 in octanol was 1.96 ± 0.08 . This value is suitable for brain penetration (Waterhouse, 2003).

9.4.3. BIODISTRIBUTION STUDIES

9.4.3.1. *Biodistribution study in FVB mice*

The tissue distribution of [¹¹C]-MC80 in wild-type mice with saline pretreatment is depicted in Table 9.1.

[¹¹C]-MC80 is cleared from plasma via the hepatobiliary system as shown by the high liver uptake (8.71 ± 2.44 % ID/g) and the increase in radioactivity uptake

over time in small intestine (from 3.89 ± 0.30 % ID/g at 1 min p.i. to 11.78 ± 3.38 % ID/g at 90 min p.i.) and large intestine (from 1.83 ± 0.72 % ID/g at 1 min p.i. to 2.18 ± 0.82 % ID/g at 90 min p.i.). [¹¹C]-MC80 also demonstrated high initial kidney uptake (11.32 ± 0.95 % ID/g at 1 min p.i.), and subsequently urinary clearance was observed (data not shown). Since radioactivity uptake in the intestines already occurred at the earliest time point, it is probably not only caused by excretion of [¹¹C]-MC80 but is possibly also P-gp mediated.

Table 9.1 Tissue distribution of [¹¹C]-MC80 in wild-type mice

	% ID/g \pm SD (<i>n</i> =3)				
	1 min	10 min	30 min	60 min	90 min
Blood	2.56 ± 0.67	1.12 ± 0.09	0.93 ± 0.09	0.73 ± 0.05	0.85 ± 0.15
Brain	7.66 ± 1.38	3.73 ± 0.46	2.03 ± 0.20	1.09 ± 0.18	0.90 ± 0.20
Heart	10.69 ± 2.49	3.19 ± 0.37	2.26 ± 0.24	1.54 ± 0.19	1.27 ± 0.22
Lungs	31.35 ± 11.60	8.44 ± 0.58	4.24 ± 0.98	2.86 ± 0.56	1.84 ± 0.25
Stomach	4.60 ± 0.39	6.00 ± 1.39	7.72 ± 6.74	3.37 ± 0.62	4.05 ± 1.68
Spleen	3.24 ± 0.75	2.84 ± 0.27	2.53 ± 0.38	1.52 ± 1.12	1.47 ± 0.35
Liver	7.68 ± 0.27	8.71 ± 2.44	6.10 ± 0.20	4.86 ± 0.33	5.71 ± 1.51
Kidneys	11.32 ± 0.95	5.31 ± 2.08	3.62 ± 0.59	2.46 ± 1.61	3.00 ± 0.80
Small intestine	3.89 ± 0.30	4.51 ± 0.69	8.03 ± 0.91	11.68 ± 0.13	11.78 ± 3.38
Large intestine	1.83 ± 0.72	1.58 ± 0.20	1.33 ± 0.07	1.45 ± 0.78	2.18 ± 0.82
Bladder	4.27 ± 0.63	5.28 ± 2.11	4.45 ± 1.16	4.00 ± 1.77	7.08 ± 1.31
Pancreas	7.13 ± 1.77	9.99 ± 3.35	10.63 ± 1.68	6.85 ± 0.66	5.12 ± 1.64
Testes	1.66 ± 0.41	2.23 ± 0.28	2.83 ± 0.36	2.46 ± 0.51	1.91 ± 0.16

[¹¹C]-MC80 displayed good uptake in mouse brain (7.66 ± 1.38 % ID/g at 1 min p.i.) followed by efficient wash-out (0.90 ± 0.20 % ID/g at 90 min p.i.). Blood activity never exceeded brain uptake. Compared to [¹¹C]verapamil (Hendrikse et al., 1998; Lee et al., 2006) and [¹¹C]N-desmethyl-loperamide, [¹¹C]-MC80 displayed a high baseline brain uptake. This could be an advantage for imaging small fluctuations in P-gp expression or function. With a low initial brain uptake, it is not possible to image a small increase in P-gp function or a small reduction in

P-gp expression. It will be difficult to observe significant reductions in brain radioactivity uptake in the very low brain radioactivity levels.

9.4.3.2. Biodistribution study after CsA pretreatment

Pretreatment of animals with CsA caused a significant increase (except at 90 min p.i.) of radioactivity uptake in mice brain compared to FVB mice treated with physiological saline (Figure 9.3). The calculated p-values are 0.003, 0.007, 0.011, 0.009 and 0.293 at 1, 10, 30, 60 and 90 min p.i., respectively. Brain uptake raised 1.3 - 2 fold compared to mice without CsA pretreatment.

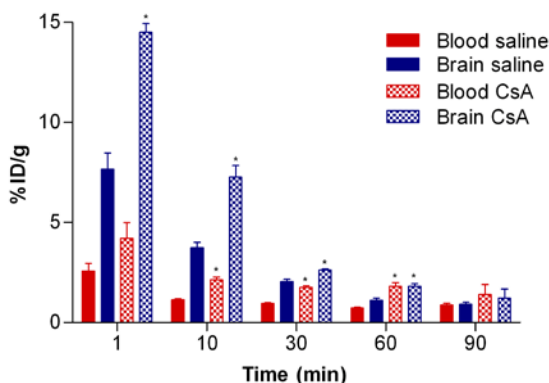


Figure 9.3 Blood-brain distribution of [¹¹C]-MC80 in FVB mice with saline or CsA pretreatment

Values are expressed as % ID/g \pm SD ($n=3$); * $p < 0.05$ with the student's *t*-test

Except at 1 min p.i., CsA also increased the uptake of [¹¹C]-MC80-derived radioactivity in several peripheral organs including testes (from 2.56 ± 0.51 % ID/g to 3.73 ± 0.66 % ID/g at 60 min p.i.), pancreas (from 6.85 ± 0.66 % ID/g to 8.19 ± 0.79 % ID/g at 60 min p.i.), spleen (from 1.52 ± 1.12 % ID/g to 2.31 ± 0.15 % ID/g at 60 min p.i.), kidneys (from 2.46 ± 1.61 % ID/g to 4.53 ± 0.28 % ID/g at 60 min p.i.), and liver (from 4.86 ± 0.33 % ID/g to 8.25 ± 0.99 % ID/g at 60 min p.i.) (Figure 9.4). This increase however was not significant at every time point. Compared to mice treated with saline, radioactivity uptake in

blood (from 2.56 ± 0.67 % ID/g to 4.97 ± 0.26 % ID/g), heart (from 10.69 ± 2.49 % ID/g to 28.55 ± 1.35 % ID/g) and lungs (from 31.35 ± 11.60 % ID/g to 71.59 ± 15.79 % ID/g) was already higher at 1 min p.i. and remained higher at each time point. These observations suggest a slower distribution of [^{11}C]-MC80 to the peripheral organs after CsA administration. In contrast, intestinal uptake was significantly lower with CsA pretreatment. A possible reason is the reduced binding to P-gp caused by CsA modulation. Taken together, CsA administration has an effect on tissue uptake of [^{11}C]-MC80 suggesting P-gp plays a role in the kinetics of [^{11}C]-MC80.

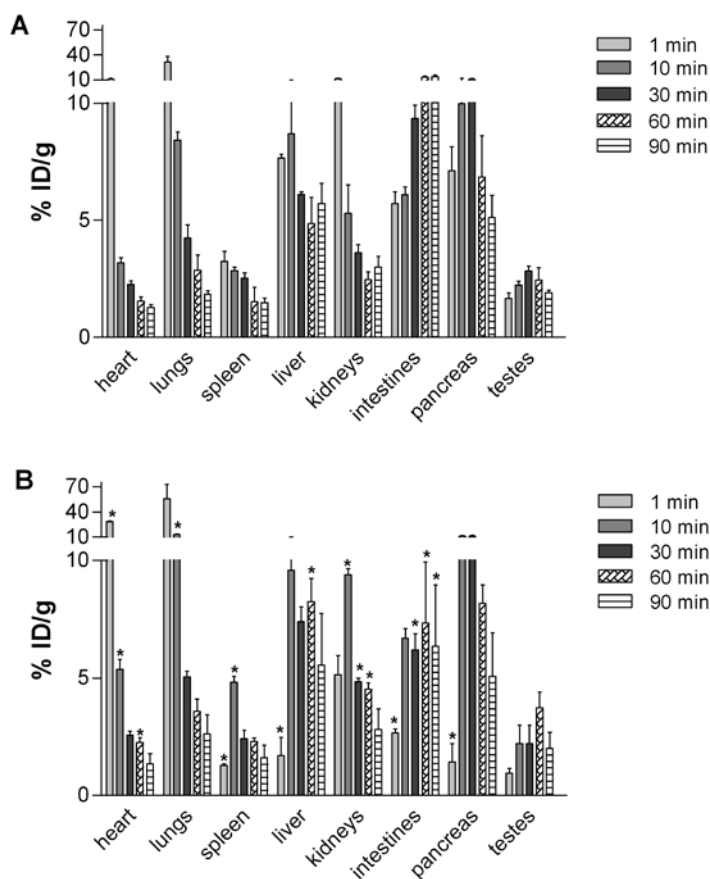


Figure 9.4 Tissue distribution of [^{11}C]-MC80 in FVB mice with saline (A) or CsA (B) pretreatment

Values are expressed as % ID/g \pm SD ($n=3$); * $p < 0.05$ with the student's t -test

9.4.3.3. Biodistribution study in *mdr1a* (-/-) mice

In *mdr1a* (-/-) mice, cerebral uptake of [¹¹C]-MC80 (Figure 9.5) was significantly increased at 10 min ($p = 0.014$) and 60 min p.i. ($p = 0.001$) compared to wild-type mice. The highest increase in brain uptake was 1.96 ± 0.38 (from 1.09 ± 0.18 % ID/g to 2.15 ± 0.65 % ID/g) at 60 min p.i. Significant differences in [¹¹C]-MC80 levels in plasma were measured between the two types of mice at 10 min ($p = 0.021$) and 30 min ($p = 0.032$) p.i.

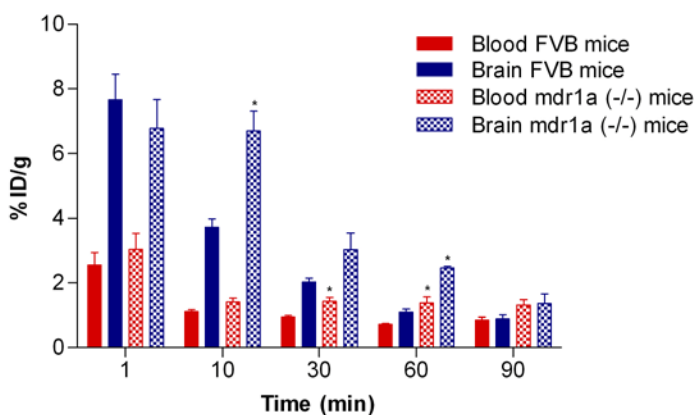


Figure 9.5 Blood-brain distribution of [¹¹C]-MC80 in normal FVB mice or *mdr1a* (-/-) mice

Values are expressed as % ID/g \pm SD ($n=3$); * $p < 0.05$ with the student's *t*-test

At 1 min p.i. most organs displayed a reduced radioactivity uptake. In contrast lungs (from 31.35 ± 11.60 % ID/g to 45.85 ± 13.79 % ID/g) and heart (from 10.69 ± 2.49 % ID/g to 13.06 ± 1.72 % ID/g) showed an increased uptake at 1 min p.i. As with CsA, these observations suggest also a slower distribution of [¹¹C]-MC80 to peripheral organs when using *mdr1a* (-/-) mice (Figure 9.6). Genetic disruption of the *mdr1a* gene appears to affect retention of the tracer in the excretory organs. Radioactivity uptake in the kidney raised from 2.46 ± 1.61 % ID/g to 4.41 ± 0.63 % ID/g at 60 min p.i., and liver uptake increased from 4.86 ± 0.33 % ID/g to 8.47 ± 0.57 % ID/g at 60 min p.i. The elevation in testes

(significant at 10 min ($p = 0.015$) and 30 min ($p = 0.003$) p.i.) uptake is in accordance with P-gp distribution. Contrary to the effect seen with CsA pretreatment, intestinal uptake did not alter. This can be explained by the fact that *mdr1b* encoded P-gp is also found in the gastrointestinal tract resulting in an unchanged intestinal uptake when using *mdr1a* (-/-) mice.

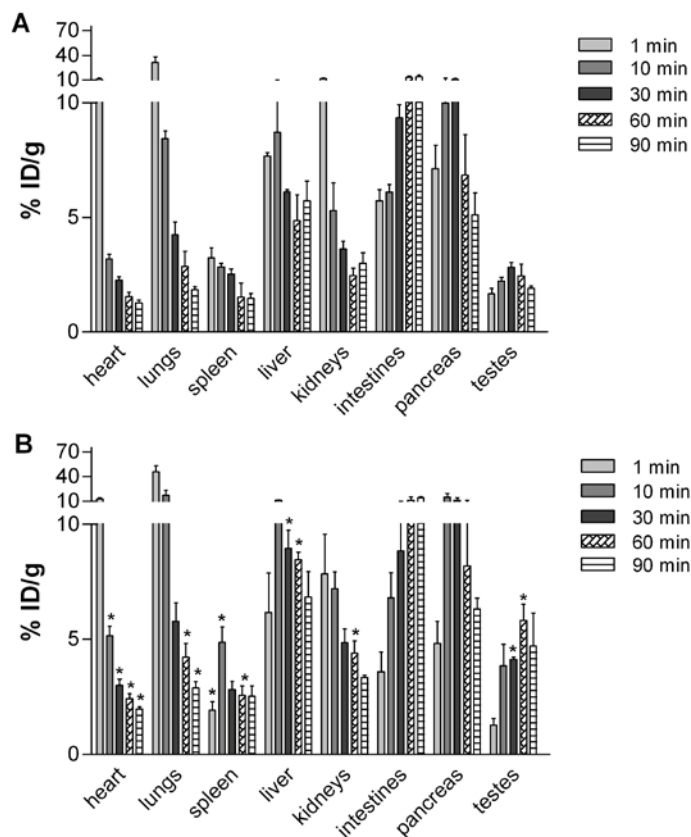


Figure 9.6 Radioactivity uptake in tissues of [¹¹C]-MC80 in normal FVB mice (A) and *mdr1a* (-/-) mice (B)

Values are expressed as % ID/g \pm SD ($n=3$); * $p < 0.05$ with the student's *t*-test

9.4.3.4. Biodistribution study after pretreatment with cold compound

The tissue distribution of [¹¹C]-MC80 in wild-type mice with and without cold MC80 pretreatment is depicted in Table 9.2.

Table 9.2 Tissue distribution of [¹¹C]-MC80 in FVB mice with and without administration of non-radioactive MC80 (15 mg/kg)

	% ID/g ± SD (<i>n</i> =3)			
	Control group		Test group	
	30 min	60 min	30 min	60 min
Blood	0.93 ± 0.09	0.73 ± 0.05	0.82 ± 0.06	0.78 ± 0.13
Brain	2.03 ± 0.20	1.09 ± 0.18	1.64 ± 0.28*	0.89 ± 0.16
Heart	2.26 ± 0.24	1.54 ± 0.19	1.75 ± 0.25*	1.21 ± 0.16*
Lungs	4.24 ± 0.98	2.86 ± 0.56	3.08 ± 0.33	1.70 ± 0.11*
Stomach	7.72 ± 6.74	3.37 ± 0.62	2.21 ± 1.17	2.46 ± 0.71
Spleen	2.53 ± 0.38	1.52 ± 1.12	1.80 ± 0.70	1.31 ± 0.13
Liver	6.10 ± 0.20	4.86 ± 0.33	5.39 ± 0.80	5.63 ± 0.26
Kidneys	3.62 ± 0.59	2.46 ± 1.61	2.99 ± 0.93	2.10 ± 0.31
Small intestine	8.03 ± 0.91	11.68 ± 0.13	4.77 ± 0.88*	6.54 ± 1.62*
Large intestine	1.33 ± 0.07	1.45 ± 0.78	0.98 ± 0.02*	0.95 ± 0.10*
Bladder	4.45 ± 1.16	4.00 ± 1.77	3.86 ± 0.60	4.71 ± 1.34
Pancreas	10.63 ± 1.68	6.85 ± 0.66	5.15 ± 0.30*	3.53 ± 0.37*
Testes	2.26 ± 0.24	1.54 ± 0.19	2.15 ± 0.12*	2.10 ± 0.28

* *p* < 0.05 using one-sided, unpaired student's *t*-test

The brain uptake of [¹¹C]-MC80 was reduced by 20 % after pretreatment of the animals with non-radioactive MC80. This reduced uptake was significant at 30 min p.i. (*p* = 0.037). In the pancreas, pretreatment caused the most outstanding decline in tracer uptake (reduction with 52 % and 49 % at 30 min and 60 min p.i., respectively). A significantly decreased uptake of [¹¹C]-MC80 was also noticed in the heart (reduction with 22 % and 21 % at 30 min and 60 min p.i.), lungs (reduced with 47 % at 60 min p.i.), small intestines (reduction with 41 % and 44 % at 30 min and 60 min p.i., respectively), large intestines (reduction with 26 % and 35 % at 30 min and 60 min p.i., respectively) and testes (reduced with 24 % at 30 min p.i.). This study indicates that MC80 act as an inhibitor for the P-gp transporter and not as a substrate (an increased brain uptake should be observed since MC-80 will compete with [¹¹C]-MC80 for its interaction with P-gp).

Summarizing, the highest amount of specific binding of [¹¹C]-MC80 occurred in the pancreas, lungs and intestine. A lower fraction of specific binding occurred in the brain (reduction with 19 % and 18 % at 30 min and 60 min p.i., respectively),

testes and heart. This tissue distribution of the specific binding of [¹¹C]-MC80 is in accordance with the known expression levels of P-gp (see Chapter 2).

9.4.4. METABOLITE ANALYSIS

The stability of [¹¹C]-MC80 *in vivo* was studied at 10 min and 30 min p.i. After protein elimination, the recovery of radioactivity in the supernatant solutions was 97 ± 1 % in plasma and 87 ± 7 % in brain. HPLC measurements of plasma and brain spiked with [¹¹C]-MC80, displayed one radioactive peak ($T_r = 10$ min). This peak corresponds with [¹¹C]-MC80 as it was found to co-elute with authentic MC80.

Table 9.3 Metabolic profile of [¹¹C]-MC80

Treatment group	Tissue	Time	Retention time on RP-HPLC	
			2.5 min	10 min [¹¹ C]-MC80
Control^a	Brain	10 min	2 ± 2 %	98 ± 2 %
		30 min	9 ± 1 %	91 ± 1 %
	Plasma	10 min	37 ± 6 %	63 ± 6 %
		30 min	42 ± 6 %	58 ± 6 %
CsA pretreatment^b	Brain	10 min	1 %	99 %
		30 min	7 ± 1 %	93 ± 1 %
	Plasma	10 min	35 ± 9 %	65 ± 9 %
		30 min	78 ± 3 %	22 ± 3 %
mdr1a(-/-) mice^c	Brain	10 min	2 ± 1 %	98 ± 1 %
		30 min	8 ± 2 %	92 ± 2 %
	Plasma	10 min	23 ± 7 %	77 ± 7 %
		30 min	40 ± 3 %	60 ± 3 %

^a pretreatment with saline in FVB mice ($n=3$), ^b pretreatment with CsA (50 mg/kg) in FVB mice ($n=3$), ^c pretreatment with saline in mdr1a (-/-) mice ($n=3$)

The metabolic profile of [¹¹C]-MC80 in the three different treatment regiments is summarized in Table 9.3.

9.4.4.1. *Metabolism study in FVB mice*

In brain, [¹¹C]-MC80 remained very stable with over 98 % and 91 % intact product at 10 min and 30 min p.i., respectively. The tracer underwent a more extensive metabolism in plasma. Plasma metabolite analysis showed 63 ± 6 % and 58 ± 6 % intact [¹¹C]-MC80 at 10 and 30 min, respectively. Only one polar metabolite was found, that eluted at the void volume of the column. When [¹¹C]-MC80 is demethylated, it is anticipated that [¹¹C]methyl is removed and metabolized to [¹¹C]CH₃OH, [¹¹C]CH₂O, [¹¹C]CO₂H or [¹¹C]CO₂. These compounds are very polar and are believed to correspond with the radioactive peak of the solvent front.

9.4.4.2. *Metabolism study after CsA pretreatment*

In both tissues, the same radioactive products were found as without CsA injection (Table 9.3). Administration of CsA did not affect the metabolic profile of [¹¹C]-MC80 in brain. The percentage intact [¹¹C]-MC80 was 99 % and 93 % at 10 min and 30 min, respectively. Those values are similar to the values found in the mice pretreated with saline. Blood metabolite studies indicated that [¹¹C]-MC80 underwent an elevated metabolism when CsA was given; at 30 min p.i., the percentage unchanged [¹¹C]-MC80 was 58 ± 6 % without and 22 ± 3 % with CsA pretreatment.

9.4.4.3. *Metabolism study in mdr1a (-/-) mice*

Similar to the previous reported treatment regimens, two radioactive products are detected (Table 9.3). The use of mdr1a (-/-) mice did not affect the amount of unchanged [¹¹C]-MC80 present in brain. At 10 min p.i., 98 ± 1 % of parent compound remained in the brain and at 30 min p.i. 92 ± 2 % was still present as unchanged [¹¹C]-MC80. The fraction of radioactivity in plasma that represented

[¹¹C]-MC80 was 77 ± 7 % at 10 min p.i. and 60 ± 3 % at 30 min p.i. representing the same metabolic profile as in FVB mice.

9.5. Conclusion

MC80 was evaluated *in vitro* using three biological assays. The [³H]vinblastine transport inhibition assay defined MC80 as a potent inhibitor of [³H]vinblastine transport. The second assay showed that MC80 did not activate ATPase within the monolayer. The ratio of drug transport through Caco-2 monolayers in the basolateral-apical and apical-basolateral directions was 3.6, indicating that MC80 is effluxed by P-gp (Colabufo et al., 2008).

[¹¹C]-MC80 was readily prepared (radiochemical yield of 25 %) for intravenous injection by methylation of MC90 with [¹¹C]methyl iodide, itself prepared from cyclotron-produced [¹¹C]methane. Purification by RP-HPLC and Sep-pak provided [¹¹C]-MC80 in high radiochemical purity (> 98 %) and very high specific activity (> 0.3 TBq/μmol).

Biodistribution studies in wild-type mice demonstrated brain uptake which quickly maximized and then washed out. Compared to [¹¹C]N-desmethyl-loperamide and the clinical used [¹¹C]verapamil (Hendrikse et al., 1998; Lee et al., 2006), [¹¹C]-MC80 has a high initial brain uptake. CsA administration, as well as genetic disruption of the *mdr1a* gene, resulted in significant changes in tissue distribution, confirming that [¹¹C]-MC80 is modulated by P-gp not only *in vitro* but also *in vivo*. However, the increase in brain radioactivity is not as high as for [¹¹C]N-desmethyl-loperamide and [¹¹C]verapamil (Hendrikse et al., 1998; Lee et al., 2006). This is probably caused by a difference in pumping efficiency. Blocking studies indicated that radioactivity uptake in intestines and pancreas is highly specific. In brain, the specific binding is not so apparent indicating non-specific binding. Since the blocking study with cold MC80 caused a reduced brain uptake of [¹¹C]-MC80 it was hypothesized that [¹¹C]-MC80 is an inhibitor of P-gp. CsA pretreatment as well as the genetic disruption of *mdr1a* on the other hand caused

an increased brain uptake, indicating that [¹¹C]-MC80 is a substrate for P-gp. Taken together, it was assumed that [¹¹C]-MC80 is a mixed substrate/inhibitor for P-gp.

Summarizing, [¹¹C]-MC80 is modulated by P-gp and shows specific binding to P-gp. In brain however a high degree of non-specific binding is observed. In contrast, intestinal [¹¹C]-MC80 radioactivity uptake is highly specific and sensitive towards P-gp indicating [¹¹C]-MC80 has the potential for imaging intestinal P-gp function or expression.

HPLC measurements demonstrated that [¹¹C]-MC80 has an outstanding metabolic profile compared to [¹¹C]*N*-desmethyl-loperamide and [¹¹C]verapamil (Hendrikse et al., 1998; Lee et al., 2006). At 30 min p.i. over 90 % of the measured radioactivity in brain was related to unchanged [¹¹C]-MC80. Structural analogues possessing the same metabolic stability *in vivo*, but with a higher affinity and specificity for P-gp may be extremely useful for imaging of P-gp expression at the BBB.

9.6. References

- Ballinger JR, Hua HA, Berry BW, Firby P and Boxen I. ^{99m}Tc-sestamibi as an agent for imaging P-glycoprotein-mediated multi-drug resistance: *in vitro* and *in vivo* studies in a rat breast tumour cell line and its doxorubicin-resistant variant. *Nuc Med Comm* 1995; 16:253-7.
- Colabufo NA, Berardi F, Cantore M, Perrone MG, Contino M, Inglese C et al., 4-Biphenyl and 2-naphthyl substituted 6,7-dimethoxytetrahydroisoquinoline derivatives as potent P-gp modulators. *Bioorg Med Chem* 2008; 16:3732-43.
- Gottesman MM and Pastan I. Biochemistry of multidrug resistance mediated by the multidrug transporter. *Annu Rev Biochem* 1993; 62:385-427.
- Gottesmann MM, Fojo T and Bates SE. Multidrug resistance in cancer: Role of ATP-dependent transporters. *Nat Rev Cancer* 2002; 2:48-58.
- Hendrikse NH, Schinkel AH, de Vries EGE, Fluks E, van der Graaf WTA, Willemsen ATM et al. Complete *in vivo* reversal of P-glycoprotein pump function in the blood-brain barrier visualized with positron emission tomography. *Br J Pharmacol* 1998; 124:1413-8.
- Kim RB, Fromm MF, Wandel C, Leake B, Wood AJJ, Roden DM et al. The drug transporter P-glycoprotein limits oral absorption and brain entry of HIV-1 protease inhibitors. *J Clin Invest* 1998; 101:289-94.

- Kortekaas R, Leenders KL, van Oostrom JCH, Vaalburg W, Bart J, Willemsen ATM et al. Blood-brain barrier dysfunction in parkinsonian midbrain in vivo. *Ann Neurol* 2005; 57:176-9.
- Kostakoglu L, Elahi N, Kiratli P, Ruacan S, Sayek I, Baltali E et al. Clinical validation of the influence of P-glycoprotein on technetium-99m-sestamibi uptake in malignant tumors. *J Nucl Med* 1997; 38:1003-8.
- Kwan P and Brodie MJ. Potential role of drug transporters in the pathogenesis of medically intractable epilepsy. *Epilepsia* 2005; 46:224-35.
- Lam FC, Liu R, Lu P, Shapiro AB, Renoir J-M, Sharom FJ et al. B-amyloid efflux mediated by P-glycoprotein. *J Neurochem* 2001; 76:1121-8.
- Langford D, Grigorian A, Hurford R, Adame A, Ellis RJ, Hansen L et al. Altered P-glycoprotein expression in AIDS patients with HIV encephalitis. *J Neuropath Exp Neurol* 2004; 63:1038-46.
- Lazarova N, Zoghbi SS, Hong J, Seneca N, Tuan E, Gladding RL et al. Synthesis and evaluation of [¹¹C]-N-Desmethyl-loperamide as a new and improved PET radiotracer for imaging P-gp function. *J Med Chem* 2008; 51:6034-43.
- Lee Y-J, Maeda J, Kusahara H, Okauchi T, Inaji M, Nagai Y, Obayashi S et al. In vivo evaluation of P-glycoprotein function at the blood-brain barrier in nonhuman primates using [¹¹C]verapamil. *J Pharmacol Exp Ther* 2006; 316:647-53.
- Linnet K and Ejlsing TB. A review on the impact of P-glycoprotein on the penetration of drugs into the brain. Focus on psychotropic drugs. *Eur Neuropsychopharmacol* 2008; 18:157-69.
- Luna-Tortós C, Fedrowitz M and Löscher W. Several major antiepileptic drugs are substrates for human P-glycoprotein. *Neuropharmacology* 2008; 55:1364-75.
- Schinkel AH, Wagenaar E, Mol CAAM and van Deemter L. P-glycoprotein in the blood-brain barrier of mice influences the brain penetration and pharmacological activity of many drugs. *J Clin Invest* 1996; 97:2517-24.
- Schinkel AH and Jonker JW. Mammalian drug efflux transporters of the ATP binding cassette (ABC) family: an overview. *Adv Drug Deliv Rev* 2003; 55:3-29.
- Szabo D, Szabo G, Ocsosvzki I, Aszalos A and Molnar J. Anti-psychotic drugs reverse multidrug resistance of tumor cell lines and human AML cells ex-vivo. *Cancer Letters* 1999; 139:115-9.
- Thiebaut F, Tsuruo T, Hamada H, Gottesman MM, Pastan I and Willingham MC. Cellular localization of the multidrug-resistance gene product P-glycoprotein in normal human tissues. *Proc Natl Acad Sci* 1987; 84:7735-8.
- Turgut G, Bastemir M, Turgut S, Akin F, Kursunluoglu R and Kaptanoglu B. P-glycoprotein polymorphism in hypo- and hyper-thyroidism patients. *Mol Biol Rep* 2008; 35:693-8.
- Vogelgesang S, Cascorbi I, Schroeder E, Pahnke J, Kroemer HK, Siegmund W et al. Deposition of Alzheimer's beta-amyloid is inversely correlated with P-glycoprotein expression in the brains of elderly non-demented humans. *Pharmacogenetics* 2002; 12:535-41.
- Waterhouse RN. Determination of lipophilicity and its use as a predictor of blood-brain barrier penetration of molecular agents. *Mol Imaging Biol* 2003; 5:376-389.
- Zoghbi SS, Liow J-SL, Yasuno F, Hong J, Tuan E, Lazarova N et al. ¹¹C-Loperamide and its N-desmethyl radiometabolite are avid substrates for brain permeability-glycoprotein efflux. *J Nucl Med* 2008; 49:649-56.

Summary



SUMMARY

The human brain is a complex organ, consisting of millions of intercommunicating neurons. Due to the complexity of the brain our knowledge about CNS disorders is still limited. SPECT and PET imaging of the living brain are unique tools for clinical researchers to elucidate the causes and consequences of brain disorders. *In vivo* brain mapping with PET or SPECT is of great importance in drug development as well as in the effective diagnosis, treatment and management of neurological and psychiatric illness.

In this thesis, new SPECT or PET radioligands directed towards two different brain systems, were developed and evaluated *in vivo*.

Chapter 1 gave a short overview of the medical imaging techniques and described the requirements of a valuable radiopharmaceutical for SPECT and PET imaging. The first part of **Chapter 2** described the blood-brain barrier and the transport of compounds across this barrier. One of the most important transport mechanisms limiting brain uptake of drugs, P-gp, was detailed in the second part of this chapter. After a brief description of the discovery, structure, expression and physiological role, the potential modulation agents of P-gp were reviewed. The second brain system, the catecholamine system, was addressed in **Chapter 3**. The dopamine and norepinephrine system were discussed briefly, followed by a more detailed description of the mechanisms responsible for terminating the neurotransmission. After the history, structure and function of the catecholamine transporters in general were discussed, the physiological role of NET and DAT in health and disease was illustrated. The last part of chapter 3 is dedicated to MAO, one of the main enzymes causing degradation of catecholamines. In **Chapter 4** the general material and methods were described.

Chapter 5 reported the synthesis, radiosynthesis and preliminary evaluation of [^{123}I]-(*S,S*)-IPBM, an iodinated reboxetine analogue. [^{123}I]-(*S,S*)-IPBM aimed at imaging the norepinephrine transporter. The precursor was prepared in an overall

chemical yield of 8 % with an enantiomeric excess of 95 %. Radiosynthesis afforded [^{123}I]-(*S,S*)-IPBM with an excellent radiochemical purity. Biodistribution studies demonstrated a high brain uptake of [^{123}I]-(*S,S*)-IPBM followed by efficient wash-out. Since [^{123}I]-(*S,S*)-IPBM was reported by others at the moment we performed our biodistribution studies, we did not conduct additional *in vivo* studies. Regarding their results (Tamagnan et al., 2007; Kanigawara et al., 2006), the choice to develop [^{123}I]-(*S,S*)-IPBM as radiotracer for NET was an excellent suggestion.

In **Chapter 6** the radiolabelling as well as the *in vivo* characterization of two [^{11}C]-labelled pyrrole-2-carboxamide derivatives, [^{11}C]-RS 2315 and [^{11}C]-RS 2360, were described. *In vitro*, RS 2315 and RS 2360 are potent inhibitors of MAO-A. Both tracers were obtained with a good radiochemical yield, excellent radiochemical purity and high specific activity. Both radiotracers displayed high brain uptake followed by rapid brain clearance. Blocking studies in mice could not demonstrate specificity of [^{11}C]-RS 2315 towards MAO-A or B. The blocking study with [^{11}C]-RS 2360 on the other hand indicated specific binding at MAO-A at the earliest time point. In the imaging study with [^{11}C]-RS 2360, administration of clorgyline caused an overall significant reduced brain uptake indicating specific binding at MAO-A. These results indicated that [^{11}C]-RS 2315 is not suitable for mapping MAO-A *in vivo* and that further research is necessary to investigate the potential of [^{11}C]-RS 2360 in MAO-A imaging.

The (radio)synthesis and *in vivo* evaluation of [^{123}I]-FMIP as a selective radiotracer for DAT was reported in **Chapter 7**. FMIP has nanomolar affinity for DAT and better selectivity over the other monoamine transporters compared to the already existing ligands for DAT imaging with SPECT. The tributylstannyl precursor was synthesized using a five-step synthetic procedure. [^{123}I]-FMIP was synthesized with a high radiochemical yield and purity. The specific activity of the compound was at least 667 GBq/ μmol . Biodistribution studies showed low brain uptake and high blood activity. Blocking studies indicated no selectivity of [^{123}I]-FMIP towards DAT. A metabolite study demonstrated that in brain, over 80 % was

present as intact [^{123}I]-FMIP upon 60 min p.i. In rats, regional brain distribution of [^{123}I]-FMIP was not in agreement with DAT distribution. These results indicated that [^{123}I]-FMIP is not suitable for mapping DAT *in vivo*.

The contribution of P-gp to the low brain uptake of [^{123}I]-FMIP along with its potential as P-gp imaging agent was investigated in **Chapter 8**. To date, no iodinated SPECT ligands for P-gp imaging have been published. Brain uptake of [^{123}I]-FMIP was very low in wild-type mice with saline pretreatment, consistent with the rapid action and high capacity of P-gp. Modulation of P-gp with CsA as well as *mdr1a* gene depletion resulted in a significant increase in cerebral uptake of [^{123}I]-FMIP with only minor effect on blood activity. A dose-dependent sigmoidal increase in brain uptake of [^{123}I]-FMIP with increasing doses of CsA was observed. *In vivo* ROI-based SPECT measurements confirmed the observations of the biodistribution studies. These findings indicated that [^{123}I]-FMIP is a very promising radiotracer to visualize P-gp at the BBB.

Chapter 9 described the radiolabelling of an *in vitro* characterized substrate (MC80) of the P-gp pump with ^{11}C and the evaluation of this tracer *in vivo* for its potential to image P-gp function and expression. [^{11}C]-MC80 was synthesized with high radiochemical purity and high specific activity. Cerebral uptake was increased in *mdr1a* knock-out mice as well as after CsA pretreatment. Administration of non-radioactive MC80 caused a reduced uptake in brain, heart, lungs, testes, pancreas and intestines. In brain, [^{11}C]-MC80 displayed an excellent metabolic profile (> 90 % intact). Since [^{11}C]-MC80 showed specific binding to target organs, this compound can be a lead compound for the development of novel radioligands for measuring the expression of P-gp in the brain.

References

- Kanegawa N, Kiyono Y, Kimura H, Sugita T, Kajiyama S, Kawashima H et al. Synthesis and evaluation of radioiodinated (S,S)-2-(alpha-(2-iodophenoxy)benzyl)morpholine for imaging brain norepinephrine transporter. *Eur J Nucl Med Mol Imaging* 2006; 33:639-47.
- Tamagnan GD, Brenner E, Alagille D, Staley JK, Haile C, Koren A et al. Development of SPECT imaging agents for the norepinephrine transporter: [^{123}I]INER. *Bioorg Med Chem* 2007; 17:533-7.

Samenvatting



SAMENVATTING

De menselijke hersenen zijn een complex orgaan die bestaan uit miljoenen communicerende neuronen. Door de complexiteit van de hersenen is onze kennis over aandoeningen van het central zenuwstelsel nog steeds beperkt. Beeldvorming van de hersenen met SPECT en PET zijn unieke hulpmiddelen voor klinische onderzoekers om de oorzaken en de gevolgen van hersenaandoeningen op te helderen. *In vivo* beeldvorming van de hersenen met PET of SPECT is van groot belang in zowel geneesmiddelenontwikkeling als in het stellen van de juiste diagnose, behandeling en controle van neurologische en psychiatrische ziektes. In deze thesis werden nieuwe SPECT en PET radioliganden gericht naar twee verschillende hersensystemen ontwikkeld en *in vivo* geëvalueerd.

Hoofdstuk 1 gaf een overzicht van de medische beeldvormingstechnieken en beschreef de voorwaarden van een waardevol radiofarmacon voor SPECT en PET beeldvorming. Het eerste deel van **Hoofdstuk 2** beschreef de bloed-hersen barrière en het transport van bestanddelen doorheen deze barrière. Een van de belangrijkste transport mechanismen die de hersenopname van geneesmiddelen beperkt, P-gp, werd gespecificeerd in het tweede deel van dit hoofdstuk. Na een korte beschrijving van de ontdekking, structuur, expressie en fysiologische rol werden de mogelijke modulerende agentia van P-gp besproken. Het tweede hersensysteem, het catecholamine systeem, werd behandeld in **Hoofdstuk 3**. Het dopamine en norepinephrine systeem werden kort besproken, gevolgd door een meer gedetailleerde beschrijving van de mechanismen die verantwoordelijk zijn voor het beëindigen van de neurotransmissie. Nadat de geschiedenis, structuur en functie van de catecholamine transporters in het algemeen besproken waren, werd de fysiologische rol van de norepinephrine transporter en dopamine transporter in ziekte en gezondheid toegelicht. Het laatste deel van hoofdstuk 3 was toegewijd aan monoamine oxidase, één van de belangrijke enzymen die de

afbraak van catecholamines veroorzaken. In **Hoofdstuk 4** werden de algemene materialen en methoden beschreven.

Hoofdstuk 5 rapporteerde de synthese, radiosynthese en preliminaire evaluatie van [^{123}I]-(*S,S*)-IPBM, een geïodeerd reboxetine analoog. [^{123}I]-(*S,S*)-IPBM had als doel de beeldvorming van de norepinephrine transporter. De precursor werd aangemaakt met een chemisch rendement van 8 % met een enantiomere overmaat van meer dan 95 %. Radiosynthese leverde [^{123}I]-(*S,S*)-IPBM op met een uitstekende radiochemische zuiverheid. Biodistributie studies toonden een hoge hersenopname van [^{123}I]-(*S,S*)-IPBM gevolgd door een efficiënte klaring. Doordat [^{123}I]-(*S,S*)-IPBM gerapporteerd werd door anderen op het moment dat wij onze biodistributies deden, voerden we geen bijkomende *in vivo* studies uit. Hun resultaten in beschouwing nemend (Tamagnan et al., 2007; Kanigawara et al., 2006), was de keuze om [^{123}I]-(*S,S*)-IPBM als radiotracer voor de norepinephrine transporter te ontwikkelen een uitstekend voorstel. In **Hoofdstuk 6** werd zowel de merking met radioactiviteit als de *in vivo* karakterisatie van twee [^{11}C]-gemerkte pyrrool-2-carboxamide derivaten, [^{11}C]-RS 2315 and [^{11}C]-RS 2360, beschreven. *In vitro*, zijn RS 2315 en RS 2360 sterke inhibitoren van MAO-A. Beide tracers werden bekomen met een goed radiochemisch rendement, uitstekende radiochemische zuiverheid en hoge specifieke activiteit. Beide radiotracers vertoonden hoge hersenopname gevolgd door snelle klaring uit de hersenen. Blokkeringstudies in muizen konden geen selectiviteit aantonen van [^{11}C]-RS 2315 voor MAO-A of MAO-B. De blokkeringstudie met [^{11}C]-RS 2360 toonde specifieke binding aan MAO-A op het eerste tijdstip. In de beeldvorming studie met [^{11}C]-RS 2360 veroorzaakte toedoening van clorgyline een algemeen significante gedaalde hersenopname wat een specifieke binding aan MAO-A indiceerde. Deze resultaten wezen aan dat [^{11}C]-RS 2315 niet bruikbaar is voor het in kaart brengen van MAO-A *in vivo* en dat verdere onderzoek nodig is om de mogelijkheid van [^{11}C]-RS 2360 in beeldvorming van MAO-A te analyseren.

De radiosynthese en *in vivo* evaluatie van [¹²³I]-FMIP als een selectieve radiotracer voor DAT werd gerapporteerd in **Hoofdstuk 7**. FMIP heeft nanomolaire affiniteit voor DAT en een betere selectiviteit vergeleken met de reeds bestaande liganden voor DAT beeldvorming met SPECT. De tributyltin precursor werd gesynthetiseerd gebruik makend van een vijf-staps synthese. [¹²³I]-FMIP werd aangemaakt met hoog radiochemisch rendement en zuiverheid. De specifieke activiteit van de component was minstens 667 GBq/μmol. Biodistributie studies toonden een lage hersenopname en hoge bloedactiviteit. Blokkeringstudies wezen geen selectiviteit van [¹²³I]-FMIP voor DAT aan. Een metabolietaalyse demonstreerde dat in de hersenen meer dan 80 % aanwezig was als intact [¹²³I]-FMIP tot 60 min na injectie. In ratten, bleek de regionale hersendistributie van [¹²³I]-FMIP niet in overeenkomst met de DAT verdeling. Deze resultaten toonden aan dat [¹²³I]-FMIP niet bruikbaar is voor het in beeld brengen van DAT *in vivo*.

De deelname van P-gp aan de lage hersenopname van [¹²³I]-FMIP samen met zijn potentieel als agens voor beeldvorming van P-gp werd onderzocht in **Hoofdstuk 8**. Tot op heden werden nog geen geïodeerde SPECT liganden voor beeldvorming van P-gp gepubliceerd. Hersenopname van [¹²³I]-FMIP was zeer laag in wildtype muizen voorbehandeld met zoutoplossing, in overeenstemming met de snelle actie en hoge capaciteit van P-gp. Zowel modulatie van P-gp met CsA als verwijderen van het *mdr1a* gen resulteerde in een significantie stijging van de hersenopname van [¹²³I]-FMIP met slechts een klein effect op de bloedactiviteit. Een dosisafhankelijke sigmoïdale stijging in hersenopname van [¹²³I]-FMIP met stijgende concentraties CsA werd waargenomen. *In vivo* ROI-gebaseerde SPECT metingen bevestigden de observatie van de biodistributie studies. Deze bevindingen wezen erop dat [¹²³I]-FMIP een veelbelovende radiotracer is voor de visualisatie van P-gp ter hoogte van de bloed-hersen barrière.

Hoofdstuk 9 beschreef de radioactieve merking van een *in vitro* gekarakteriseerd substraat (MC80) van de P-gp pomp met ¹¹C en de evaluatie van deze tracer *in*

in vivo voor zijn potentieel om P-gp functie en expressie in beeld te brengen. [¹¹C]-MC80 werd zeer snel gesynthetiseerd met hoge radiochemische zuiverheid en hoge specifieke activiteit. De hersenopname werd verhoogd zowel in *mdr1a* knock-out muizen als na voorbehandeling met CsA in gewone muizen. Toediening van niet radioactief MC80 veroorzaakte een gereduceerde opname in de hersenen, hart, longen, testes, pancreas en darmen. In de hersenen vertoonde [¹¹C]-MC80 een uitstekend metabolisch profiel (> 90 % intact). Omdat [¹¹C]-MC80 specifieke binding vertoont aan de doelorganen kan deze component een goede basismolecule zijn voor de ontwikkeling van nieuwe radioliganden voor het meten van P-gp expressie in de hersenen.

Referenties

- Kanegawa N, Kiyono Y, Kimura H, Sugita T, Kajiyama S, Kawashima H et al. Synthesis and evaluation of radioiodinated (S,S)-2-(alpha-(2-iodophenoxy)benzyl)morpholine for imaging brain norepinephrine transporter. *Eur J Nucl Med Mol Imaging* 2006;33:639-47.
- Tamagnan GD, Brenner E, Alagille D, Staley JK, Haile C, Koren A et al. Development of SPECT imaging agents for the norepinephrine transporter: [I-123]INER. *Bioorg Med Chem* 2007;17:533-7.

Curriculum Vitae



CURRICULUM VITAE

PERSONALIA

Name	De Bruyne
First names	Sylvie Julie Suzie
Nationality	Belgian
Place and date of birth	Eeklo, Oktober 15 th , 1981
Civil status	Not married
Private address	Molenstraat 29 - 9880 Aalter Mobile + 32 (0)499 23 11 89 sylviedebruyne@hotmail.com

EDUCATION BACKGROUND

June, 1999	Secondary school: Mathematics-Sciences - Emmaüsinstituut – Aalter
June, 2004	Pharmacist with distinction – Faculty of Pharmaceutical Sciences – Ghent University
November, 2005	Symposium on in vivo small animal imaging – Faculty of Medicine and Pharmacy – VU Brussel
June, 2006	Methodology and radiochemical counting techniques - Faculty of Pharmaceutical Sciences - Ghent University

Nuclear chemistry - Faculty of Pharmaceutical Sciences - Ghent University

Radiobiology and radiopathology - Faculty of Medicine and Health Sciences - Ghent University

Molecular Spectroscopy - Faculty of Sciences - Ghent University

March, 2007

PET: Technology and application professional development programme - Department of Chemistry and Centre for Professional Development - Imperial College London

April, 2007

^{18}F Radiochemistry course - VU Amsterdam

June, 2007

Radioprotection and legislation - Faculty of Medicine and Health Sciences - Ghent University

Radiation dosimetry - Faculty of Medicine and Health Sciences - Ghent University

Basic course in laboratory animal sciences, partim 1 & 2: experiment leader - Faculty of Veterinary Medicine - Ghent University

Basic principles of nuclear chemistry and radiopharmacy - Faculty of Medicine and Health Sciences - Ghent University

PEER REVIEWED PUBLICATIONS

Blanckaert P., Burvenich I., wyffels L., **De Bruyne S.**, Moerman L., De Vos F. In vivo evaluation in rodents of [I-¹²³]-3-I-CO as a potential SPECT tracer for the serotonin 5-HT_{2A} receptor. *Nuclear Medicine and Biology* **2008**; 35: 861-867.

wyffels L., **De Bruyne S.**, Blanckaert P., Lambert D.M., De Vos F. Radiosynthesis, in vitro and in vivo evaluation of ¹²³I-labeled anandamide analogues for mapping brain FAAH. *Bioorganic and Medicinal Chemistry* **2009**; 17 (1): 49-56.

Blanckaert P., Burvenich I., Staelens S., **De Bruyne S.**, Moerman L., wyffels L., De Vos F. Effect of cyclosporine A on the biodistribution and μ SPECT imaging of [I-123]-R91150 in rodent brain. *European Journal of Nuclear Medicine and molecular imaging* **2009**; 36 (3): 446-453.

De Bruyne S., Boos T.L., wyffels L., Goeman J.L., Rice K.C., De Vos F. Synthesis, radiosynthesis and *in vivo* evaluation of [¹²³I]-4-(2-(bis(4-fluorophenyl)methoxy)ethyl)-1-(4-iodobenzyl)piperidine as a selective tracer for imaging the dopamine transporter. *Journal of Labelled Compounds and Radiopharmaceuticals* **2009**; 52 (8): 304-311.

wyffels L., Muccioli G.G., **De Bruyne S.**, Moerman L., Sambre J., Lambert D.M., De Vos F. Synthesis and in vitro evaluation of aryl anandamide analogues as candidate radioligands for in vivo imaging of fatty acid amide hydrolase in the brain. *Journal of Medicinal Chemistry* **2009**; 52 (15): 4613-4622.

wyffels L., **De Bruyne S.**, Moerman L., Lambert D.M., De Vos F. Radiosynthesis and biological evaluation of ¹¹C-labeled aryl anandamide analogues for in vivo

evaluation of brain fatty acid amide hydrolase. *Bioorganic and Medicinal Chemistry*, submitted.

De Bruyne S., La Regina G., wyffels L., Staelens S., Deleye S., Silvestri R., De Vos F. Radiosynthesis and *in vivo* evaluation of [¹¹C] labeled 1*H*-pyrrole-2-carboxamide derivatives as novel radioligands for PET imaging of monoamine oxidase A. *Nuclear Medicine and Biology*, accepted for publication.

De Bruyne S., wyffels L., Boos T.L., Staelens S., Deleye S., Rice K.C., De Vos F. Preclinical evaluation of [¹²³I]-4-(2-(bis(4-fluorophenyl)methoxy)ethyl)-1-(4-iodobenzyl)piperidine, an iodinated SPECT tracer for imaging P-gp function. *Nuclear Medicine and Biology*, submitted.

De Bruyne S., wyffels L., Moerman L., Sambre J., Colabufo N.A., De Vos F. Radiosynthesis and *in vivo* evaluation of [¹¹C]-MC80 for P-glycoprotein imaging. *Nuclear Medicine and Biology*, submitted.

wyffels L., Muccioli G., Kapanda C., Labar G., **De Bruyne S.**, De Vos F., Lambert D. PET imaging of fatty acid amide hydrolase in the brain: synthesis and biological evaluation of a ¹¹C-labelled URB597 analogue. *British Journal of Pharmacology*, submitted.

CONFERENCES WITH ORAL PRESENTATION

Blanckaert P., Burvenich I., Schoonooghe S., **De Bruyne S.**, wyffels L., De Vos F., Slegers G. Precursor synthesis, radiosynthesis and *in vivo* evaluation in mice of [¹²³I]-(4-fluorophenyl)[1-3-iodophenethyl]piperidine-4-yl]methanone as a potential SPECT tracer for the 5-HT_{2A} receptor. *European Journal of Nuclear Medicine and molecular imaging* **2006**; 33: S211-S212. European Association of Nuclear Medicine Congress, **October 2006**, Athens, Greece.

De Bruyne S., wyffels L., Blanckaert P., Rice K.C., Boos T., De Vos F. Synthesis, radiosynthesis and biodistribution in mice of [¹²³I]-4-(2-(bis(4-fluorophenyl)methoxy)ethyl)-1-(4-iodobenzyl)piperidine. The quarterly journal of nuclear medicine and molecular imaging **2008**; 52 (S1): 25. 14th European Symposium on Radiopharmacy and Radiopharmaceuticals, **April 2008**, Skopje, Macedonia.

wyffels L., **De Bruyne S.**, Blanckaert P., Lambert D.M., De Vos F. Synthesis, radiosynthesis and in vitro evaluation of iodinated anandamide analogues for mapping brain FAAH in vivo. The quarterly journal of nuclear medicine and molecular imaging **2008**; 52 (S1): 23. 14th European Symposium on Radiopharmacy and Radiopharmaceuticals, **April 2008**, Skopje, Macedonia.

De Bruyne S., wyffels L., Rice K., Boos T., De Vos F. Influence of cyclosporin A administration on the biodistribution of [¹²³I]-4-(2-(bis(4-fluorophenyl)methoxy)ethyl)-1-(4-iodobenzyl)piperidine. European Journal of Nuclear Medicine and Molecular Imaging **2008**; 35 (S2): S163. European Association of Nuclear Medicine Congress, **October 2008**, Munchen, Germany.

wyffels L., Muccioli G.G., **De Bruyne S.**, Moerman L., Lambert D.M., De Vos F. Synthesis and evaluation of N-(4-[¹¹C]methoxyphenethyl)linoleoylamide as a FAAH PET tracer. Journal of Nuclear Medicine **2009**; 50 (S2): S161. Society of Nuclear Medicine 56th annual Meeting, **June 2009**, Toronto, Canada.

wyffels L., Muccioli G.G., **De Bruyne S.**, Moerman L., Lambert D.M., De Vos F. Synthesis and evaluation of N-(4-[¹¹C] methoxyphenethyl)arachidonoylamide as PET radioligand for in vivo imaging of FAAH in the brain. Journal of Labelled

Compounds and Radiopharmaceuticals **2009**; 52 (S1): 83. 18th International Symposium on Radiopharmaceutical Sciences **July 2009**, Edmonton, Canada.

wyffels L., Muccioli G.G., Kapanda C.N., **De Bruyne S.**, Lambert D.M., De Vos F. Radiosynthesis and in vivo evaluation of [¹¹C]-biphenyl-3-yl 4-methoxyphenylcarbamate as PET tracer for in vivo evaluation of FAAH in the brain. 19th Annual Symposium of the International Cannabinoid Research Society **July 2009**, St-Charles, Illinois, USA.

CONFERENCES WITH POSTER PRESENTATION

De Bruyne S., wyffels L., Rice K.C., Boos T., Staelens S., Deleye S., De Vos F. Influence of Cyclosporin A on the SPECT scan of [¹²³I]-(4-(2-(bis(4-fluorophenyl)methoxy)ethyl)-1-(4-iodobenzyl)piperidine. First World Molecular Imaging Congress, **September 2008**, Nice, France.

Blanckaert P., Burvenich I., wyffels L., **De Bruyne S.**, De Vos F. Influence of cyclosporine A on the regional brain biodistribution of [¹²³I]-3-I-CO in rodents. European Journal of Nuclear Medicine and molecular imaging 2008; 35: S217. European Association of Nuclear Medicine Congress, **October 2008**, Munchen, Germany.

wyffels L., **De Bruyne S.**, BLanckaert P., Lambert D.M., De Vos F. Radiosynthesis, in vitro and in vivo evaluation of iodinated anandamide analogues for mapping brain FAAH in vivo. European Journal of Nuclear Medicine and Molecular Imaging 2008; 35 (S2): S330. European Association of Nuclear Medicine Congress, **October 2008**, München, Germany.

De Bruyne S., wyffels L., Blanckaert P., Rice K., Boos T., De Vos F. In vivo evaluation and metabolite analysis of [¹²³I]-(4-(2-(bis(4-fluorophenyl)

methoxy)ethyl)-1-(4-iodobenzyl)piperidine. *Journal of Nuclear Medicine* 2008; 49 (S1): 285. Society of Nuclear Medicine 55th annual Meeting, **June 2008**, New Orleans, USA.

De Bruyne S., wyffels L., Moerman L., Cantore M., Capparelli E., Colabufo N.A., De Vos F. Radiosynthesis and in vivo evaluation of a [¹¹C] labelled tracer for imaging P-gp. 4th European Molecular Imaging Meeting, **May 2009**, Barcelona, Spain.

De Bruyne S., wyffels L., Boos T., Staelens S., Rice K.C., De Vos F. Influence of Cyclosporin A administration on the brain uptake of [¹²³I]-(4-(2-(bis(4-fluorophenyl)methoxy)ethyl)-1-(4-iodobenzyl)piperidine. Scientific afternoon Faculty Pharmaceutical Sciences **May 2009**, Gent, Belgium.

De Bruyne S., wyffels L., Moerman L., La Regina G., Silvestri R., De Vos F. Radiosynthesis and in vivo evaluation of [¹¹C]-N-methyl-N-phenethyl-1H-pyrroile-2-carboxamide. *Journal of Nuclear Medicine* 2009; 50 (S2): 401. Society of Nuclear Medicine 56th annual Meeting, **June 2009**, Toronto, Canada.

De Bruyne S., wyffels L., Moerman L., La Regina G., Silvestri R., De Vos F. Radiosynthesis and in vivo evaluation of [¹¹C]-(R)-N-(1-cyclohexylethyl)-N-methyl-1H-pyrrole-2-carboxamide. *Journal of Labelled Compounds and Radiopharmaceuticals* 2009; 52 (S1): 328. 18th International Symposium on Radiopharmaceutical Sciences, **July 2009**, Edmonton, Canada.

Moerman L., wyffels L., **De Bruyne S.**, De Vos F. Phenytoin is a weak modulator of P-glycoprotein transporters: evaluation with ¹¹C-desmethylloperamide in mice. *Journal of Labelled Compounds and Radiopharmaceuticals* 2009; 52 (S1): 333. 18th International Symposium on Radiopharmaceutical Sciences, **July 2009**, Edmonton, Canada.

Moerman L., wyffels L., **De Bruyne S.**, De Vos F. Influence of sodium valproate, levetiracetam and topiramate on the P-glycoprotein transporters: evaluation with ¹¹C-desmethyloperamide in mice. European Association of Nuclear Medicine Congress, **October 2009**, Barcelona, Spain.

Slaets D., **De Bruyne S.**, Moerman L. De Vos F. Reduction of dimethylaminoethanol levels in [18F]fluoromethylcholine: *in vitro* and *in vivo* evaluation. European Association of Nuclear Medicine Congress, **October 2009**, Barcelona, Spain.

